Titre: Title:	Synergistic Gelation Properties of Gelatin and Polysaccharide Aqueous Mixtures
Auteur: Author:	Changsheng Wang
Date:	2017
Type:	Mémoire ou thèse / Dissertation or Thesis
Référence: Citation:	Wang, C. (2017). Synergistic Gelation Properties of Gelatin and Polysaccharide Aqueous Mixtures [Thèse de doctorat, École Polytechnique de Montréal]. PolyPublie. https://publications.polymtl.ca/2705/

UNIVERSITÉ DE MONTRÉAL

SYNERGISTIC GELATION PROPERTIES OF GELATIN AND POLYSACCHARIDE AQUEOUS MIXTURES

CHANGSHENG WANG

DÉPARTEMENT DE GÉNIE CHIMIQUE

ÉCOLE POLYTECHNIQUE DE MONTRÉAL

THÈSE PRÉSENTÉE EN VUE DE L'OBTENTION

DU DIPLÔME DE PHILOSOPHIAE DOCTOR

(GÉNIE CHIMIQUE)

AOÛT 2017

UNIVERSITÉ DE MONTRÉAL

ÉCOLE POLYTECHNIQUE DE MONTRÉAL

Cette thèse intitulée :

SYNERGISTIC GELATION PROPERTIES OF GELATIN AND POLYSACCHARIDE AQUEOUS MIXTURES

présentée par : WANG Changsheng

en vue de l'obtention du diplôme de : Philosophiae Doctor

a été dûment acceptée par le jury d'examen constitué de :

M. FAVIS Basil, Ph. D., président

Mme HEUZEY Marie-Claude, Ph. D., membre et directrice de recherche

M. VIRGILIO Nick, Ph. D., membre et codirecteur de recherche

Mme WOOD-ADAMS Paula, Ph. D., membre et codirectrice de recherche

M. CARREAU Pierre, Ph. D., membre

Mme ORSAT Valérie, Ph. D., membre externe

DEDICATION

To my beloved daughter, my wife, my parents and my grandparents

ACKNOWLEDGEMENTS

I would like to take this opportunity to thank all those who have supported and helped me during my study in École Polytechnique de Montréal.

First and foremost, I would like to express my deep acknowledgements to my supervisors: Prof. Marie-Claude Heuzey, Prof. Nick Virgilio and Prof. Paula Wood-Adams for their fundamental advices, constructive comments and unrelenting support throughout this project. Their meaningful instructions and recommendations were invaluable to my time as a PhD student and will be remembered and looked upon in years to come. I appreciate all of their contributions, time, and ideas. It was a great honor to work with them.

I would like to take this opportunity to thank Xiaoyan and Jun for their continuous support in my project and my life. Special thanks are extended to Dr. Giovanniantonio Natale for his contributions to the first part of this project.

I am very grateful for all the technical assistance of our previous and current research associates, Ms Melina Hamdine and Mr. Matthieu Gauthier. A sincere acknowledgement to Dr. Nicolas Tran-Khanh for his help in performing CLSM observations. Many thanks go to Prof. Françoise M. Winnik for allowing me to use their micro-DSC instrument, Dr. Evgeniya Korchagina for her help using micro-DSC and useful discussions, Ms Helia Sojoudiasli for useful discussions, Dr. Ross Clark from CP Kelco U.S., Inc for providing the xanthan gum samples, and Mr Bertrand Floure (Malvern Instruments Ltd) for kindly allowing the use of the Malvern Zetasizer Nano ZSP instrument and for useful discussions.

I would also like to express my gratitude to friends and colleagues for their support and help during my PhD study and my life, especially Shiming, Xiang, Qinghua, Yinghao, Nury, Mounia, Faezeh, Gilles, Quentin, Benoît, Fatemeh, Davood, Hanan, Chao and Lu.

I gratefully thank the China Scholarship Council (CSC), the Natural Sciences and Engineering Research Council of Canada (NSERC) and the Center for Applied Research on Polymers and Composites (CREPEC) for financial support.

Finally, I would like to thank my family for all their love, encouragement and support. In particular to my parents who raised me with love and supported me in all my pursuits; to my wife Lan who always encouraged me and took care of our kid to give me the time to work and write; to my brother

Changzi. A special word also goes to my grandparents, whose persistence and love continue to be an aspiration. I am so happy that they are able to see the completion of my studies before passing away.

RÉSUMÉ

Les protéines et les polysaccharides sont deux composants essentiels de la nourriture qui contribuent à leurs microstructures et textures. En conséquence, des gels composés de mélanges de protéines et de polysaccharides sont actuellement développés et utilisés, à des fins de recherche, en tant que modèles pour comprendre la structure et les propriétés des aliments réels. Récemment, ces gels multicomposants ont également attiré beaucoup d'attention comme systèmes d'encapsulation et de distribution de molécules bioactives, car la gélification peut se produire sans l'utilisation d'agents de réticulation, d'enzyme, ou de traitement thermique. Les gels composés de mélanges de protéines et de polysaccharides, ou gels mixtes, peuvent souvent être formés à des concentrations beaucoup plus faibles et affichent des propriétés mécaniques améliorées par rapport aux gels composés d'un seul composant. Ces gels mixtes sont connus pour être sensibles à des facteurs environnementaux tels que le pH, la force ionique, le rapport massique protéine/polysaccharide et les caractéristiques intrinsèques des biopolymères (type de polysaccharide, poids moléculaire, etc.). Par conséquent, une compréhension fondamentale des interactions entre protéines et polysaccharides en solutions est nécessaire pour concevoir de nouveaux épaississants et/ou gélifiants, systèmes d'encapsulation et de livraison. Dans ce projet, nous avons systématiquement étudié le comportement gélifiant de mélanges binaires composés de quatre types de gélatine (la protéine gélifiante la plus connue et l'une des plus utilisées) et de deux polysaccharides aux charges opposées: le chitosane, à charge positive (le deuxième biopolymère naturel le plus abondant) et la gomme de xanthane, chargée négativement (XG) (en raison de ses applications importantes dans les industries alimentaire, cosmétique et pharmaceutique). L'objectif général de cette thèse est de comprendre et de proposer un mécanisme général de gélification pour des mélanges de gélatine et de polysaccharides.

La première partie de cette thèse démontre qu'un équilibre délicat des charges est nécessaire pour former un gel mixte de gélatine et de gomme de xanthane à des concentrations très diluées (à une concentration environ 10 fois moindre par rapport à la concentration de gélification critique de la gélatine B uniquement) - illustrant le rôle important des interactions électrostatiques dans ces systèmes. Les expériences de rhéométrie ont montré que des systèmes composés de gélatine B de faible indice de Bloom (L-GB) et de XG gélifient légèrement au-dessus du point isoélectrique (pI) de L-GB (pI = 5.3) et affichent un module de stockage beaucoup plus élevé (G') par rapport à des solutions composées de XG ou de L-GB uniquement, avec G' atteignant un maximum à pH 5.5.

En outre, l'addition de sel entraîne une diminution significative de *G'* en raison de l'écrantage des charges. En outre, la microscopie confocale à balayage laser (CLSM) a révélé que la L-GB et le XG forment des agrégats dispersés à des pH inférieurs à 5.0, des réseaux colocalisés à pH 5.5 et enfin des réseaux complémentaires à des pH plus élevés (par exemple pH 8.0) - la structure du réseau se brisant avec l'addition de sel. Ces microstructures corrèlent avec les résultats de rhéologie et de potentiel zêta. Enfin, comme pour les gels de gélatine purs, les gels mixtes sont thermoréversibles, ce qui indique que les liaisons hydrogène jouent également un rôle important pendant le processus de gélification.

Dans la deuxième partie de cette thèse, nous avons étudié les effets de l'indice de Bloom pour la GB, du rapport GB à XG, et du poids moléculaire de la XG sur les propriétés de gélification des mélanges GB/XG. Comme pour les mélanges L-GB/XG (faible indice de Bloom), les mélanges composés de GB à indice de Bloom élevé H-GB/XG présentent un *G'* maximum à un pH proche du pI de H-GB. Les mélanges (L- et H-GB)/XG possèdent des compositions optimales au-delà desquelles *G'* diminue. L'augmentation de l'indice de Bloom entraîne l'augmentation de *G'*, alors que l'augmentation du poids moléculaire de la XG provoque l'effet inverse (ce qui peut sembler contre-intuitif) en raison des limitations de transfert de masse (diffusion). En fait, au pH optimal, le CLSM révèle que les mélanges GB/XG présentent également des transitions microstructurales reliées à la composition: d'agrégats discontinus (rapport GB/XG $\leqslant$ 1) à des réseaux superposés de GB et XG (ratio = 2-6), puis finalement une fragmentation du réseau (ratio = 8-10). Ces transitions microstructurales sont également corrélées aux propriétés rhéologiques mesurées. La micro-calorimétrie (micro-DSC) a finalement révélé que la XG adopte une conformation moléculaire plus stable avec l'addition de GB, ce qui augmente la gélification GB par la formation de triples hélices, comme l'indiquent la position et la surface des pics de transition.

Dans la troisième partie de cette thèse, nous avons étendu notre étude en analysant les effets des types de gélatine (type A et B) et de la charge des polysaccharides (XG chargé négativement, chitosane chargé positivement (CHI)), afin d'évaluer si les caractéristiques observées dans les systèmes GB/XG constituent un comportement général, ou sont spécifiques à cette combinaison protéine/polysaccharide. Les deux types de gélatine ont des compositions différentes en acides aminés, et donc différents points isoélectriques. Les mélanges GB/polysaccharides présentent toujours un *G'* à un pH sensiblement supérieur au pI, tandis que les mélanges gélatine A

(GA)/polysaccharides se comportent quelque peu différemment. Par exemple, les mélanges GA/XG montrent un *G'* maximum à un pH bien au-dessous du pI de GA (un résultat qui, nous soupçonnons, pourrait être dû à la distribution des charges dans la molécule de GA, mais cette hypothèse reste à être validée), tandis que les systèmes GA/CHI montrent une augmentation monotone de G' avec le pH, jusqu'à ce que le chitosane ne soit plus soluble en solution (au-delà de pH 6,0-6,5). Dans tous les cas, les microstructures des gels mixtes, dans les conditions optimales, sont caractérisées par des domaines pauvres et riches en biopolymères, et les résultats de micro-DSC révèlent que l'ajout des polysaccharides mène à l'augmentation de la formation de triples hélices de gélatine.

La synthèse des résultats suggère que le mécanisme de gélification des systèmes mixtes de gélatine/polysaccharide peut être divisé en trois étapes principales: 1) la formation de complexes de gélatine/polysaccharide par attraction électrostatique à une température initialement élevée (au-dessus de la température de transition pelote/hélice de la gélatine); 2) la réduction de la distance entre les molécules de polysaccharide avec une modification de la conformation du polysaccharide, à des températures intermédiaires; 3) l'augmentation de la concentration locale en biopolymères due à un effet de pontage provoqué par la formation de triples hélices de la gélatine, sous la température de transition pelote-hélice de la gélatine, ainsi que la formation d'un réseau.

Enfin, dans la quatrième et dernière partie de ce projet, nous avons commencé à étudier l'impact de la cinétique de gélification et du pH initial en comparant les propriétés des gels de gélatine/polysaccharide préparés selon 3 méthodes différentes: 1) par addition de HCl ou de NaOH en solution - c'est-à-dire par titration, un processus très rapide (~ 1 s) qui a été utilisé dans les trois premières parties de cette thèse; 2) par l'addition de glucono delta-lactone (GDL), ce qui ralentit l'acidification du milieu (~ 4-5 h); 3) par gélification induite par une phase vapeur (acidification très lente sans agitation, ~ 24 h). Nous avons constaté que les procédés d'acidification lente étendent significativement la gamme des compositions et des pH pour la formation de gels. Les gels mixtes obtenus par exposition à une vapeur d'acide présentent les meilleures propriétés mécaniques. Il apparaît que le processus de gélification est affecté par l'agitation, le taux d'acidification, le pH initial et le pH final.

Ce projet a utilisé une gamme de techniques complémentaires incluant la rhéométrie, la calorimétrie et la microscopie, qui pourraient être utilisées pour explorer et comprendre le mécanisme de gélification propre à d'autres mélanges aqueux de protéines linéaires ou globulaires, et de polysaccharides. Il ouvre la voie à l'exploration et à la compréhension du comportement de systèmes plus complexes, tels que des émulsions préparées avec des mélanges aqueux de protéines et de polysaccharides. En résumé, ce projet fournit un ensemble de lignes directrices fondamentales pour la conception de nouveaux épaississants et/ou gélifiants à base de protéines et de polysaccharides, pour des applications alimentaires ou pharmaceutiques.

ABSTRACT

Proteins and polysaccharides are two essential components in food, which contribute to structural and textural properties. As a result, gels comprising mixtures of proteins and polysaccharides are currently used, for research purposes, as models of multicomponent structures found in real foods. Recently, these multicomponent gels have attracted much attention for the protection of bioactive molecules when used as encapsulation and delivery systems, since gelation can occur without the use of crosslinking agents, heating or enzymes. Proteins/polysaccharides mixed gels can often be formed at much lower concentrations, and display enhanced mechanical properties compared to gels composed of only one component. These mixed gels are known to be sensitive to environmental factors like pH, ionic strength, protein to polysaccharide ratio, and biopolymer intrinsic characteristics (polysaccharide type, molecular weight, etc.). Therefore, a fundamental understanding of the interactions between proteins and polysaccharides in solutions is required to provide the guidelines to design such novel thickeners and/or gelling agents, encapsulation and delivery systems. In this project, we have systematically investigated the gelation behavior of binary mixtures comprising four types of gelatin (the most well-known and employed gelling protein), and two oppositely charged polysaccharides: the positively charged chitosan (the second most abundant natural biopolymer), and the negatively charged xanthan gum (XG) (due to its extensive applications in food, cosmetics and pharmaceutical industries). The general objective of this thesis is to understand and to propose a general gelation mechanism for gelatin/polysaccharide mixtures.

The first part of this thesis demonstrates that a delicate charge balance is required to form a mixed gel of gelatin and xanthan gum at very dilute concentrations (about 10 times less concentrated compared to the critical gelling concentration of gelatin B (GB) alone) – illustrating the important role of electrostatic interactions in these systems. Rheometry experiments showed that mixed gels comprised of low Bloom index gelatin B (L-GB) and XG form slightly above the isoelectric point (pI) of L-GB (pI = 5.3) and display much higher storage modulus (*G'*) compared to neat XG and L-GB solutions, with *G'* reaching a maximum at pH 5.5. Furthermore, salt addition causes a significant decrease in *G'* due to charge screening. Moreover, confocal laser scanning microscopy (CLSM) has revealed that L-GB and XG form dispersed aggregates at pH 5.0 and below, colocalized networks at pH 5.5, and finally complementary networks at higher pHs (*e.g.* pH 8.0) - the network structure however breaks down when salt is added. These microstructures correlate

well with rheology and zeta potential results. Finally, like pure gelatin gels, mixed L-GB and XG gels are thermoreversible, indicating that hydrogen bonding also plays an important role during the gelling process.

In the second part of this thesis, we further investigated the effects of GB Bloom index, GB to XG ratio, and XG molecular weight on the gelation properties of GB/XG mixtures. Similar to L-GB/XG, high Bloom index gelatin B (H-GB)/XG mixtures exhibit a maximum *G'* at a pH near the pI of H-GB. Both (L- and H-GB)/XG mixtures possess optimal compositions, beyond which *G'* decreases. Increasing the GB Bloom index results in a higher *G',* whereas increasing XG molecular weight causes the opposite effect (which might seem counter-intuitive) due to mass transfer (diffusion) limitations. In fact, at the optimum pH, CLSM reveals that GB/XG mixtures also display composition-dependent microstructural transitions: from discontinuous aggregates (GB/XG ratio $\leq$ 1) to continuous GB and XG colocalized networks (ratio = 2-6), followed by a fragmentation of the network (ratio = 8-10). These microstructural transitions also correlate well with the measured rheological properties. Micro-calorimetry (micro-DSC) finally revealed that XG adopts a more stable molecular conformation with the addition of GB, which in turn enhances GB gelling by triple helix formation, as indicated by the position and area of the transition peaks.

In the third part of this thesis, we extended our investigation by analyzing the effects of gelatin types (Type A and B) and polysaccharide charge (negatively charged XG, positively charged chitosan (CHI)), to assess whether or not the observed features observed in GB/XG systems constitute a general behavior, or are particular to this protein/polysaccharide combination. The two types of gelatin have different compositions of amino acids, and thus isoelectric point. Gelatin B (GB)/polysaccharides mixtures always exhibit the highest *G'* at a pH near the pI of GB, whereas gelatin A (GA)/polysaccharides mixtures behave somewhat differently. For example, GA/XG displays the highest *G'* at a pH far below the pI of GA (a result which we suspect could be due to the charge distribution in GA at a molecular level, but that remains to be validated), while GA/CHI shows a monotonous increase in *G'* with pH, until chitosan is no longer soluble over pH (~6.0-6.5). In all cases, the microstructures of the mixed gels under the optimal conditions are characterized by biopolymer-rich and biopolymer-poor domains, and micro-DSC results reveal that both polysaccharides always enhance gelatin gelling by triple helix formation.

Overall, our results indicate that the gelation mechanism of gelatin/polysaccharide mixed systems can be divided into three main steps: 1) the formation of gelatin/polysaccharide complexes via electrostatic attraction at an initially elevated temperature (above the coil-to-helix transition temperature of gelatin); 2) the reduction of the distance between polysaccharide molecules along with a change in polysaccharide conformation at intermediate temperatures; 3) the increase in local biopolymer concentration due to a bridging effect caused by gelatin triple helices formation below the coil-to-helix transition temperature of gelatin, along with a network formation.

Finally, in the fourth and last part of this project, we have started to investigate the impact of the gelling kinetics and initial starting pH by comparing the properties of gelatin/polysaccharide gels prepared following 3 different methods: 1) by the addition of HCl or NaOH solutions – *i.e.* titration, a very fast process (~ 1 s), which was used in the first three parts of this thesis; 2) by the addition of glucono delta-lactone (GDL), which slows down the acidification of the medium (~ 4-5 hrs); 3) by vapor-induced gelification (very slow acidification without stirring, ~ 24 hrs). It was found that slow acidification methods extend the range of compositions and pHs for gel formation. The vapor-induced mixed gels display the best mechanical properties. The gelation process is affected by stirring, acidification rate, initial pH and final pH.

This project has used an extensive array of techniques including rheometry, calorimetry and microscopy, which could be used to explore and understand the gelation mechanism of other linear protein/polysaccharide or globular protein/polysaccharide aqueous mixtures. It paves the way to understand the behavior of more complicated systems, such as emulsions prepared by protein/polysaccharide aqueous mixtures. In summary, this project provides a set of fundamental guidelines to design novel thickeners and/or gelling agents based on proteins and polysaccharides, for food or pharmaceutical applications.

TABLE OF CONTENTS

DEDICATION III

ACKNOWLEDGEMENTS IV

RÉSUMÉ VI

ABSTRACT X

TABLE OF CONTENTS XIII

LIST OF TABLES XVIII

LIST OF FIGURES XIX

LIST OF SYMBOLS AND ABBREVIATIONS XXIV

CHAPTER 1 INTRODUCTION 1

1.1 Background and problem identification 1

1.2 Organization of the thesis 3

CHAPTER 2 LITERATURE REVIEW 4

2.1 Proteins 4

2.1.1 Protein structure 4

2.1.2 Proteins functional properties 6

2.1.2.1 Gelation 6

2.1.2.2 Interfacial properties 8

2.1.3 Gelatin 11

2.2 Polysaccharides 13

2.2.1 Polysaccharide functional properties 16

2.2.1 Xanthan gum 16

2.2.2 Chitosan 18

2.3 Protein-polysaccharide interactions 20

2.4 Protein/polysaccharide gels 22
2.4.1 Interpenetrating networks 23
2.4.2 Phase-separated networks 23
2.4.3 Coupled gel networks 24
2.5 Factors influencing protein/polysaccharide gels 26
2.6 Rheology of gels 27
2.7 Summary 32
CHAPTER 3 RESEARCH OBJECTIVES AND COHERENCE OF ARTICLES 33
3.1 Research objectives 33
3.2 Presentation of articles and coherence with research objectives 33
CHAPTER 4 ARTICLE 1: SYNERGISTIC GELATION OF GELATIN B WITH XANTHAN GUM 35
4.1 Abstract 35
4.2 Introduction 35
4.3 Materials and methods 37
4.3.1 Materials 37
4.3.2 Preparation of GB, XG and mixed GB/XG solutions 38
4.3.3 Zeta potential measurements 38
4.3.4 Rheological measurements 38
4.3.4.1 Small amplitude oscillatory shear (SAOS) 38
4.3.4.2 Time-resolved small amplitude oscillatory shear 39
4.3.5 Confocal laser scanning microscopy (CLSM) 39
4.4 Results 40
4.4.1 Zeta potential 40
4.4.2 Turbidity observations 42

4.4.3 Rheological behavior 44
4.4.3.1 Small amplitude oscillatory shear (SAOS) 44
4.4.3.2 Time-resolved small amplitude oscillatory shear 48
4.4.4 CLSM analysis 49
4.5 Discussion 56
4.6 Conclusions 58
4.7 Acknowledgement 58
4.8 Supporting information 58
4.9 References 60
CHAPTER 5 ARTICLE 2: A MECHANISM FOR THE SYNERGISTIC GELATION PROPERTIES OF GELATIN B AND XANTHAN GUM AQUEOUS MIXTURES 64
5.1 Abstract 64
5.2 Introduction 64
5.3 Materials and methods 66
5.3.1 Materials 66
5.3.2 Preparation of GB, XG and GB/XG solutions 66
5.3.3 Zeta potential measurements 66
5.3.4 “Table-top” rheology 67
5.3.5 Time-resolved small amplitude oscillatory shear 67
5.3.6 Confocal laser scanning microscopy (CLSM) 67
5.3.7 Micro-differential scanning calorimetry (Micro-DSC) 68
5.4 Results and discussion 69
5.4.1 Zeta potential of GB and XG 69
5.4.2 “Table-top” rheology 71
5.4.3 Time-resolved small amplitude oscillatory shear 73

5.4.4 CLSM 77
5.4.5 Micro-DSC 82
5.4.6 Proposed synergistic gelation mechanism 85
5.5 Conclusions 87
5.6 Acknowledgements 88
5.7 Supporting Information 88
5.8 References 99
CHAPTER 6 ARTICLE 3: A GELATION MECHANISM FOR GELATIN/POLYSACCHARIDE AQUEOUS MIXTURES 102
6.1 Abstract 102
6.2 Introduction 102
6.3 Materials and methods 104
6.3.1 Materials 104
6.3.2 Sample preparation 104
6.3.3 Zeta potential measurements 104
6.3.4 “Table-top” rheology 105
6.3.5 Time-resolved small amplitude oscillatory shear 105
6.3.6 Confocal laser scanning microscopy 105
6.3.7 Micro-differential scanning calorimetry (Micro-DSC) 106
6.4 Results and discussion 107
6.4.1 Zeta potential 107
6.4.2 “Table-top” rheology 109
6.4.3 Time-resolved small amplitude oscillatory shear 111
6.4.4 CLSM 114
6.4.5 Micro-DSC 118

6.4.6 Discussion 119
6.5 Conclusions 121
6.6 Acknowledgements 122
6.7 Supporting information 122
6.8 References 123
CHAPTER 7 ARTICLE 4: PROTEIN/POLYSACCHARIDE BASED HYDROGELS PREPARED BY VAPOR-INDUCED PHASE SEPARATION 126
7.1 Abstract 126
7.2 Results and discussion 126
7.3 Experimental section 134
7.3.1 Materials 134
7.3.2 Preparation of GB, XG and GB/XG solutions 135
7.3.3 Preparation of GB/XG mixed gels 135
7.3.4 Confocal laser scanning microscope (CLSM) 135
7.3.5 Mechanical properties 136
7.4 Acknowledgements 136
7.5 Supporting information 137
7.6 References 140
CHAPTER 8 GENERAL DISCUSSION 142
CHAPTER 9 CONCLUSIONS AND RECOMMENDATIONS 146
9.1 Conclusions 146
9.2 Recommendations 147
BIBLIOGRAPHY 148

LIST OF TABLES

Table 2.1: The 20 amino acids composing proteins 4

Table 2.2: Molecular characteristics of some food-grade proteins [28] 6

Table 2.3 Published studies on emulsifying properties of some protein/polysaccharide complexes 10

Table 2.4: Amino acid composition of collagen and gelatin per 1000 residues [25] 12

Table 2.5: Molecular characteristics food-grade polysaccharides [27] 13

Table 2.6: Different structural levels of polysaccharides 14

Table 2.7: Published studies on protein/polysaccharide mixed gels 24

Table 5.1 Specific enthalpies and transition temperatures (peak maximum) of L-GB, R-XG and their mixtures during the second micro-DSC heating segment. 84

Table 6.1 Specific enthalpies and transition temperatures (peak maximum) of neat components and their mixtures during the second micro-DSC heating segment. 119

LIST OF FIGURES

Figure 2.1 The four different levels of protein structure [26]. 5

Figure 2.2 Schematic of unfolding and aggregation of a protein. 7

Figure 2.3 Schematic of stranded and particulate gels formed by globular proteins. The circles with or without thick red borders represent the native or denatured soy proteins, respectively. Modification of sketch by Peng et al. [39]. 8

Figure 2.4 Overview of the different steps in the formation of an adsorbed protein layer: A) diffusion and adsorption protein molecules to the interface; B) unfolding and rearrangement of protein molecules at interface; C) film formation at interface. 9

Figure 2.5 Illustration of two alternative procedures for stabilization of oil droplets by protein–polysaccharide complexes. A) layer-by-layer procedure, with polysaccharide (ps) added after emulsification with protein (pr); (B) premixing procedure, with both biopolymers present together during emulsification. 9

Figure 2.6 The thermoreversible gelation process for gelatin [25]. 11

Figure 2.7 Thermally reversible helix-to-coil (order-to-disorder) conformational transition of polysaccharides for a) single- and b) double-helical structures [54]. 15

Figure 2.8 Molecular structure of xanthan gum [57]. 17

Figure 2.9 Schematic model for the XG order–disorder transition [57]. 18

Figure 2.10 Chemical structure of chitin and chitosan [82]. 19

Figure 2.11 Possible interactions for proteins/polysaccharides mixtures and consequences in the formation of mixed gels. Based on the work by Ghosh et al. [17], and Stokes [53]. 21

Figure 2.12 Different structures formed by the electrostatic complexation of proteins and polysaccharides: (a) coacervates; (b) insoluble complexes; and (c) electrostatic gel. The scale bar is 40 μm [95]. 22

Figure 2.13 Network structures: (a) coupled network, (b) interpenetrating network, (c) phase-separated network [96]. 23

Figure 2.14 Schematic of the interaction and gel formation process between β-lg (circles) and XG (rod shapes); rectangle presents aggregation zones of β-lg on XG chains, arrow presents electrostatic cross-linking zones of XG chains by β-lg [24]. 26

Figure 2.15 Stress versus strain response of a Hookean solid, Newtonian liquid and a viscoelastic material in dynamic oscillatory tests. 28

Figure 2.16 The mechanical spectra of four principle categories: a) dilute solution, b) entangled solution, c) strong gel and d) weak gel [125]. 29

Figure 2.17 Schematic of the divergence of zero-shear viscosity, η_0, and equilibrium modulus, G_e. The extent of crosslinking is marked by p [126]. 31

Figure 4.1 Zeta potential of GB, XG and their mixtures. ■: GB, ●: GB:XG = 5:1, ▲: XG. 41

Figure 4.2 a) Effects of pH (3.5-7.0) and NaCl concentration (0-300 mM) on the visual aspect of GB/XG mixtures (GB:XG = 5:1, total concentration = 1.2% w/v); b) close-up view of mixtures without NaCl at pHs 5.0-7.0 43

Figure 4.3 a) Storage modulus (G') and b) complex viscosity (|η*|) as functions of frequency at 20°C for the mixtures (GB:XG=5:1, total concentration = 1.2 %) at various pHs (pH=5.0-10.0). XG at a concentration of 0.2 % (w/v) is shown for comparison purposes. No salt added. 45

Figure 4.4 Comparisons of storage modulus (G') and complex viscosity (|η*|) at different pHs for the mixtures (GB:XG = 5:1, total concentration = 1.2 % w/v) and XG solutions (c = 0.2-0.8 % w/v, pH = 6.0) at ω = 1 rad/s. No salt added. 46

Figure 4.5 Comparison of storage modulus (G') of the mixtures (GB:XG = 5:1, total concentration = 1.2 % w/v) at different pHs and salt concentrations (0 - 100 mM) at a ω = 1 rad/s. 47

Figure 4.6 Evolution of G' of the mixtures (GB:XG=5:1, total concentration = 1.2 % w/v) at different pHs (5.0-9.0) as a function of time. The samples were first heated up to 60°C, then cooled down to 20°C, and the process was repeated a second time. 48

Figure 4.7 CLSM images of mixtures (GB:XG = 5:1, total concentration = 1.2 % w/v) at different pHs, at 0 h and 24 h after solution preparation. GB was stained with Nile Blue A (red). Image size: 210 μm x 210 μm. No salt added. 52

Figure 4.8 Average size of GB-poor domains as a function of pH. At least 10 small bright regions (50 μm x 50 μm) from no less than 2 different CLSM images for each sample are selected for calculation. The insert shows G' against the diameter of GB-poor domains.....53

Figure 4.9 CLSM images of mixtures (GB:XG = 5:1, total concentration = 1.2 % w/v) at different pHs. XG is labelled with DTAF (green). Image size: 210 μm x 210 μm. No salt added. The pictures were taken 24 h after solution preparation. 55

Figure 4.10 Effect of salt addition on the microstructure of GB/XG mixture (GB:XG = 5:1, total concentration = 1.2 % w/v) at pH = 5.5, salt concentration = 50 mM. Image size: 210 μm x 210 μm. The pictures were taken after 24 h. Left: XG stained with DTAF; right: GB stained with Nile Blue A. 55

Figure 5.1 Zeta potential values of the GB (a) and XG (b) grades used in this work.....70

Figure 5.2 a) Effect of L-GB concentration (c_{GB} = 0.2-2.0 % w/v) on the visual aspect of L-GB/R-XG aqueous mixtures, at pH 5.5; b) effects of pH (4.0-7.0) and H-GB concentration (c_{GB} = 0.2–1.6 % w/v) on the visual aspect of H-GB/R-XG mixtures, H-GB/R-XG ratio = 1-8; c) effects of pH (4.0-7.0) and XG molecular weight on the visual aspect of L-GB/XG mixtures (L-GB:XG ratio = 6, c_{XG} = 0.2 % w/v). The photos were taken after overnight storage.....73

Figure 5.3 a) Evolution of G' as a function of time for the L-GB/R-XG mixtures at ratios (1-10), at pH 5.5; b) G' and G" after 8 hrs, as a function of L-GB/R-XG ratio. c_{XG} = 0.2 % w/v, ω = 1 rad/s. 75

Figure 5.4 G' as a function of time, for the mixtures of L-GB and Low-XG, Med-XG and High-XG respectively, at ratio 6 and pH 5.5. XG concentration = 0.2 % w/v, ω = 1 rad/s. 76

Figure 5.5 Comparison of G_{8h}' of H-GB solution with and without R-XG after 8 hrs in the rheometer at 20°C, ω = 1 rad/s, c_{XG} = 0.2 % w/v. The insert shows the ratio of the G_{8h}' of H-GB/R-XG mixtures over the sum of the G_{8h}' of neat H-GB and R-XG at concentrations in the corresponding mixtures, as a function of H-GB concentration.....77

Figure 5.6 Microstructures of L-GB (red) and R-XG (green) domains in the mixtures at different ratios (1, 2 6 and 10) and merge of the two imaging, at pH 5.5. The images were taken after storage for 24 hrs. Image size: 210 μm x 210 μm.....79

Figure 5.7 Microstructure of L-GB (red) when mixed with Low-XG, Med-XG and High-XG, respectively, at different ratios (2, 6, and 8) and pH 5.5. The images were taken after storage for 24 hrs at room temperature. Image size: 210 μm x 210 μm. 80

Figure 5.8 a) Average size of biopolymer-poor (BP-poor) domains in L-GB/R-XG and H-GB/R-XG mixtures, as a function of GB/R-XG ratio; and b) average size of biopolymer-poor domains in L-GB/Low-XG, L-GB/Med-XG and L-GB/High-XG mixtures, as a function of L-GB/XG ratio. 82

Figure 5.9 Micro-DSC heating curves, shifted vertically for clarity. Scanning rate = 1 ^{o}C/min. ..83

Figure 5.10 Proposed gelation mechanism in GB/XG mixtures, based on their interactions and molecular conformations. 85

Figure 5.11 Evolution of G' during heating of three systems: (◄) L-GB = 4.0 % w/v, (▲) L-GB/R-XG = 6, total concentration = 1.4 % w/v and (■) R-XG 0.2 % w/v. Heating rate: 0.2 ^{o}C/min 87

Figure 6.1 Zeta potential values of the gelatins (a), XG (b) and CHI (c) used in this work. 108

Figure 6.2 Effects of pH and gelatin concentration on the visual aspect of different mixtures: a) L-GA/XG, b) H-GA/CHI, c) L-GA/CHI and d) H-GB/CHI. The photos were taken after overnight storage. 110

Figure 6.3 Evolution of G' as a function of time for a) the L-GA/ XG mixtures at ratio = 3 and different pHs, b) the L-GA/ XG mixtures at different ratios and pH 6.0, c_{XG} = 0.2 %, c) the H-GB/CHI mixtures at ratio = 2.5 and different pHs, d) the H-GB/CHI mixtures at different ratios and pH 5.0, c_{CHI}= 0.4 %, e) the L-GA/CHI mixtures at ratio= 3 and different pHs, and f) the L-GA/XG mixtures at different ratios and pH 6.0, c_{CHI} = 0.4 % 112

Figure 6.4 The ratio of G' of a) H-GB/CHI and b) L-GA/CHI mixtures over the sum of the G' of neat compositions at concentrations in the corresponding mixtures, as a function of gelatin concentration, 8 h after solution preparation (c_{CHI} = 0.4 % w/v). 114

Figure 6.5 Microstructures of L-GA/XG (Panel A, ratio 3, 120 μm x 120 μm), H-GB/CHI (Panel B, ratio 4, 105 μm x 105 μm) and L-GA/CHI (Panel C, ratio 4, 105 μm x 105 μm) mixtures.

Gelatin appears in red and XG or CHI in green. The images were taken after storage for 24 hrs. 117

Figure 6.6 Micro-DSC heating curves shifted vertically for clarity. Scanning rate = 1 ^{o}C/min. . 118

Figure 6.7 Gelation mechanism in gelatin/polysaccharide mixtures, based on their interactions and molecular conformations. XG molecules undergo a disorder-to-order transition and CHI molecules become less flexible upon cooling in step b. 120

Figure 6.8 Time-resolved rheological and turbidity measurements at different temperatures, a) and c) H-GB/CHI, ratio = 4, pH 5.0; b) and d) L-GB/XG, ratio = 6, pH 5.5. Turbidity data were obtained at 600 nm. 121

Figure 7.1. pH of a gelatin B solution (1.0 % w/v) as a function of time under different acidification conditions: acetic acid vapor (solid symbols, wt% in water) and GDL addition (open symbols). 128

Figure 7.2. State of the mixtures in terms of gelation (upside down vials) and syneresis (tilted vials) after 24 h: a) initial pH = 5.5 and prepared (i) by exposing to vapor of 80 wt% acetic acid; (ii) with 0.1 wt% GDL; (iii) with 0.5 wt% GDL; (iv) gel destabilization after heating; b) initial pH = 10.0 prepared (i) by exposing to vapor of 80 wt% acetic acid and (ii) with GDL addition; c) effects of (i) XG and (ii) GB concentration. 129

Figure 7.3. Microstructures of GB/XG (c_{XG} = 0.2 wt%) mixed gels prepared from an initial pH of 5.5 by VIPS using 80 wt% acetic acid (Panel A), and by GDL addition (Panel B); Panel C: mixed gels prepared from an initial pH of 10.0 by VIPS using 80 wt% acetic acid vapor. GB appears in red and XG in green with colocalized networks appearing yellow. The images were taken after 24 h storage. 132

Figure 7.4. Force at break in compression of mixed gels at different GB/XG ratios, prepared by different methods after 24 h storage (c_{XG} = 0.2 wt%). 133

LIST OF SYMBOLS AND ABBREVIATIONS

GA	Gelatin type A
GB	Gelatin type B
XG	Xanthan gum
CHI	Chitosan
CLSM	Confocal laser scanning microscope
DDA	Degree of deacetylation
5-DTAF	5-(4,6-Dichlorotriazinyl) Aminofluorescein
pI	Isoelectric point
SAOS	Small amplitude oscillatory shear
WPI	Whey protein isolate
LVE	Linear viscoelastic regime
FITC	Fluorescein isothiocyanate
VIPS	Vapor induced phase separation
GDL	Glucono delta-lactone

CHAPTER 1 INTRODUCTION

1.1 Background and problem identification

Food formulations are complicated mixtures since they usually contain water, proteins, polysaccharides, fats and other minor components. Proteins and polysaccharides are two essential ingredients in food products, and perform complementary nutritional, structural and textural functions [1]. The interactions between proteins and polysaccharides greatly affect the rheological behavior of the final product [2], and their importance in food formulations has been emphasized by Tolstoguzov [3]. In addition, proteins and polysaccharides are also commonly used in the cosmetic, pharmaceutical and biomedical industries.

The interactions between proteins and polysaccharides were first reported at the turn of the 19th century by the observation of the incompatibility between gelatin and starch, and since then they have been extensively investigated. Two general cases occur when mixing proteins and polysaccharides in aqueous solution, depending on the pH and ionic strength: segregative phase separation (thermodynamic incompatibility) and associative phase separation (thermodynamic compatibility) [4,5]. Further details on protein/polysaccharide interactions are presented in section §2.3. Protein/polysaccharide interactions have gained much attention since they can result in the enhancement of functional properties (stability, interfacial and gelation properties, encapsulation) as compared to those of the individual components.

Polysaccharides can enhance the stability of proteins via complexation, which is of great importance in protein beverages [6]. For example, the ideal pH for whey protein beverages (*e.g.* sports drinks) is at pH 4-6, where astringency and off-flavors can be avoided [7,8]. However, the stability of whey protein is a concern since the isoelectric point of whey protein is located in the pH range mentioned above, which may result in protein precipitation, microphase separation or gelation after heating [9,10]. The problem can be solved by adding pectin to form whey protein/pectin soluble complexes having a narrower size distribution, reduced hydrodynamic volume and greater magnitude of surface charge [11]. This successfully overcomes the limitation mentioned above and allows the manufacture of high whey protein beverages at pH 4.

Protein/polysaccharide complexes can also be used as emulsion or foam stabilizers. As it is well known, the mechanical strength of the interfacial layer, the electrostatic (repulsion between the

emulsion droplets) and the steric (barrier of thick interfacial layer) effects are the most important factors contributing to the stability of emulsions [12]. There are two ways to prepare emulsions using proteins and polysaccharides: a) premix proteins and polysaccharides under appropriate conditions to form complexes, followed by emulsion processing with the formed complexes [13,14]; b) use a layer-by-layer method by adding proteins and polysaccharides sequentially during emulsion preparation [15,16]. Both techniques can result in a thicker adsorption layer. For example, the interfacial elastic modulus is higher for an interfacial film formed by β-lactoglobulin/acacia gum electrically neutral complexes at pH 4.2 compared to the protein alone. In addition, complexation increases the magnitude of the zeta potential, which enhances the stability of emulsions. Finally, the presence of polysaccharides provides steric stabilization and increases the viscosity of the continuous phase, which reduce emulsion droplets movements and collisions.

Protein/polysaccharide mixed gels are receiving more and more interest because they can be formed without heat, enzyme or crosslinking agent and at extremely low concentrations. As a result, they are of high interest for the development of novel thickeners and gelling agents [4,17] for the protection of bioactive molecules, when used as encapsulation and delivery systems [4,5]. Therefore, understanding the underlying principles of how proteins and polysaccharides interact in solution with each other is a prerequisite to design and prepare systems with the desired properties and functionalities.

Protein/polysaccharide mixed gel formation depends on the nature and characteristics of the biopolymers. For both proteins [18] and polysaccharides [19], a higher biopolymer concentration is needed to form a gel when the molecular weight and charge density are lower. Electrostatic forces are the dominant interactions between proteins and polysaccharides in solution, but other interactions such as hydrogen bonding and hydrophobic interactions can also be involved [6,20]. Proteins and polysaccharides can both repel and attract each other even when they carry the same net charge due to the amphiprotic properties of proteins [4,21,22]. Electrostatic forces are affected by the protein/polysaccharide ratio, pH, ionic strength and biopolymer charge density [4,20]. The gelation properties of protein/polysaccharide electrostatic hydrogels are the result of a delicate balance between repulsive and attractive interactions [4,23].

The gelation properties of different protein/polysaccharide mixtures have been investigated extensively, as summarized later in Table 2.7. However, no related studies have been found for the

mixtures of gelatin and xanthan gum. In addition, the majority of protein/polysaccharide mixed gel studies focus on proteins and anionic polysaccharides, with fewer works on proteins and cationic polysaccharides. A mechanism was proposed to explain the synergistic gelation of β-lactoglubulin/XG mixtures [24]. However, it has several limitations: a) it neglects the conformation of xanthan gum when complexing with β-lactoglubulin, which can also be a driving force for the gelation process; b) it is not ideal to explain the gelation systems at a constant pH due to the used acidifier (glucono delta-lactone, GDL), which changes pH gradually with time; c) it is not suitable to explain the gelation process of gelatin/polysaccharide mixtures due to the differences between globular and linear proteins.

In this project, we aim at understanding the interactions between gelatin and two polysaccharides (xanthan gum, an anionic polysaccharide and chitosan, a cationic polysaccharide), which still remain unknown. We also target to propose a general mechanism on a molecular level to explain the gelation behavior of gelatin/polysaccharide aqueous mixtures, in order to better control the mechanical properties according to needs and to design novel thickeners and/or gelling agents, encapsulation and delivery systems.

1.2 Organization of the thesis

This thesis is based on three articles that have been published by or submitted to scientific journals, and consists of the following chapters:

- Chapter 2 provides a literature review considering the related issues.
- Chapter 3 describes the objectives and the coherence of the articles.
- Chapters 4, 5, 6 and 7 present the four articles describing the main achievements obtained in this study.
- Chapter 8 reports a general discussion about the main results.
- Chapter 9 states the conclusions as well as recommendations for future work.

CHAPTER 2 LITERATURE REVIEW

2.1 Proteins

2.1.1 Protein structure

Proteins constitute one of the most important class of biopolymers, which are encountered in areas such as food, cosmetics, pharmaceutical, medicine, packaging, coatings, etc [25]. Proteins can be composed of up to 20 different amino acids (**Table 2.1**).

Table 2.1: The 20 amino acids composing proteins

Acidic and polar (positive)	pI	**Neutral and non-polar**	pI
Aspartic acid (Asp)	2.77	Alanine (Ala)	6.00
Glutamic acid (Glu)	3.22	Glycine (Gly)	5.97
Basic and polar (negative)		Isoleucine (Ise)	6.02
Arginine (Arg)	10.76	Leucine (Leu)	5.98
Histidine (His)	7.59	Methionine (Met)	5.74
Lysine (Lys)	9.74	Phenylalanine (Phe)	5.48
Neutral and polar		Proline (Pro)	6.30
Asparagine (Asn)	5.41	Serine (Ser)	5.68
Cysteine (Cys)	5.07	Tryptophan (Try)	5.89
Glutamine (Gln)	5.65	Valine (Val)	5.96
Threonine (Thr)	5.60		
Tyrosine (Tyr)	5.66		

Each amino acid contains a primary amine and a carboxylic acid group with the general formula:

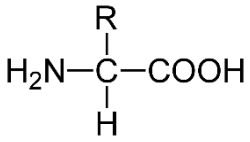

The R group (guanidinium of arginine, imidazole of histidine, carboxyl group of aspartic acid, etc.) differs for various amino acids and determines the polarity and charge. Amino acids are linked together through peptide bonds (amide bonds between -NH_2 of one amino acid and -COOH of another). Sequences with fewer than 50 amino acids are referred to as peptides, while longer sequences are termed as polypeptides or proteins. A protein can consist of one or more polypeptides.

The two termini of a polypeptide or protein sequence contain a free carboxyl group and a free amino group, and are designated as carboxy-terminus (C-terminus) and amino terminus (N-terminus), respectively. The (ionic or neutral) R group, amino- and carboxyl termini give a protein its positive, negative or neutral charge, depending on the pH. The isoelectric point (pI) is defined as the pH at which a protein possesses no net charge. The amphiprotic charge properties of proteins are important for understanding protein/protein and protein/polysaccharide interactions.

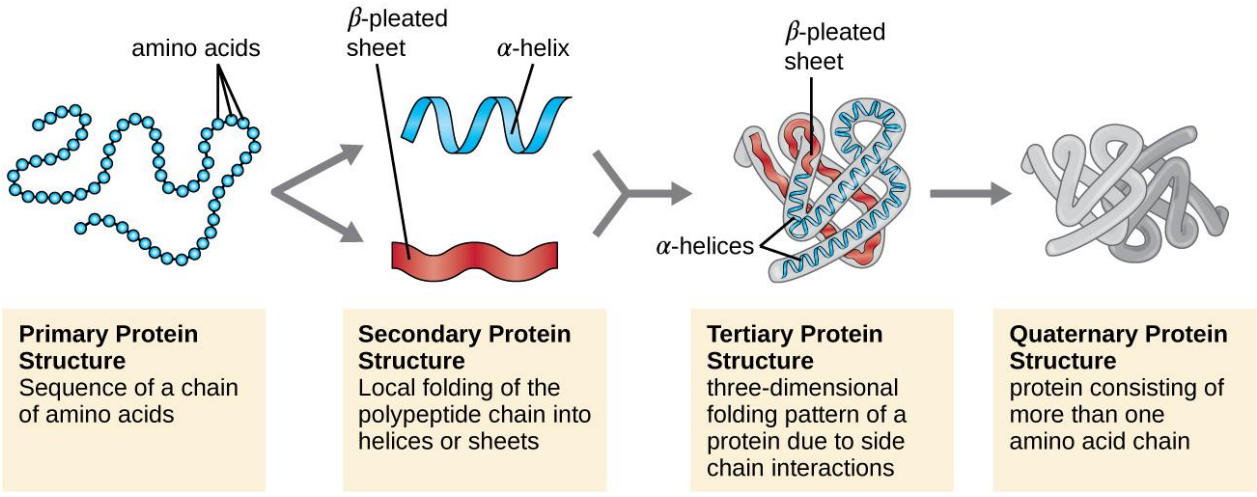

Figure 2.1 The four different levels of protein structure [26].

Protein structure has four different levels – primary, secondary, tertiary and quaternary (**Figure 2.1**). The primary structure is defined by the unique sequence, composition and distribution of amino acids in the polypeptide chain. Certain amino acids within the chain give rise to local secondary structures such as α-helix and β-sheets. After complex arrangement and/or folding, protein molecules adopt linear conformations or globular structures, which is referred to as tertiary structure. The tertiary structure is mainly stabilized by hydrogen bonding, disulfide bonding and salt bridges. Globular proteins are formed by folding polypeptide chains into a compact spherical shape with an irregular surface; hydrophobic amino acids tend to reside inside globular proteins with hydrophilic amino acids being outside; they are usually soluble in an aqueous environment and are involved in the transport processes or dynamic functions in cells (*e.g.* enzymes, bovine serum albumin). Linear proteins are characterized by their long parallel polypeptide chains. They function as structural elements, such as in the connective tissue of animals (*e.g.* collagen, keratin). The structure of protein can vary in response to changes in environmental conditions, for example, pH, temperature, salts and nature of solvent. Usually, protein molecules exist in the lowest

attainable free energy. The free energy may not be the global minimum, but it will be the lowest that the protein can achieve in a reasonable period of time [27]. Generally, proteins are made of multiple polypeptide chains, which are defined as protein subunits. The associations between multiple protein subunits are referred to as the quaternary structure.

2.1.2 Proteins functional properties

The unique sequence, composition and distribution of amino acids (primary structure) endow a given protein with different physicochemical characteristics, such as solubility, thermal stability, hydrophobicity and hydrophilicity, and further determine its functional properties, such as gelation, foaming and emulsifying properties. Some common proteins are listed in **Table 2.2**.

Table 2.2: Molecular characteristics of some food-grade proteins [28]

Name	Source	Structure	pI
Bovine serum albumin	Bovine blood/milk	Globular	4.7
Gelatin	Collagen	Linear	7-9.4[a]; 4.8-5.5[b]
Ovalbumin	Egg white	Globular	4.5-4.7
Soy glycinin	Soybean	Globular	5
β-Lactoglobulin	Whey protein	Globular	4.8-5.1

[a] Type A gelatin; [b] Type B gelatin.

2.1.2.1 Gelation

Since a protein is usually stable in solution, denaturation/destabilization is a prerequisite for gelation [29]. The denaturation/destabilization techniques include heating, pressure [30,31], enzymatic crosslinking [32,33] and denaturants [34,35]. Denaturation also occurs at extremes of solution pH and ionic strength. The protein molecules under these conditions are unfolded and then aggregate into a network through non-covalent crosslinks such as electrostatic forces, hydrogen bonding, hydrophobic and covalent bonds (*e.g.* disulfide bonds) (**Figure 2.2**). The functional properties of protein hydrogels (gel strength, elasticity, water holding capacity, etc.) depend on the protein intrinsic characteristics, protein concentration, pH, salt concentration and type, as well as denaturation conditions (heating temperature, time, pressure, etc.) [4].

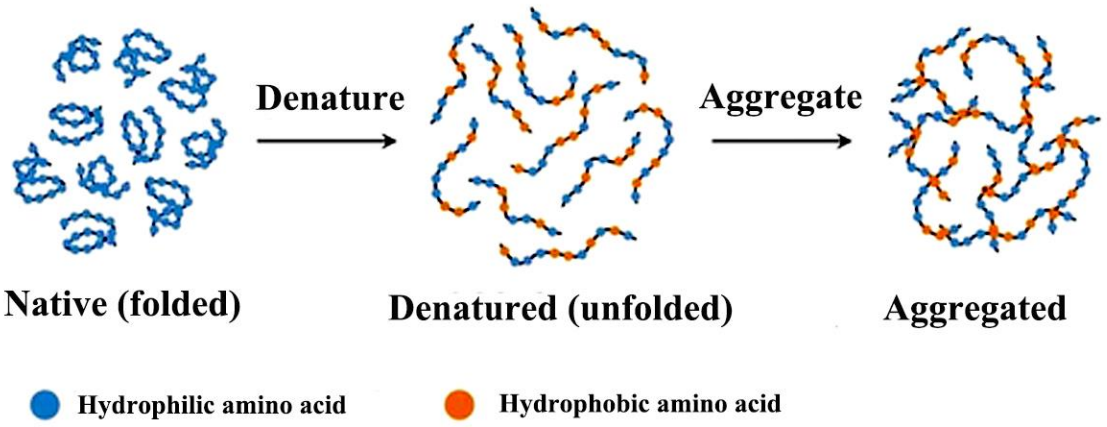

Figure 2.2 Schematic of unfolding and aggregation of a protein.

Globular proteins can form two categories of gels: particulate gels and fine-stranded gels. Particulate gels are obtained when heated at a pH close to the pI and/or at high ionic strength when electrostatic repulsion is low [36,37], whereas the fine-stranded gels are formed at pH far from the pI at low ionic strength when electrostatic repulsion is high [38] (**Figure 2.3**). The former gels have coarse, opaque and brittle structures; in contrast, the latter ones are usually transparent, more elastic, smoother and less sticky. The gels formed by globular proteins are usually thermally irreversible. In contrast, linear proteins are able to form thermally reversible gels, such as collagen and gelatin. More details are given in §2.1.3.

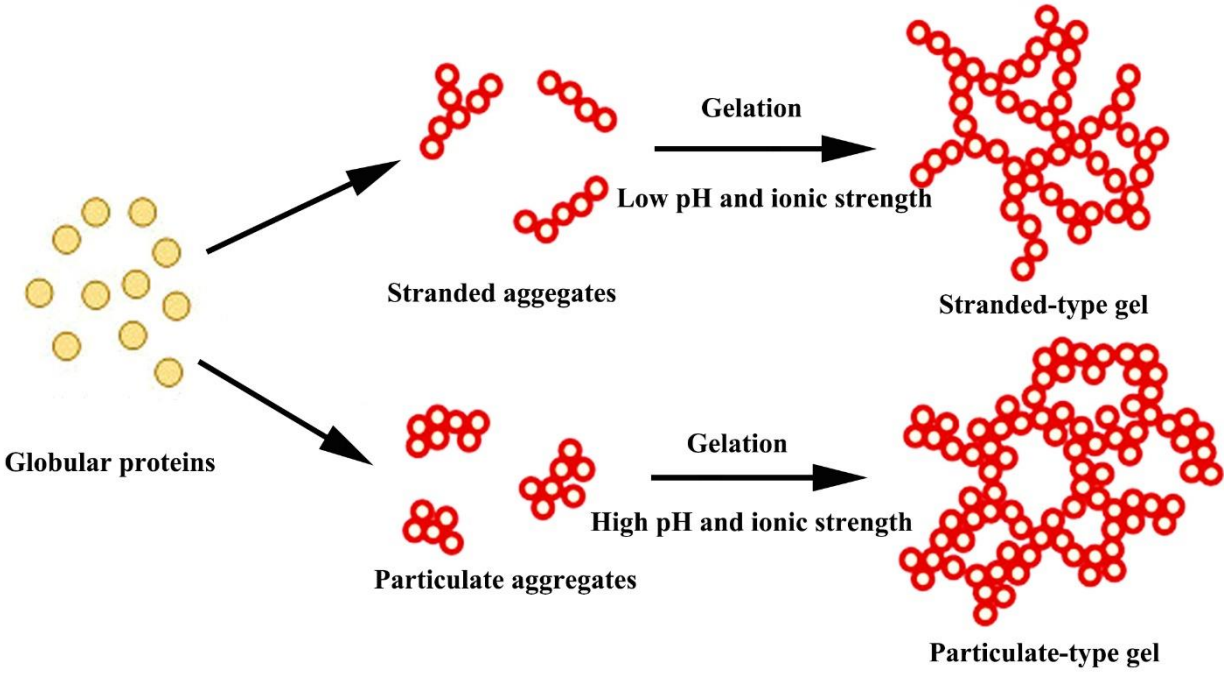

Figure 2.3 Schematic of stranded and particulate gels formed by globular proteins. The circles with or without thick red borders represent the native or denatured soy proteins, respectively. Modification of sketch by Peng et al. [39].

2.1.2.2 Interfacial properties

Proteins are commonly used as emulsifiers due to their surface-activity properties. During emulsification, protein molecules adsorb at the newly-created interfaces by diffusion and undergo a structural rearrangement in order to optimize their conformation to pack inside the adsorbed layer (**Figure 2.4**). Smaller protein molecules are expected to be more effective since they diffuse to the interface at a faster rate. Solvent conditions like pH or ionic strength also affect the adsorption and emulsion stability due to their effects on the net charges and conformations of protein molecules. It has been shown that increasing the exposed hydrophobic segments on a protein reduces its kinetic barrier [40] for adsorption while increasing the net charge increases the kinetic barrier [41].

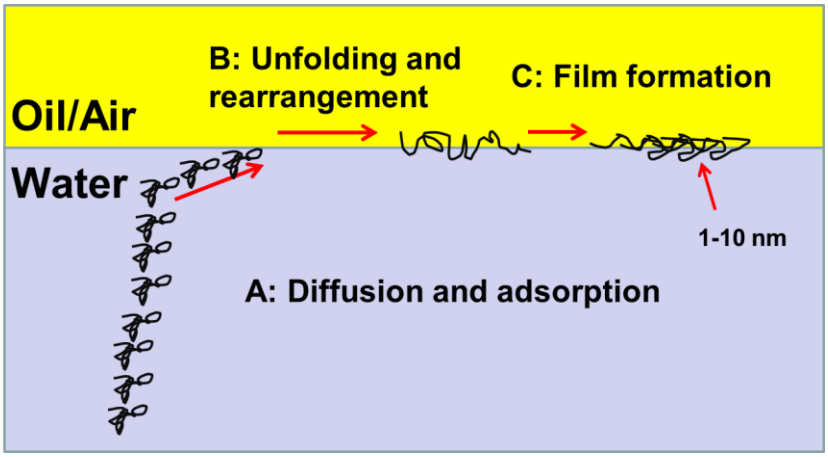

Figure 2.4 Overview of the different steps in the formation of an adsorbed protein layer: A) diffusion and adsorption protein molecules to the interface; B) unfolding and rearrangement of protein molecules at interface; C) film formation at interface.

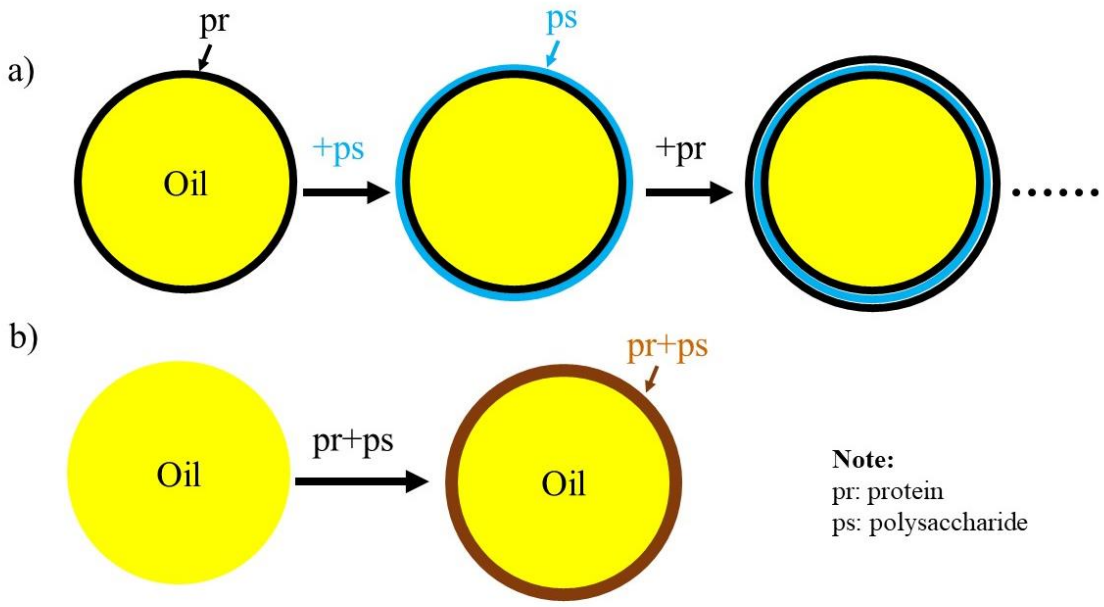

Figure 2.5 Illustration of two alternative procedures for stabilization of oil droplets by protein–polysaccharide complexes. A) layer-by-layer procedure, with polysaccharide (ps) added after emulsification with protein (pr); (B) premixing procedure, with both biopolymers present together during emulsification.

Table 2.3 Published studies on emulsifying properties of some protein/polysaccharide complexes

	$Protein_1$	$Polysaccharide_1$	$Polysaccharide_2$ or $protein_2$	Experimental conditions (pH; incorporation order)
Complexes	WPI	Chitosan	-	pH 5.5; pr_1/ps_1 premixed [13]
		Pectin	-	pH 2-8; pr_1/ps_1 premixed [14]
	β-lg	Gum Arabic	-	pH 4.2; pr_1/ps_1 premixed [42]
Bi-layer	β-lg	Pectin	-	pH 4-7; pr_1 then ps_1 [16]
		Alginate	-	pH 3-7; pr_1 then ps_1 [43]
	WPI	Xanthan gum	-	pH 7; pr_1 then ps_1 [44]
Tri-layer	β-lg	Pectin	Chitosan	pH 4; pr_1, ps_1 then ps_2 [16]
		Chitosan	Pectin	pH 3-7; pr_1, ps_1 then ps_2 [15]
		Chitosan	Alginate	pH 3-7; pr_1, ps_1 then ps_2 [15]

Note: pr: protein; ps: polysaccharide; WPI: whey protein isolate; β-lg: β-lactoglobulin; 1 and 2 indicates the different types of proteins or polysaccharides.

Protein molecules associate with neighboring molecules after adsorbing at an interface, resulting in the formation of a viscoelastic interfacial layer. The interfacial layer stabilizes oil droplets against flocculation and coalescence through electrostatic repulsion (at a pH far from the pI) and steric effects (at a pH close to the pI). However, the adsorbed protein layer is too thin to provide steric stabilization in many cases. In order to overcome this, protein/polysaccharide complexes are of great interest since they combine the advantages of proteins (*e.g.* surface-activity, fast adsorption) and polysaccharide (*e.g.* steric repulsion). There are two alternative procedures to prepare emulsions using protein/polysaccharide complexes (**Figure 2.5**) and related work has been reported in **Table 2.3**. One approach is to prepare emulsions initially with a protein, followed by the addition of a polysaccharide which can interact with the adsorbed proteins, forming a bilayer [15,16] . Larger charge and thickness of the bilayer increase the stability of oil droplets against

flocculation and coalescence. Another procedure is premixing proteins and polysaccharides to form protein/polysaccharide complexes, then use the complex as the emulsifier [13,14].

2.1.3 Gelatin

Gelatin is one of the most well-known gelling proteins. It has numerous applications in many areas, such as confectionery, pharmaceutical/medical, and cosmetic products. The global gelatin market is expected to reach 4.08 billion USD by 2024, growing at a compound annual growth rate (CAGR) of 5.3% from 2016 to 2024, according to a report by Grand View Rearch, Inc [45]. It is a denatured protein derived from collagen by either acid (type A) or alkaline (type B) treatment [46]. The two types of gelatin differ in amino acid composition. Type A gelatins have similar amino acid composition to collagen, whereas type B gelatins do not contain glutamine and asparagine due to the alkaline processing [25](**Table 2.4**). Therefore, gelatin A has an identical isoelectric point as collagen in a pH range of 7-9.4, while gelatin B has a lower pI in a range of 4.8-5.4 [46]. Typically, the gelatin primary structure consists of repeating sequences of glycine-X-Y, where proline occurs in the X and Y positions and hydroproline exclusively in the Y position [46]. Glycine, as the smallest amino acid, allows the three peptides units to come closely together, whereas proline and hydroproline enhance rigidity due to their pyrrolidine rings and stabilize gelatin structure by hydrogen bonding [47].

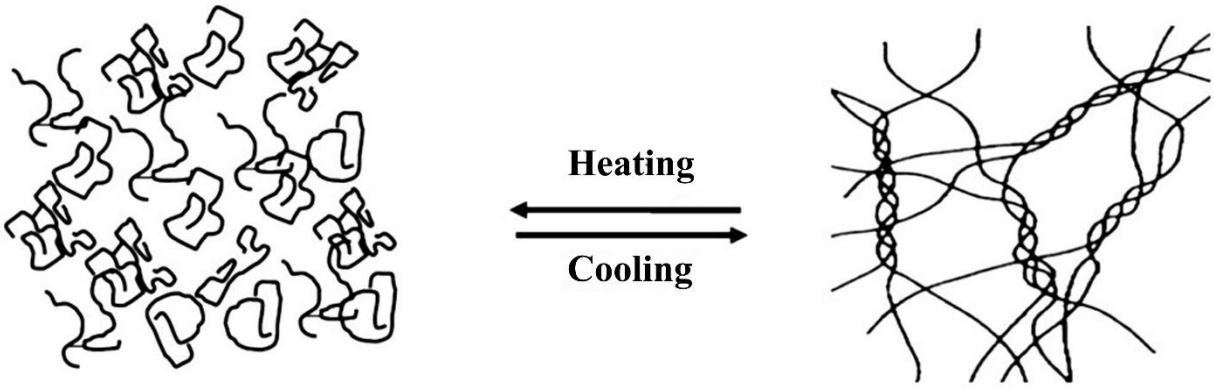

Figure 2.6 The thermoreversible gelation process for gelatin [25].

Table 2.4: Amino acid composition of collagen and gelatin per 1000 residues [25]

Amino acid	Type I collagen (bovine)	Type A gelatin*	Type B gelatin**
Alanine	114	112	117
Arginine	51	49	48
Aspargine	16	16	-
Aspartic acid	29	29	46
Glutamine	48	48	-
Glutamic acid	25	25	72
Glycine	332	330	335
Histidine	4	4	4
4-Hydroxyproline	104	91	93
ε-Hydroxylysine	5	6	4
Isoleucine	11	10	11
Leucine	24	24	24
Lysine	28	27	28
Methionine	6	4	4
Phenylalanine	13	14	14
Proline	115	132	124
Serine	35	35	33
Threonine	17	18	18
Tyrosine	4	3	1
Valine	22	26	22

* Type A gelatin: acid-pretreated pigskin gelatin.

**Type B gelatin: alkali-pretreated bone gelatin

Like collagen, gelatin also has a helix-to-coil transition temperature, which is located at about 15-40 ^{o}C depending on gelatin sources (*e.g.* fish gelatin: ~15 ^{o}C and bovine ~40 ^{o}C). Above this temperature, gelatin molecules exist in solution as random coils, and once cooling down below this temperature, the coils start to form a triple helices structure driven by hydrogen bonding (**Figure 2.6**), which can induce chain associations and a thermally reversible three-dimensional network [47,48].

Gelatin gel formation is proposed as a two-step process: the formation of locally ordered regions by partial random return (renaturation) of gelatin to collagen-like helices, followed by a continuous

fibrillar three-dimensional network of fringed micelles due to nonspecific bond formation between the more ordered segments of the chains [46,47]. The possible bonds involved during physical crosslinking are hydrogen bonding, hydrophobic and electrostatic forces, which can be disrupted upon heating. The gel state rarely reaches an equilibrium since the junctions are continuously reorganizing and new junctions are slowly formed with time [25,49]. Rheology and optical rotation measurements tests reveal that the gel strength is determined by the helix concentration [50,51]. Industrially, the Bloom index (also called Bloom value, Bloom number or Bloom strength), rather than the storage modulus, is used to characterize the gel strength. It is defined as the weight in grams that is required for a 12.7 mm diameter flat bottomed cylindrical plunger to depress the surface of a 6.67 % (w/w) gelatin gel (matured at 10 ^{o}C for 16-18 h) to a depth of 4 mm. A linear relationship can be found between the Bloom index and storage modulus.

2.2 Polysaccharides

Polysaccharides are another family of very important biopolymers widely used in different areas such as food, cosmetics, pharmaceutical, medicine, packaging, coatings, etc. [52]. Polysaccharides are long chains of carbohydrate polymers and are composed of at least 20 repeating monosaccharide residues linked by O-glycosidic linkages [52,53]. The number of monosaccharide units in a polysaccharide is referred to as the degree of polymerization (DP). Some common polysaccharides are listed in **Table 2.5**.

Table 2.5: Molecular characteristics food-grade polysaccharides [27]

Name	Main structure type	Major monomer	Charge
Chitosan	Linear	2-Amino-2-deoxy-β-D-	Positive
Xanthan gum	Branched	Glucose, mannose	Negative
Carrageenan	Linear/helical	Sulfated galactan	Negative
Gum Arabic	Branched coil domains on	Galactose	Negative
Pectin	Highly branched coil	Glucuronate (backbone)	Negative
Alginate	Linear	β-D-Mannuronic Acid, Guluronic acid	Negative
Starch	Linear/branched	Glucose	Neutral
Cellulose	Linear	Glucose	Neutral

Unlike proteins and nucleic acids, polysaccharides are both poly-disperse and poly-molecular. A particular polysaccharide possesses a range of degree of polymerizations (DPs) and molecular weights rather than a defined monomeric unit or a defined molecular weight. In addition, most polysaccharides are chemically heterogeneous [54]. They are poly-molecular in the sense that individual molecules within a polysaccharide type may differ from one to another with respect to monosaccharide sequence, composition, linkage type, branching frequency, etc. [54]

Table 2.6: Different structural levels of polysaccharides

Structural level	Description
Primary structure	Monosaccharide composition, sequence, linkage types
Secondary structure	Helix, ribbon and random coil
Tertiary structure	Double helices
Quaternary structure	Aggregates of secondary or tertiary structure

Analogous to proteins, the polysaccharide structure can also be defined on several different organization levels (**Table 2.6**). The primary structure of a polysaccharide refers to the monosaccharide composition, sequence, linkage types, and it determines the development of secondary, tertiary and quaternary structures. Glycosidic linkage type is believed to exert a greater influence on molecular conformation than the monosaccharide type [55], as illustrated by the comparison of three polysaccharides, cellulose, amylose and dextran, which are all linear chains of polyglucose, differing only in the nature of their glycosidic linkages. The secondary structure refers to the helix, ribbon and random coil conformations, and the arrangements such as double helices and aggregates of helices and ribbons can be regarded as tertiary or higher levels of structure [54,56]. Most polysaccharide secondary and tertiary structures are stabilized by intra- and intermolecular hydrogen bonding. Therefore, temperature influences the adoption of an ordered secondary and tertiary structure. A polysaccharide in an ordered conformation typically undergoes an order-to-disorder (helix-to-coil) transition upon increasing temperature, which disrupts the hydrogen bonds that stabilize the ordered conformation (**Figure 2.7**). When cooling down below

the transition temperature, polysaccharide molecules regain their secondary and/or tertiary structure. The alignment and aggregation of secondary- and/or tertiary ordered polysaccharide structures result in the quaternary structure, which is usually stabilized by non-covalent interactions such as electrostatic forces, hydrogen bonding and hydrophobic interactions. The intermolecular associations in the quaternary structure level leads to the development of gels or crystalline structures.

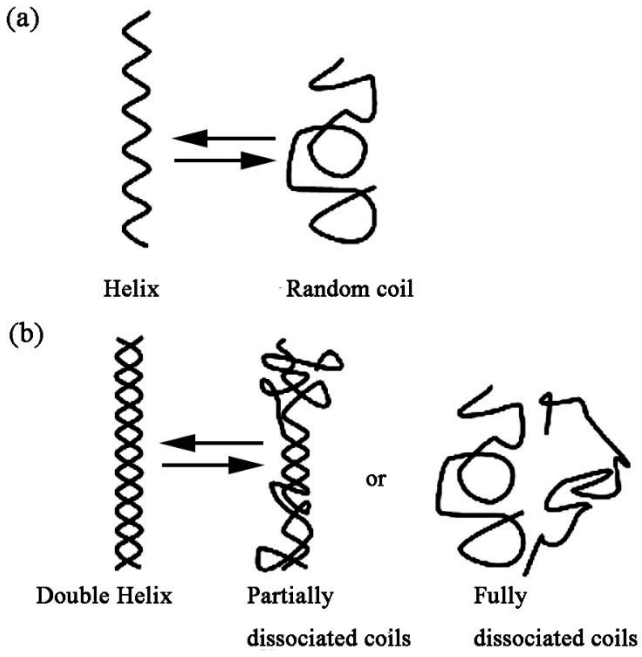

Figure 2.7 Thermally reversible helix-to-coil (order-to-disorder) conformational transition of polysaccharides for a) single- and b) double-helical structures [54].

Polysaccharides can be neutral (starch, cellulose), negatively charged (xanthan gum, alginate, carrageenan) or positively charged (chitosan) depending on the ionic groups along the chain background and solution conditions. The electrical charge magnitude is related to the pHs. Anionic polysaccharides are neutral at pHs sufficiently below their pKa but negative above, whereas cationic polysaccharides are neutral at pHs sufficiently above their pKa but positive below [27]. The electrical charge of polysaccharides alters their solubilization in water and interactions with other ionic species, such as salt and other charged biopolymers. The alteration of electrical charges induces changes in the secondary and/or tertiary structures of polysaccharides, which in turn results in different functional properties.

2.2.1 Polysaccharide functional properties

The monosaccharide composition, sequence, linkage types, chain shapes and degree of polymerization dictate the molecular properties, such as molecular weight, degree of branching, flexibility and electrical charges, which in turn determine the functional properties, such as solubility, gelation, thickening and interfacial properties, water holding capacity and digestibility [27,52].

The polysaccharide gel formation depends on polysaccharide intrinsic characteristics, such as flexibility, charge density, molecular weight, monosaccharide composition, etc., and extrinsic factors, such as ionic strength, pH and temperature. Variations of extrinsic factors may lead to a disorder-order conformation change, and the intermolecular associations between ordered domains result in the formation of physical links and then subsequently a network [53]. The driving forces for crosslink formation vary between polysaccharides. For example, agar gelation is driven by hydrogen bonding, whereas for alginate and low methoxyl pectin, gelation is induced by ionic interactions [53]. Some polysaccharides cannot form gels due to conformational restriction or repulsive conditions. For example, λ-carrageenan is a non-gelling polysaccharide mainly due to the repulsive conditions caused by its high density of sulfate groups [57]. Mixing two or more polysaccharides is another way to produce gels. For example, thermally reversible gels are formed when mixing xanthan gum with galactomannan, carob gum or tara gum [58].

2.2.1 Xanthan gum

Xanthan gum (XG) (M_w ~ 2-6 x 10^6 kDa) is a microbial polysaccharide produced by *Xanthomonas campestris* by a distinct fermentation process. It has extensive applications, such as thickener, stabilizer, cleaner, etc., in areas such as food, cosmetics, pharmaceutical industries and some water-based systems [59]. The XG market is expected to reach a value of 452.8 million USD by 2022, at a compound annual growth rate (CAGR) of 3.25% from 2016 [60]. XG has a cellulosic backbone with trisaccharide side chains (**Figure 2.8**). The trisaccharide side chain contains two mannose units separated by a glucuronic acid unit. Approximately half of the terminal mannose units are linked to a pyruvate group at C4- and C6-positions; whereas the non-terminal residue is usually acetylated at C6. The carboxyl groups on the side chains make XG an anionic polysaccharide. X-

ray diffraction studies indicate that oriented XG has a right-handed, fivefold helix with a pitch of 4.7 nm and side chains being aligned with the backbone [61,62].

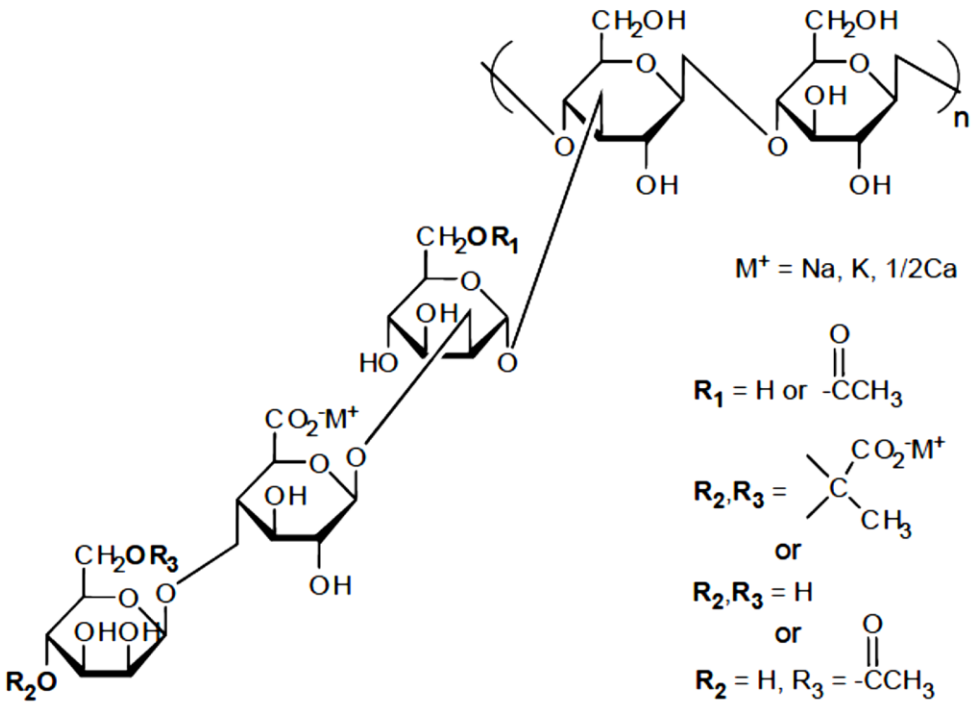

Figure 2.8 Molecular structure of xanthan gum [57].

XG molecules in solution undergo a disorder-to-order transition (coil-to-helix) depending on salinity and temperature (**Figure 2.9**) [57,59,63,64]. In the absence of salt or at intermediate salt levels, XG molecules are partially ordered due to the electrostatic repulsion between the charged carboxylic groups on the side chains [64-66]. Adding salt causes a disorder-to-order transition due to charge screening effects, in which the backbone takes on a helical conformation and the charged side chains collapse down onto the backbone and stabilize the ordered conformation [64]. The ordered structures allow the molecules to be easily aligned and associate with each other. Heating a XG solution above a certain temperature results in the "melting" of the ordered structures; the structures return to their original state upon cooling [67,68]. This temperature is defined as the helix-to-coil transition temperature (usually at 50-55 ^{o}C). Salt addition pushes the helix-to-coil transition temperature to a much higher value by promoting helix formation [64].

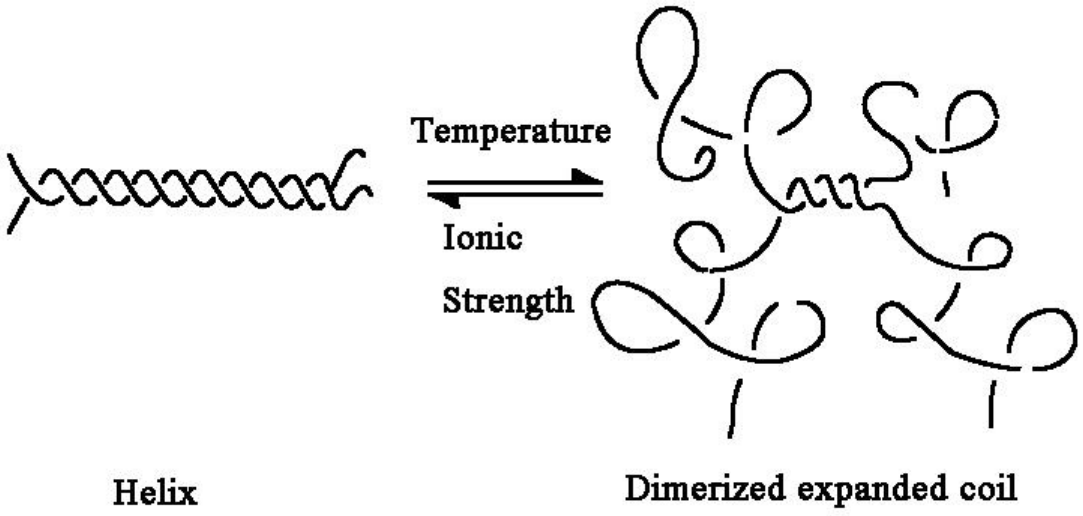

Figure 2.9 Schematic model for the XG order–disorder transition [57].

XG is commonly regarded as a non-gelling polysaccharide [61,69]. It can however form a gel in the presence of trivalent ions or when mixed with other polysaccharides [57,70,71], or even proteins [24]. Weakly associated XG microgels (XG aggregates) can be formed by side-by-side associations between the ordered regions, which gives a tenuous network structure and endows XG dispersions with a "gel-like" behavior [57,68,72]. The presence of XG microgels accounts for many unusual features, such as a highly shearing-thinning behavior. Under shear, the weak links between the microgels break, leading to the deformation of microgels, chain disentanglement and alignment, whereas the network re-establishes itself upon removal of the applied shear [66]. This rheological feature enhances sensory qualities (mouth feel, flavor release) in food products, and makes XG easy to mix, pump and pour during processing and/or actual use despite its high molecular weight [59].

2.2.2 Chitosan

Chitin is the second most abundant natural biopolymer derived from exoskeletons of crustaceans and also from cell walls of fungi and insects [73,74]. Alkaline deacetylation of chitin results in chitosan (CHI). Chitin and CHI have excellent properties like biodegradability and biocompatibility, as well as low toxicity. As a result, they have been of great interest due to their various applications, such as chelator, drug release, texture controlling agent, dietary fiber, etc, in food technology, biomedical, and pharmaceutical industries [75-77]. The global CHI market is

expected to reach USD$17.84 billion by 2025, according to a report by Grand View Research, Inc [78]. Solubility in dilute aqueous acid is used as a criterion to distinguishing chitin and CHI, since chitin is insoluble, while CHI can form viscous solutions. Another more quantitative method is to use the degree of acetylation (DA) or deacetylation (DDA). Generally, the DDA of chitosan is ≥ 60 % [79]. The DDA and degree of polymerization (DP) are two important parameters dictating the physical, chemical and biological properties of CHI, such as the ability to chelate metal ions, its immunoadjuvant activity, the tensile strength of films, etc. [80] The DDA also influences the CHI solubility and solution properties, such as charge and viscosity [57,81]. The apparent charge density increases as DDA increases (i.e. the number of NH_2 groups increases at the expense of acetylamine groups). The protonated amine groups make CHI to expand in solution at low ionic strength, thus increasing excluded volume by electrostatic repulsions, whereas acetylated units increase the rigidity of chitosan [82]. Molecular weight is another parameter that affects the properties of chitosan, such as solubility and viscosity. The relation between viscosity of chitosan in solution and molecular weight can be described by the Mark-Houwink equation ($[\eta] = KM^{\alpha}$; where $[\eta]$ is the intrinsic viscosity and M is the viscosity average of the molecular weight, K and α are constants. Decreasing the molecular weight of chitosan can thus decrease its viscosity and improve its solubility.

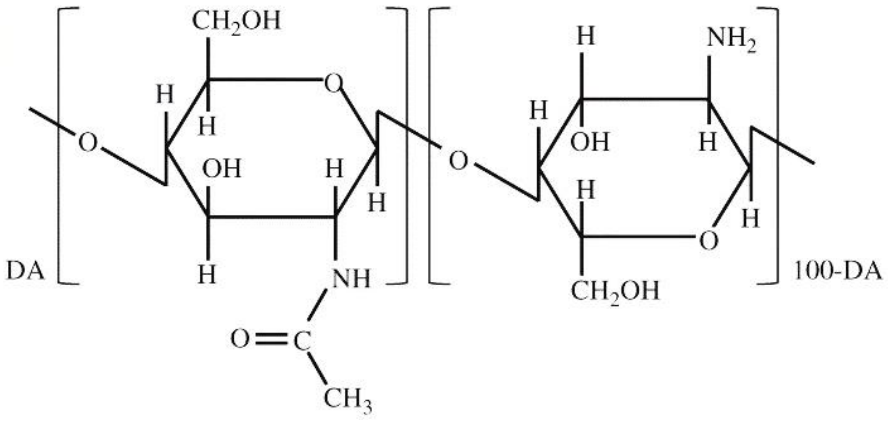

Figure 2.10 Chemical structure of chitin and chitosan [82].

CHI is composed of randomly distributed deacetylated units (β-(1-4)-linked D-glucosamine, or D-unit) and acetylated units (N-acetyl-D-glucosamine, or A-unit), as shown in **Figure 2.10**. It is a cationic polysaccharide with a pKa around 6.3-6.5, and that explains why it is only soluble in acidic

solutions. The amino groups of D-units allow chemical modification of chitosan by covalent attachment of various chemical groups, according to the targeted applications [81].

There are several ways to make CHI to form a gel. One way is to re-acetylate CHI with acetic anhydride in hydroalcoholic media, which then gives rise to a chitin gel through hydrophobic interactions [83]. Another way is to use β-glycerol phosphate (β-GP) combined with temperature [84-87]. The gel mechanism suggests that heat-stimulated proton transfer from CHI to β-GP reduces electrostatic repulsion, thus leading to CHI aggregation [88]. Other ionic crosslinker and complexing agents can also be used to gelify CHI, such as anionic molecules like phosphates and citrates [89] and metal ions like molybdate [90]. CHI gels can even be obtained without any additives by exposing CHI to well-defined conditions (*e.g.* using water-alcohol mixed solvent + heating) [91,92]. Generally, soft and easily degraded gels are formed from highly acetylated chitosan while more solid gels are obtained from highly deacetylated chitosan [93].

2.3 Protein-polysaccharide interactions

When mixing two biopolymers together in aqueous environment, two different types of interactions can occur, mainly depending on pH and ionic strength (**Figure 2.11**): segregative phase separation (thermodynamic incompatibility) and associative phase separation (thermodynamic compatibility) [4,5].

Segregative phase separation occurs when one or both biopolymers are uncharged or both biopolymers have similar charges. A one-phase solution is formed at sufficiently low biopolymer concentrations, whereas a two-phase solution containing protein-rich and polysaccharide-rich phases is formed once the biopolymer concentration exceeds a certain level [24,27]. In contrast, associative phase separation is induced by relatively strong attractions between the two biopolymers. It has been established that such interactions are primarily electrostatic in nature and will be inhibited at higher ionic concentration. The resulting two-phase system consists of solvent-rich and biopolymer-rich phases.

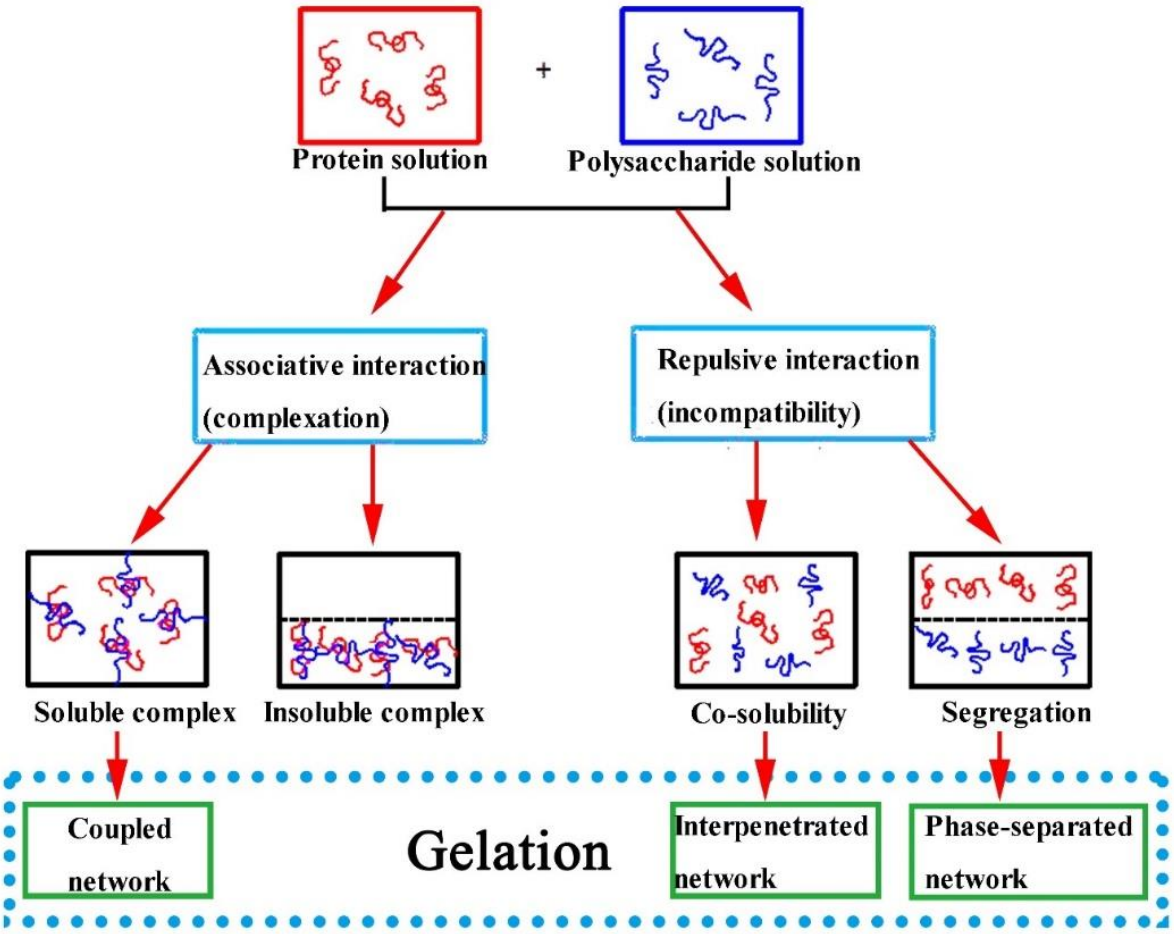

Figure 2.11 Possible interactions for proteins/polysaccharides mixtures and consequences in the formation of mixed gels. Based on the work by Ghosh et al. [17], and Stokes [53].

The biopolymer-rich phase may either form coacervates or precipitates (insoluble complexes) (**Figure 2.12**). There is some confusion in the scientific literature where in some instances complexes are referred to as "coacervates", since the two are related to phase separation. In fact, coacervates are obtained by a liquid-liquid phase separation, whereas precipitates are formed by a solid-liquid phase separation. The two structures follow the same initial path, i.e. the two biopolymers form primary soluble complexes at a critical pH (pHc), followed by the formation of interpolymer complexes when the pH is decreased to a second critical pH (pHφ), and finally bulk phase separation [5]. However, it is still not clearly understood why some protein/polysaccharide systems result in precipitates whereas others lead to coacervates, but it may be related to the flexibility and charge density of the molecules [5]. Proteins or polysaccharides with low charge density and/or very flexible backbone tend to form coacervates, *e.g.* gelatin, acacia gum, dextran

sulfate and some specific varieties of pectin; whereas the ones with high charge density with a stiff structure are prone to form complexes, *e.g.* ι- and κ-carrageenan, sodium alginate, gellan and xanthan gum. In addition, higher molecular binding affinity also favors the formation of complexes. Other weak interactions, such as hydrogen bonding and hydrophobic interactions, may also affect the complexation between proteins and polysaccharides [6]. Note that complexation is still possible between proteins and polysaccharides when they carry the same net charges at a pH near the isoelectric point of the protein because of the presence of the oppositely charged patches on the protein [6,94].

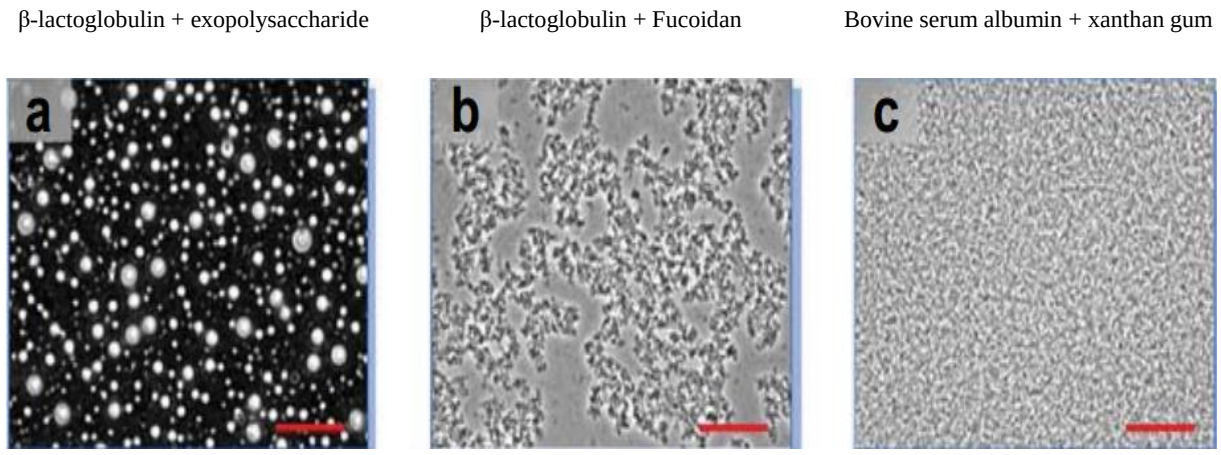

Figure 2.12 Different structures formed by the electrostatic complexation of proteins and polysaccharides: (a) coacervates; (b) insoluble complexes; and (c) electrostatic gel. The scale bar is 40 μm [95].

2.4 Protein/polysaccharide gels

Protein/polysaccharide mixed gels have been investigated for many years, and a summary of publications is shown in **Table 2.7**. Proteins and polysaccharides can form three different types of gels due to thermodynamic compatibility and incompatibility: interpenetrating, coupled and phase separated networks [53], as shown in **Figure 2.13**.

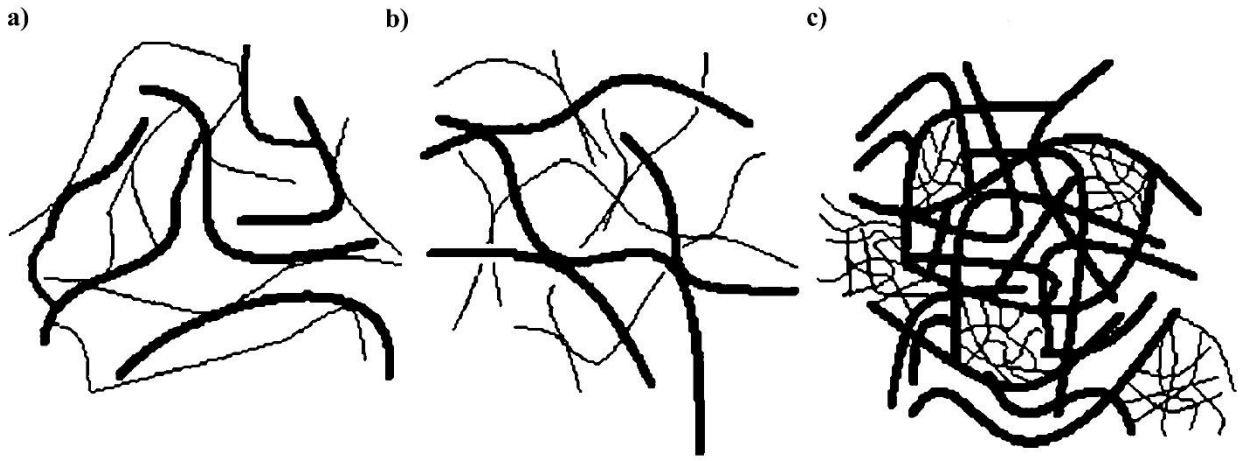

Figure 2.13 Network structures: (a) coupled network, (b) interpenetrating network, (c) phase-separated network [96].

2.4.1 Interpenetrating networks

Interpenetrating networks are the result of two continuous independent networks formed by the protein and polysaccharide that interlace into one another. Both biopolymer contents in solution need to exceed the critical gelling concentration. Bovine serum albumin and LM-pectin can form interpenetrating networks in the presence of calcium ions [97]. Another example is calcium-alginate and gelatin mixtures, but only if gelatin helices are formed inside a pre-existing calcium-alginate gel [98].

2.4.2 Phase-separated networks

Phase-separated networks are obtained under segregative conditions when proteins and polysaccharides tend to demix due to repulsion and/or varying affinity towards the solvent [99]. The final structure is determined by the relative rates of phase separation and gelation, the balance of which can be tuned by ionic strength, pH and heating/cooling kinetics [4,99]. Low heating rates extend the time to denature proteins, which enhances phase separation compared to faster heating rates; adjusting the pH far away from the pI of proteins increases the electrostatic repulsion between proteins and polysaccharides, leading to more extended phase separation [4]. Phase separation is also affected by the charge density of polysaccharides [100].

Phase separation concentrates both components by reducing the water availability for each component [1,98,101] and thus allows the biopolymers to gel at lower concentration than that

usually needed. It is thus used to explain the synergistic gelation properties of protein/polysaccharide mixtures, such as WPI/XG [69], WP/κ-carrageen [102], and WP/pectin [103].

2.4.3 Coupled gel networks

Coupled gel networks are formed through electrostatic associative conditions under specific conditions (slow acidification, quiescent conditions [104]. The gelling process follows an initial similar path to that of complexes and coacervates, but then junctions are formed due to the interactions between soluble complexes, which result in a network structure instead of coarsening and phase separation [104]. Such gels can be formed under conditions where neither polymer forms gels alone. Coupled gel networks can be formed by many protein/polysaccharide systems (caseinate, bovine serum albumin, lysozyme with xanthan gum, gellan gum, λ-carrageenan, etc.) [19].

Table 2.7: Published studies on protein/polysaccharide mixed gels

Model systems	Experimental conditions
β-lactoglobulin/κ-carrageenan	1. c_{pr} = 0.5, 5, 10 %, c_{ps} = 1 %, pH = 7.0 [105] 2. c_{pr} = 10 %, c_{ps} = 1 %, pH = 5.0, 6.0, 7.0 [106] 3. c_{pr} = 5 %, c_{ps} = 1 %, pH = 5, presheared time: 15s, 30s and 300s [107]
β-lactoglobulin /Xanthan gum	1. Ratio pr/ps = 2, 5 and 10 with total concentration = 0.1 %, 0.2 % and 0.3 %, pH = 4.4 [108] 2. Ratio pr/ps = 2, 5. 15 and 20, total concentration = 0.1 %, pH ≈ 4.5 [109] 3. Ratio pr/ps = 2, 5. 10 and 20, 1) total concentration = 0.3 %, 2) c_{ps} = 0.03 %, 3) c_{pr} = 0.3 %, pH = 4.4 [24] 4. c_{pr} = 3.4 – 16.6 %, c_{ps} = 0.9 %, pH = 6.85-6.93 [110]
β-lactoglobulin/Low- and high methoxyl pectin, sodium alginate	c_{pr} = 12 %, c_{ps} = 0.1-1.0 %, pH = 7.0 [111]
Gelatin B/κ-carrageenan	1. c_{pr} = 1-2%, c_{ps} = 0.05-1 % [112] 2. c_{pr} = 1.0 %, c_{ps} = 0.001-0.5%, pH = 5.2-5.6 [113]

Table 2.7 continued: Published studies on protein/polysaccharide mixed gels

Gelatin B/konjac glucomannan	c_{pr} = 4 %, c_{ps} = 0.1-0.5 % [114]
Bovine serum albumin/Low-methoxyl pectin	c_{pr} = 2, 4 and 8 %, c_{ps} = 0.21, 0.43 and 0.85%, pH = 6.8 0.1 M NaCl, with or without CaCl2 [97]
Whey protein isolate/pectin	c_{pr} = 5 %, c_{ps} = 0.05-0.5 %, pH = 4.7 [115]
Whey protein isolate/Xanthan gum	1. c_{pr} = 12.5 %, c_{ps} = 0.01, 0.03 and 0.06 %, pH = 5.5, 6.0, 6.5, 0.1 and 0.5 M NaCl [69] 2. c_{pr} = 14 %, c_{ps} = 0.05-0.5 %, pH = 5.5 [101] 3. c_{pr} = 8.5 %, c_{ps} = 0-0.2 %, pH = 7.0 [116]
Whey protein isolate/Low-methoxyl pectin	1. c_{pr} = 8 %, c_{ps} = 0.1-1.5 %, pH = 6.0, 5-10 mM $CaCl_2$ [103] 2. c_{pr} = 0.5, 0.75 and 1.0 %, c_{ps} = 0.5, 0.75 and 1.0 %, pH = 2.0, 2.5, 3.5 and 5.5 [117]
Whey protein isolate/κ-carrageenan	1. c_{pr} = 13 %, c_{ps} = 0-0.6 %, pH = 7.0, 50, 100 and 250 mM NaCl [118] 2. c_{pr} = 5 %, c_{ps} = 0-0.3 %, 100 mM NaCl, pH = 5.5, 6.0 and 6.5 [119]
Gelatin A/ι-carrageenan	c_{pr} = 8 %, c_{ps} = 2 %, pH = 7, 0.2 M NaCl [120]
Gelatin A/Alginate	1. c_{pr} = 1-2 %, c_{ps} = 1-1.5 %, CaEDTA 180 mM, GDL 180 mM [121] 2. c_{pr} = 1.5 and 5 %, c_{ps} = 1 %, with CaEDTA and Alginate Lyase [98]

Note: c_{pr}: protein concentration; c_{ps}: polysaccharide concentration

The gelation mechanism of β-lactoglubulin/XG (the most commonly studied system) is composed of three stages when using glucono-δ-lactone (GDL) as an acidifier, as demonstrated with the help of rheology and confocal laser scanning microscopy (CLSM) [24] (**Figure 2.14**). XG forms a tenuous network in solution by the presence of large-scale molecular assemblies due to side-by-side associations [72] or end-to-end associations [122]. During acidification, soluble complexes are formed by the interaction between positively charged patches on β-lactoglobulin and the carboxyl groups of XG, as pH decreases near the pI of the protein (stage 1). Further decreases in pH lead to more protein aggregates on the XG chains, and lower the charge density of soluble complexes. These complexes then aggregate into interpolymer complexes due to the formation of

junction zones by a possible bridging effect between neighboring proteins (stage 2). The increasing electrostatic associative interactions with decreasing pH finally results in a sol-gel transition (stage 3). The proposed mechanism is limited since it does not take the conformational change of protein and polysaccharide into consideration during the complexation, which could also be a driving force for interpolymer complexes. In addition, the mechanism proposed based on the change of pH, thus cannot explain the gelation phenomenon at a constant pH.

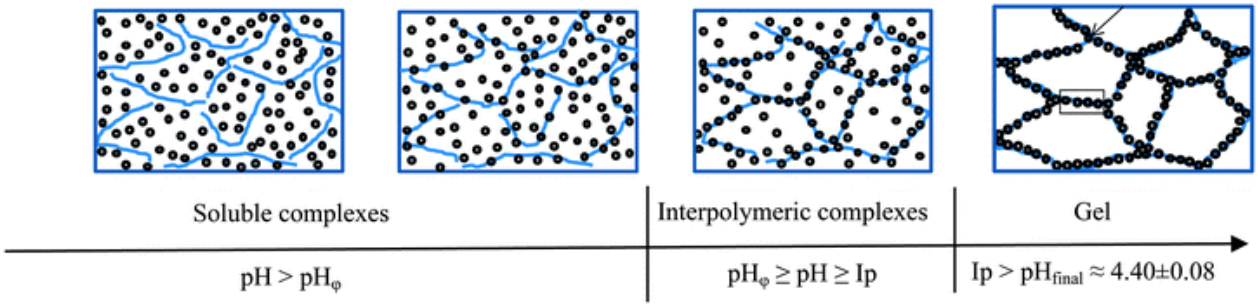

Figure 2.14 Schematic of the interaction and gel formation process between β-lg (circles) and XG (rod shapes); rectangle presents aggregation zones of β-lg on XG chains, arrow presents electrostatic cross-linking zones of XG chains by β-lg [24].

2.5 Factors influencing protein/polysaccharide gels

The dominant forces between proteins and polysaccharides in aqueous solutions are electrostatic forces. Therefore, the properties of protein/polysaccharide gels are affected by environmental factors such as pH, ionic strength and protein to polysaccharide ratio, and the biopolymers intrinsic characteristics, such as molecular conformation and charge density. A delicate charge balance is needed to tune the gelation properties [108].

The gelation properties are related to the conformation and charge density of proteins and polysaccharides. Stronger mixed gels are formed by globular proteins (BSA, β-lg, ovalbumin) than linear proteins (gelatin, caseinate) [19]. Stiff polysaccharides (*e.g.* xanthan gum and gellan gum) are more suitable for gel formation, whereas flexible polysaccharides (e.g. acacia gum) tend to form particulate complexes or coacervates [19]. Lower charge density lowers the biopolymer concentration needed for mixed gel formation. For example a higher concentration of λ-carrageenan is required to form a gel as compared to xanthan gum (XG) when mixed with different

types of proteins [19]. Similarly, a lower bovine serum albumin concentration is needed, compared to β-lactoglobulin, when mixed with polysaccharides [4].

Salt addition screens the charges on both biopolymers, thus it has a strong effect on the gelation properties of protein/polysaccharide mixtures. For example, the gelation rate of β-lactoglobulin/XG mixtures decreases with 20 mM NaCl and the gelation was inhibited with the addition of 50 mM NaCl [104]. The final *G'* value was also lower when salt was added. Pectin, gellan or alginate can form a gel alone in the presence of $CaCl_2$, which makes an interpenetrated network possible, such as bovine serum albumin/LM-pectin [97] and gelatin/alginate [98].

2.6 Rheology of gels

Rheology is widely used to follow sol-to-gel transformation and understand molecular and structural interactions involved in gel formation. Small amplitude oscillatory rheology is capable of determining the viscoelastic response of gels to dynamic shear stress. Such testing allows multiple measurements without sample destruction due to small deformations. Another advantage is that values obtained from different studies are comparable regardless of the instrumentation used.

The two prototypical behavior of a substance under an imposed stress are ideal solid and ideal liquid. The energy transferred to an ideal solid (Hookean) will be completely and reversibly stored, and stress and strain are in phase (**Figure 2.15a**), whereas for an ideal liquid (Newtonian), the transferred energy is fully converted irreversibly into internal energy via dissipative effects – in that case, stress and strain are out of phase by 90^o (**Figure 2.15b**). Gels possess both solid-like (elastic) and a liquid-like (viscous) behaviors simultaneously - stress and strain are not in phase (**Figure 2.15c**). Some important information, such as the relative contributions of the elastic and viscous components, can be obtained by the phase lag.

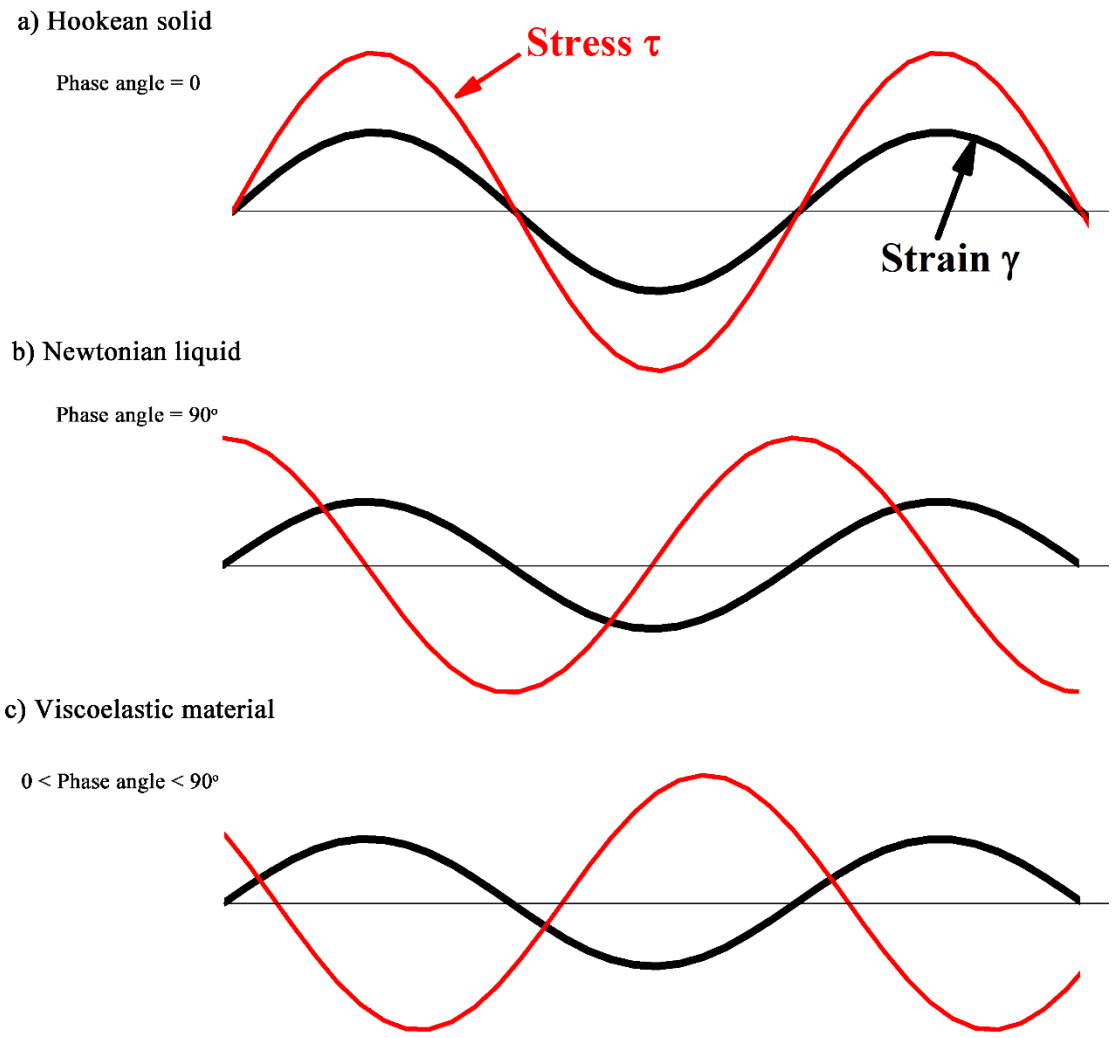

Figure 2.15 Stress versus strain response of a Hookean solid, Newtonian liquid and a viscoelastic material in dynamic oscillatory tests.

Two moduli are used to evaluate the dynamic shear stress response to small amplitude oscillation. The elastic modulus (*G'*) is a measure of the energy reversibly stored during deformation, whereas the viscous modulus (*G"*) is a measure of energy dissipated as heat/internal energy due to sample viscosity. The loss tangent (tan δ) reflects the phase angle between stress and strain and is calculated by *G"*/*G'*. A loss tangent value greater than 1 indicates more liquid-like properties whereas a value lower than 1 means more solid-like properties. For a specific gel, magnitudes of *G'* and *G"* are dependent on measurement frequency, temperature and strain. In the linear regime, the two moduli are independent of strain (or stress).

Four types of dynamic tests are commonly used to investigate the properties of gels [123,124]:

1) **Strain sweep** is used to determine the linear response range of a network to increasing strain (or stress) amplitude and is performed at a constant frequency and temperature. In the linear viscoelastic range, stress changes linearly with strain, producing constant values of *G'* and *G"*.

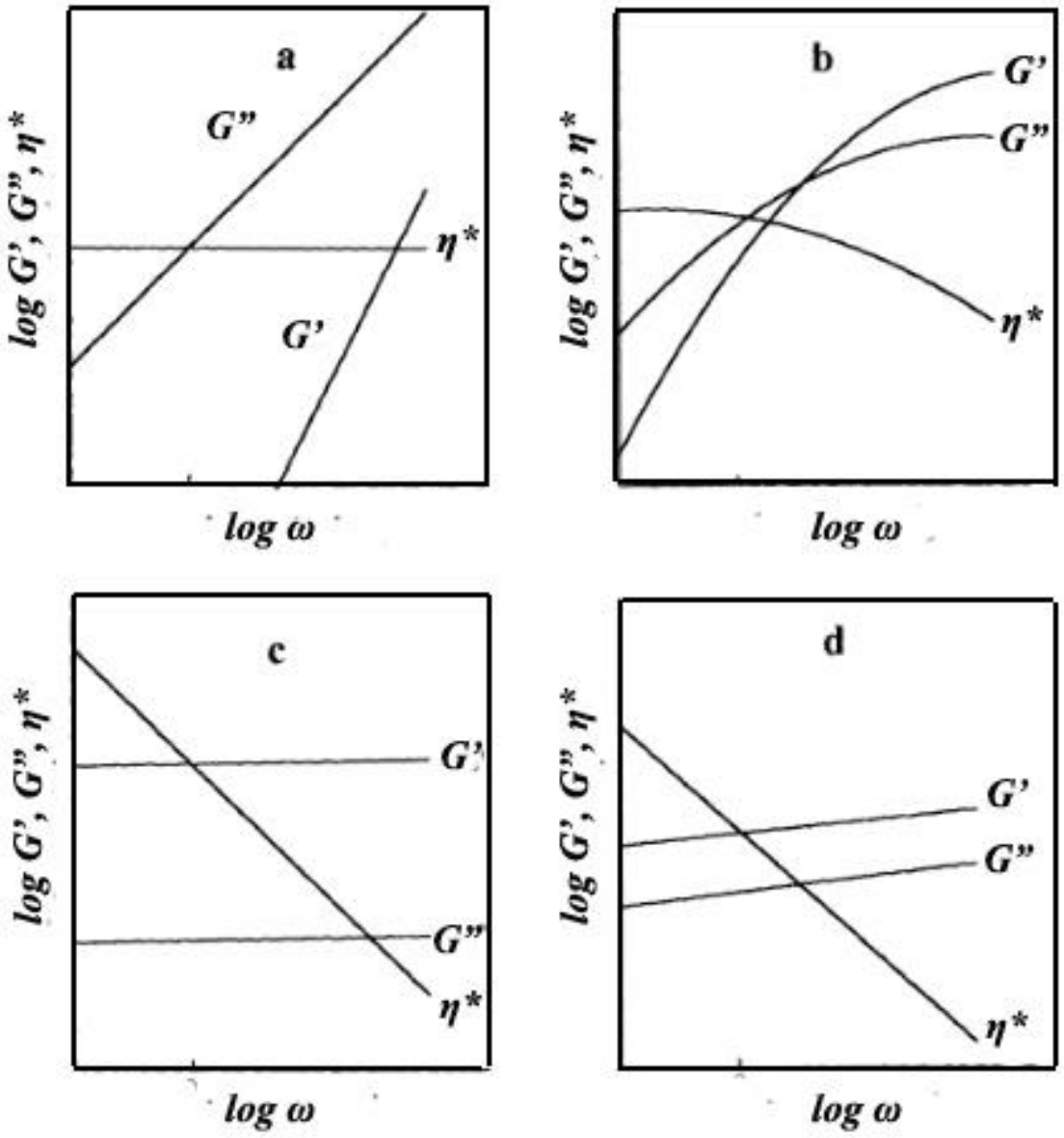

Figure 2.16 The mechanical spectra of four principle categories: a) dilute solution, b) entangled solution, c) strong gel and d) weak gel [125].

2) **Frequency sweep** illustrates the changes of *G'* and *G"* as functions of frequency and at a fixed temperature and strain amplitude. Materials can be divided into four types based on the mechanical

spectra (**Figure 2.16**): diluted solution (*e.g* fruit juice, vegetable soup), entangled solution (*e.g.* semi-dilute chitosan solution), strong gel (*e.g.* jelly) and weak gel (*e.g.* ketchup) [124,125]. Strong gels have higher *G'* than *G''* (~ 10 times) throughout the frequency range, and *G'* and *G''* are almost independent of frequency, whereas for weak gels, there is a dependency on frequency for the two moduli and lower difference between the moduli values.

3) **Temperature sweep** provides useful information for some temperature-related processes, such as the gelation of heated dispersion during cooling, starch gelatinization during heating and protein aggregates and gel formation. *G'* and *G''* are determined as functions of temperature at fixed frequency and strain in such a test.

4) **Time sweep** is used to study the structure development of gels, during which *G'* and *G''* are measured as functions of time at fixed frequency, strain and temperature.

Additional information on the gelation and melting phenomena can be obtained with time and temperature sweeps by calculating the structure development rates (*dG'/dt or dG'/dT*) or structure loss rates (*-dG'/dt or -dG'/dT*).

The **gel point** marks the phase transition of polymer solution from liquid to a soft viscoelastic solid during gelation. One can talk about the gel point as an instant in time or as a specific temperature [127]. The transition is caused by the increasing connectivity in the material. The zero-shear viscosity increases and diverges as the connectivity increases when approaching the gel point. At the gel point, the viscosity diverges to infinity but the equilibrium modulus is still zero. Beyond the gel point, the equilibrium modulus starts to increase [126,128-130] (**Figure 2.17**).

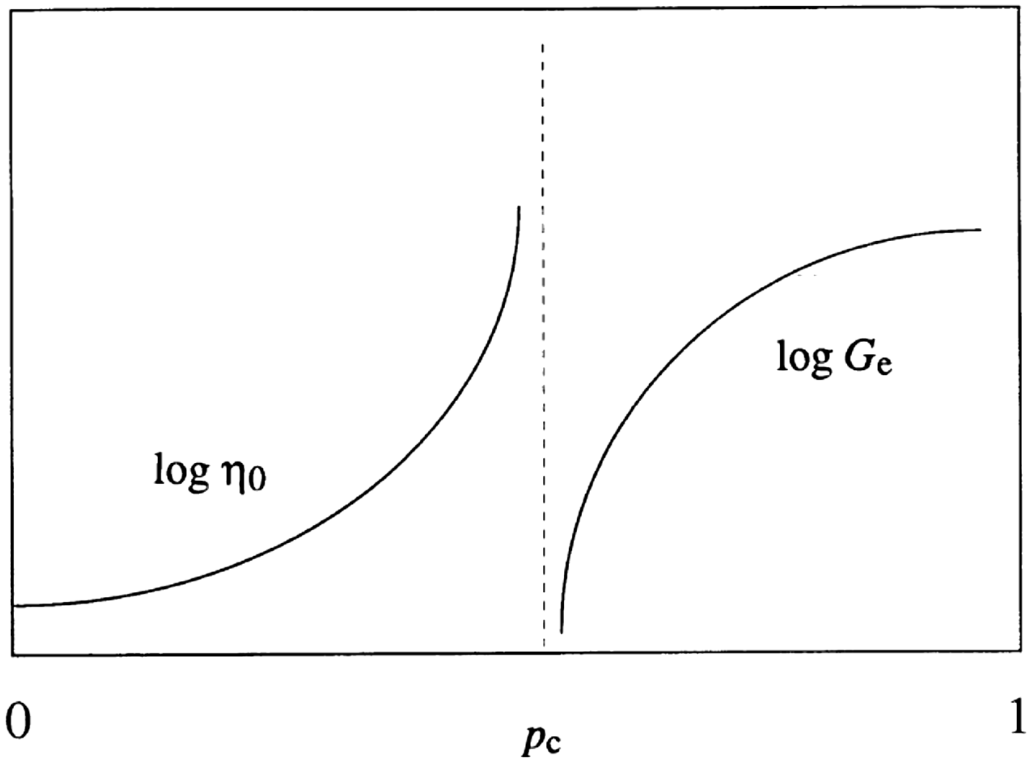

Figure 2.17 Schematic of the divergence of zero-shear viscosity, η_0, and equilibrium modulus, G_e. The extent of crosslinking is marked by *p* [126].

To determine the gel point, *G'* and *G"* are recorded as a function of time. A first approach to identify the gel point is when *G'* and *G"* cross each other at a given frequency. This criterion was applied to the gelation of some biopolymers, such as gelatin [131], β-lactoglobulin [132], κ-carrageenan [133], etc. However, the crossover of *G'* and *G"* was found to be frequency-dependent for both biopolymers [131] and synthetic polymers [130,134]. Since the gel point is an intrinsic property of the material, it should not be dependent on the measurement parameters. Therefore, Chambon and Winter proposed a new criterion [135]: at the gel point, *G'* and *G"* exhibit a power-law dependence on the oscillation frequency and the power-law exponent is the same. Alternately, tan δ is independent of frequency. This method has been applied to evaluate the gelation of many systems, such as starch [136], pectin [137], chitosan [87], etc.

$$G', G'' \propto \omega^n, \qquad \frac{G''}{G'} = \tan\delta = \tan\left(\frac{n\pi}{2}\right)$$

For ideal gels, *G'* equals *G"* at the gel point and $n = 0.5$, whereas for gels containing defects, the phase angle $\delta = n\pi/2$ will be independent of frequency with *n* ranging from 0.5 to 1.

2.7 Summary

As reviewed above, protein and polysaccharide mixed gels have attracted more and more attention from scientists. They have great potential for the protection of micronutrients in food or active molecules in pharmaceutical drugs since they are formed without heat, enzyme or crosslinking agent. There have been extensive investigations on the gelation properties of the aqueous mixtures of proteins and polysaccharides. However, no relevant studies have been found for gelatin and xanthan gum, which are the most well-known gelling agent and thickener, respectively. In addition, most work are based on proteins and negatively-charged polysaccharides. The studies on the gelation properties of proteins and the only naturally-derived cationic polysaccharide, chitosan, are rather limited, despite the abundance of chitosan and its excellent properties, such as good biodegradability, biocompatibility and low toxicity.

In order to provide a guideline to design novel thickeners and/or gelling agents, encapsulation and delivery systems, a fundamental understanding of protein and polysaccharide interactions in solution is necessary. Le and Turgeon [24] proposed a gelation mechanism based on β-lactoglobulin and xanthan gum mixtures. However, it does not take the change of polysaccharide conformation into consideration and it is not ideal to explain the gelation properties of linear proteins and polysaccharides.

CHAPTER 3 RESEARCH OBJECTIVES AND COHERENCE OF ARTICLES

3.1 Research objectives

According to the literature review, the gel properties of gelatin and xanthan gum aqueous mixtures have not been investigated yet, and few reports are found on gelatin/chitosan mixtures. Gelatin is the most well-known gelling agent; xanthan gum is an effective thickener and chitosan is abundant and all have excellent properties like biodegradability and biocompatibility. Therefore, it is of great interest to study the interactions between gelatin and the two polysaccharides to help design low-cost novel thickeners and/or gelling agents, and provide guidelines for the development of new formulations for the food, and cosmetic industries for encapsulation and delivery systems. In addition, some of the proposed mechanisms for protein/polysaccharide mixed gels are based on globular proteins and polysaccharides mixtures. They are not ideal to explain the gelation process of linear proteins and polysaccharide mixtures. Thus, the main objective of this work is **to investigate how polysaccharides and gelatin interact in mixed solutions, and to propose a general mechanism to explain their gelation properties.**

The specific objectives of the current work are:

1) To understand the effect of pH, salt concentration and temperature on the gelation properties of mixed solutions of gelatin B and xanthan gum;

2) To propose a molecular mechanism explaining the gelling properties of gelatin B and xanthan gum mixtures;

3) To assess if the proposed mechanism can be generalized and applied to other linear proteins and polysaccharides systems.

3.2 Presentation of articles and coherence with research objectives

The main scientific findings of this work are presented in the form of three peer-reviewed journal papers in the following three chapters.

Chapter 4 presents the results of the first paper “Synergistic Gelation of Gelatin B with Xanthan Gum” that has been published in *Food Hydrocolloids* (IF 4.747, Q1, Volume 60, October 2016,

Pages 374–383). In this work, we revealed that a synergistic gel can be formed by gelatin B and xanthan gum aqueous mixtures. The effects of pH, ionic strength and temperature on the gelation properties of gelatin B and xanthan gum aqueous mixtures are investigated.

Chapter 5 presents the results of the second paper "A mechanism for the synergistic gelation properties of gelatin B and xanthan gum aqueous mixtures", accepted by *Carbohydrate Polymers* (IF 4.811). In this work, we further studied the effects of gelatin Bloom index, gelatin to polysaccharide ratio, xanthan molecular weight on the gelation properties of gelation B and xanthan gum aqueous mixtures. A gelation mechanism was proposed to explain the synergistic gelation properties. The mechanism is supported by a complementary array of experimental techniques: zeta potential measurements, rheology, confocal microscopy and micro-calorimetry.

Chapter 6 reports the results of the third paper "A Gelation Mechanism for Gelatin/Polysaccharide Aqueous Mixtures", submitted to *Food Hydrocolloids* (August, 2017). In this work, we studied the gelation properties of the mixtures of four types of gelatin and two polysaccharides (a positively charged polysaccharide: chitosan and a negatively charged polysaccharide: xanthan gum). Finally, a general gelation mechanism was proposed for gelatin/polysaccharide mixtures based on all the results above.

Chapter 7 contains the results of the fourth paper "Protein/Polysaccharide Based Hydrogels Prepared by Vapor-induced Phase Separation", submitted to *ACS Macro Letters* (August, 2017). In this work, we studied the gelation kinetics of gelatin and polysaccharide mixtures. We found that using vapor induced phase separation (VIPS) yields gels at very low gelling agent content, and for a variety of other mixed systems, including globular proteins such as bovine serum albumin. The mixed gel strength is much stronger than that of gels prepared by the conventional dropwise pH adjustment technique.

CHAPTER 4 ARTICLE 1: SYNERGISTIC GELATION OF GELATIN B WITH XANTHAN GUM

Changsheng Wang [a], Giovanniantonio Natale [b], Nick Virgilio [a]* and Marie-Claude Heuzey [a]*

[a] CREPEC, Department of Chemical Engineering, Polytechnique Montréal, Montréal, Québec, H3C 3A7, Canada

[b] Department of Chemical and Biological Engineering, The University of British Columbia, Vancouver, British Columbia, V6T 1Z3, Canada.

This work was published in *Food Hydrocolloids* (IF 4.747, Q1) on January 15, 2016

4.1 Abstract

Xanthan gum (XG) and gelatin B (GB) interact synergistically in aqueous solution (0.2% XG, 1.0% GB (wt/vol.)) and form gels with an elastic modulus *G'* almost 30 times superior to a pure 0.2% XG solution. *G'* reaches a maximum at pH 5.5, near the isoelectric point of GB, and subsequently decreases with increasing pH, while it decreases significantly with salt addition due to charge screening. A delicate balance is then needed between electrostatic attraction and repulsion to maximize the rheological properties of mixed XG/GB gels. In addition, the gels display time-dependent properties originating from hydrogen bonding between gelatin molecules, as shown by full heat-reversibility behavior. The macroscopic rheological properties correlate well with confocal laser scanning microscopy (CLSM) microstructure analysis: GB forms large aggregates at pH 5.0 and a network structure at pH ≥ 5.5, while XG forms a network at pH 5.5 which disappears with increasing pH.

4.2 Introduction

Proteins and polysaccharides are two categories of natural biopolymers commonly used in various fields of applications such as the food and cosmetic industries, and biomedical engineering, to name a few. Processed food systems usually contain both proteins and polysaccharides performing complementary nutritional, structural and textural functions [1]. Their mixtures can show favorable or detrimental effects on the formation of mixed gels. Interestingly, complexation (intermolecular attraction) [2] and/or incompatibility (intermolecular repulsion) [3-7] can both enhance gelling

properties. Protein/polysaccharide interactions are usually dominated by electrostatic forces, but they also depend on other weaker interactions such as hydrogen bonding and van der Waals forces. As a consequence, the interactions between these biopolymers can usually be tuned by controlling the pH, the ionic strength, and the protein/polysaccharide ratio [3]. For example, the addition of xanthan gum (XG) (0.01-0.06 % w/v) to whey protein isolate (WPI) results in a synergistic effect on gel strength at pH 6.0-6.5, while an antagonist effect is observed at pH 5.5 [3]. In another study on the same binary combination, a synergistic effect is observed at pH ≥ 7.0, while an antagonist effect takes place at pH ≤ 6.5 when 0.05-0.1 % wt XG is added. Higher XG concentrations (0.2-0.5 wt%) led to an antagonist effect in a pH range of 5.5-7.5 [5]. In this binary system, the synergy is attributed to a segregative phase separation. Bryant et al. [7] found that 0.1 wt% XG added to a heat-denatured WPI solution can cause an appreciable increase in its opacity, gelation rate and final rigidity. Mixtures of ι-carrageenan and gelatin also show higher moduli than gelatin and ι-carrageenan systems alone [6]. Phase separation induced by heat treatment in bovine serum albumin (BSA)/pectin mixtures is believed to be the reason for the decreasing *G'*, compared to BSA gels only, while the presence of calcium in BSA/pectin mixtures leads to the formation of an interpenetrated network [8].

Gelatin, derived from the parent protein collagen by either acid (type A) or alkaline (type B) treatments, is a low-cost and one of the most widely used protein hydrocolloids because of its numerous applications in food, confectionary, pharmaceutical/medical, cosmetic and technical products [9]. Like collagen, gelatin has a helix-to-coil transition temperature. Above this temperature, gelatin molecules exist in solution as random coils, but upon cooling below this temperature, the coil structures of gelatin start to form triple helices, which can induce chain association and three-dimensional network formation [9, 10].

On the other hand, xanthan gum (XG) is a relatively expensive anionic microbial hetero-polysaccharide with a cellulosic backbone substituted at C-3 on alternate glucose residues, with a trisaccharide branch (D-glucose, D-mannose and D-gluconate). XG is known to undergo an order-to-disorder (helix-to-coil) transition in solution depending on salinity and temperature [11-14]. In aqueous solution, XG may be regarded as a highly-extended worm-like chain due to the electrostatic repulsion arising from the deprotonated carboxylic acid groups on the side chains; non-covalent associations (mainly hydrogen bonding) between the extended structures make XG a weakly structured material, thus exhibiting a weak gel-like behavior [13, 15]. Nevertheless, XG is

commonly regarded as a non-gelling polysaccharide showing a shear-thinning behavior in solution [3]. It can however form a gel in the presence of trivalent ions or when mixed with other polysaccharides, [14, 16, 17] or even proteins [18].

Lii et al. have pointed out that the interaction between XG and gelatin A involves electrostatic and non-coulombic interactions (hydrogen bonding) from -NH and -OH bonds [19]. They can form complexes when mixed at pH 2.3, or in a pH range of 9-11 when their electrosynthesis is conducted at a constant potential difference of 12 V for 1.5 h. The addition of XG can also greatly improve the mechanical properties and thermal stability of gelatin edible films through interactions caused by electrostatic forces, hydrogen bonding and entanglements between both biopolymers, and appropriately oxidized XG can further improve these properties [20]. Recently, it was reported that the addition of XG into gelatin with high levels of co-solutes (glucose syrup and sucrose) shifted the glassy state to lower temperatures, [21] making the samples more hydrated, ordered and stable, [22] and accelerated the process of vitrification (an ultra-rapid process that prohibits the formation of ice crystals) [23]. However, to the best of our knowledge, there is no rheological/microstructural study in the literature on the interactions between XG and GB in mixed solutions and the gels they can form.

The main objective of this work is to probe the rheological properties of gelatin B/xanthan gum mixed solutions and gels as functions of pH and ionic strength, and to correlate the results with solution microstructure, in order to ultimately design low-cost novel thickeners and/or gelling agents. In addition, this design provides a potential method to prepare a gel without using thermal, enzymatic or any other denaturing treatment, which is favorable for protecting micronutrients in food or active molecules in pharmaceutical drugs. Finally, this study aims to shed some light on the gelling mechanisms between proteins and polysaccharides.

4.3 Materials and methods

4.3.1 Materials

Gelatin (type B, G6650, bloom index ~75, molecular weight: 20-25 kDa, pI = 4.7-5.3) (GB) and xanthan gum (XG) (from *Xanthomonas campestris*, G1253, molecular weight ≈ 2000 kDa [24, 25]) were purchased from Sigma-Aldrich Canada. All other reagents and chemicals (HCl, NaOH, NaCl) were of analytical grade and were used without further purification.

4.3.2 Preparation of GB, XG and mixed GB/XG solutions

GB solutions (2.0 % w/v) were prepared by allowing the GB to swell in Milli-Q water (18.2 Ω) for 15-20 min, followed by gentle stirring at 40ºC for 15 min [26]. The solutions were used on the same day. XG solutions (0.2-0.8 % w/v) were prepared by dissolving the powder into Milli-Q water at a stirring speed of 600-700 rpm for at least 12 h at room temperature, to ensure complete dissolution. Mixed GB/XG solutions (GB:XG = 5:1) were prepared by mixing equal volumes of GB (2.0 % w/v) and XG (0.4 % w/v) solutions while stirring at 40ºC for approximately 30 min. The salt concentration in GB/XG mixtures was adjusted over a range of 0 to 300 mM NaCl. The pH was adjusted with 1N HCl or NaOH to the desired values. Photographs of the various solutions were taken the following day for qualitative turbidity analysis, and the samples were further characterized as detailed below.

4.3.3 Zeta potential measurements

Zeta potential values of GB and XG solutions, and their mixtures, at different pHs (3.0-7.0), were determined by laser doppler velocimetry and phase analysis light scattering (M3-PALS) using a Malvern Zetasizer Nano ZSP instrument (Malvern Instruments Ltd., Worcestershire, UK). The zeta potential was determined from the direction and velocity of the molecules in the applied electric field. The Smoluchowski model was used by the software to convert the electrophoretic mobility measurements into zeta potential values. All the samples were diluted to about 0.05 % (w/v) and then put in the cuvette to measure the zeta potential. The temperature of the cell was maintained at 25ºC. The data presented are the average values of three individual measurements.

4.3.4 Rheological measurements

4.3.4.1 Small amplitude oscillatory shear (SAOS)

Measurements were performed using a rough surface Couette flow geometry (cup and bob diameters of 18.066 mm and 16.66 mm, respectively) with a stress-controlled Physica MCR 501 rheometer (Anton Paar-Physica, Ostfildern, Germany). A rough surface was chosen since our preliminary experiments showed that wall slip occurred at GB concentrations ≥ 1.0% w/v when using a smooth geometry. After storage at room temperature (~20-21 ºC) for approximately 24 h, the samples were directly poured into the flow geometry and kept at rest at 20 ºC for 2 min before the measurements. Frequency sweeps over a range of 0.1 to 10 rad/s were performed within the

identified linear viscoelastic (LVE) regime (strain = 0.1-10 %). The storage modulus (*G'*), loss modulus (*G''*), and complex viscosity (|η*|) were recorded. For all samples, the experiments were performed at 20°C for three times.

4.3.4.2 Time-resolved small amplitude oscillatory shear

Freshly prepared solutions were directly poured into the rough surface Couette geometry. Before the time sweep tests, all systems containing GB were heated at a rate of 5°C/min up to 60°C. The systems were kept at this temperature for 10 min to erase the previous thermal histories of the samples, and were subsequently cooled down to 20°C at a rate of 5°C/min. Dynamic time sweep measurements were then performed at 1 rad/s and 20°C in the LVE regime (strain = 0.1-10 %) for 8 h. After that, the mixtures were heated again at a rate of 5°C/min up to 60°C, were kept at this temperature for 10 min, were next cooled down to 20°C at the same rate, followed by a second 8 h time sweep. The storage modulus (*G'*), loss modulus (*G''*), and related complex viscosity (|η*|) were recorded as functions of time. Samples were covered with a thin film of low viscosity mineral oil to prevent water evaporation. The oil was shown not to affect the measurements. The experiments were performed for three times.

4.3.5 Confocal laser scanning microscopy (CLSM)

CLSM observations of the GB/XG solutions were performed with an Olympus IX 81 inverted Confocal Microscope (Olympus Canada Inc., Richmond Hill, ON, Canada). GB was stained with Nile Blue A (N0766, Sigma) under magnetic stirring for 30 min before mixing with XG solutions. On the other hand, XG was covalently labeled with 5-(4,6-dichlorotriazinyl) aminofluorescein (DTAF) (D0531, Sigma). This fluorescent dye directly reacts with hydroxyl, amino, thiol or amide groups to form stable, covalent links between the dye and substrate at room temperature in an aqueous solution at pH ≥ 9 [27, 28]. 10 mg of DTAF was first dissolved into a 50 mL Na_2CO_3-$NaHCO_3$ buffer solution (0.1 M, pH = 10). 200 mg of XG was then dispersed into the prepared DTAF solution. The mixture was allowed to react overnight at room temperature at a stirring speed of 600-700 rpm. The pH was adjusted to 7.0 to stop the reaction, as well as to ensure a quick diffusion rate for counterions in the following dialysis step. The mixture was dialyzed against Milli-Q water for 48 h to remove unreacted DTAF and the counterions. Sodium azide (0.02 wt%) was added to inhibit bacteria growth, and the Milli-Q water was changed every 2 h during dialysis.

Fractions corresponding to XG were cooled at -20ºC. After freeze-drying, a yellow powder (DTAF-XG) was obtained (yield = 91 ± 5 %). Preliminary experiments showed that labeling did not change the rheological behavior of the solutions. After mixing, solution samples were poured in Petri dishes (P35G-1.5-14-C, MatTek), closed with cover slips and hermetically sealed with oil. Observation of XG was made by excitation of DTAF at 488 nm, the emission being recorded between 510 and 550 nm. Observation of GB was made by excitation of Nile Blue A at 633 nm, the emission being recorded between 650 and 680 nm. Micrographs were taken after approximately 24 h using a 60x objective lens at a 2048 x 2048 pixels resolution. All micrographs were subsequently analyzed using Image J software.

4.4 Results

4.4.1 Zeta potential

The zeta potential as a function of pH was measured for GB, XG and their mixtures, without salt, and the results are displayed in **Figure 4.1**. The zeta potential for the mixture is an indicator of the overall charges (all the charged molecules in the system). The isoelectric point (pI) of a protein is actually related to the amount of $-NH^{3+}$ and $-COO^{-}$ groups. Once the balance between the $-NH^{3+}$ and $-COO^{-}$ is disturbed, the pI also changes. The zeta potential of GB progressively increased from negative to positive values with pH decreasing from 7.0 to 3.5, which indicates that the electrostatic pattern is gradually changing from an overall negatively charged to a positively charged protein, due to the protonation of the gelatin carboxyl and amino groups. As expected, the pI of GB is around 5.3 [9].

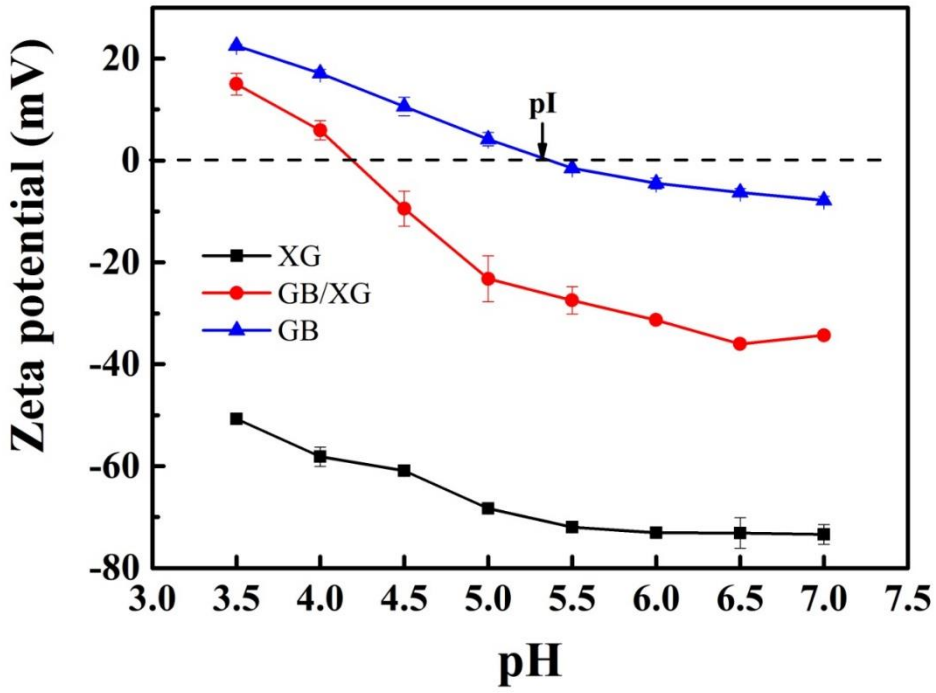

Figure 4.1 Zeta potential of GB, XG and their mixtures. ■: GB, ●: GB:XG = 5:1, ▲: XG.

For XG, the negative zeta potential increases with decreasing pH because of the protonation of the carboxyl groups, as reported by Le and Turgeon [18].

The zeta potential of GB/XG 5:1 mixtures lies in-between, and is more positive than the average values of GB and XG at pH ≥ 5.5, indicating that the two biopolymers still interact with each other through electrostatic attraction even though they are both negatively charged. Similar results have been reported for other protein/polysaccharide systems, such as β-lactoglobulin/chitosan [29], soy globulin/chitosan [30] or β-lactoglobulin/XG systems [18]. The zeta potential of the mixtures reaches 0 around pH 4.2-4.3, which is lower than the pI of GB, showing that electrostatic interactions occur between the amino groups of GB and carboxyl groups of XG. In fact, complexation of proteins and polysaccharides can cause the pI of the protein to shift to a lower [18, 31] or higher pH, [29, 30] depending on the polysaccharide nature and mixing ratio [18, 30-33]. The zeta potential of the mixture is positive at pHs below 4.2, indicating an excess of GB – since the positive net charge of the system can solely be due to free proteins. Such an infer was also made by Le and Turgeon [18].

4.4.2 Turbidity observations

Photos of the samples at varying pHs and salt concentrations are reported in **Figure 4.2** after overnight storage at room temperature. From **Figure 4.2a**, it is clear that pH and ionic strength have a great influence on the turbidity of the GB/XG mixtures. Phase separation occurs below the pI of GB (5.2~5.3) in a certain range of NaCl concentrations (0-50 mM), and gradually shifts to lower pH values as the NaCl concentration increases up to 50 mM. It then disappears when the NaCl concentration increases further (>100 mM). GB is overall positively charged at pH < 5.0 (< pI, **Figure 4.2**) and can interact strongly with the negatively charged XG at relatively low salt concentrations (0-50 mM) by electrostatic forces. This results in the formation of insoluble GB/XG complexes (phase separation). However, salt addition screens the charges and therefore weakens the electrostatic interactions between GB and XG. This explains why phase separation occurs at lower pH values as salt concentration increases, leading ultimately to a single-phase system if salt concentration is high enough (≥ 100 mM). Such a phenomenon was also reported for other protein/polysaccharide systems, such as bovine serum albumin (BSA)/pectin, [34] BSA/gum arabic [33] and whey protein/gum arabic systems [35]. In fact, the addition of salt usually reduces or completely suppresses the formation of protein-polysaccharide complexes [34, 36].

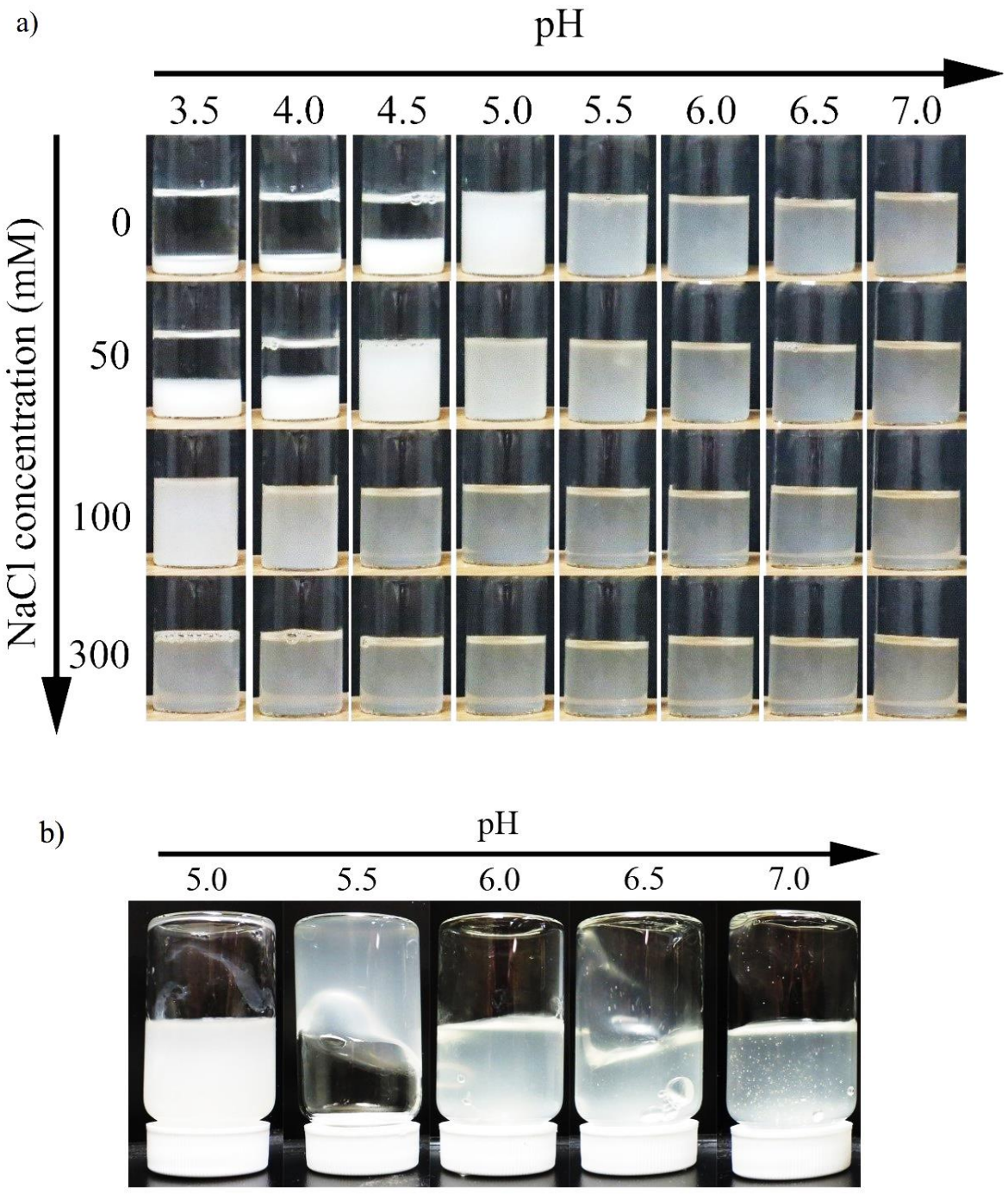

Figure 4.2 a) Effects of pH (3.5-7.0) and NaCl concentration (0-300 mM) on the visual aspect of GB/XG mixtures (GB:XG = 5:1, total concentration = 1.2% w/v); b) close-up view of mixtures without NaCl at pHs 5.0-7.0.

When no salt is added, weak self-supporting properties are observed at pH 5.5 but not for the samples below or above this pH, indicating the highest viscosity/elasticity, as observed when the samples are turned upside down (**Figure 4.2b,** "tabletop rheology"). The samples are viscoelastic fluids at pH 6.0~7.0, whereas those at pH 5.0 or below are more water-like. At pH ≥ 5.5, the two biopolymers start to be more and more thermodynamically incompatible since both of them carry net negative charges. Because of this peculiar effect, these samples were selected for further rheological analysis.

4.4.3 Rheological behavior

4.4.3.1 Small amplitude oscillatory shear (SAOS)

Dynamic rheological measurements were carried out to investigate the flow properties of the GB/XG mixtures, without salt and at different pHs - the results are presented in **Figure 4.3** for the storage modulus *G'* **(4.3a)** and complex viscosity $|\eta^*|$ **(4.3b)**. The rheological properties of XG alone, at a concentration of 0.2 % (w/v), are also shown for comparison purposes, while the results for GB are too low and noisy to be reported. At pH = 5.0, *G'* of the mixture is comparable to a 0.2% XG solution. A first important feature is the sudden and sharp increase of *G'* and $|\eta^*|$ of the mixture as the pH increases from 5.0 to 5.5. Then, at pHs ranging from 5.5-7.0, *G'* gradually decreases in magnitude, but remains significantly higher as compared to the 0.2 % XG solution alone: 10-30 times for *G'* and $|\eta^*|$, depending on the pH. These results clearly illustrate the synergistic effect occurring between GB and XG in solution. However, this effect gradually disappears when the pH increases up to 10.0.

a)

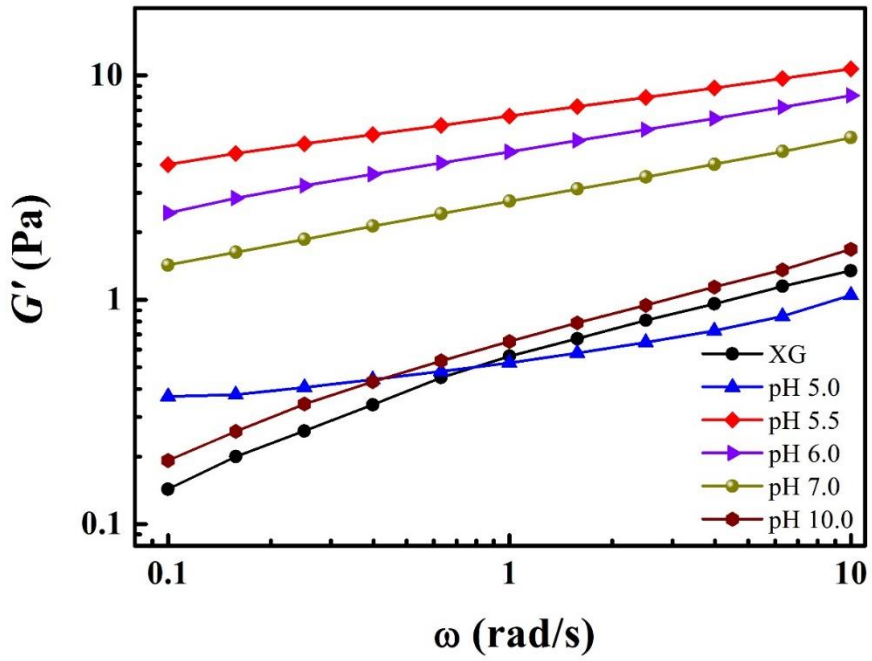

b)

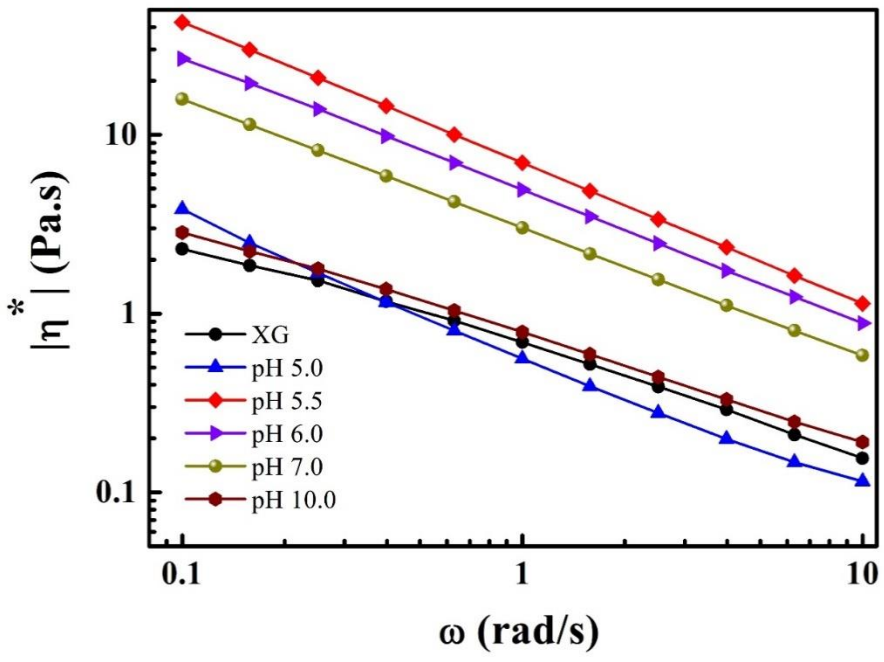

Figure 4.3 a) Storage modulus (*G'*) and b) complex viscosity (|η*|) as functions of frequency at 20ºC for the mixtures (GB:XG=5:1, total concentration = 1.2 %) at various pHs (pH=5.0-10.0). XG at a concentration of 0.2 % (w/v) is shown for comparison purposes. No salt added.

In **Figure 4.4b**, $|\eta^*|$ of the mixtures shows a similar trend to *G'*. In addition, at pHs ranging from 5.0 to 7.0, $|\eta^*|$ decreases with increasing ω (log-log scale), hence showing a somehow solid-like behavior with a slope in-between (-0.70) – (-0.75), with no indication of a low-frequency Newtonian plateau in the range of frequencies investigated. In comparison, the mixture at pH = 10.0 and the 0.2 % XG solution show similar behavior with a less pronounced shear-thinning behavior (slope ≈ 0.60).

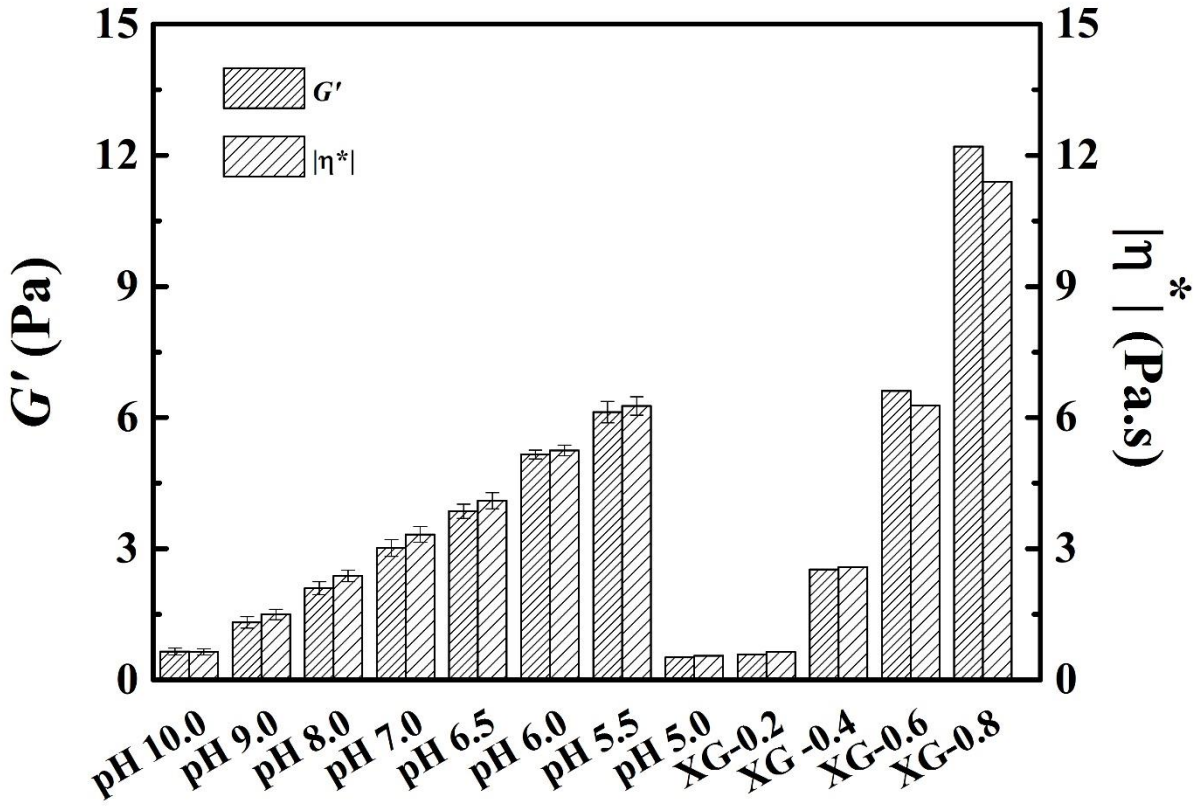

Figure 4.4 Comparisons of storage modulus (*G'*) and complex viscosity ($|\eta^*|$) at different pHs for the mixtures (GB:XG = 5:1, total concentration = 1.2 % w/v) and XG solutions (c = 0.2-0.8 % w/v, pH = 6.0) at ω = 1 rad/s. No salt added.

Figure 4.4 presents *G'* and $|\eta^*|$ of the mixtures at different pHs, as well as neat XG solutions at different concentrations, at ω = 1 rad/s. Mixture values are in fact comparable to neat XG solutions at concentrations ranging from 0.4-0.6 % w/v. Further increase in pH over 7.0 still shows a gradual decrease of *G'* and $|\eta^*|$. The storage modulus (*G'*) is 2.0-3.0 times higher than the loss modulus

(*G''*) depending on pH, indicating that the mixtures behave as weak gels. Our experiments also show that *G'* and $|\eta^*|$ of the 0.2% XG solution are only slightly sensitive to pH within the selected pH and salt concentration ranges investigated here (data not shown).

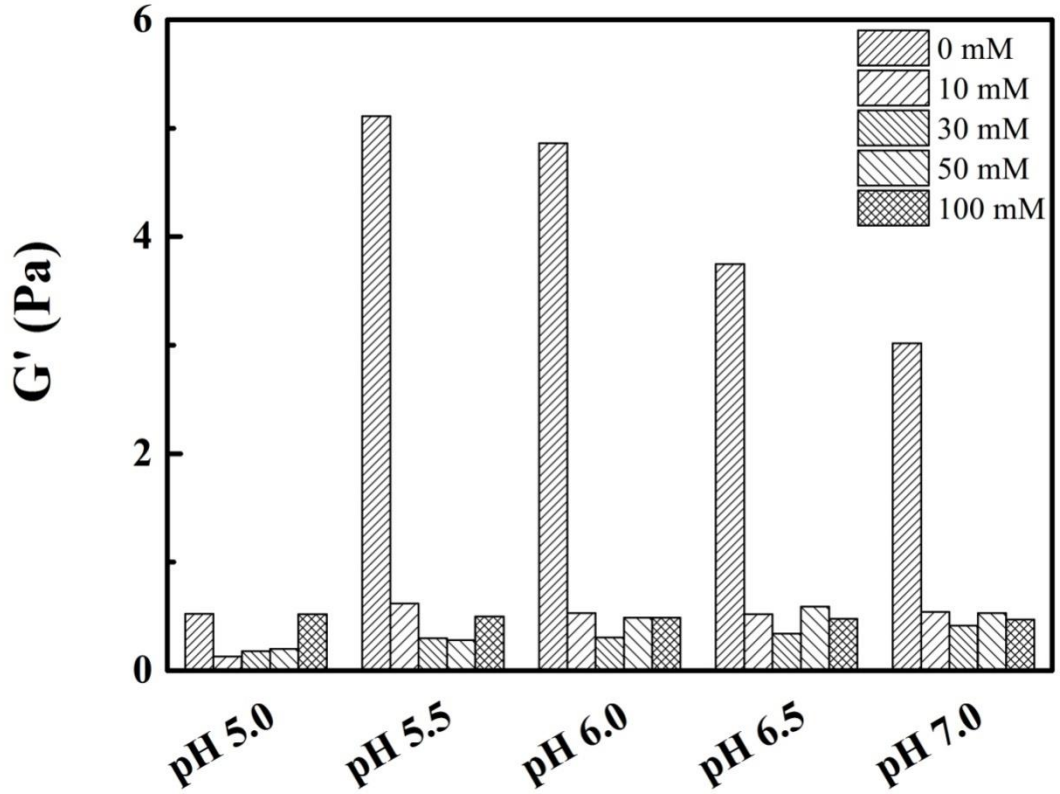

Figure 4.5 Comparison of storage modulus (*G'*) of the mixtures (GB:XG = 5:1, total concentration = 1.2 % w/v) at different pHs and salt concentrations (0 - 100 mM) at a ω = 1 rad/s.

To understand what causes this synergy between XG and GB and the complex behavior of their mixtures, examining the effect of salt on *G'* may be useful. The results are presented in **Figure 4.5**. Clearly, ionic strength has a strong influence since *G'* decreases significantly as salt is added. This further demonstrates that this synergy is due, to a large extent, to electrostatic interactions between GB and XG.

4.4.3.2 Time-resolved small amplitude oscillatory shear

The time-dependent rheological properties of the GB/XG mixtures without salt at different pHs were studied by dynamic time sweep tests at ω = 1 rad/s, and the results are presented in **Figure 4.6**. *G'* of the XG solution alone changes slightly with time, but when mixed with GB, *G'* steadily increases, regardless of pH. The mixture at pH 5.0 shows the lowest *G'* at the beginning of the measurement (lowest curve), while a maximum value is observed at pH = 5.5. Further increase (> 5.5) in pH results in the overall decrease of *G'*. Nevertheless, the values remain above those of XG alone (data not shown). The same trend remains during the whole period of measurement. This indicates that the relative magnitude of the solutions' rheological properties is determined by the initial electrostatic interactions between the two biopolymers.

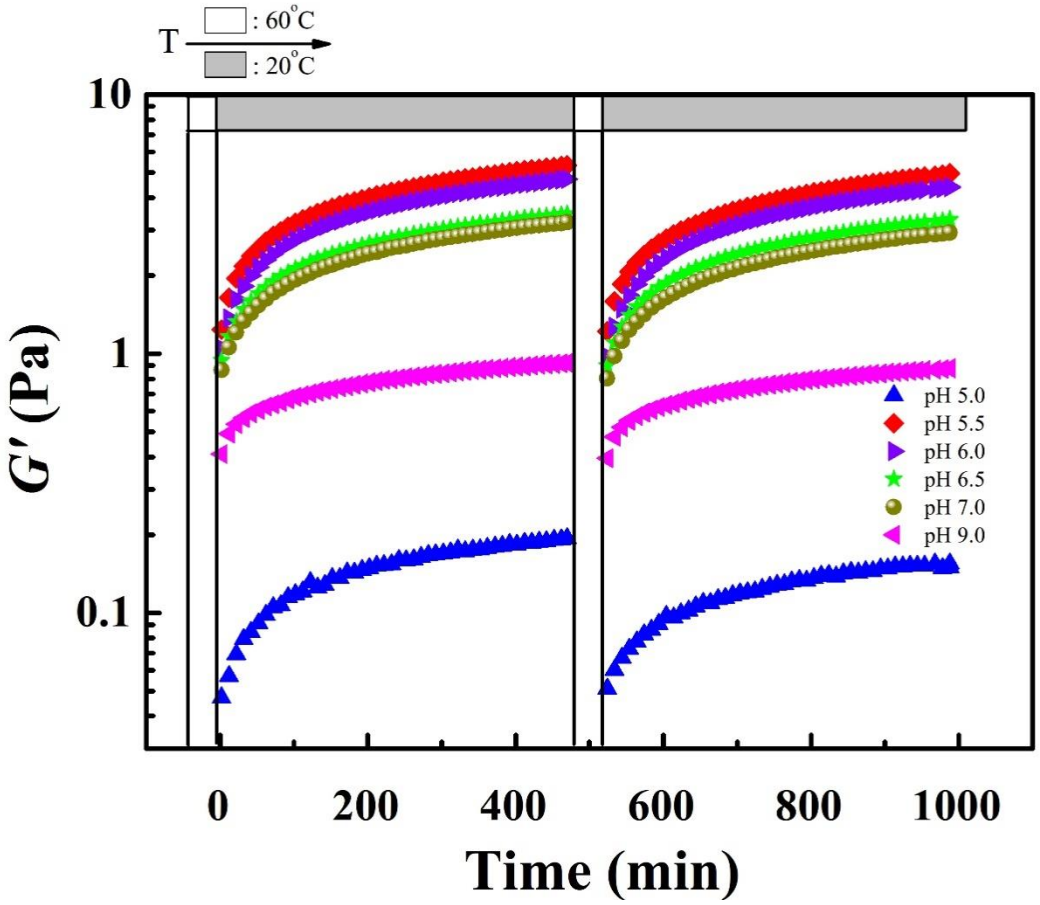

Figure 4.6 Evolution of *G'* of the mixtures (GB:XG=5:1, total concentration = 1.2 % w/v) at different pHs (5.0-9.0) as a function of time. The samples were first heated up to 60°C, then cooled down to 20°C, and the process was repeated a second time.

The mixed solutions also exhibit heat-reversible properties (**Figure 4.6**). Heating at 60°C for 10 minutes after a period of 8 h at 20ºC brings the solutions back to a low viscosity liquid state. When cooling back a second time to 20°C, the rheological properties start to increase again following the same trends that were observed in the previous set of experiments at similar conditions. This heat-reversible behavior indicates that no covalent crosslinking but only physical interactions are involved during gel formation and evolution, most probably hydrogen bonds that are easily disturbed at high temperature. *G'* of the GB/XG mixtures increases rapidly at the beginning (< 100 min), and then slows down, as shown in **Figure 4.6**. The initial fast increase can be explained by the solutions' initial low viscosity, which allows the molecules to interact with each other more easily by diffusion. However, diffusion slows down with time due to the progressive interlocking between molecules, ultimately leading to the slower evolution of *G'*.

When the same data are plotted in log-log scale, two regimes can be identified: 1) first a transient regime (< 15 min), followed by 2) a second regime with a constant slope (≥ 15 min). Modeling the second regime with a power-law function $\propto t^n$ (n corresponding to the slope on a (log *G'*) vs (log *t*) plot) shows that n = 0.32-0.35, hence is nearly constant over a pH range of 5.0 to 7.0. The pH-independency of the exponent indicates that the evolution of the system is self-similar and possibly due to hydrogen bonding, as mentioned above. This is further confirmed by the full heat-reversibility of the rheological properties (**Figure 4.6**). However, the exponent decreases to 0.19 when pH = 9.0, probably because of the electrostatic repulsions that are finally strong enough to weaken hydrogen bonding by changing the distance between molecules, illustrating again the importance of electrostatic forces.

4.4.4 CLSM analysis

To shed more light on the underlying mechanisms of this synergistic effect on rheological properties between XG and GB, the microstructure of the mixtures was examined by CLSM. 24 h after solution preparation, GB, when mixed with XG, gradually evolves from discontinuous aggregates (pH = 5.0) to a network structure as pH increases above the pI of GB (**Figure 4.7**, right column). In comparison, GB alone shows a homogeneous distribution and no apparent microstructure (data not shown). The aggregates at pH 5.0 are caused by the strong electrostatic attraction between the two biopolymers, while the network structure, comprised of GB-rich (in red) and GB-poor (in black) domains, can be attributed to an excluded volume effect due to the

increasing electrostatic repulsion at pH ≥ 5.5. This excluded volume effect increases the GB local concentration, therefore favoring gelation of hydrocolloids [1, 5, 37] – in this case GB, explaining the enhanced rheological properties.

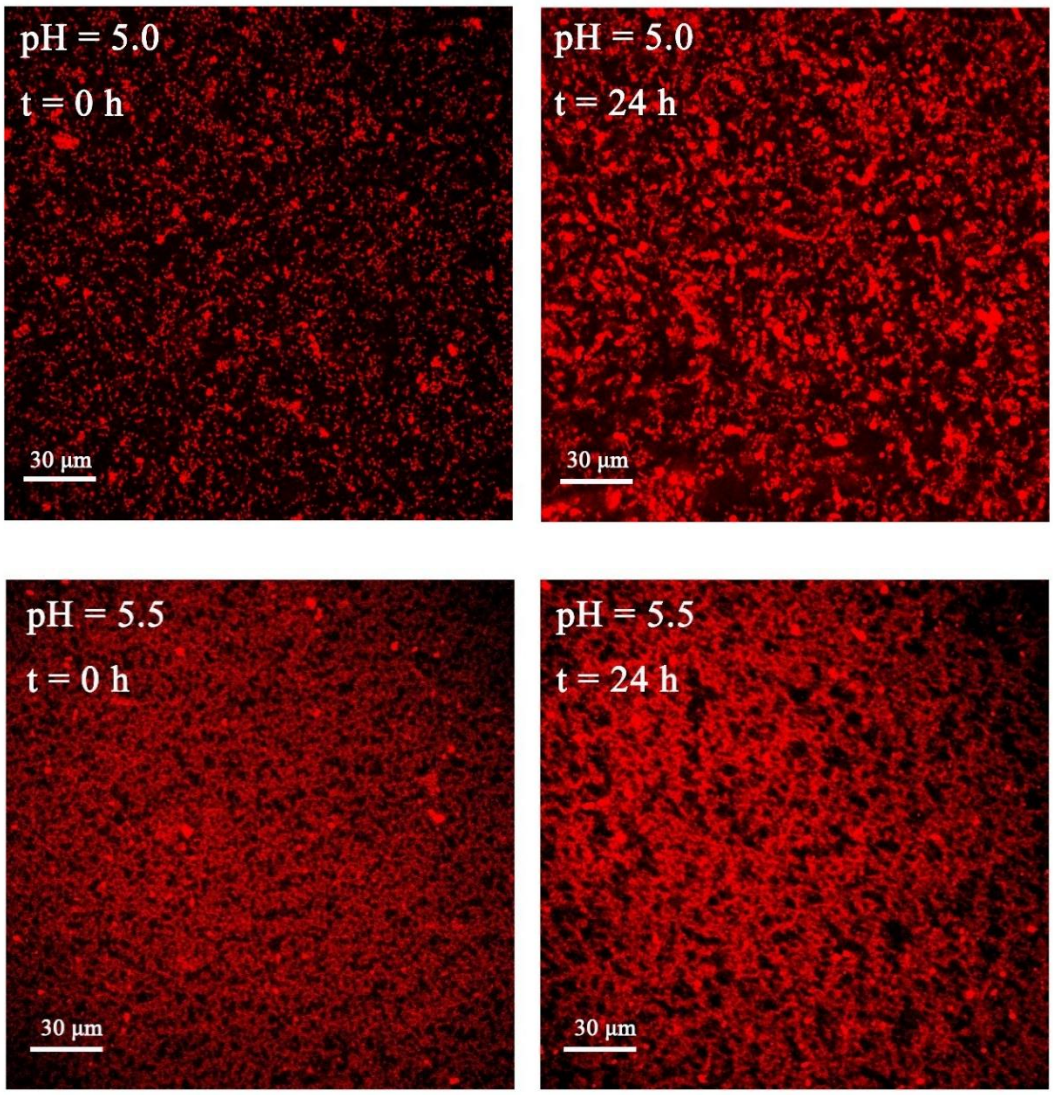

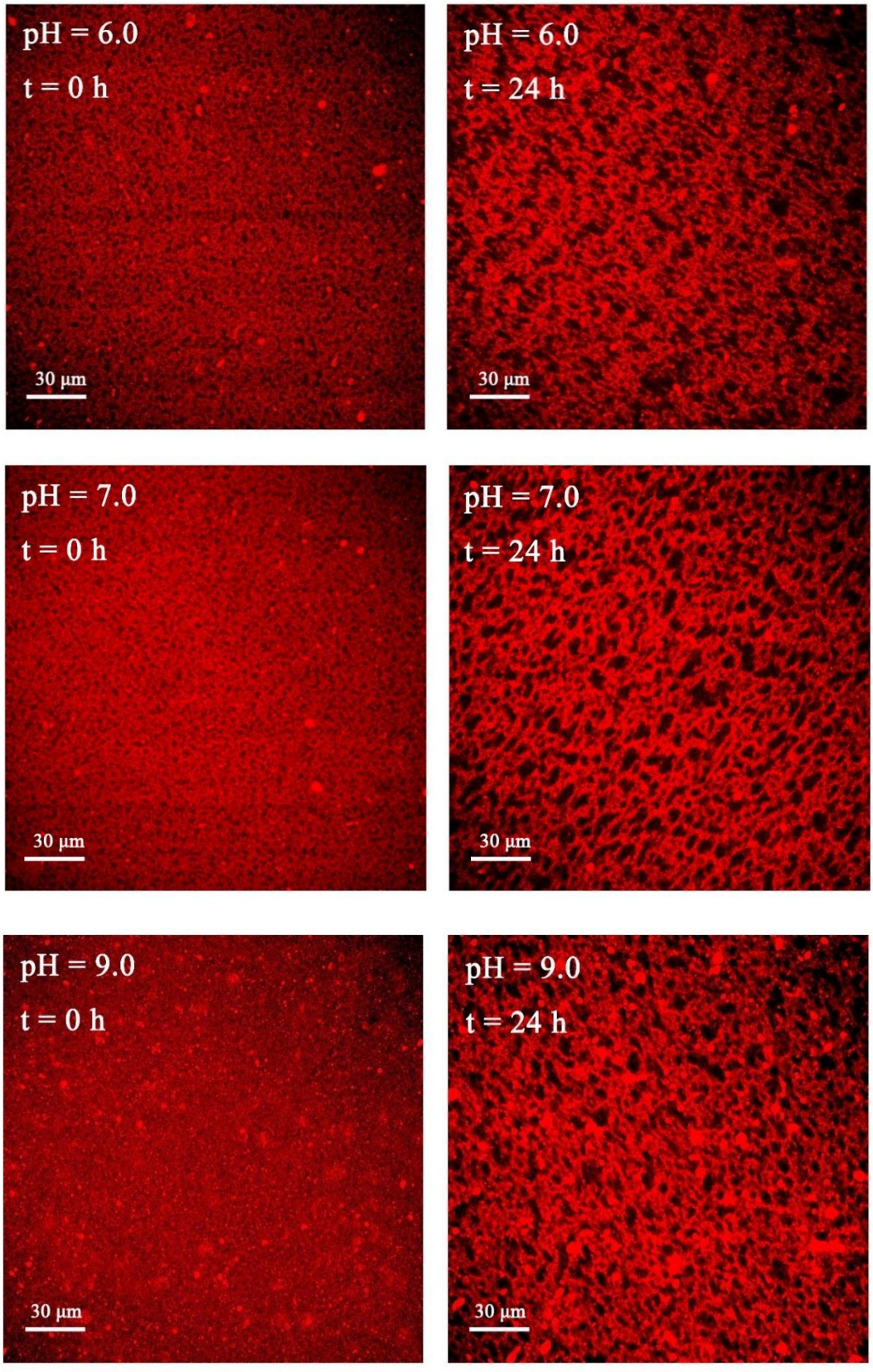
pH = 6.0
t = 0 h
30 µm
pH = 6.0
t = 24 h
30 µm
pH = 7.0
t = 0 h
30 µm
pH = 7.0
t = 24 h
30 µm
pH = 9.0
t = 0 h
30 µm
pH = 9.0
t = 24 h
30 µm

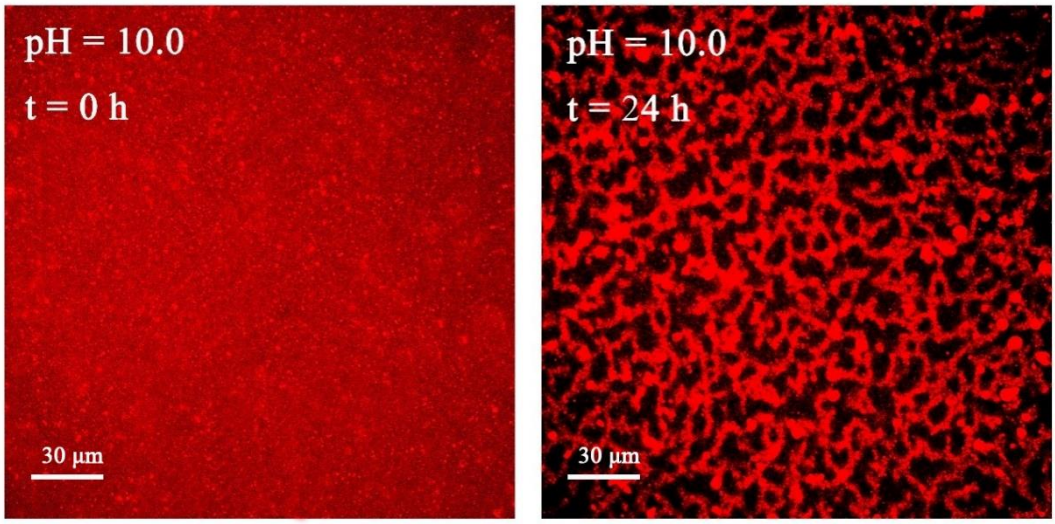

Figure 4.7 CLSM images of mixtures (GB:XG = 5:1, total concentration = 1.2 % w/v) at different pHs, at 0 h and 24 h after solution preparation. GB was stained with Nile Blue A (red). Image size: 210 µm x 210 µm. No salt added.

If the GB-poor domains are modeled as cylinders (see **Supporting information**), we can next obtain an average diameter value corresponding to a microstructure length scale [38-40]. The interfacial perimeter *P* between GB-rich and GB-poor domains is obtained by a contour analysis on the binarized CLSM micrographs (after adjusting brightness, contrast, and removing noise with a median filter, see **Supporting information**). The specific interfacial area, *S*, between GB-rich domains and GB-poor domains is then given by:

$$S = \frac{P}{A} \tag{1}$$

where A is the micrograph's area. The average diameter *d* of GB-poor domains is then obtained as follows:

$$d = \frac{4\Phi_{GB-poor}}{S} \tag{2}$$

where $\phi_{GB\text{-}poor}$ is the volume fraction of GB-poor domains in solution, also obtained by image analysis (because of microstructure isotropy, the GB-poor domains surface fraction on the micrographs is equal to the volume fraction in solution). The average size of the GB-poor domains (after 24 h) shows a gradual increase with pH due to increasing electrostatic repulsion between the molecules (**Figure 4.8**). The mixture at pH 5.5 has the smallest characteristic microstructure length

scale after 24 h, which may be one reason for the most favorable gelling properties. The increase in diameter of the GB-poor domains may explain the decrease in gelling properties. In fact, *G'* decreases exponentially with the diameter of GB-poor domains, with an exponent approximately -4.2.

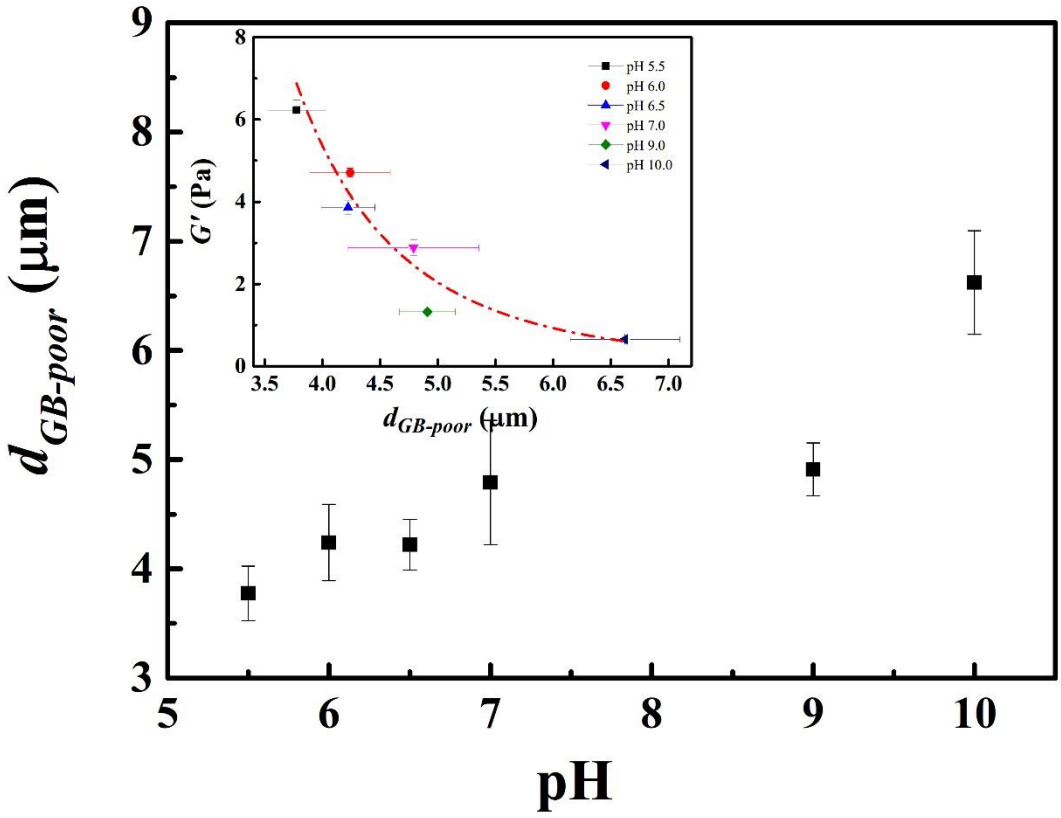

Figure 4.8 Average size of GB-poor domains as a function of pH. At least 10 small bright regions (50 μm x 50 μm) from no less than 2 different CLSM images for each sample are selected for calculation. The insert shows *G'* against the diameter of GB-poor domains.

In addition, the electrostatic repulsion between GB molecules also needs to be considered. Above the pI of GB, the association between GB molecules is the strongest at pH 5.5 among all samples due to the weakest electrostatic repulsion between GB molecules. This is a second possible reason for the enhanced gelling properties at pH 5.5. Too strong electrostatic repulsion between GB molecules does not favor gel formation, which explains the decrease in gelling properties at pH 9.0 and above.

As mentioned before, DTAF was also used to stain XG – the micrographs are shown in **Figure 4.9**. Similarly to GB, XG shows large aggregates after 24 h at pH 5.0. It indicates that the two biopolymers can form aggregates by electrostatic attraction. These aggregates start to disappear with increasing pH. XG shows a network structure at pH 5.5 with XG-rich and poor domains (d = 2.3 ± 0.2 μm), which are smaller than GB-poor domains. The XG network structure might be induced by GB positive patches through electrostatic attraction. This attraction becomes weaker with increasing pH, and correspondingly, the electrostatic repulsion between GB and XG molecules increases, as well as in-between XG molecules. This makes XG more dispersed. The electrostatic attraction allows XG to cooperatively interact with the GB network structure, making it the strongest at pH 5.5. This also explains the decreasing gelling properties with increasing pH **(Figure 4.4**).

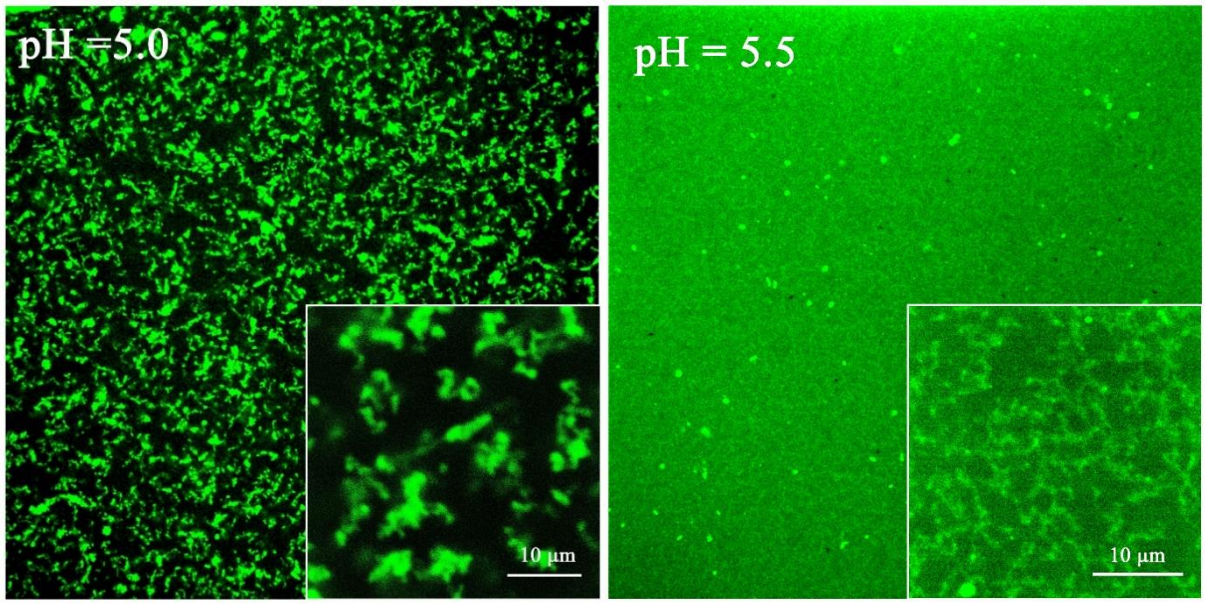

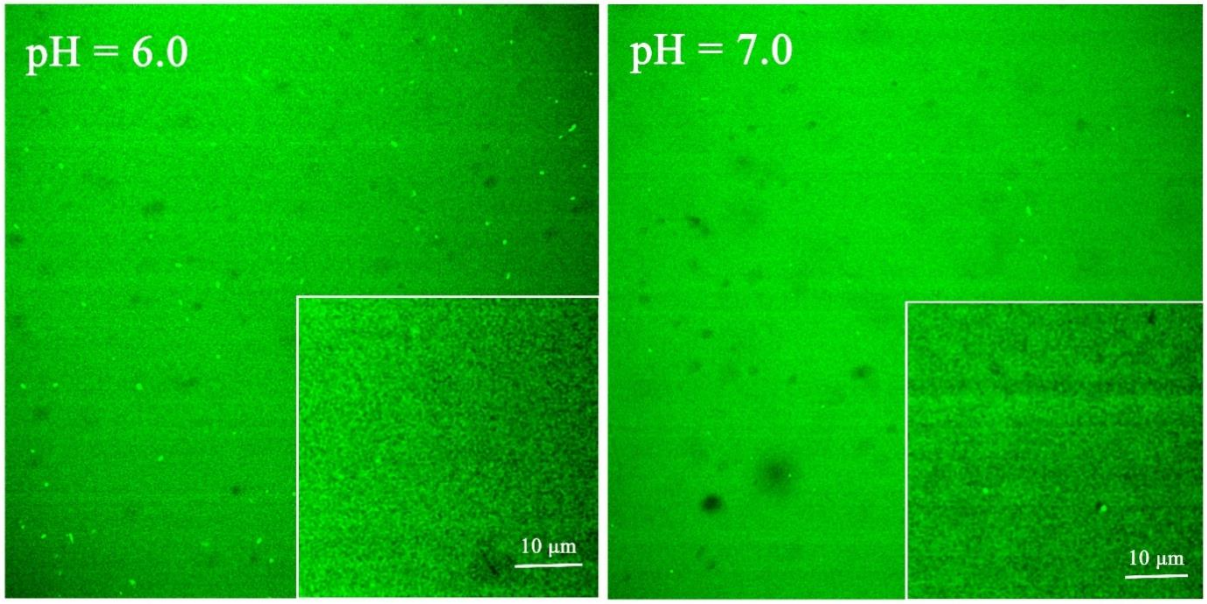

Figure 4.9 CLSM images of mixtures (GB:XG = 5:1, total concentration = 1.2 % w/v) at different pHs. XG is labelled with DTAF (green). Image size: 210 µm x 210 µm. No salt added. The pictures were taken 24 h after solution preparation.

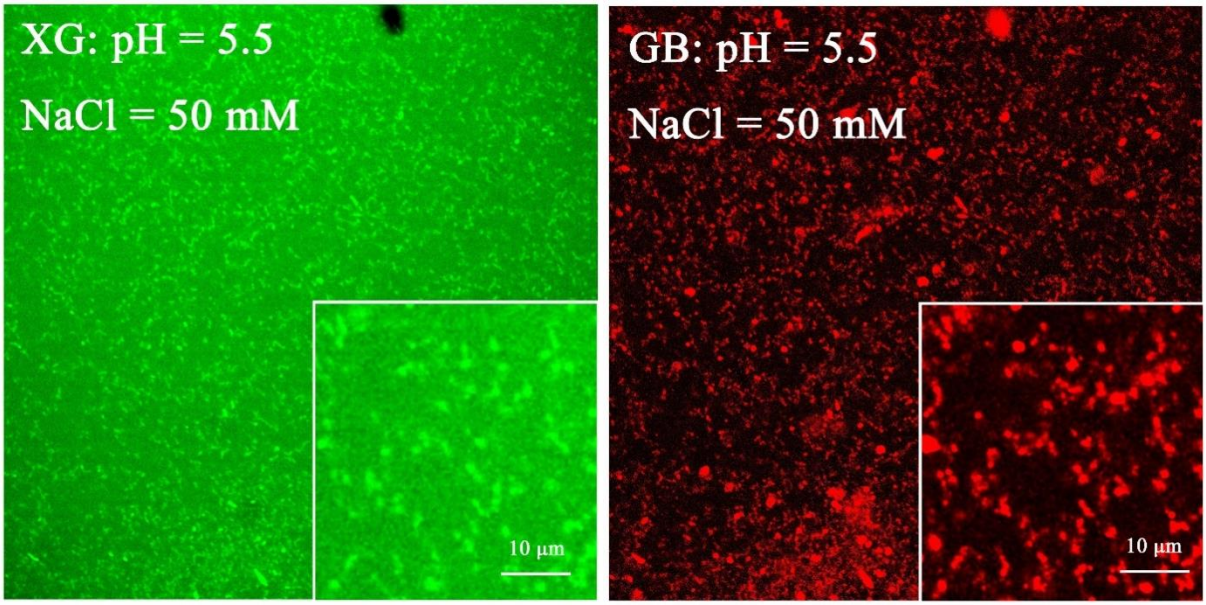

Figure 4.10 Effect of salt addition on the microstructure of GB/XG mixture (GB:XG = 5:1, total concentration = 1.2 % w/v) at pH = 5.5, salt concentration = 50 mM. Image size: 210 µm x 210 µm. The pictures were taken after 24 h. Left: XG stained with DTAF; right: GB stained with Nile Blue A.

Figure 4.10 shows the significant effect of salt on the mixture microstructure. The fine networks of GB and XG at pH 5.5, as observed in **Figure 4.7** and **Figure 4.9**, are broken down into particles when salt is added, explaining the sudden decrease in rheological properties, as illustrated in **Figure 4.6**. The existence of particles indicates that 50 mM NaCl is high enough to destroy the network structure, but possibly not enough to suppress the formation of GB/XG complexes. Interestingly, Wyatt and Liberatore showed that 50mM of NaCl added to XG solutions was sufficient to result in viscosity scaling typical of neutral/uncharged polymers [41].

4.5 Discussion

GB/XG mixtures show a synergistic effect on the rheological properties when the two biopolymers repel each other (pH ≥ 5.5), and a maximum *G'* is observed at pH 5.5. The excluded volume effect due to incompatibility between XG and GB increases the local concentration of GB and thus lowers its critical gelling concentration [1, 5, 37]. This mechanism also explains the synergistic gelling properties observed for other protein/polysaccharide systems, such as WPI/XG, [3] WP/κ-carrageen, [42] and WP/pectin [43]. It does not completely explain however why, in our case, *G'* and $|\eta^*|$ first increase, and then decrease, with increasing pH. This tends to indicate that the attraction between GB and XG also plays an important role. Strong attraction does not favor the synergistic effect either, as the mixtures at pH 5.0 and below illustrate through complexation and agglomeration (**Figures 4.2, 4.7** and **4.9**). A delicate balance between electrostatic attraction and repulsion is hence needed to obtain an optimum synergistic effect on gelling properties in mixed GB/XG systems.

GB and XG interact with each other through electrostatic forces in the pH range investigated, as inferred from zeta potential results (**Figure 4.1**), visual inspection (**Figure 4.2**), rheological results (**Figures 4.3 to 4.5**) and CLSM images (**Figures 4.7, 4.9 and 4.10**). The electrostatic forces between GB and XG lead to different microstructures in solution, depending on pH. At pH ≤ 5.0, the two biopolymers form discontinuous aggregates. GB forms a continuous network structure at pH ≥ 5.5 (**Figure 4.7**), while XG forms a network (pH 5.5) and then becomes more and more dispersed with increasing pH (**Figure 4.9**). The GB network structure is due to the excluded volume effect caused by the repulsion between the two biopolymers, which increases the GB local concentration. Therefore, GB can form a weak gel with the help of XG. The shift from discontinuous aggregates to a continuous network, as well as the excluded volume effect, explain

the enhanced gelling properties for the mixtures at pH ≥ 5.5. GB gels are known to evolve with time through the formation of helical structures, and the gel state can never reach an equilibrium [44], whereas XG alone shows stable rheological properties with time in our preliminary experiments. The GB structure becomes coarser after 24 h (**Figure 4.7**), while the XG structure shows no significant difference (data not shown). This indicates that GB controls the time dependent properties, and hydrogen bonding is commonly regarded as the driving force for coil-to-helix transition [9, 10]. This explains the full heat-reversibility and the fact that *G'*, independently of the pH (5.0-7.0), increases with the same power-law exponent after an initial period of time (t ≥ 15 min, **Figure 4.6**). However, strong electrostatic repulsions can weaken hydrogen bonding, leading to a decrease in the exponent at pH 9.0. This also explains why *G'* decreases at pH 9.0 and above.

Besides the excluded volume effect, XG could potentially reinforce the GB network structure through its interaction with GB positive patches. As for proteins, positive patches will still be present even at pHs above the pI, although the net charge is negative [45, 46]. Similar effects have also been reported for other protein/polysaccharide systems [18, 46, 47]. The reinforcement effect weakens with pH due to increasing electrostatic repulsion between XG and GB molecules (fewer and fewer positive patches are present on GB molecules with increasing pH). In addition, the repulsion between GB molecules also increases with pH, resulting in a decrease of associations between GB molecules. Therefore, the increasing repulsion between GB and XG as well as between GB molecules explains why *G'* decreases with pH. The optimum gelling properties are obtained at pH 5.5, which can be due to the densest GB network structure (**Figure 4.8b**), the strongest association between GB molecules, as well as the strongest reinforcement effect by XG. The phenomena is different from that of the β-lactoglobulin/XG system, in which both *G'* and $|\eta^*|$ increase with decreasing pH, even below the pI of β-lactoglobulin [18]. This difference may be related to the method of preparation of this protein/polysaccharide system, where glucono delta lactone (GDL) was used as an acidifier to induce gelation.

Based on the discussion above, it is clear that electrostatic forces play a crucial role in the synergistic effect. The interplay between attractive and repulsive electrostatic interactions between XG and GB determines the rheological properties at a given pH (**Figures 4.4, Figure 4.6**). Adding salt can break down the network structure by screening the charges (**Figure 4.10**), which is the reason for the large decrease in *G'* with salt addition (**Figure 4.5**).

4.6 Conclusions

GB can form synergistic gels with XG above the pI of GB – the elastic modulus measured in small amplitude oscillatory shear reaching nearly 30 times the value of a pure XG solution at the same concentration used in the mixture. XG has two main functions: it enhances the local concentration of GB thanks to electrostatic repulsions (excluded volume effect) and it interacts with GB's positive patches by electrostatic attraction. The excluded volume effect leads to the formation of a microstructured network comprised of GB-rich and GB-poor domains, and allows GB to form a gel at low concentration. GB is also responsible for the observed time dependent properties of the gels due to the gradual coil-to-helix transitions induced by hydrogen bonding stabilization. The best gelling properties are obtained at pH 5.5 - where the densest GB network is observed with the strongest GB association (nearest to the pI of GB), as well as XG cooperative interaction. Salt addition can break down the network structure through screening of the charges, causing a significant drop in rheological properties and confirming the involvement of electrostatic interactions. These gels represent a first step towards the design of physical gels for food and biomedical applications, since pH and ionic strength sensitivity of the structure could be used to control the release of bioactive molecules. Moreover, they are of interest as novel thickeners and/or gelling agents.

4.7 Acknowledgement

The authors acknowledge Bertrand Floure (Malvern Instruments Ltd) for kindly allowing the use of the Malvern Zetasizer Nano ZSP instrument and Xiaoyan Wang for useful discussions. The authors also thank the Natural Sciences and Engineering Research Council of Canada (NSERC) for financial support and China Scholarship Council (CSC) for providing a scholarship to Mr. Wang.

4.8 Supporting information

Image analysis procedure (taking the sample at pH 5.5 for example):

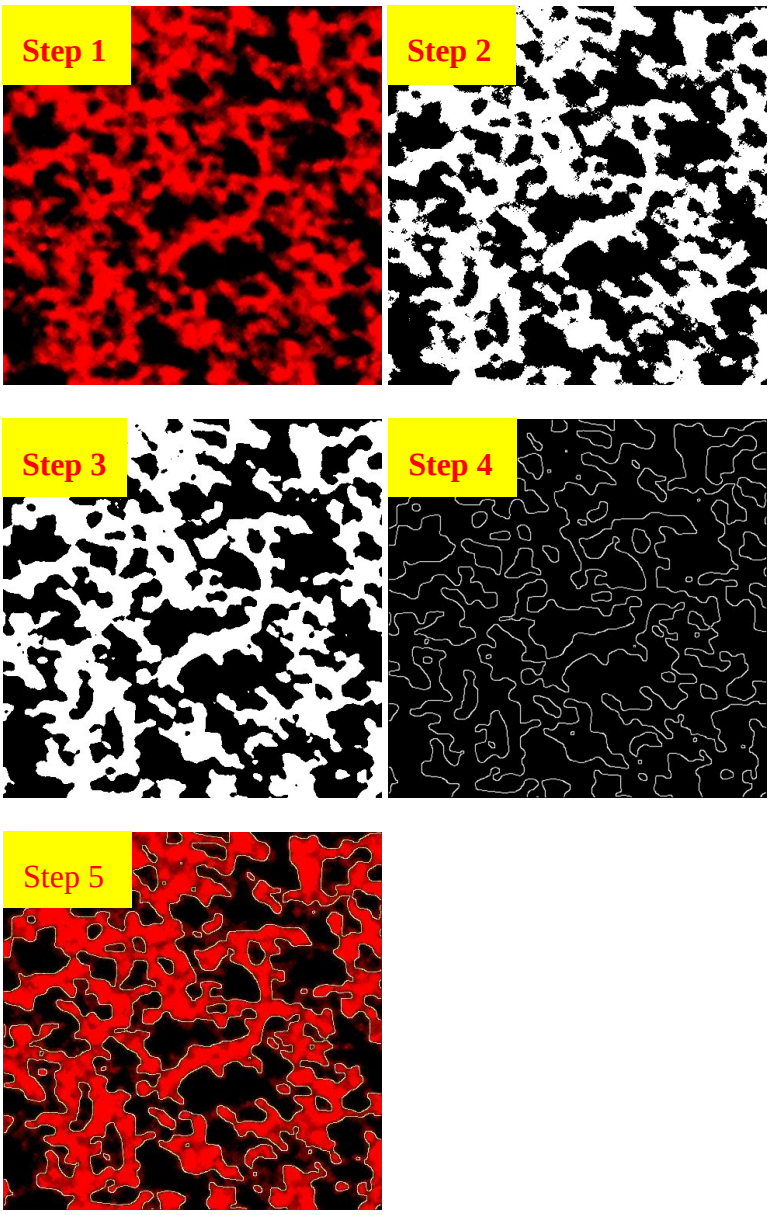

Step 1. A small bright region is obtained from the original image. The size is 50.26μm x 50.26 μm. Brightness and contrast is adjusted to make GB-poor region clearer,

Step 2. Turn micrograph into a binary image using Image J (1.49v)

Step 3. Use median filter to remove noise and smooth contour. The volume fraction of GB-poor domains is determined by Image J.

Step 4. Contour is extracted using an Image Edge plugin with a thickness of 1 pixel. The interfacial perimeter, P, of GB/XG interface is then obtained by counting the pixels in the contour by Image J.

Step 5. A colocalization plugin is then used to check the superposition of contour and initial image to ensure the reliability of data.

Finally, gelatin-poor domain size (assumption: cylinders) is determined by:

$$d = \frac{4V}{S}(1 - \varphi_{GB})$$

4.9 References

1. Tolstoguzov, V.B., *Some physico-chemical aspects of protein processing in foods. Multicomponent gels.* Food Hydrocolloids, 1995. **9**(4): p. 317-332.
2. Wang, Q. and Qvist, K.B., *Investigation of the composite system of β-lactoglobulin and pectin in aqueous solutions.* Food Research International, 2000. **33**(8): p. 683-690.
3. Bertrand, M.-E. and Turgeon, S.L., *Improved gelling properties of whey protein isolate by addition of xanthan gum.* Food Hydrocolloids, 2007. **21**(2): p. 159-166.
4. Ould Eleya, M.M. and Turgeon, S.L., *Rheology of κ-carrageenan and β-lactoglobulin mixed gels.* Food Hydrocolloids, 2000. **14**(1): p. 29-40.
5. Sanchez, C., et al., *Rheology of whey protein isolate-xanthan mixed solutions and gels. Effect of pH and xanthan concentration.* Food / Nahrung, 1997. **41**(6): p. 336-343.
6. Michon, C., et al., *Viscoelastic properties of ι-carrageenan/gelatin mixtures.* Carbohydrate Polymers, 1996. **31**(3): p. 161-169.
7. Bryant, C.M. and McClements, D.J., *Influence of xanthan gum on physical characteristics of heat-denatured whey protein solutions and gels.* Food Hydrocolloids, 2000. **14**(4): p. 383-390.
8. Donato, L., et al., *Heat-induced gelation of bovine serum albumin/low-methoxyl pectin systems and the effect of calcium ions.* Biomacromolecules, 2005. **6**(1): p. 374-385.
9. Williams, P., Phillips, G., and McKenna, B., *The use of hydrocolloids to improve food texture.* Texture in food. Volume 1: Semi-solid foods, 2003: p. 251-274.
10. Djabourov, M., Leblond, J., and Papon, P., *Gelation of aqueous gelatin solutions. I. Structural investigation.* Journal de physique, 1988. **49**(2): p. 319-332.
11. Katzbauer, B., *Properties and applications of xanthan gum.* Polymer Degradation and Stability, 1998. **59**(1): p. 81-84.
12. Pelletier, E., et al., *A rheological study of the order–disorder conformational transition of xanthan gum.* Biopolymers, 2001. **59**(5): p. 339-346.
13. Rochefort, W.E. and Middleman, S., *Rheology of Xanthan Gum: Salt, Temperature, and Strain Effects in Oscillatory and Steady Shear Experiments.* Journal of Rheology (1978-present), 1987. **31**(4): p. 337-369.
14. Stephen, A.M. and Phillips, G.O., *Food polysaccharides and their applications*. Bacterial Polysaccharides. Vol. 160. 2010: CRC Press.

15. Song, K.-W., Kim, Y.-S., and Chang, G.-S., *Rheology of concentrated xanthan gum solutions: Steady shear flow behavior.* Fibers and Polymers, 2006. **7**(2): p. 129-138.

16. Stokke, B.T., Christensen, B.E., and Smidsrod, O., *Macromolecular properties of xanthan*. Polysaccharides, Structural Diversity and Functional Versatility. 1998. 433-472.

17. Copetti, G., et al., *Synergistic gelation of xanthan gum with locust bean gum: a rheological investigation.* Glycoconjugate Journal, 1997. **14**(8): p. 951-961.

18. Le, X.T. and Turgeon, S.L., *Rheological and structural study of electrostatic cross-linked xanthan gum hydrogels induced by [small beta]-lactoglobulin.* Soft Matter, 2013. **9**(11): p. 3063-3073.

19. Lii, C.y., et al., *Xanthan gum–gelatin complexes.* European Polymer Journal, 2002. **38**(7): p. 1377-1381.

20. Guo, J., et al., *Periodate oxidation of xanthan gum and its crosslinking effects on gelatin-based edible films.* Food Hydrocolloids, 2014. **39**(0): p. 243-250.

21. Altay, F. and Gunasekaran, S., *Mechanical spectra and calorimetric evaluation of gelatin–xanthan gum systems with high levels of co-solutes in the glassy state.* Food Hydrocolloids, 2013. **30**(2): p. 531-540.

22. Altay, F. and Gunasekaran, S., *Rheological evaluation of gelatin–xanthan gum system with high levels of co-solutes in the rubber-to-glass transition region.* Food Hydrocolloids, 2012. **28**(1): p. 141-150.

23. Altay, F. and Gunasekaran, S., *Gelling properties of gelatin–xanthan gum systems with high levels of co-solutes.* Journal of Food Engineering, 2013. **118**(3): p. 289-295.

24. Gagnon, D., Shen, X., and Arratia, P., *Undulatory swimming in fluids with polymer networks.* EPL (Europhysics Letters), 2013. **104**(1): p. 14004.

25. Sato, T., et al., *Double-Stranded Helix of Xanthan in Dilute Solution: Further Evidence.* Polym J, 1984. **16**(5): p. 423-429.

26. Milanović, J., et al., *Complex coacervation in gelatin/sodium caseinate mixtures.* Food Hydrocolloids, 2014. **37**: p. 196-202.

27. Schumann, R. and Rentsch, D., *Staining particulate organic matter with DTAF-a fluorescence dye for carbohydrates and protein: a new approach and application of a 2D image analysis system.* Marine Ecology Progress Series, 1998. **163**(1): p. 77-88.

28. Gonçalves, M.S., *Optimized UV/Visible Fluorescent Markers*, in *Advanced Fluorescence Reporters in Chemistry and Biology I*, A.P. Demchenko, Editor. 2010, Springer Berlin Heidelberg. p. 27-64.

29. Guzey, D. and McClements, D.J., *Characterization of β-lactoglobulin–chitosan interactions in aqueous solutions: a calorimetry, light scattering, electrophoretic mobility and solubility study.* Food Hydrocolloids, 2006. **20**(1): p. 124-131.

30. Liu, C., et al., *Complex coacervation of chitosan and soy globulins in aqueous solution: a electrophoretic mobility and light scattering study.* International Journal of Food Science & Technology, 2011. **46**(7): p. 1363-1369.

31. Ye, A., *Complexation between milk proteins and polysaccharides via electrostatic interaction: principles and applications – a review.* International Journal of Food Science & Technology, 2008. **43**(3): p. 406-415.

32. Espinosa-Andrews, H., et al., *Interrelationship between the zeta potential and viscoelastic properties in coacervates complexes.* Carbohydrate Polymers, 2013. **95**(1): p. 161-166.

33. Vinayahan, T., Williams, P.A., and Phillips, G., *Electrostatic interaction and complex formation between gum arabic and bovine serum albumin.* Biomacromolecules, 2010. **11**(12): p. 3367-3374.

34. Ru, Q., et al., *Turbidity and rheological properties of bovine serum albumin/pectin coacervates: Effect of salt concentration and initial protein/polysaccharide ratio.* Carbohydrate Polymers, 2012. **88**(3): p. 838-846.

35. Weinbreck, F., Tromp, R., and De Kruif, C., *Composition and structure of whey protein/gum arabic coacervates.* Biomacromolecules, 2004. **5**(4): p. 1437-1445.

36. Kizilay, E., Kayitmazer, A.B., and Dubin, P.L., *Complexation and coacervation of polyelectrolytes with oppositely charged colloids.* Advances in colloid and interface science, 2011. **167**(1): p. 24-37.

37. Doumèche, B., Picard, J., and Larreta-Garde, V., *Enzyme-catalyzed phase transition of alginate gels and gelatin-alginate interpenetrated networks.* Biomacromolecules, 2007. **8**(11): p. 3613-3618.

38. Esquirol, A.-L., Sarazin, P., and Virgilio, N., *Tunable Porous Hydrogels from Cocontinuous Polymer Blends.* Macromolecules, 2014. **47**(9): p. 3068-3075.

39. Galloway, J.A., Montminy, M.D., and Macosko, C.W., *Image analysis for interfacial area and cocontinuity detection in polymer blends.* Polymer, 2002. **43**(17): p. 4715-4722.

40. Li, J. and Favis, B., *Characterizing co-continuous high density polyethylene/polystyrene blends.* Polymer, 2001. **42**(11): p. 5047-5053.

41. Wyatt, N.B. and Liberatore, M.W., *Rheology and viscosity scaling of the polyelectrolyte xanthan gum.* Journal of Applied Polymer Science, 2009. **114**(6): p. 4076-4084.

42. Turgeon, S.L. and Beaulieu, M., *Improvement and modification of whey protein gel texture using polysaccharides.* Food Hydrocolloids, 2001. **15**(4–6): p. 583-591.

43. Beaulieu, M., Turgeon, S.L., and Doublier, J.-L., *Rheology, texture and microstructure of whey proteins/low methoxyl pectins mixed gels with added calcium.* International Dairy Journal, 2001. **11**(11–12): p. 961-967.

44. Djabourov, M., *Architecture of gelatin gels.* Contemporary Physics, 1988. **29**(3): p. 273-297.

45. van der Wielen, M.W.J., van de Heijning, W., and Brouwer, Y., *Cellulose Gum as Protective Colloid in the Stabilization of Acidified Protien Drinks*, in *Gums and Stabilisers for the Food Industry 14*, P.A. Williams and G.O. Phillips, Editors. 2008, The Royal Society of Chemistry: London, UK. p. 495-502.

46. Seyrek, E., et al., *Ionic strength dependence of protein-polyelectrolyte interactions.* Biomacromolecules, 2003. **4**(2): p. 273-282.

47. Laneuville, S.I., et al., *Small-angle static light-scattering study of associative phase separation kinetics in [small beta]-lactoglobulin + xanthan gum mixtures under shear*, in *Food Colloids: Interactions, Microstructure and Processing*, E. Dickinson, Editor. 2005, The Royal Society of Chemistry. p. 443-465.

CHAPTER 5 ARTICLE 2: A MECHANISM FOR THE SYNERGISTIC GELATION PROPERTIES OF GELATIN B AND XANTHAN GUM AQUEOUS MIXTURES

Chang-Sheng Wang, [a] Nick Virgilio, [a*] Paula M. Wood-Adams, [b] Marie-Claude Heuzey [a*]

[a] Centre de Recherche sur les Systèmes Polymères et Composites à Haute Performance (CREPEC), Department of Chemical Engineering, Polytechnique Montréal, Montréal, Québec, H3C 3A7, Canada

[b] CREPEC, Department of Mechanical and Industrial Engineering, Concordia University, Montréal, Québec, H3G 1M8, Canada

This work was accepted by *Carbohydrate Polymers*

5.1 Abstract

Gelatin B and xanthan gum aqueous mixtures (GB/XG, (0.2-2%)/0.2% w/v) exhibit enhanced gelling properties compared to their pure component solutions at similar compositions. The mixed gels comprise co-localized networks of GB and XG–rich domains. Our results show that these domains are composed of intermolecular complexes and their aggregates stabilized by the neutralization effect of GB, and linked together by formation of GB triple helices. GB/XG mixtures display composition-dependent microstructural transitions: from discontinuous aggregates (GB/XG ratio ≤ 1) to a continuous GB/XG network (ratio = 2-6), followed by network fragmentation (ratio = 8-10). Increasing the GB Bloom index accelerates network formation and results in higher elastic modulus (G'), while increasing the XG molecular weight causes the opposite effect due to diffusion limitations. This work provides a set of fundamental guidelines to design novel thickeners and/or gelling agents based on proteins and polysaccharides, for food or pharmaceutical applications.

5.2 Introduction

Proteins and polysaccharides are two of the most important functional biopolymers in food products. Their interactions in aqueous solutions can result in coacervates, complexes or gels depending on charge density, protein/polysaccharide binding affinity and other molecular

characteristics (conformation, contour length, chain flexibility and molecular weight) [1]. These three phase states consequently exhibit different functional properties. For example, protein/polysaccharide coacervates and electrostatic gels can be utilized for ingredient encapsulation [1, 2]; complexes and electrostatic gels have excellent texturing properties [1, 3]; and complexes can provide stabilization due to their interfacial properties [1, 4]. Protein/polysaccharide electrostatic gels can be formed without heat, enzyme or crosslinking agents, and are therefore promising for the protection of bioactive molecules when used as encapsulation and delivery systems [1, 4]. In addition, they can be formed at extremely low concentrations of biopolymers [1]. In order to fully control their functional properties for application design, it is necessary to understand the mechanisms involved in the interactions between proteins and polysaccharides and the way in which these interactions can be tuned [5].

Protein/polysaccharide mixed gel formation depends on the nature and characteristics of the biopolymers. For both proteins [4] and polysaccharides [6], a higher biopolymer concentration is needed to form a gel when the molecular weight and charge density are lower. Electrostatic forces are the dominant interactions between proteins and polysaccharides in solution, but other interactions such as hydrogen bonding and hydrophobic interactions can also be involved [7, 8]. Proteins and polysaccharides can both repel and attract each other even when they carry the same net charge due to the amphiprotic properties of proteins [9-11]. Electrostatic forces are affected by the protein/polysaccharide ratio, pH, ionic strength and biopolymer charge density [8, 10].

The gelation properties of protein/polysaccharide electrostatic hydrogels are the result of a delicate balance between repulsive and attractive interactions [10, 12]. Optimal pH, protein/polysaccharide ratio and ionic strength are required to tune their gelation properties. For example, our previous study demonstrated that the highest elastic modulus (G') of a gelatin B (referred to here as L-GB) and XG mixed gel occurs at pH 5.5 [12]. Similarly, β-lactoglobulin/XG and whey protein isolate (WPI)/XG mixtures require an optimum pH and protein to polysaccharide ratio for gelation [13-15].

We have also shown that GB/XG aqueous mixtures exhibit time-dependent, pH sensitive synergistic gelation properties [12]. The objective of this work is to investigate the effects of composition, GB Bloom index and XG molecular weight on the rheological properties and

microstructure of GB/XG aqueous mixtures, in order to elucidate the mechanism behind the synergistic gelation of this specific protein/polysaccharide pair.

5.3 Materials and methods

5.3.1 Materials

Two grades of gelatin (type B), G6650 (Bloom index = 75, *Mw* = 20-25 kDa, critical gelling concentration $c_{crit} \approx 4.0$ % w/v) (L-GB) and G9382 (Bloom index = 225, *Mw* = 50 kDa, $c_{crit} \approx 2.0$ % w/v) (H-GB) were purchased from Sigma-Aldrich, Canada. Four grades of xanthan gum (XG) were used: one grade (G1253) was purchased from Sigma-Aldrich Canada (the grade used in our previous work [12], referred to here as R-XG), while the other three grades with different viscosities (see Figure S1), i.e. Keltrol SF (Low-XG), Keltrol (Med-XG) and Keltrol AP (High-XG), were kindly supplied by CP Kelco U.S., Inc. Other chemicals (HCl, NaOH, Nile Blue A and 5-(4,6-dichlorotriazinyl) aminofluorescein) were of analytical grade (Sigma Aldrich, Canada), and used as received.

5.3.2 Preparation of GB, XG and GB/XG solutions

GB solutions (0.4-4.0 % w/v) were prepared by allowing GB powder to swell in Milli-Q water (18.2 Ω) for 15-20 min at room temperature, followed by gentle stirring at 60 ^{o}C for 15 min. XG solutions (0.2 and 0.4 % w/v) were prepared by dissolving the powder into Milli-Q water at a magnetic stirring speed of 600-700 rpm for at least 12 h at room temperature. Mixed GB/XG solutions with a fixed XG concentration (0.2 % w/v) and different GB concentrations (0.2-2.0 % w/v) were prepared by mixing equal volumes of GB and XG primary solutions while magnetic stirring at 60 ^{o}C for approximately 30 min. The pH of the mixtures was adjusted using 1M HCl or NaOH to the desired values.

5.3.3 Zeta potential measurements

Zeta potential values of GB and XG solutions were determined by laser doppler velocimetry and phase analysis light scattering (M3-PALS) using a Malvern Zetasizer Nano ZSP instrument (Malvern Instruments Ltd., Malvern, Worcestershire, UK). The zeta potential was determined from the direction and velocity of the molecules in the applied electric field. The Smoluchowski model

was used by the software to convert the electrophoretic mobility measurements into zeta potential values. All the samples were diluted to about 0.05 % (w/v) and then put into a disposable folded capillary cell (DTS1060) to measure the zeta potential. The temperature of the cell was maintained at 25 ^{o}C. The data presented are the average values of three individual measurements.

5.3.4 "Table-top" rheology

Small volumes (7-8 mL) of freshly prepared GB/XG mixed solutions were transferred into 20 mL vials (Fisherbrand, O.D. × H (with cap): 28 x 61 mm) and kept at room temperature for 24 h. The vials were then inverted to qualitatively assess gel formation and strength.

5.3.5 Time-resolved small amplitude oscillatory shear

Freshly prepared GB, XG or GB/XG mixed solutions were directly poured into a rough surface Couette flow geometry (cup and bob diameters of 18.066 mm and 16.66 mm, respectively) and measurements were performed using a stress-controlled Physica MCR 501 rheometer (Anton Paar, Graz, Austria). Before the time sweep tests, all systems were heated at a rate of 5 °C/min up to 60 °C. The samples were kept at this temperature for 10 min to erase the previous thermal histories and were subsequently cooled down to 20 °C at a rate of 5 °C/min. Dynamic time sweep measurements were performed at 1 rad/s and 20 °C in the LVE regime (strain = 3 %) for 8 h. The elastic modulus *(G'*), loss modulus (*G"*), and related complex viscosity (|η*|) were recorded as functions of time. Samples were covered with a thin film of low viscosity mineral oil to prevent water evaporation. The oil was shown not to affect the rheological measurements. The experiments were performed at least twice with good reproducibility (< 5 %). The results of L-GB solutions alone in the investigated concentration range (0.2 - 2.0 %, w/v) and of H-GB at concentrations less than 1.0 % w/v were too low and noisy to be reported.

5.3.6 Confocal laser scanning microscopy (CLSM)

CLSM observations of the GB/XG solutions were performed with an Olympus IX 81 inverted Confocal Microscope (Olympus Canada Inc., Richmond Hill, ON, Canada). GB was stained with Nile Blue A (N0766, Sigma) in solution under magnetic stirring for 30 min before mixing with XG solutions. On the other hand, XG was covalently labeled with 5-(4,6-dichlorotriazinyl) aminofluorescein (DTAF) (D0531, Sigma) using a method described previously [12]. Preliminary

experiments showed that labeling did not change the rheological behavior of the solutions. After mixing, solution samples were poured into Petri dishes (P35G-1.5-14-C, MatTek), which were closed with cover slips and hermetically sealed with oil. Observation of XG was made by excitation of DTAF at 488 nm, the emission being recorded between 510 and 550 nm. Observation of GB was made by excitation of Nile Blue A at 633 nm, the emission being recorded between 650 and 680 nm. Micrographs were taken using a 60x objective lens at a 2048 x 2048 pixels resolution. All micrographs were subsequently analyzed using Image J software. To calculate the average size of GB-poor domains, at least 10 small bright regions (50 x 50 μm) from no less than 2 different CLSM images for each sample were selected. Brightness and contrast were adjusted to make GB-poor domains clearer, and the micrographs were then transformed into 8-bit binary images. A median filter was used to remove noise and smooth contours. By modeling GB-poor domains as cylinders, an average diameter value corresponding to a microstructure length scale could be obtained [16-18]. The calculation method is briefly described next [12].

The specific interfacial area, *S*, between GB-rich domains and GB-poor domains is first given by

$$S = \frac{P}{A} \quad (1)$$

where *P* is the interfacial perimeter between GB-rich and GB-poor domains (obtained by image analysis), and *A* is the micrograph area. The average diameter *d* of GB-poor domains is then obtained as follows:

$$d = \frac{4\Phi_{GB-poor}}{S} \quad (2)$$

where $\Phi_{GB\text{-}poor}$ is the volume fraction of GB-poor domains in solution, also obtained by image analysis (because of microstructure isotropy, the GB-poor domains surface fraction on the micrographs is taken equal to the volume fraction in solution).

In this work, GB-rich domains can also be referred to as biopolymer-rich domains since XG and GB are mixed at pH close to the pI of GB, where strong complexation occurs.

5.3.7 Micro-differential scanning calorimetry (Micro-DSC)

Micro-DSC experiments were performed on a micro-calorimeter (Microcal Inc., Northampton, MA, US) with a cell volume of 0.520 mL and under an external pressure of 180 kPa. The samples were first degassed using a bath sonicator (FS110, Fisher Scientific, Pittsburgh, PA, US) operated

at 135 W for 30 min while heating (final temperature ≈ 80 ºC), and were then injected into the sample cell and kept at 90 ºC for 15 min to remove any effects of thermal history. The samples were subjected to cooling and heating cycles over a temperature range of 10-90 ºC at a rate of 1 ºC/min. The sample cell was cleaned by a continuous flow of hot deionized water after each experiment followed by a water-water baseline test to ensure there was no contamination of the sample cell. The experimental data were analyzed using the Origin-based software provided by the manufacturer. The transition temperatures were taken at the transition peaks maxima, and the transition enthalpies were determined from the area of the endothermic or exothermic peaks.

5.4 Results and discussion

5.4.1 Zeta potential of GB and XG

Figure 5.1 shows the zeta potential values of all GB and XG grades. The isoelectric point (pI) of L-GB is around 5.2-5.3, which is higher than that of H-GB (≈ 4.9) (**Figure 5.1a**). The values agree with those reported in the literature [19, 20], and both GB grades show positive zeta potential at pH below the pI, while negative values are exhibited above the pI, indicating a change of the overall charge.

Consistent with literature [13], the different XG grades show no significant difference in zeta potential values **(Figure 5.1b**): a strong negative dependency of zeta potential on pH occurs over the range of pH 3.5-5.0. This is due to the deprotonation of -COOH groups with increasing pH, and is followed by a plateau after deprotonation is complete. Note that the data for R-XG were reported in our previous work [12].

a)

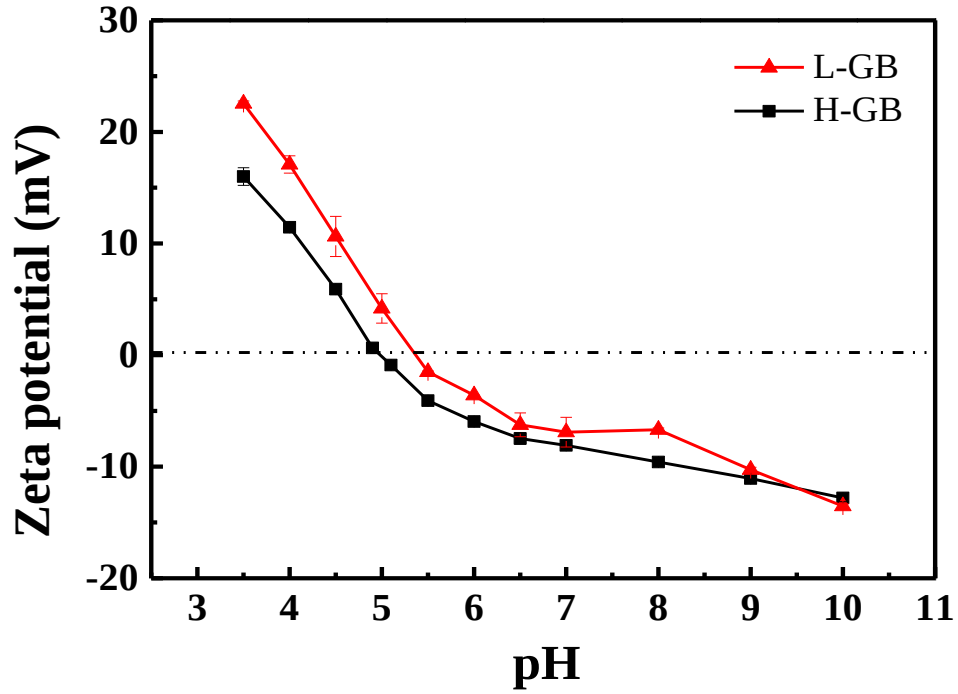

b)

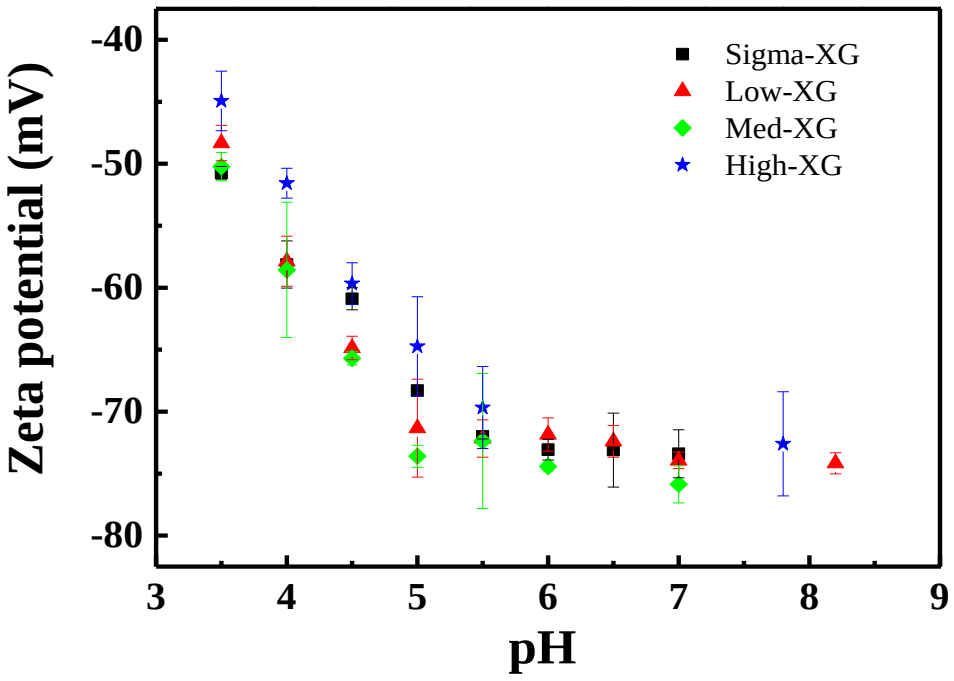

Figure 5.1 Zeta potential values of the GB (a) and XG (b) grades used in this work.

5.4.2 "Table-top" rheology

The effects of pH, GB concentration, GB Bloom index and XG molecular weight on the visual aspects of the GB/XG mixed gels are exhibited in **Figure 5.2**. The properties of GB/XG mixed gels are primarily controlled by a delicate charge balance and are therefore affected by pH and GB concentration. At a given XG concentration, increasing the GB content decreases the charge density of XG due to complexation, which favors the eventual formation of a network. However, the GB content should be carefully controlled to avoid low XG charge densities, which may reduce stability and lead to aggregate formation. For example, L-GB/R-XG mixed gels become more elastic with increasing L-GB concentration and as shown in **Figure 5.2a**, they exhibit self-supporting properties at L-GB concentrations between 1.0-1.6 % w/v. At 2.0 % w/v L-GB, the system loses its self-holding ability. The decrease in gelation properties is not observed by "table-top" rheology when the GB concentration is close to the critical gelling concentration, as indicated by H-GB/R-XG mixed gels (**Figure 5.2b**). Here the gels become firmer with increasing H-GB concentration at a given pH.

Similarly, at a pH below the pI of GB, positively charged GB can interact strongly with negatively charged XG. This results in phase separation via the formation of insoluble complexes. At a pH equal to or above the pI of GB, complexation decreases, which makes network formation unlikely. In other words, an optimal pH exists to obtain the strongest gelation properties. For example, see the results for L-GB/R-XG [12], H-GB/R-XG in **Figure 5.2b**, and L-GB/Low-, Med-, High-XG mixed gels in **Figure 5.2c**.

The "table-top" rheology (**Figure 5.2c**) indicates that the elastic properties decrease with increasing XG molecular weight. These results also show that a synergistic gelation effect occurs since the critical gelling concentration is much lower for the mixture ($c_{L\text{-}GB}$ = 1.0-1.6 % w/v and $c_{H\text{-}GB} \geq 0.4$ % w/v) than for GB alone ($c_{crit} \approx 4.0$ % w/v for L-GB and $c_{crit} \approx 2.0$ % w/v for H-GB).

a)

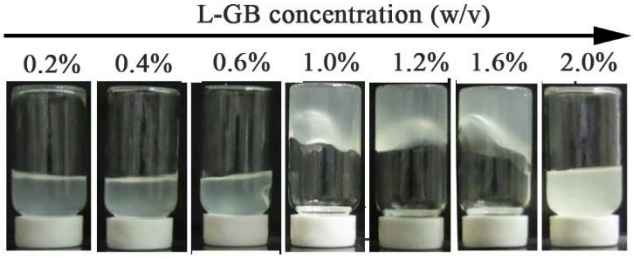
L-GB concentration (w/v)
0.2%
0.4%
0.6%
1.0%
1.2%
1.6%
2.0%

b)

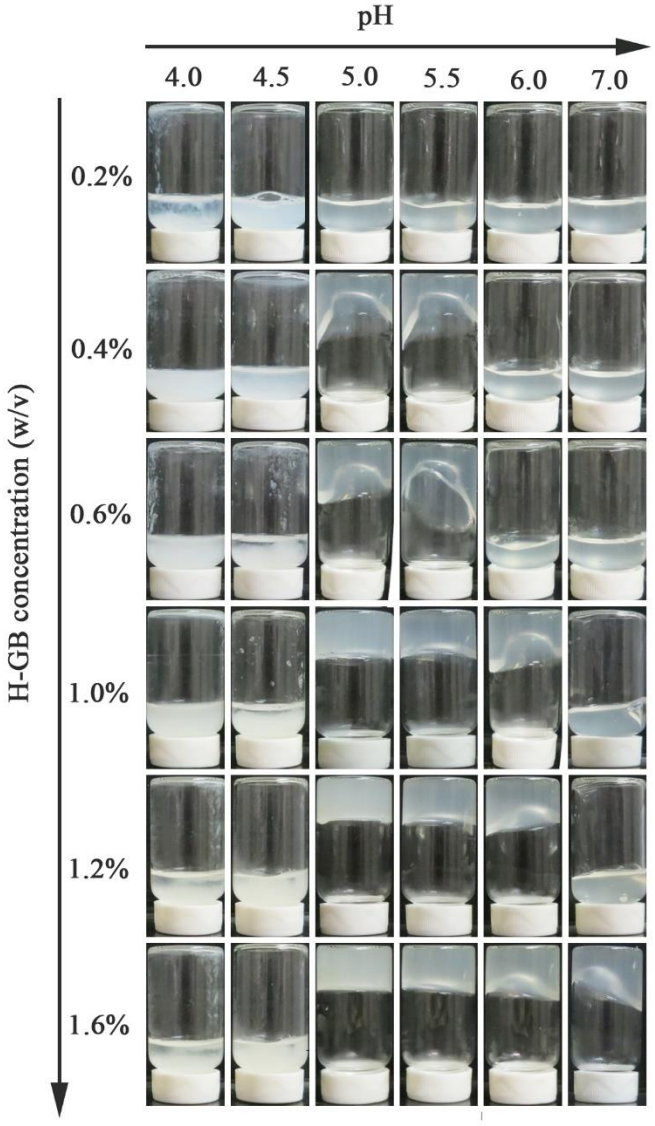
pH
4.0
4.5
5.0
5.5
6.0
7.0
H-GB concentration (w/v)
0.2%
0.4%
0.6%
1.0%
1.2%
1.6%

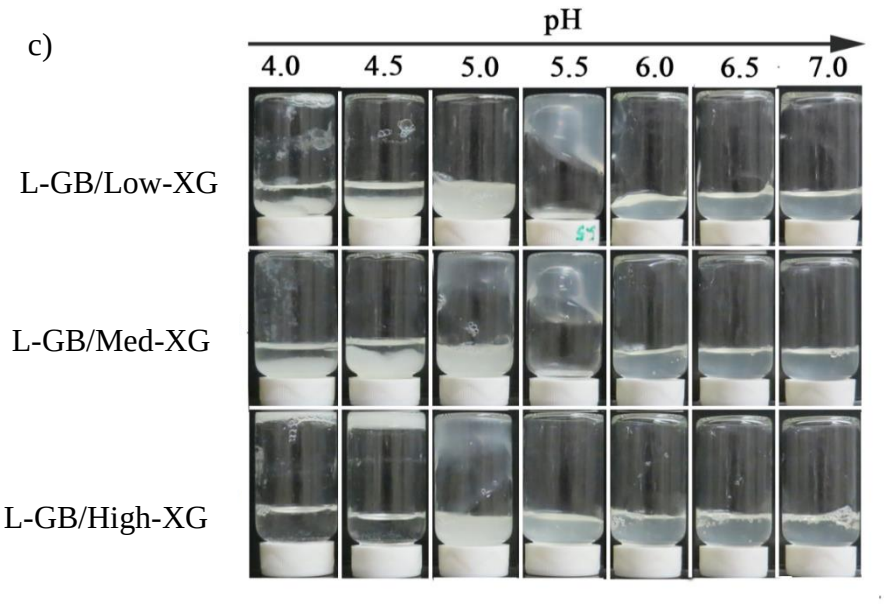

Figure 5.2 a) Effect of L-GB concentration (c_{GB} = 0.2-2.0 % w/v) on the visual aspect of L-GB/R-XG aqueous mixtures, at pH 5.5; b) effects of pH (4.0-7.0) and H-GB concentration (c_{GB} = 0.2–1.6 % w/v) on the visual aspect of H-GB/R-XG mixtures, H-GB/R-XG ratio = 1-8; c) effects of pH (4.0-7.0) and XG molecular weight on the visual aspect of L-GB/XG mixtures (L-GB:XG ratio = 6, c_{XG} = 0.2 % w/v). The photos were taken after overnight storage.

5.4.3 Time-resolved small amplitude oscillatory shear

The effects of L-GB concentration and XG molecular weight on the time-dependent rheological properties of GB/XG mixtures were evaluated by dynamic time sweep tests, and the results are presented, respectively, in **Figures 5.3** and **5.4**. The elastic modulus (*G'*) of the XG solution is almost constant in time and always less than the values of the mixtures. The LVE properties of the L-GB solutions are below the resolution limit of our instrument and are therefore not reported. Mixing GB and XG significantly enhances the rheological properties and endows the system with time-dependent properties. In addition, *G'* is always higher than *G"* for these GB/XG mixtures after 8 hrs (**Figures 5.3b** and **5S2**), showing a soft solid-like behavior.

The *G'* of the mixtures initially increases rapidly followed in most cases by a slow rise, as shown in **Figures 5.3a**, **5.4** and **5S2**. The elastic modulus after 8 hrs (G_{8h}') increases significantly for the mixtures containing H-GB as compared to those containing L-GB (compare **Figures 5.3** and **5S2**)

but decreases as XG molecular weight increases (**Figure 5.4**). Note that we observe the inverse effect of XG molecular weight on the initial *G'* (at t = 0 s). The mixtures show a maximum *G'* at a certain GB concentration ($c_{L\text{-}GB}$ = 1.2 % w/v and $c_{H\text{-}GB}$ = 1.6 % w/v) and further increasing the GB content leads to a decrease in gelation properties. These results are coherent with the "table-top" rheology observations presented in section §5.2.

a)

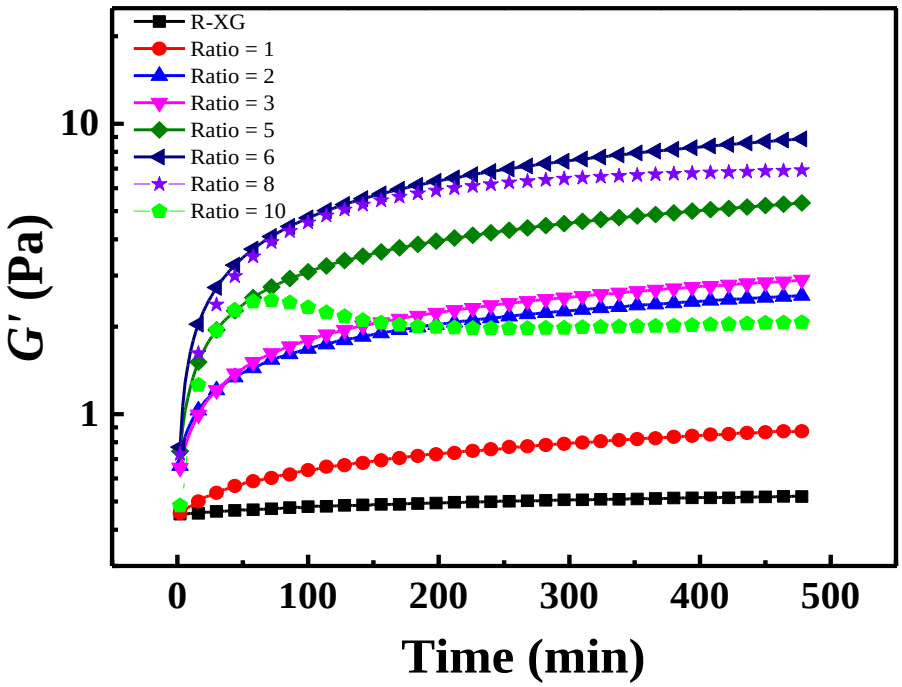

b)

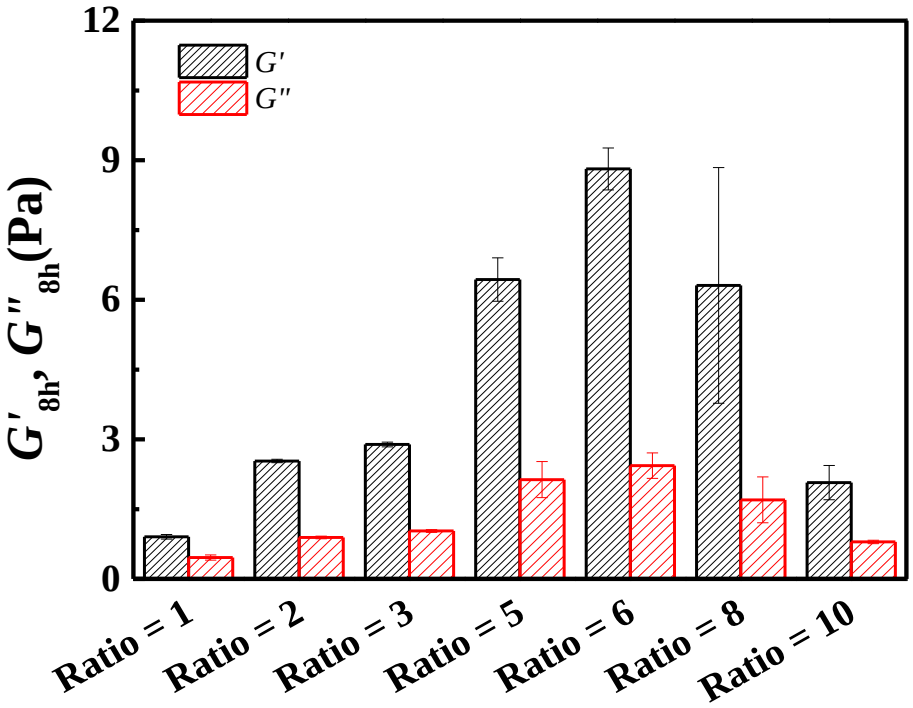

Figure 5.3 a) Evolution of *G'* as a function of time for the L-GB/R-XG mixtures at ratios (1-10), at pH 5.5; b) *G'* and *G"* after 8 hrs, as a function of L-GB/R-XG ratio. c_{XG} = 0.2 % w/v, ω = 1 rad/s.

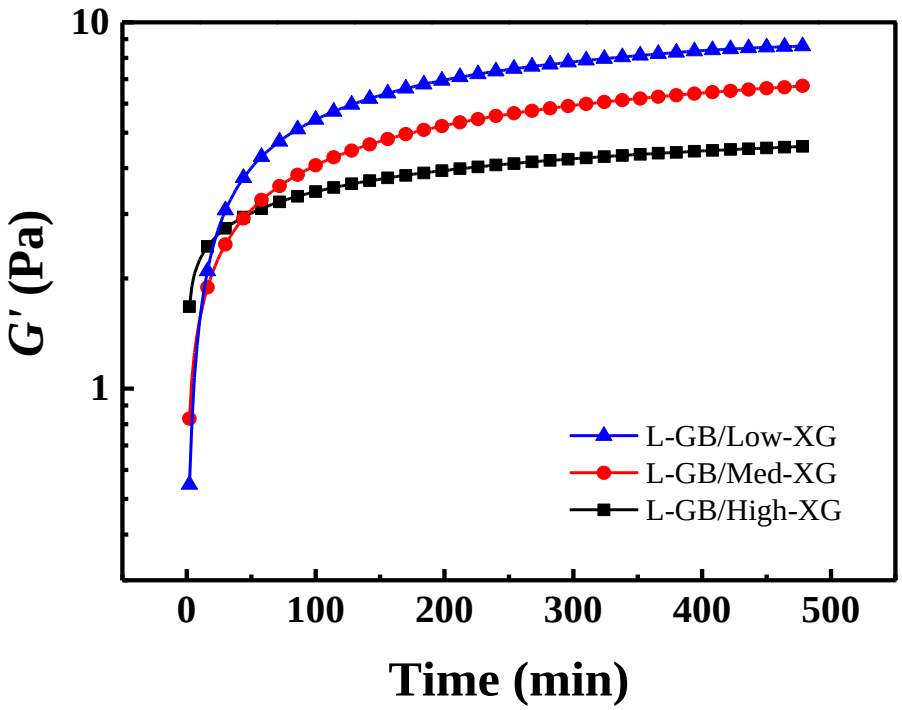

Figure 5.4 *G'* as a function of time, for the mixtures of L-GB and Low-XG, Med-XG and High-XG respectively, at ratio 6 and pH 5.5. XG concentration = 0.2 % w/v, ω = 1 rad/s.

The ratios of the G_{8h}' of H-GB/R-XG mixtures, to the sum of the G_{8h}' of neat H-GB and R-XG solutions at the concentrations in the corresponding mixtures, were calculated to better evaluate the synergistic effects and are presented in **Figure 5.5**. This ratio is 22.2 at a GB/XG ratio of 5 (c_{GB} = 1 % w/v and c_{XG} = 0.2 % w/v), and decreases exponentially as GB concentration increases, clearly showing a weakening synergistic effect when the ratio ≥ 5. The H-GB/R-XG mixture even shows a lower G_{8h}' than H-GB alone at ratio GB/XG ratio of 10, showing antagonist or detrimental gelation properties.

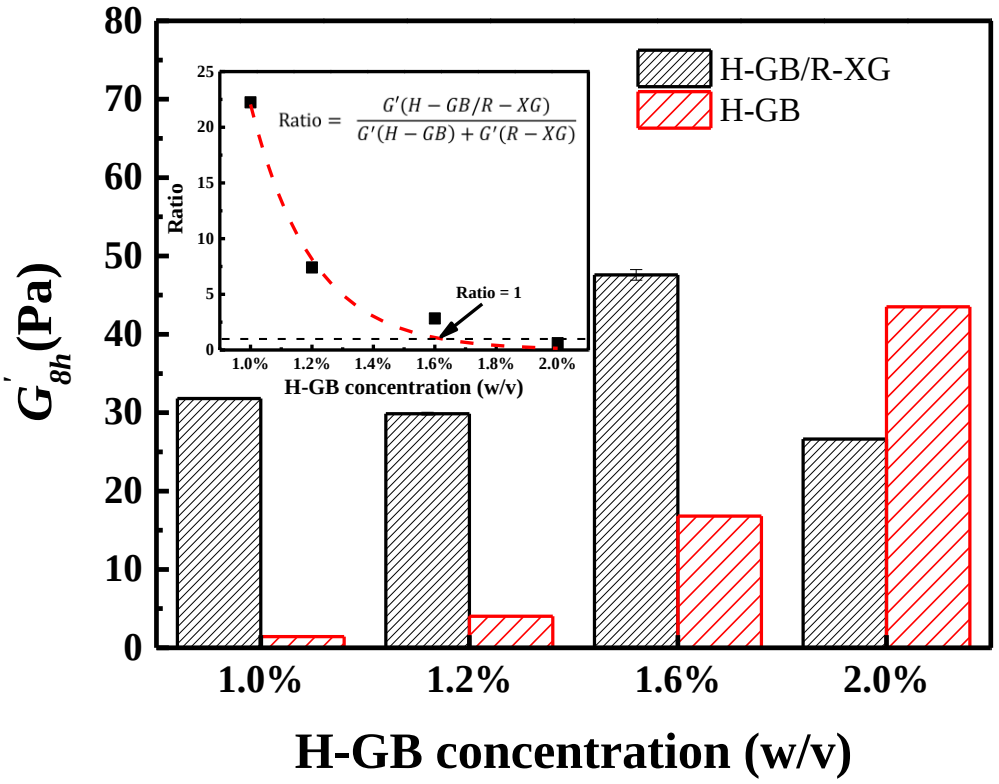

Figure 5.5 Comparison of G_{8h}' of H-GB solution with and without R-XG after 8 hrs in the rheometer at 20°C, ω = 1 rad/s, c_{XG} = 0.2 % w/v. The insert shows the ratio of the G_{8h}' of H-GB/R-XG mixtures over the sum of the G_{8h}' of neat H-GB and R-XG at concentrations in the corresponding mixtures, as a function of H-GB concentration.

In the next section, confocal laser scanning microscopy is employed to analyze the microstructure of the mixtures.

5.4.4 CLSM

Figure 5.6 shows a set of images for L-GB/Sigma-XG mixtures at different ratios, while **Figure 5.7** exhibits the effect of XG molecular weight on L-GB microstructure. The microstructure of GB/XG mixed gels generally consists of biopolymer-rich and biopolymer-poor domains. In comparison, neat GB and XG solutions at similar concentrations have no visible structure and appear homogeneous (images not shown). Both GB and XG exhibit a composition-dependent

structural transition in mixed gels. GB has a discontinuous agglomerated morphology at low GB content ($c_{GB} \leq 0.2$ % w/v); a continuous network structure at intermediate GB content followed by a fragmented network structure at high GB content ($c_{L\text{-}GB} = 1.6$ % w/v and $c_{H\text{-}GB} = 2.0$ % w/v). This is seen in the left column of **Figures 5.6**, **5.7**, **5S4** and **5S5**. No XG structure is observed at GB concentrations of 0.2-0.6 % w/v, but a network structure appears when the GB concentration ≥ 1.0 % w/v (middle column of **Figures 5.6** and **5S4**). In this composition range the biopolymer-rich domains consists of GB-rich domains colocalized with XG-rich domains (right column of **Figures 5.6**, and **5S4**). For the systems with GB/XG ratios of 5 and 6 we observe significant XG content in the biopolymer-poor domains whereas at higher ratios most of the XG appears to be colocalized with the GB-rich domains. The biopolymer-rich domains first decrease in size (up to ratio 6) and then grow again (ratio ≥ 8) with increasing GB concentration. As we reported previously, the XG network disappears when increasing pH to 7.0 (**Figure 5S5**), probably due to the stronger electrostatic repulsion between the molecules [12].

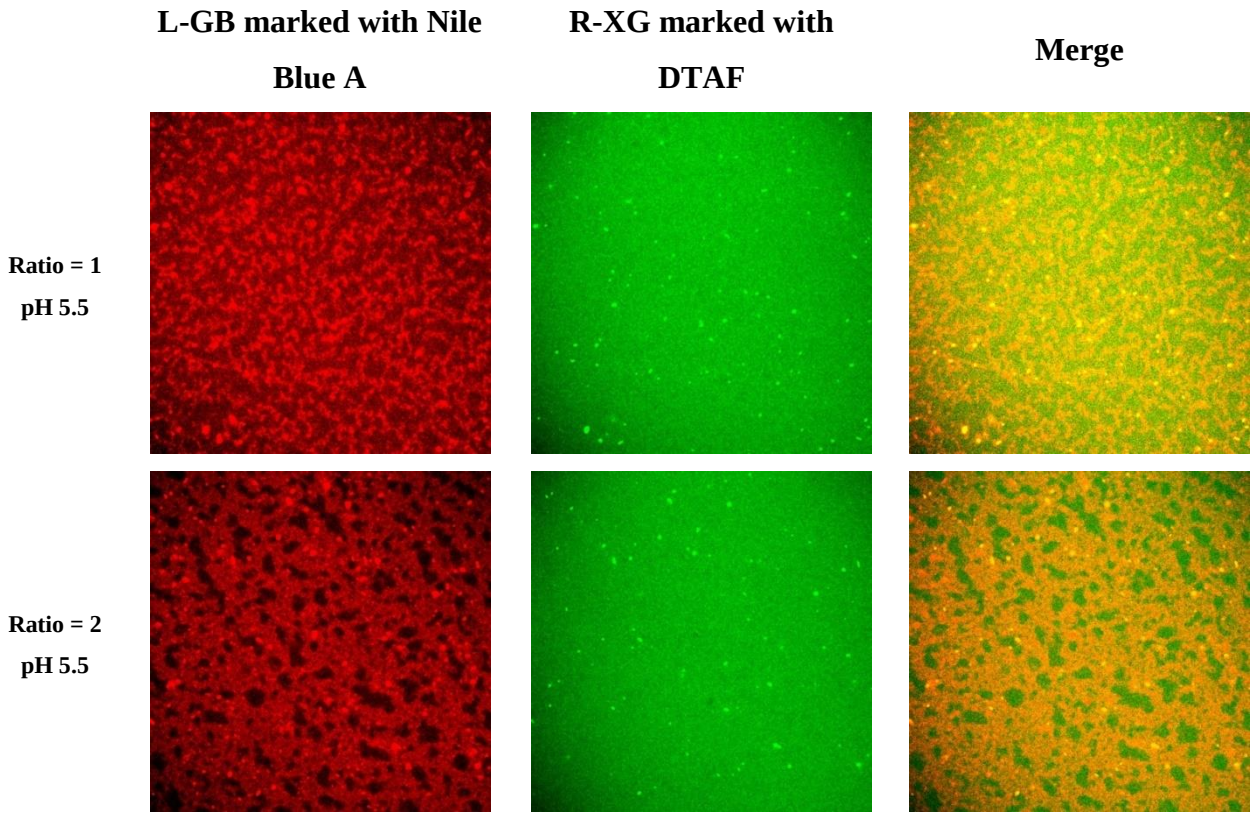

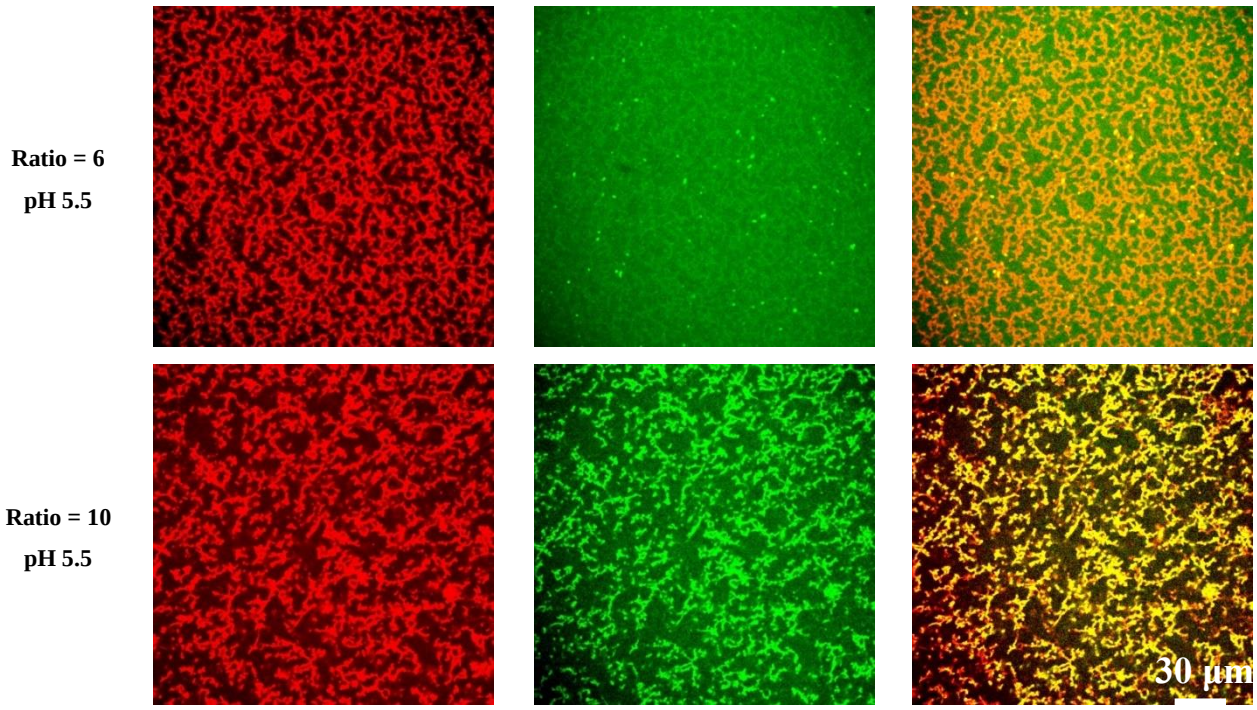

Figure 5.6 Microstructures of L-GB (red) and R-XG (green) domains in the mixtures at different ratios (1, 2 6 and 10) and merge of the two imaging, at pH 5.5. The images were taken after storage for 24 hrs. Image size: 210 µm x 210 µm.

Increasing GB Bloom index leads to much finer microstructures (compare **Figures 5.6** and **5S5**), whereas increasing XG molecular weight reduces the connectivity of the co-localized networks at ratio 6, finally leading to a granular microstructure (L-GB/High-XG) (**Figure 5.7**).

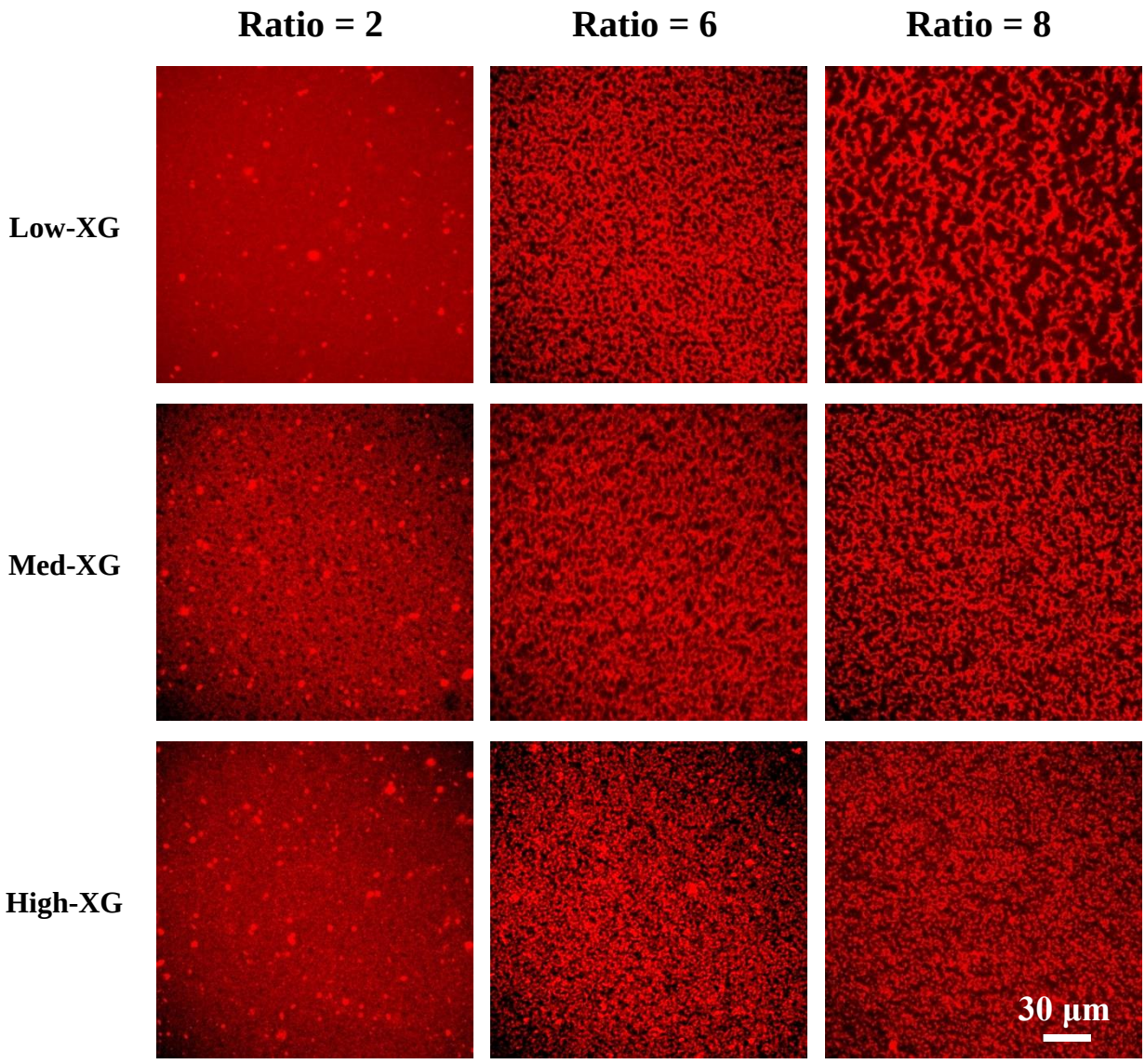

Figure 5.7 Microstructure of L-GB (red) when mixed with Low-XG, Med-XG and High-XG, respectively, at different ratios (2, 6, and 8) and pH 5.5. The images were taken after storage for 24 hrs at room temperature. Image size: 210 µm x 210 µm.

By modeling biopolymer-poor domains as cylinders, an average diameter value $d_{biopolymer\text{-}poor}$ can be calculated, corresponding to a characteristic microstructural length scale [12, 16-18]. The results are shown in **Figure 5.8**. The average size of biopolymer-poor domains increases with GB content. The biopolymer-poor domain size is always higher for L-GB/R-XG gels as compared to that of H-GB/R-XG gels.

a)

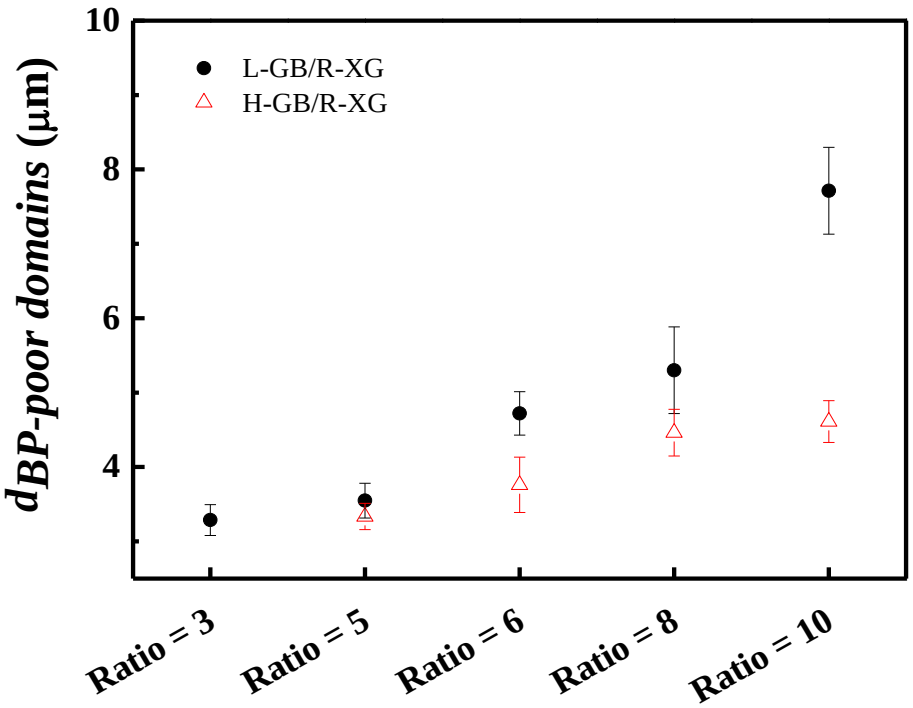
10
8
6
4
$d_{BP\text{-}poor\ domains}$ (μm)
L-GB/R-XG
H-GB/R-XG
Ratio = 3
Ratio = 5
Ratio = 6
Ratio = 8
Ratio = 10

b)

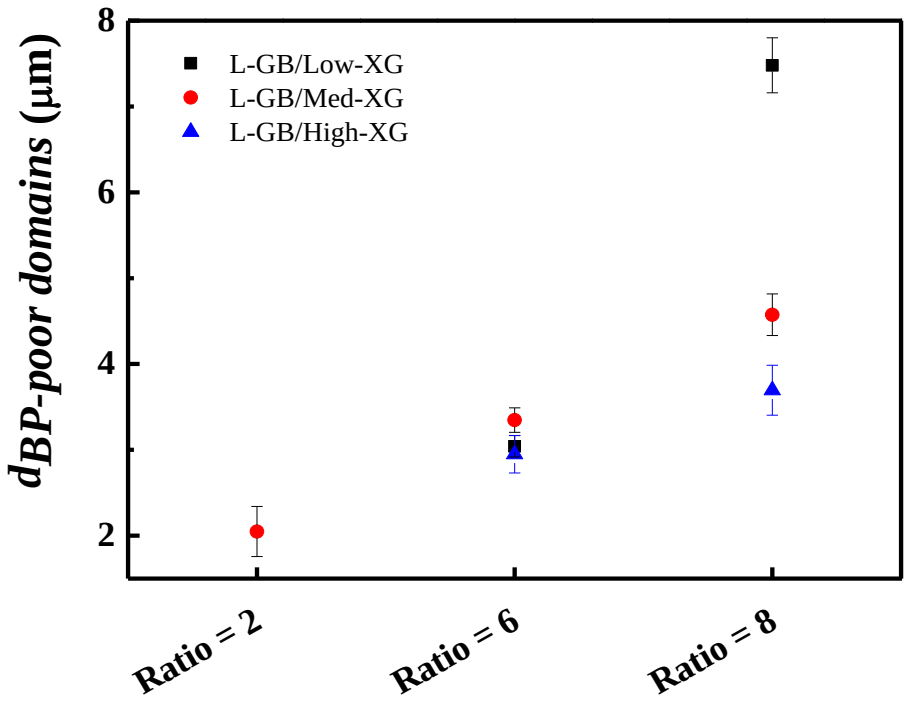

Figure 5.8 a) Average size of biopolymer-poor (BP-poor) domains in L-GB/R-XG and H-GB/R-XG mixtures, as a function of GB/R-XG ratio; and b) average size of biopolymer-poor domains in L-GB/Low-XG, L-GB/Med-XG and L-GB/High-XG mixtures, as a function of L-GB/XG ratio.

5.4.5 Micro-DSC

Micro-DSC is a powerful technique to study the helix-to-coil (order-to-disorder) transition of polysaccharides and proteins, such as XG [21-24], DNA [25, 26], carrageenan [27, 28] and gelatin [29, 30]. Here, micro-DSC was used to study the R-XG and L-GB conformation transitions in L-GB/R-XG mixtures, shedding more light on the gelation mechanism.

As shown in **Figure 5.9**, the R-XG solution at 1.0 % w/v exhibits two peaks located at 35.6 (T_2) and 52.3 ^{o}C (T_3) in the heating cycle. The second peak is consistent with the transition temperatures of 52 ^{o}C observed by Pelletier et al [24] and ~50 ^{o}C observed by Fitzsimons et. al [22]. This peak is therefore attributed to the XG order-to-disorder (helix-to-coil) transition upon heating [21-24]. The reason for the first peak remains unknown, but it is likely related to impurities in the XG sample, as discussed at the end of this section.

L-GB at 1 % (**Figure 5.9**) exhibits a peak located at 23.5 ºC attributed to the gelatin helix-to-coil transition [29-31].

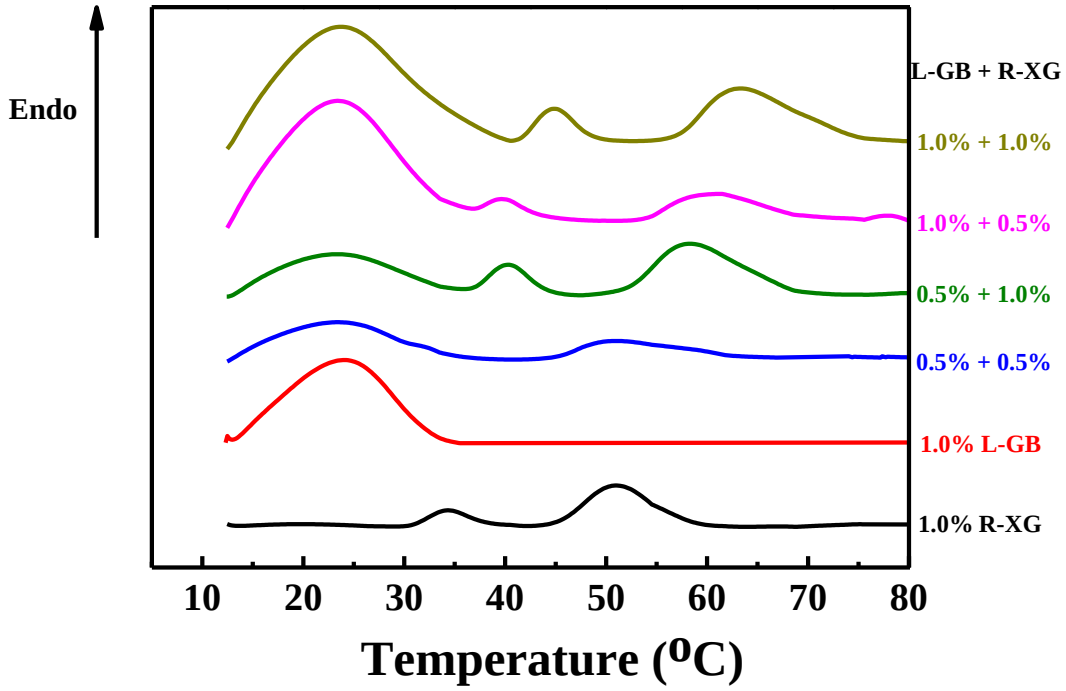

Figure 5.9 Micro-DSC heating curves, shifted vertically for clarity. Scanning rate = 1 ºC/min.

Table 5.1 Specific enthalpies and transition temperatures (peak maximum) of L-GB, R-XG and their mixtures during the second micro-DSC heating segment.

			Peak 1		Peak 2		Peak 3	
GB (%)	XG (%)	GB/XG ratio	T_1 (°C)	ΔH_1^a (J/g)	T_2 (°C)	ΔH_2^b (J/g)	T_3 (°C)	ΔH_3^b (J/g)
0.5	1.0	0.5	23.3	5.74	40.3	0.34	58.3	2.66
0.5	0.5	1	23.4	4.91	-	-	51.0	2.06
1.0	1.0	1	23.7	8.64	45.0	1.09	63.3	2.99
1.0	0.5	2	23.4	8.02	39.6	0.82	61.3	2.52
0	1.0	-	-	-	35.6	0.49	52.3	1.54
1.0	0	-	23.5	5.03	-	-	-	-
2.0	0	-	23.6	7.78	-	-	-	-

a: normalized by the mass of GB;

b: normalized by the mass of XG;

The mixtures (**Figure 5.9**) exhibit three peaks: peak 1 corresponds to L-GB and peak 2 and 3 to R-XG. When R-XG concentration is 1.0 % w/v, the two peaks of the R-XG shift to higher temperatures in the presence of L-GB as compared to those of neat R-XG. The enthalpy of XG also increases with increasing L-GB concentration (**Table 5.1**). At a XG concentration of 0.5% w/v, peak 2 is no longer visible. These features indicate that more stable XG microstructures are formed with the help of GB. This phenomenon is due to the neutralization of XG molecules after complexation with GB, which then promotes the formation of the XG ordered structure. Furthermore, the enthalpy of L-GB increases in the presence of R-XG. The enthalpy values of 1.0 % w/v L-GB in the mixtures are even higher than that of 2.0 % w/v L-GB alone (**Table 5.1**). This suggests that XG also enhances or promotes L-GB gelling by triple helix formation.

Note that clarified XG and its mixtures with L-GB were also studied, and they exhibit similar results except that there is only one peak instead of two for the neat clarified XG, and two peaks rather than three for the mixtures (see **Figure 5S7**).

5.4.6 Proposed synergistic gelation mechanism

XG molecules are known to undergo a disorder-to-order (coil-to-helix) transition in response to charge screening and/or temperature decrease. The XG backbone takes on a helical conformation and the trisaccharide side chains collapse onto the backbone and stabilize the ordered conformation [32-34]. Weakly associated XG aggregates can subsequently form side-by-side associations between neighboring ordered regions, which gives a tenuous network structure and endows XG dispersions with a weak "gel-like" behavior [23, 35, 36]. Based on the properties of XG, the results above and previous observations [12], a mechanism is proposed to explain the synergistic gelation behavior displayed by GB/XG mixtures (**Figure 5.10**).

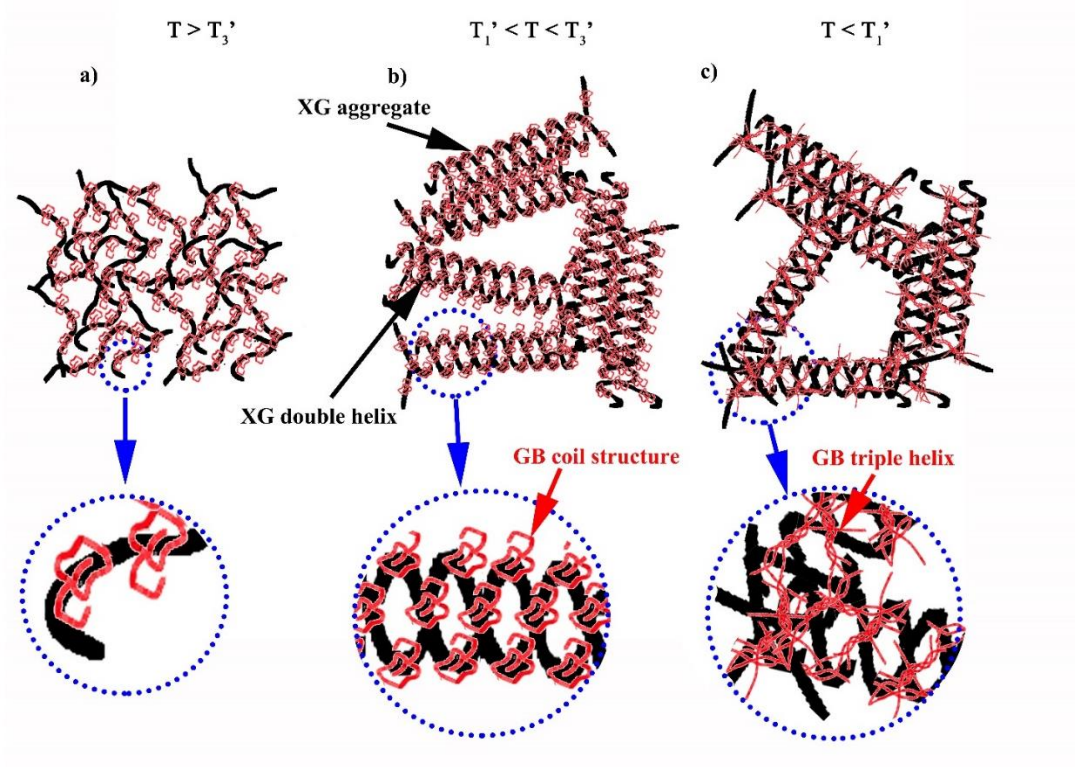

Figure 5.10 Proposed gelation mechanism in GB/XG mixtures, based on their interactions and molecular conformations.

When mixing the two biopolymers in aqueous solution near the pI of GB, and above the coil-to-helix transition temperature of XG (represented by T_3'), the electrostatic attraction between the negative charges of XG and the positive patches of GB gives rise to soluble GB/XG complexes (**Figure 5.10a**). This complexation decreases the XG charge density. When the temperature is in-

between T_3' and T_1' (representing the coil-to-helix transition of GB), the soluble complexes assemble into interpolymer complexes in the form of XG ordered structures (**Figure 5.10b**). Since factors that stabilize the ordered structure also favor the formation of XG aggregates [57,68], it is reasonable to say that large scale assemblies of interpolymer complexes stabilized by GB are also formed under these conditions through side-by-side associations between the ordered XG domains. The local concentrations of both GB and XG are therefore increased. When the system is cooled down below *T_1'*, GB triple helix formation occurs, promoted by its enhanced local concentration. With time, GB/XG interpolymer complexes and aggregates concentrate locally in space and become linked together due to GB gelling (**Figure 5.10c**). This finally results in a percolated network of biopolymer-rich domains, explaining the observed increase in *G'* of GB/XG mixtures with time (**Figure 5.3**, **Figure 5.4** and **Figure5 S2**). When the network is heated again, the system first goes through the helix-to-coil transition of GB (*T_1* in **Table 5.1**), then through the helix-to-coil transition of XG (*T_3* in **Table 5.1**), since the process is reversible.

The proposed mechanism is further supported by a rheological temperature sweep (**Figure 5.11**). Starting at 20 °C, when the temperature increases, we can clearly observe the helix-to-coil transition in the 4.0 % L-GB system at ~25 °C, while no such features are evident in the case of 0.2 % w/v R-XG due to the low concentration. However, we do see the helix-to-coil transition at around 52 ^{o}C if increasing R-XG concentration to 1 % w/v (**Figure 5S8**), which is well consistent with micro DSC results (**Figure 5.9** and **Table 5.1**). For the mixture, we observe the helix-to-coil transition of the GB at just above 25 °C with the characteristic drop in the *G'*. This demonstrates that the viscoelastic properties of the GB/XG gels, are mainly the result of the GB network up to about 30 °C.

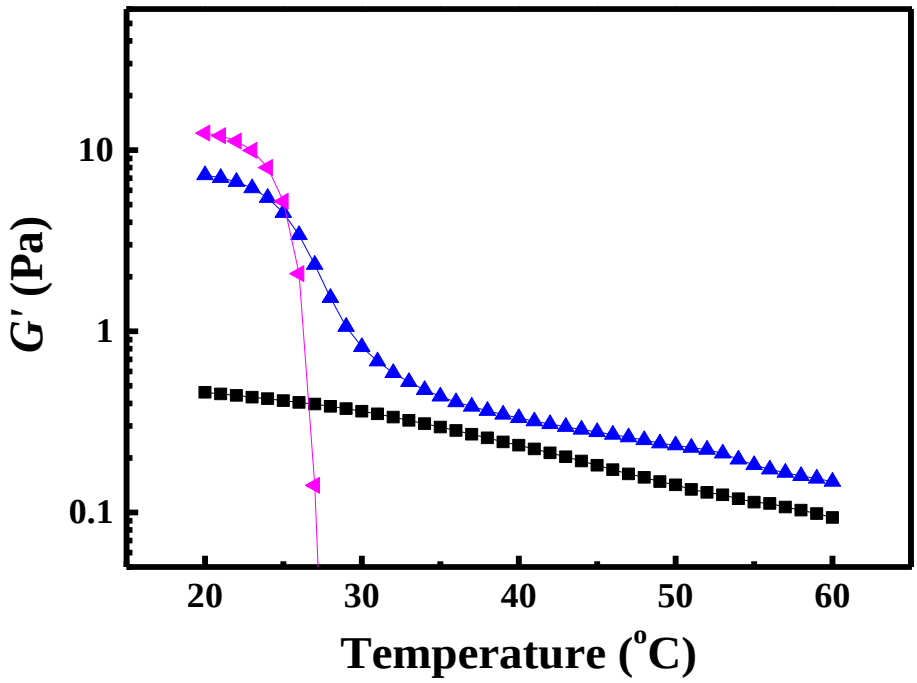

Figure 5.11 Evolution of *G'* during heating of three systems: (◀) L-GB = 4.0 % w/v, (▲) L-GB/R-XG = 6, total concentration = 1.4 % w/v and (■) R-XG 0.2 % w/v. Heating rate: 0.2 °C/min

5.5 Conclusions

A gelation mechanism is proposed for gelatin B (GB)/xanthan gum (XG) aqueous mixtures. Soluble GB/XG complexes form near the isoelectric point of GB, above the coil-to-helix transition temperature of XG, followed by a disorder-to-order transition of XG due to the GB neutralization effect when the temperature is in-between the coil-to-helix transition temperature of XG and GB. The two biopolymers are locally concentrated due to the formation of large scale assemblies of interpolymer complexes stabilized by GB, and once cooled below the transition temperature of GB, a network composed of biopolymer-rich domains forms and develops over time. Increasing GB concentration favors the disorder-to-order transition of XG by decreasing its charge density - however, too low XG charge density destabilizes the system and results in aggregation. Therefore, the GB/XG ratio must be carefully controlled to maintain the network structure and the gelation properties. Stronger interactions between GB/XG interpolymer complexes when cooling down

leads to a faster initial evolution and higher *G'*, as well as a denser network. Increasing the XG molecular weight decreases the mobility of soluble and/or interpolymer complexes, which then weakens the concentrating effect and resulting gel properties. We are now currently investigating if this mechanism applies to other protein/polysaccharide systems. This work brings a fundamental understanding to the effects of proteins and polysaccharides interactions in solutions, and provides important guidelines to design novel thickeners and/or gelling agents, encapsulation and delivery systems.

5.6 Acknowledgements

The authors acknowledge Dr. Nicolas Tran-Khanh from École Polytechnique de Montréal for performing the CLSM observations, Dr. Françoise M. Winnik from University of Montreal for allowing us to use her micro-DSC, Dr. Evgeniya Korchagina from University of Montreal for her help using micro-DSC and useful discussions, Ms Helia Sojoudiasli from École Polytechnique de Montréal for useful discussions and Dr. Ross Clark from CP Kelco U.S., Inc for providing the XG samples. The authors also thank the Natural Sciences and Engineering Research Council of Canada (NSERC) and CREPEC for financial support, and the China Scholarship Council (CSC) for providing a scholarship to Mr. Wang.

5.7 Supporting Information

Figure 5S1 shows the shear rate dependence of the steady shear viscosity of XG solutions at a concentration of 0.2 % w/v. The steady shear viscosity differs significantly at low shear rates (≤ 10 s^{-1}), with High-XG having the highest viscosity, followed by (R-XG, Med-XG) and finally Low-XG. Low-XG shows a Newtonian plateau at shear rates below 0.1 s^{-1}, while the plateau appears at a lower shear rate (below 0.02 s^{-1}) for R-XG and Med-XG, and is not observed in the investigated shear rate range for High-XG. After the Newtonian plateau, the steady shear viscosity of all grades decreases with increasing shear rate, demonstrating a pronounced non-Newtonian shear-thinning behavior: the viscosity decreases by 2-3 orders of magnitude from low to high shear rates. When at rest, XG microgels (XG aggregates) form in solution due to side-by-side associations between neighboring ordered regions, which gives a tenuous network structure and endows XG dispersions with a weak "gel-like" behavior [23, 35, 36]. The microgels are stabilized by hydrogen bonding, resulting in high viscosity at low shear rates or at rest [32]. However, high shear rates result in the

breakdown and deformation of XG microgels, leading to a decrease in steady shear viscosity [37]. This rheological feature enhances sensory qualities (mouth feel, flavor release) in food products, and makes XG easy to mix, pump and pour during processing and/or actual use despite its high molecular weight [32].

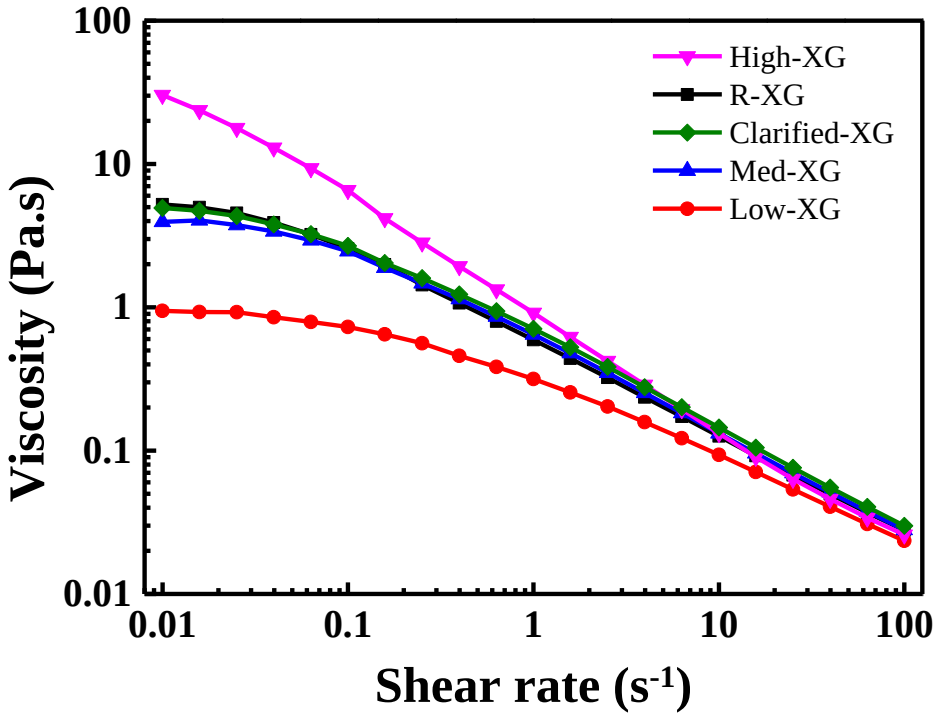

Figure 5-S1. Steady shear viscosity of different grades of XG in solution (c_{XG} = 0.2 % w/v).

a)

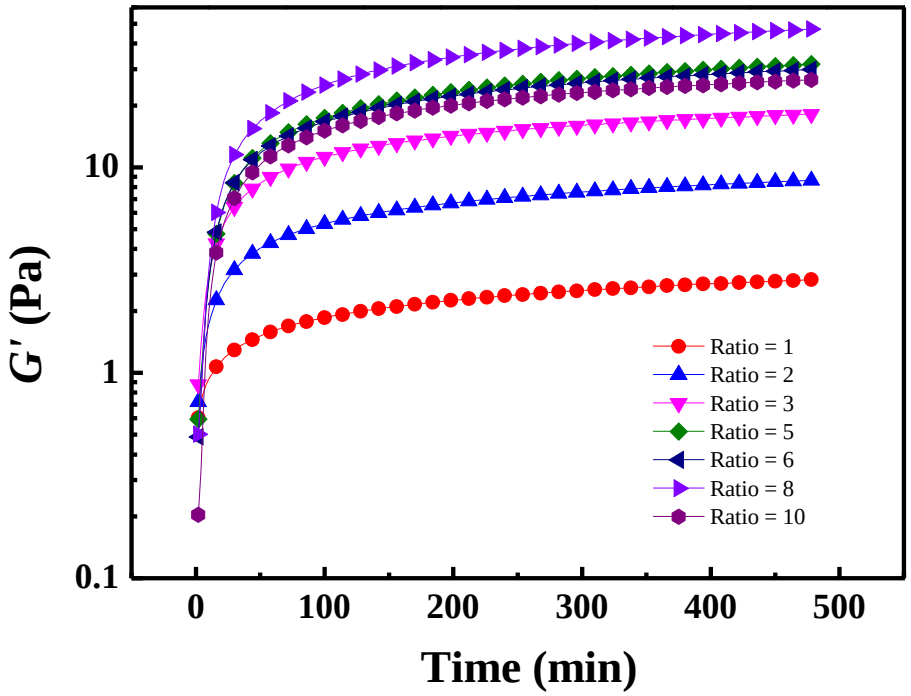
G' (Pa)
10
1
0.1
0
100
200
300
400
500
Time (min)
Ratio = 1
Ratio = 2
Ratio = 3
Ratio = 5
Ratio = 6
Ratio = 8
Ratio = 10

b)

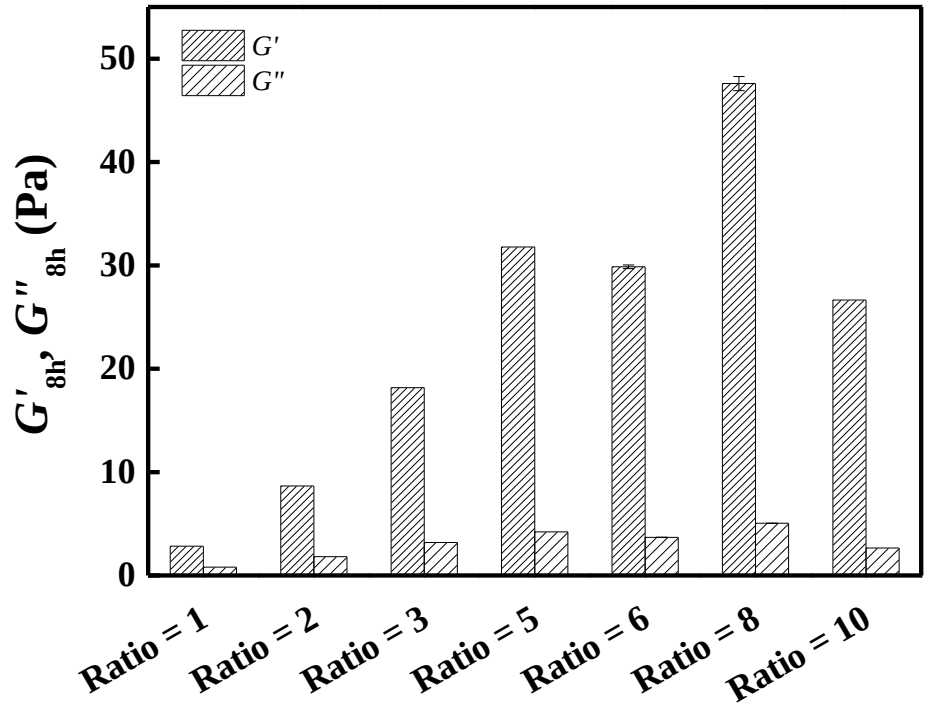

Figure 5-S2. a) Evolution of *G'* as a function of time for the H-GB/R-XG mixtures at ratios = (1-10) and pH 5.0; b) *G'* and *G"* after 8h, as a function of H-GB/R-XG ratio. c_{XG} = 0.2 % w/v, ω = 1 rad/s.

a)

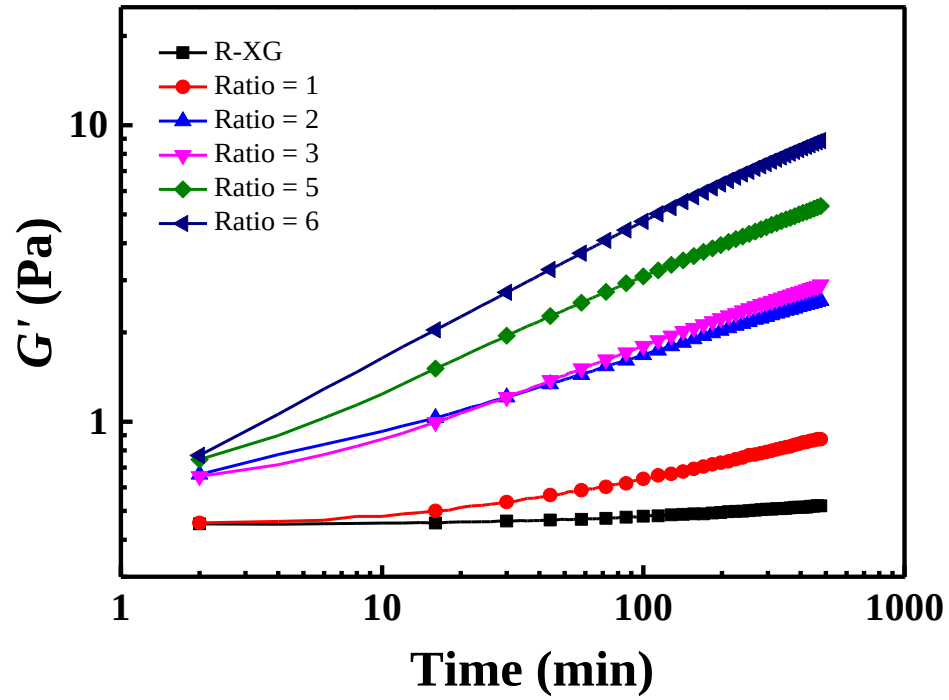
R-XG
Ratio = 1
Ratio = 2
Ratio = 3
Ratio = 5
Ratio = 6
G′ (Pa)
10
1
1
10
100
1000
Time (min)

b)

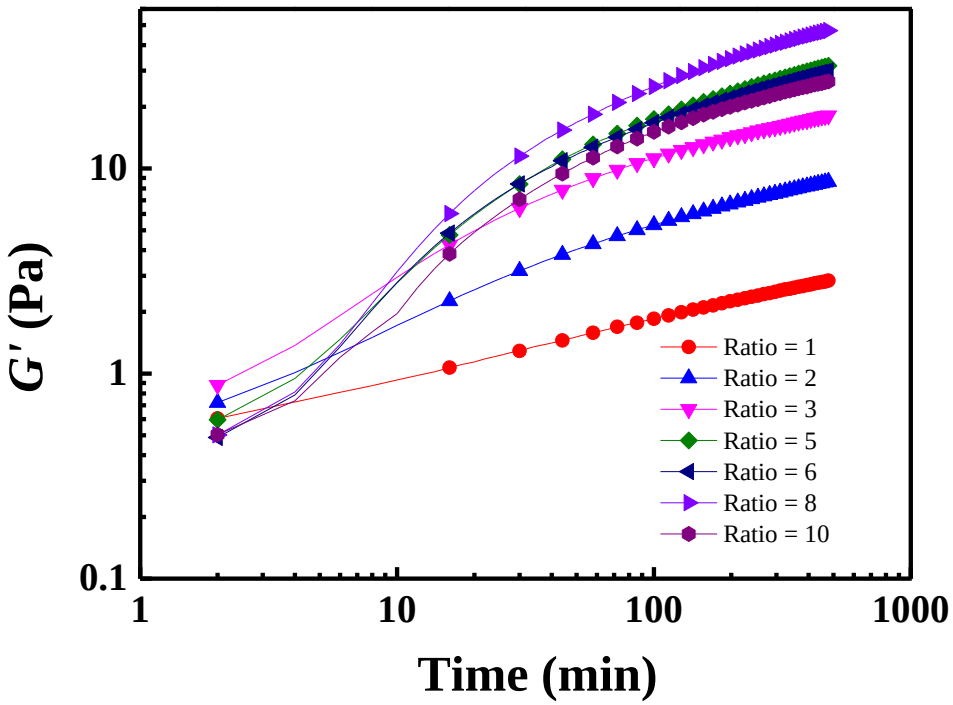
Ratio = 1
Ratio = 2
Ratio = 3
Ratio = 5
Ratio = 6
Ratio = 8
Ratio = 10
G′ (Pa)
10
1
0.1
1
10
100
1000
Time (min)

c)

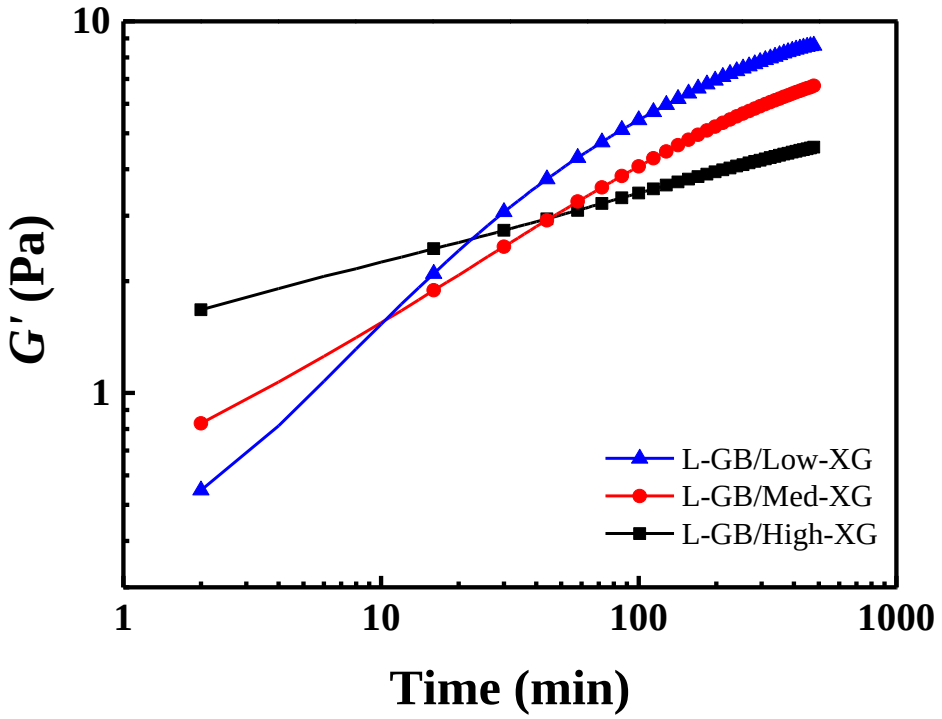

Figure 5-S3 *G'* as a function of time on a log-log scale, for a) L-GB/R-XG at pH 5.5, b) H-GB/R-XG at pH 5.0 at different ratios and c) L-GB and Low-XG, Med-XG and High-XG respectively, at ratio 6 and pH 5.5. XG concentration = 0.2 % w/v, ω = 1 rad/s.

Time sweep data show a transient regime (≤ 15 min) and a regime with a constant slope (> 15 min) on a log-log scale [12]. Modeling the second regime using a power-law function $\propto t^n$ (n corresponding to the slope on a (log G') vs. (log t) plot) shows that n increases with GB concentration (**Table 5S1**), which confirms the significant effect of GB on the time-dependent properties of the mixtures.

On the other hand, n decreases with increasing XG molecular weight (**Table 5S1**). Low viscosity XG most probably allows the molecules to diffuse more rapidly, resulting in increased intermolecular interactions, faster time evolution, and ultimately a higher G' value. The results are consistent with "table-top rheology" observations (**Figure 5.1** in article).

Table 5-S1 Fitting parameter *n* (log *G'* = n*log(t)* + *C*) for G' of GB/XG mixtures at ratios (1-10) (data of Figures 5.3a, 5.3b and 5.3c) and at long times (t ≥ 100 min), using linear regression.

	L-GB/R-XG	H-GB/R-XG	L-GB/Low-XG	L-GB/Med-XG	L-GB/High-XG
Ratio = 1	0.21	0.27	-	-	-
Ratio = 2	0.27	0.31	0.36	0.29	0.12
Ratio = 3	0.30	0.30	-	-	-
Ratio = 5	0.35	0.38	-	-	-
Ratio = 6	0.40	0.37	0.29	0.31	0.18
Ratio = 8	-	0.39	-	-	-
Ratio = 10	-	0.35	-	-	-

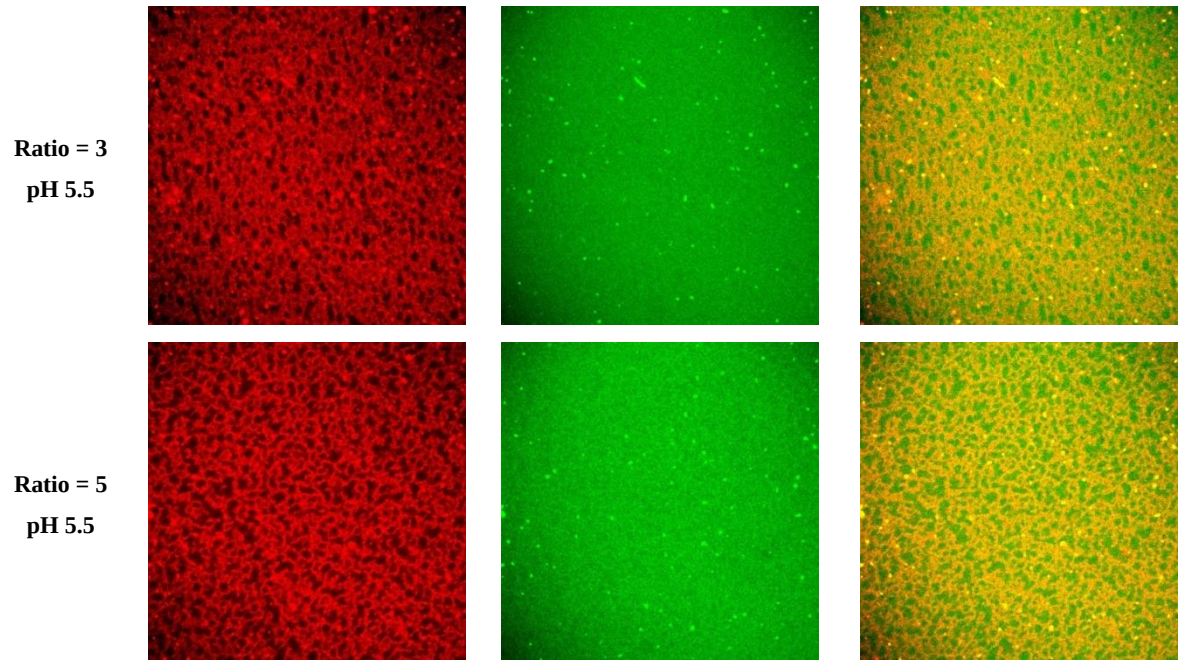

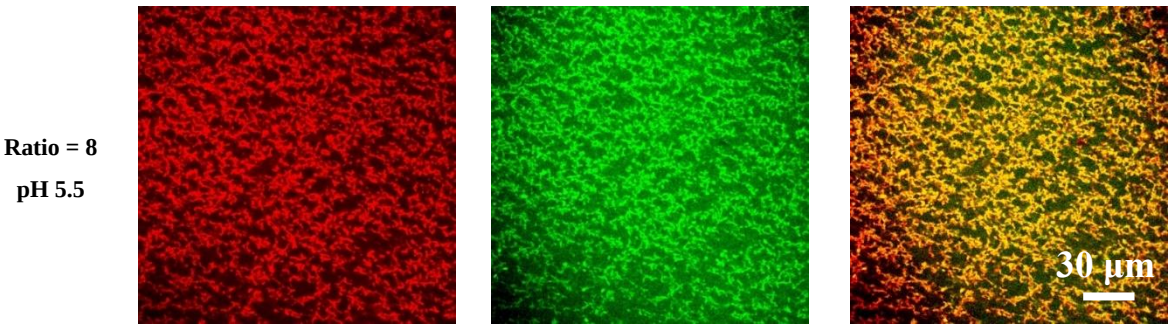

Figure 5-S4. Microstructures of L-GB (red) and R-XG (green) in the mixtures at different ratios (3, 5 and 8), at pH 5.5. The images were taken after storage for 24 h. Image size: 210 µm x 210 µm.

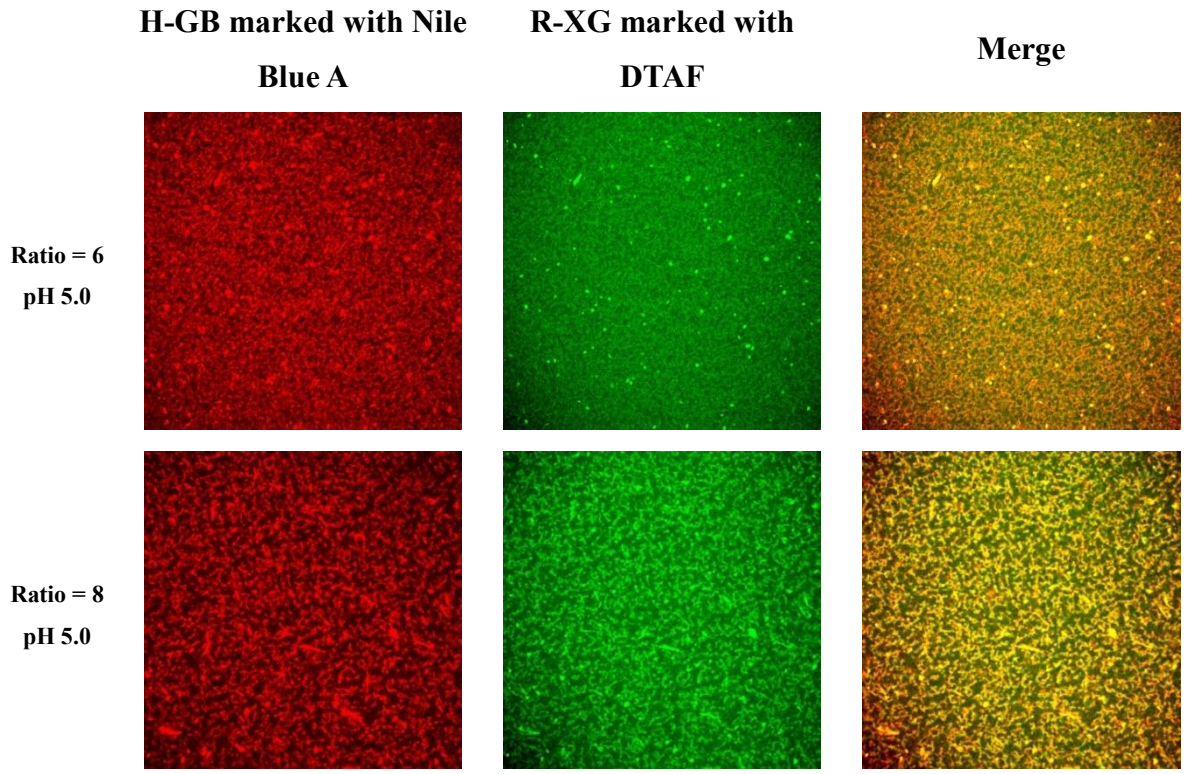

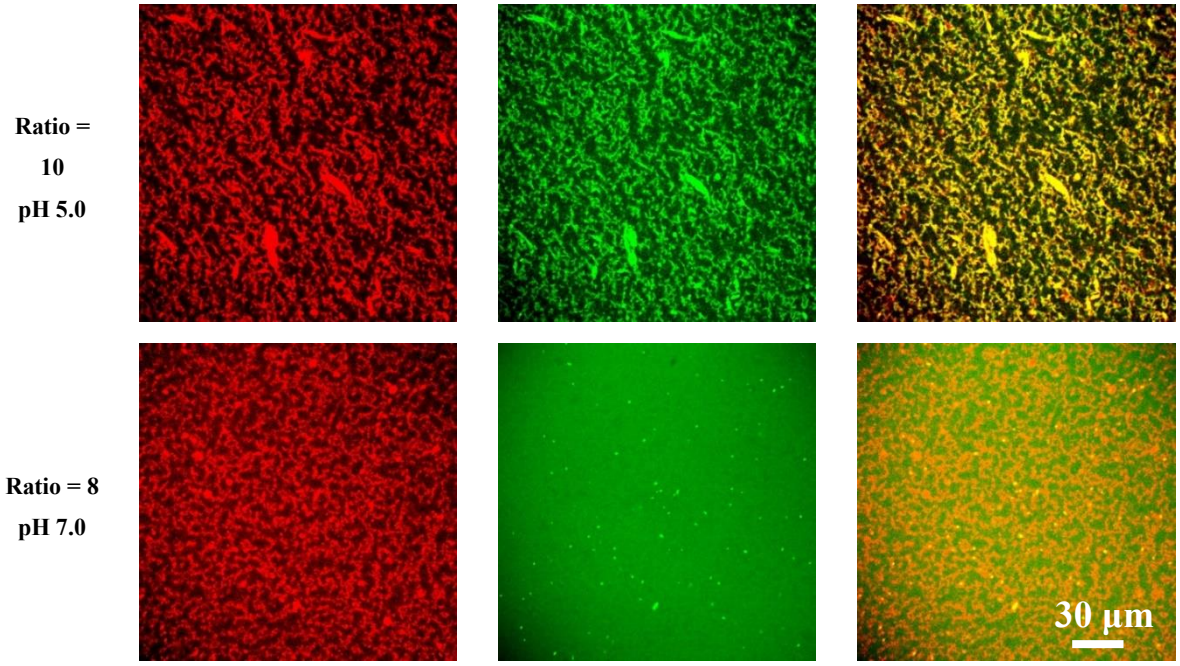

Figure 5-S5. Microstructures of H-GB (red) and R-XG (green) in mixtures at ratios (6-10), pH 5.0, compared to a mixture at ratio 8, pH 7.0. The images were taken after storage for 24 h. Image size: 210 µm x 210 µm

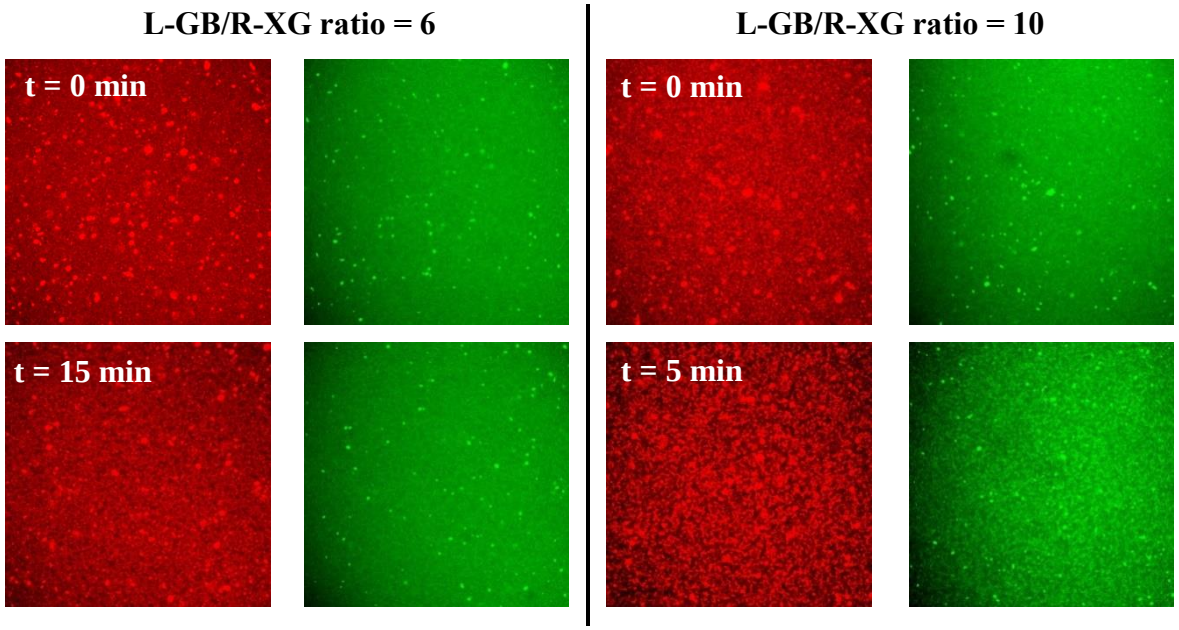

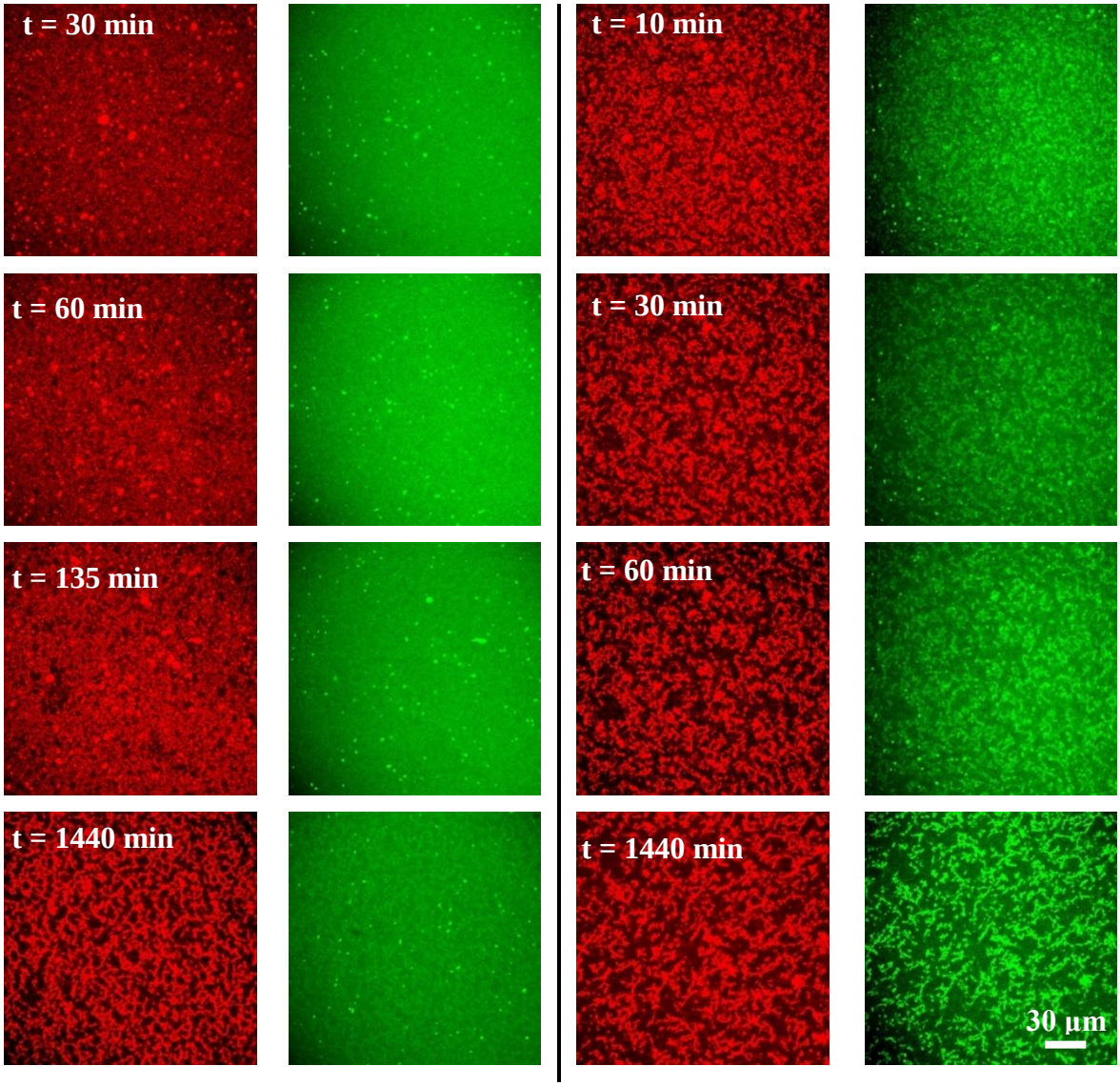

Figure 5-S6. Microstructures of L-GB (red) and R-XG (green) in mixtures at ratios 6 and 10, pH 5.5. The images were taken after different storage times. Image size: 210 µm x 210 µm

To elucidate the mechanism of the synergistic gelation effect, time-resolved CLSM was performed (**Figure 5.9 and Figure 5S6**). For the sample at ratio 6, the microstructure of L-GB evolves slowly, with a barely visible microstructure at t = 0, followed by a slow increase of (L-GB)-poor domain size with time. No clear R-XG microstructure is observed during the first 135 min. The microstructure evolves differently for the sample at ratio 10. In this case, L-GB shows a quick microstructure transition during the first 30 min, followed by a slow change. A network microstructure is already apparent after the first 10 min, but falls apart after 30 min (**Figure 5.9**

and Figure 5S6). This microstructural evolution could explain the overshoot in the rheological measurements (**Figure 5.3**), since network breakdown would result in a decreasing *G'*. Furthermore, Sigma-XG always shows a microstructure colocalized with that of L-GB, with the biopolymer-poor domain size increasing with time.

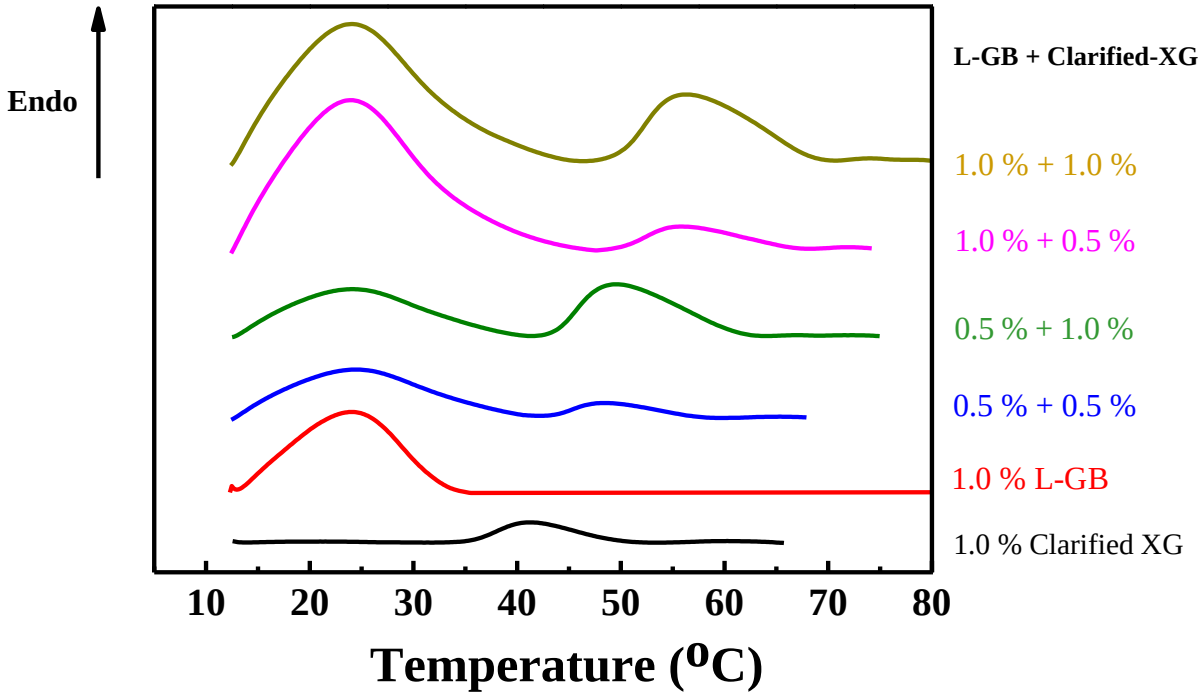

Figure 5-S7. Micro-DSC heating curves of L-GB 1 % w/v, clarified-XG 1 % w/v, and L-GB/clarified-XG mixtures (0.5 %/0.5 %, 0.5 %/1.0 %, 1.0 %/0.5 % and 1.0 %/1.0 %, from bottom to top. Scanning rate = 1°C/min. The curves were shifted vertically for clarity.

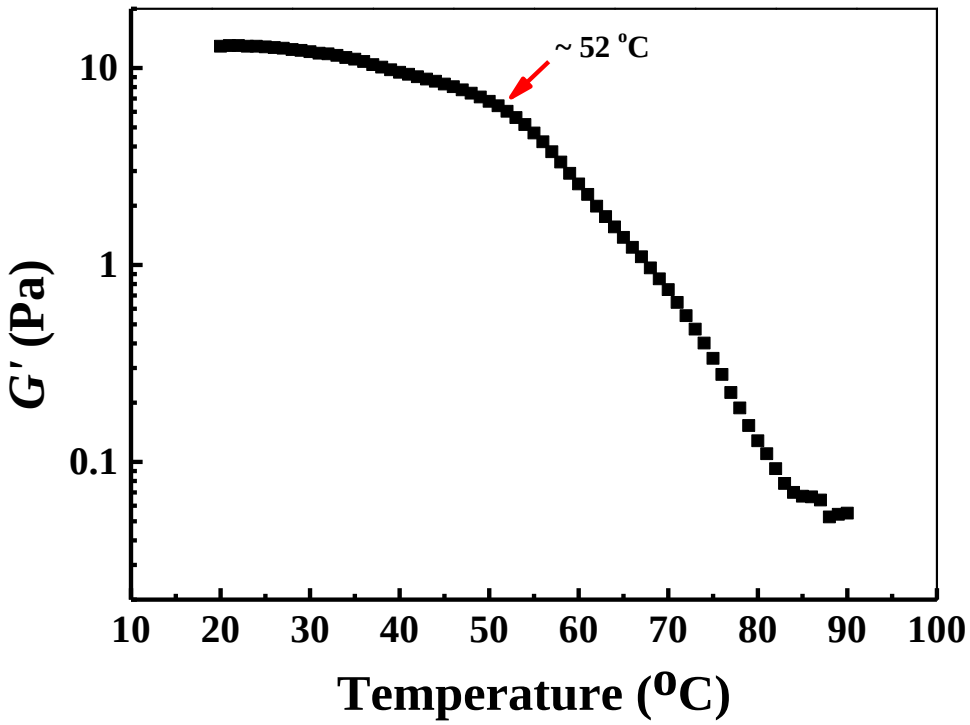

Figure 5-S8 Evolution of *G'* during heating of R-XG at a concentration of 1.0 % w/v

5.8 References

1. Turgeon, S.L. and Laneuville, S.I., *CHAPTER 11 - Protein + Polysaccharide Coacervates and Complexes: From Scientific Background to their Application as Functional Ingredients in Food Products A2 - Kasapis, Stefan*, in *Modern Biopolymer Science*, I.T. Norton and J.B. Ubbink, Editors. 2009, Academic Press: San Diego. p. 327-363.
2. Schmitt, C. and Turgeon, S.L., *Protein/polysaccharide complexes and coacervates in food systems.* Advances in Colloid and Interface Science, 2011. **167**(1–2): p. 63-70.
3. Schmitt, C., et al., *Structure and Technofunctional Properties of Protein-Polysaccharide Complexes: A Review.* Critical Reviews in Food Science and Nutrition, 1998. **38**(8): p. 689-753.
4. Le, X.T., Rioux, L.-E., and Turgeon, S.L., *Formation and functional properties of protein-polysaccharide electrostatic hydrogels in comparison to protein or polysaccharide hydrogels.* Advances in Colloid and Interface Science, 2017. **239**: p. 127-135.
5. Bernal, V.M., et al., *Interactions in Protein/Polysaccharide/Calcium Gels.* Journal of Food Science, 1987. **52**(5): p. 1121-1125.

6. Ballester, S.I.L., et al., *Gelation of Undenatured Proteins with Polysaccharides*. 2005, Google Patents.
7. Turgeon, S.L., Schmitt, C., and Sanchez, C., *Protein–polysaccharide complexes and coacervates.* Current Opinion in Colloid & Interface Science, 2007. **12**(4–5): p. 166-178.
8. Cooper, C., et al., *Polyelectrolyte–protein complexes.* Current opinion in colloid & interface science, 2005. **10**(1): p. 52-78.
9. Weinbreck, F., et al., *Complex Coacervation of Whey Proteins and Gum Arabic.* Biomacromolecules, 2003. **4**(2): p. 293-303.
10. van der Wielen, M.W.J., van de Heijning, W., and Brouwer, Y., *Cellulose Gum as Protective Colloid in the Stabilization of Acidified Protien Drinks*, in *Gums and Stabilisers for the Food Industry 14*, P.A. Williams and G.O. Phillips, Editors. 2008, The Royal Society of Chemistry: London, UK. p. 495-502.
11. Seyrek, E., et al., *Ionic strength dependence of protein-polyelectrolyte interactions.* Biomacromolecules, 2003. **4**(2): p. 273-282.
12. Wang, C.-S., et al., *Synergistic gelation of gelatin B with xanthan gum.* Food Hydrocolloids, 2016. **60**: p. 374-383.
13. Le, X.T. and Turgeon, S.L., *Rheological and structural study of electrostatic cross-linked xanthan gum hydrogels induced by [small beta]-lactoglobulin.* Soft Matter, 2013. **9**(11): p. 3063-3073.
14. Bertrand, M.-E. and Turgeon, S.L., *Improved gelling properties of whey protein isolate by addition of xanthan gum.* Food Hydrocolloids, 2007. **21**(2): p. 159-166.
15. Sanchez, C., et al., *Rheology of whey protein isolate-xanthan mixed solutions and gels. Effect of pH and xanthan concentration.* Food / Nahrung, 1997. **41**(6): p. 336-343.
16. Esquirol, A.-L., Sarazin, P., and Virgilio, N., *Tunable Porous Hydrogels from Cocontinuous Polymer Blends.* Macromolecules, 2014. **47**(9): p. 3068-3075.
17. Galloway, J.A., Montminy, M.D., and Macosko, C.W., *Image analysis for interfacial area and cocontinuity detection in polymer blends.* Polymer, 2002. **43**(17): p. 4715-4722.
18. Li, J. and Favis, B., *Characterizing co-continuous high density polyethylene/polystyrene blends.* Polymer, 2001. **42**(11): p. 5047-5053.
19. Derkach, S.R., et al., *The rheology of gelatin hydrogels modified by κ-carrageenan.* LWT-Food Science and Technology, 2015. **63**(1): p. 612-619.
20. Williams, P., Phillips, G., and McKenna, B., *The use of hydrocolloids to improve food texture.* Texture in food. Volume 1: Semi-solid foods, 2003: p. 251-274.
21. Fitzpatrick, P., et al., *Control of the properties of xanthan/glucomannan mixed gels by varying xanthan fine structure.* Carbohydrate Polymers, 2013. **92**(2): p. 1018-1025.
22. Fitzsimons, S.M., Tobin, J.T., and Morris, E.R., *Synergistic binding of konjac glucomannan to xanthan on mixing at room temperature.* Food Hydrocolloids, 2008. **22**(1): p. 36-46.
23. Norton, I.T., et al., *Mechanism and dynamics of conformational ordering in xanthan polysaccharide.* Journal of Molecular Biology, 1984. **175**(3): p. 371-394.

24. Pelletier, E., et al., *A rheological study of the order–disorder conformational transition of xanthan gum.* Biopolymers, 2001. **59**(5): p. 339-346.

25. Sturtevant, J.M., *Biochemical Applications of Differential Scanning Calorimetry.* Annual Review of Physical Chemistry, 1987. **38**(1): p. 463-488.

26. Chiu, M.H. and Prenner, E.J., *Differential scanning calorimetry: An invaluable tool for a detailed thermodynamic characterization of macromolecules and their interactions.* Journal of Pharmacy and Bioallied Sciences, 2011. **3**(1): p. 39-59.

27. Liu, S., Huang, S., and Li, L., *Thermoreversible gelation and viscoelasticity of κ-carrageenan hydrogels.* Journal of Rheology (1978-present), 2016. **60**(2): p. 203-214.

28. Liu, S. and Li, L., *Thermoreversible gelation and scaling behavior of Ca 2+-induced κ-carrageenan hydrogels.* Food Hydrocolloids, 2016. **61**: p. 793-800.

29. Sarbon, N.M., Badii, F., and Howell, N.K., *The effect of chicken skin gelatin and whey protein interactions on rheological and thermal properties.* Food Hydrocolloids, 2015. **45**: p. 83-92.

30. Alqahtani, N.K., et al., *Effect of Oat Particle Concentration and Size Distribution on the Phase Behaviour of Mixtures with Gelatin.* Journal of Food and Nutrition Research, 2016. **4**(2): p. 69-75.

31. Cheow, C.S., et al., *Preparation and characterisation of gelatins from the skins of sin croaker (Johnius dussumieri) and shortfin scad (Decapterus macrosoma).* Food Chemistry, 2007. **101**(1): p. 386-391.

32. Katzbauer, B., *Properties and applications of xanthan gum.* Polymer Degradation and Stability, 1998. **59**(1): p. 81-84.

33. Rochefort, W.E. and Middleman, S., *Rheology of Xanthan Gum: Salt, Temperature, and Strain Effects in Oscillatory and Steady Shear Experiments.* Journal of Rheology (1978-present), 1987. **31**(4): p. 337-369.

34. Stephen, A.M., *Food polysaccharides and their applications*. Vol. 67. 1995: CRC Press.

35. Morris, V.J., Franklin, D., and I'Anson, K., *Rheology and microstructure of dispersions and solutions of the microbial polysaccharide from Xanthomonas campestris (xanthan gum).* Carbohydrate research, 1983. **121**: p. 13-30.

36. Stephen, A.M. and Phillips, G.O., *Food polysaccharides and their applications*. Bacterial Polysaccharides. Vol. 160. 2010: CRC Press.

37. McClements, D.J., *Understanding and controlling the microstructure of complex foods*. 2007: Elsevier.

CHAPTER 6 ARTICLE 3: A GELATION MECHANISM FOR GELATIN/POLYSACCHARIDE AQUEOUS MIXTURES

Chang-Sheng Wang, [a] Nick Virgilio, [a] Paula M. Wood-Adams, [b*] Marie-Claude Heuzey [a*]

[a] Centre de Recherche sur les Systèmes Polymères et Composites à Haute Performance (CREPEC), Department of Chemical Engineering, Polytechnique Montréal, Montréal, Québec, H3C 3A7, Canada

[b] CREPEC, Department of Mechanical and Industrial Engineering, Concordia University, Montréal, Québec, H3G 1M8, Canada

This work has been submitted to *Food Hydrocolloids*

6.1 Abstract

Gelatin/xanthan gum (XG, an anionic polysaccharide) and gelatin/chitosan (CHI, a cationic polysaccharide) aqueous mixtures exhibit enhanced gelation properties compared to the neat components solutions. The gelation properties are determined by the extent of complexation, and therefore are affected by pH and protein to polysaccharide ratio. Inhibition or low extent of complexation results in a slow increase in elastic modulus (G'), whereas too strong complexation leads to phase separation by precipitation. Gelatin/polysaccharide mixtures display a pH-dependent structural transition. Low Bloom index grade gelatin A (L-GA) and XG form colocalized microstructures at pH 5.5 and 6.0 but complementary microstructures at higher pH, even when the two biopolymers carry opposite net charges. A colocalized microstructure is observed at pH 5.0-5.5 for high Bloom index grade gelatin B (H-GB) and CHI mixtures, but no clear structure is observed for H-GB/CHI at pH 4.0-4.5 and L-GA/CHI at pH 6.0. A general gelation mechanism for gelatin/polysaccharide aqueous mixtures is proposed based on the results of rheology, confocal microscopy and micro-differential scanning calorimetry.

6.2 Introduction

The interactions between proteins and polysaccharides in solution have received increasing interest in recent years since they can be utilized to control the functional properties of food products [1-4], separate proteins [5], and design delivery matrices for bioactive molecules [2, 4, 6]. Two types

of interactions occur depending on environmental factors such as pH and ionic strength: segregative phase separation (thermodynamic incompatibility) and associative phase separation (thermodynamic compatibility) [2, 7]. Segregative phase separation leads to the formation of protein-rich and polysaccharide-rich phases due to electrostatic repulsion, whereas associative phase separation results in solvent-rich and biopolymer-rich phases caused by electrostatic complexation. Three different mixed protein/polysaccharide networks can form through the two types of interactions, namely interpenetrating gels, phase-separated gels and coupled gels [8]. Mixed gels can also display a combination of those features, and have greater flexibility in terms of mechanical properties compared to those of individual components. For example, enhanced and tunable gelation properties are obtained for some mixtures by controlling the pH, ionic strength and protein-to-polysaccharide ratio, such as gelatin B (GB)/xanthan gum (XG) [9] and β-lactoglobulin/XG systems [10-12]. For the moment, the majority of protein/polysaccharide mixed gel studies have focused on proteins and anionic polysaccharides, with fewer works on proteins and cationic polysaccharides.

Chitosan (CHI), as the only naturally derived cationic polysaccharide, has been of great interest in various areas, such as in food technology, biomedical and pharmaceutical industries due to its good biodegradability, high biocompatibility, low toxicity and excellent antibacterial activity [13-15]. CHI has a pKa around 6.3-6.5, thus is soluble only in acidic solutions [16, 17]. Recently, it was reported that GB and CHI can form a gel in a pH range where the two biopolymers are oppositely-charged, although a long storage time is required [18]. More detailed studies are needed to understand this gelation mechanism.

Previously, we proposed a gelation mechanism for GB/XG aqueous mixtures displaying enhanced (synergistic) viscoelastic properties. In this work, the gelation behavior of mixed gels of gelatin (Type A and B) and 2 types of oppositely charged polysaccharides (XG and CHI) was investigated in order to propose a more general mechanism behind the gelation of protein/polysaccharide aqueous mixtures.

6.3 Materials and methods

6.3.1 Materials

Four grades of gelatin, namely: 48720, (type A, Bloom index = 50-75, $c_{crit} \approx 2.5$ % w/v, L-GA); G1890 (type A, Bloom index = 300, $c_{crit} \approx 1.0$ % w/v, H-GA); G6650 (type B, Bloom index = 75, $c_{crit} \approx 4.0$ % w/v, L-GB) and G9382 (type B, Bloom index = 225, $c_{crit} \approx 2.0$ % w/v, H-GB), were purchased from Sigma-Aldrich, Canada. Xanthan gum (XG) (G1253, *Mw*: ~2-4 x 10^6 kDa) was also purchased from Sigma Aldrich, while chitosan (CHI) (degree of deacetylation 90 %, dynamic viscosity 1000 mPa·s, *Mw*: 200-300 kDa) was supplied by BioLog Biotechnologie und Logistik GmbH (Landsberg, Germany). Other chemicals (HCl, NaOH, Nile Blue A and 5-(4,6-dichlorotriazinyl) aminofluorescein, Fluorescein 5(6)-isothiocyanate) were of analytical grade (Sigma Aldrich, Canada), and used as received.

6.3.2 Sample preparation

Gelatin solutions (0.4-4.0 % w/v) were prepared by allowing gelatin powder to swell in Milli-Q water (18.2 Ω) for 15-20 min at room temperature, followed by gentle stirring at 60 ^{o}C for 15 min. XG solutions (0.2 and 0.4 % w/v) were prepared by dissolving the powder into Milli-Q water at a stirring speed of 600-700 rpm for at least 12 h at room temperature. CHI solutions (0.4 and 0.8 %, w/v) were obtained by dissolving CHI powder into 50 mM acetic acid at a stirring speed of 600-700 rpm for at least 6 h at room temperature. Mixed gelatin/XG and gelatin/CHI solutions with fixed XG concentration (0.2 % w/v) and CHI concentration (0.4 % w/v), and different gelatin concentrations (0.2-1.6 % w/v), were prepared by mixing equal volumes of gelatin and XG or gelatin and CHI primary solutions while stirring at 60 ^{o}C for approximately 30 min. The pH of the mixtures was adjusted using 1M HCl or NaOH.

6.3.3 Zeta potential measurements

Zeta potential values of gelatin, XG and CHI solutions were determined by laser doppler velocimetry and phase analysis light scattering (M3-PALS) using a Malvern Zetasizer Nano ZSP instrument (Malvern Instruments Ltd., Malvern, Worcestershire, UK). The zeta potential was determined from the direction and velocity of the molecules in the applied electric field. The Smoluchowski model was used by the software to convert the electrophoretic mobility

measurements into zeta potential values. All the samples were diluted to about 0.05 % (w/v) and then put into a disposable folded capillary cell (DTS1060) to measure the zeta potential. The temperature of the cell was maintained at 25 ^{o}C. The data presented are the average values of three individual measurements.

6.3.4 "Table-top" rheology

Small volumes (7-8 mL) of freshly prepared gelatin/XG or gelatin/CHI mixed solutions were transferred into 20 mL vials (Fisherbrand, O.D. × H (with cap): 28 x 61 mm) and kept at room temperature for 24 h. The vials were then inverted to qualitatively assess gel formation and strength.

6.3.5 Time-resolved small amplitude oscillatory shear

Freshly prepared neat or mixed solutions were directly poured into a rough surface Couette flow geometry (cup and bob diameters of 18.066 mm and 16.66 mm, respectively) and measurements were performed using a stress-controlled Physica MCR 501 rheometer (Anton Paar, Graz, Austria). Before the time sweep tests, all systems were heated at a rate of 5 °C/min up to 60 °C. The samples were kept at this temperature for 10 min to erase the previous thermal histories and were subsequently cooled down to 20 °C at a rate of 5 °C/min. Dynamic time sweep measurements were performed at 1 rad/s and 20 °C in the LVE regime (3 %) for 8 h. The storage modulus (G'), loss modulus (G''), and related complex viscosity ($|\eta^*|$) were recorded as functions of time. Samples were covered with a thin film of low viscosity mineral oil to prevent water evaporation. The oil was shown not to affect the rheological measurements. The experiments were performed for three times with good reproducibility (< 5 %).

6.3.6 Confocal laser scanning microscopy

CLSM observations of the gelatin/XG and gelatin/CHI solutions were performed with an Olympus IX 81 inverted confocal microscope (Olympus Canada Inc., Richmond Hill, ON, Canada). Gelatin (A and B) was stained with Nile Blue A (N0766, Sigma) in solution under magnetic stirring for 30 min before mixing with XG or CHI solutions. On the other hand, XG was covalently labeled with 5-(4,6-dichlorotriazinyl) aminofluorescein (DTAF) (D0531, Sigma) using a method described previously [9]. CHI was covalently labelled with Fluorescein 5(6)-isothiocyanate (FITC) using a

modified method of Qaqish et al [19]. CHI and FITC were first dissolved in 200 mL 0.1 M HCl and 200 mL dehydrated methanol, respectively. The two solutions were then mixed together and kept in the dark at room temperature for 3 h with gentle stirring for chemical grafting. The pH was adjusted to 10.0 by adding 0.1 M NaOH to precipitate FITC-labelled CHI. The precipitate was obtained by centrifugation (10,000 g, 30 min) and was then dissolved in 0.1 M HCl. The FITC-labelled CHI solution was exhaustively dialyzed against Milli-Q water under darkness for 3 days to remove any unreacted FITC and the counterions. Sodium azide (0.02 wt%) was added to inhibit bacteria growth, and the Milli-Q water was changed every 2 h during dialysis. After freeze-drying, FITC-labelled CHI (yellow powder) was obtained (yield = 98 %). Preliminary experiments showed that labeling does not change the rheological behavior of the solutions. After mixing, solution samples were poured in Petri dishes (P35G-1.5-14-C, MatTek), closed with cover slips and hermetically sealed with oil. Observation of XG and CHI was made by excitation of DTAF and FITC at 488 nm, the emission being recorded between 510 and 550 nm. Observation of gelatin was made by excitation of Nile Blue A at 633 nm, the emission being recorded between 650 and 680 nm. Micrographs were taken after approximately 24 h using a 60x objective lens at a 2048 x 2048 pixels resolution. All micrographs were subsequently analyzed using Image J software.

6.3.7 Micro-differential scanning calorimetry (Micro-DSC)

Micro-DSC experiments were performed on a micro-calorimeter (Microcal Inc., Northampton, MA, US) with a cell volume of 0.520 mL and under an external pressure of 180 kPa. The samples were first degassed using a bath sonicator (FS110, Fisher Scientific, Pittsburgh, PA, US) operated at 135 W for 15 min while heating (final temperature ≈ 80 ^{o}C), and were then injected into the sample cell and kept at 90 ^{o}C for 15 min to remove any effects of thermal history. The samples were subjected to cooling and heating cycles over a temperature range of 5-90 ^{o}C at a rate of 1 ^{o}C/min. The sample cell was cleaned by a continuous flow of hot deionized water after each experiment followed by a water-water baseline test to ensure there was no contamination of the sample cell. The experimental data were analyzed using the Origin-based software provided by the manufacturer. The transition temperatures were taken at the transition peaks maxima, and the transition enthalpies were determined from the area of the endothermic or exothermic peaks.

6.4 Results and discussion

6.4.1 Zeta potential

The zeta potential values of XG, CHI and the gelatins are shown in **Figure 6.1**. H-GB has an isoelectric point (pI) at around pH 5.0, whereas L-GA and H-GA exhibit a pI at 9.3 (**Figure 6.1a**). The zeta potentials of the two grades of GA are essentially the same over the pH range investigated, and their curves are shaped differently from that of H-GB, decreasing steeply in the pH range of 4.0-6.0, and slowly in a pH range of 6.0-9.0. Above their respective pI, all gelatins are negatively-charged.

a)

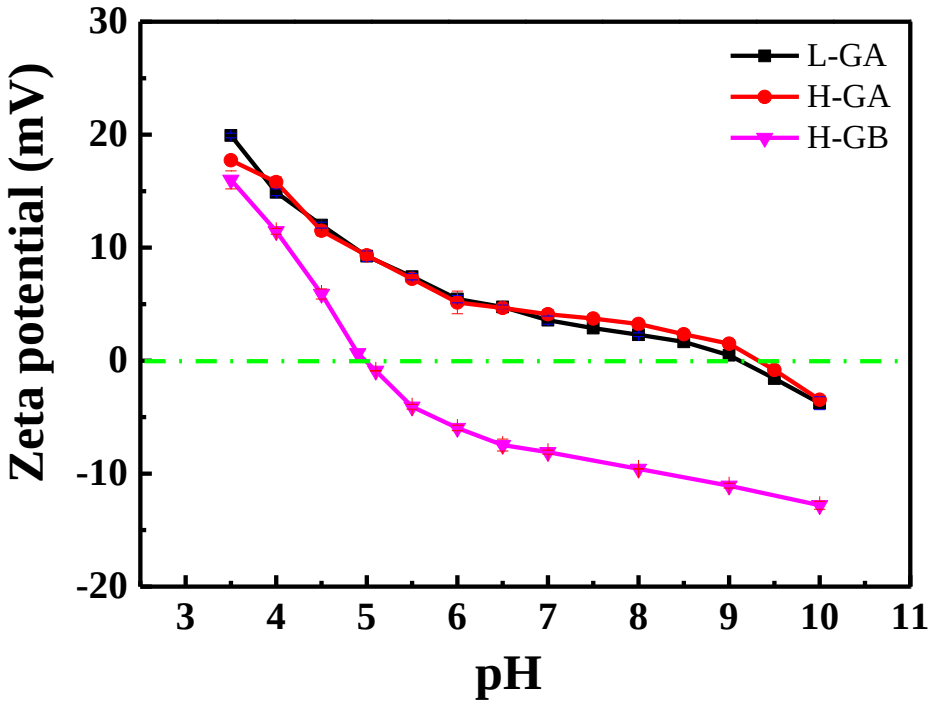

b)

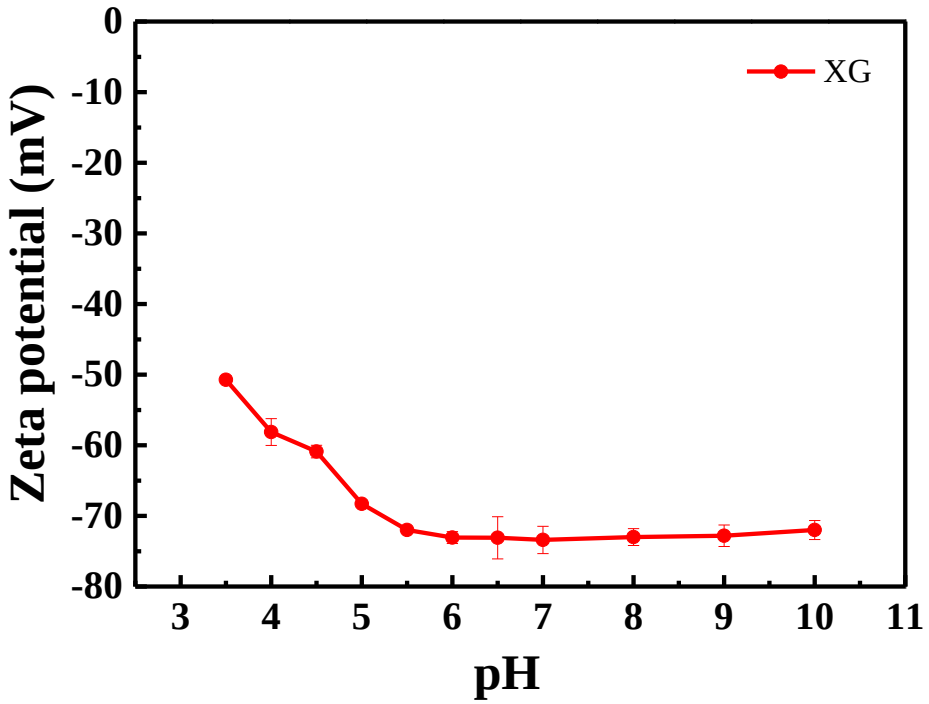

c)

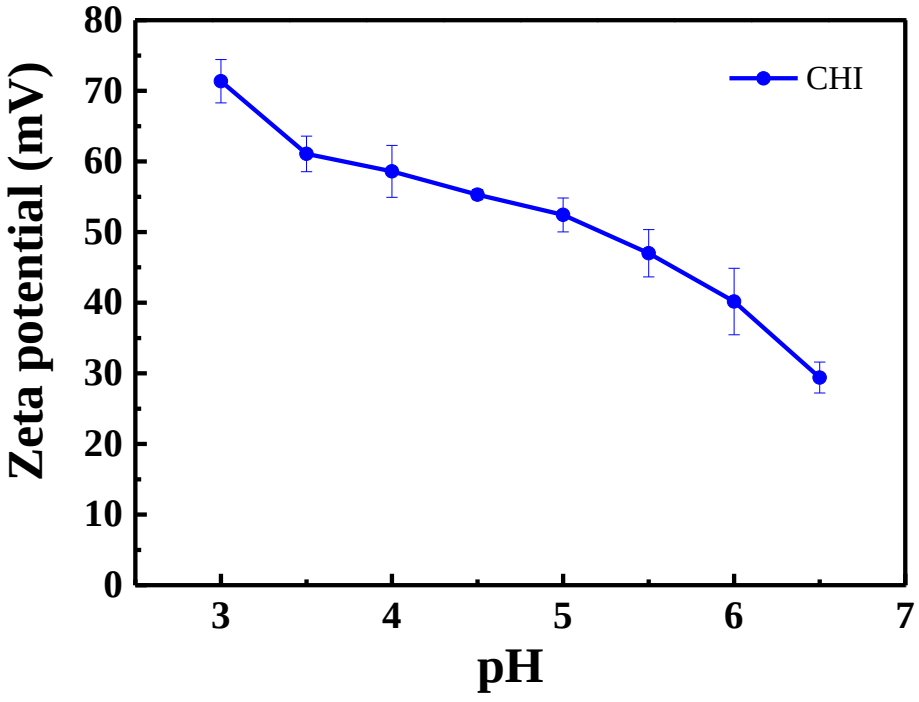

Figure 6.1 Zeta potential values of the gelatins (a), XG (b) and CHI (c) used in this work.

XG is negatively-charged in the whole investigated pH range (**Figure 6.1b**). Consistent with previous studies [9, 10], we observe a steep decrease in zeta potential at pH 3.5-5.0 due to the deprotonation of -COOH groups as pH increases, and is followed by a plateau regime after complete deprotonation.

CHI is positively-charged over the pH range investigated (**Figure 6.1c**), in agreement with the trend reported by Wang et al [18] and Liu et al [20]. The decrease of the chitosan zeta potential is due to the deprotonation of NH_3^+ groups with increasing pH.

6.4.2 "Table-top" rheology

The effects of pH and gelatin concentration on the visual aspects of L-GA/XG, H-GB/CHI, L-GA/CHI and H-GA/CHI mixed gels are shown in **Figure 6.2**. These mixtures display different gelation behavior depending on pH, composition and biopolymer type.

Complexation occurs when proteins and polysaccharides are mixed in an aqueous solution near the pI of proteins [2, 21]. The charge density of polysaccharides after complexation, which can be tuned by pH and protein/polysaccharide ratio, is a critical factor for network formation [22]. A high polysaccharide charge density limits the associations between the complexes, which makes a network formation unlikely, whereas low charge density causes phase instability and leads to aggregate formation. Therefore, an optimum balance of pH and protein/polysaccharide ratio is typically needed to obtain the best gelation properties. For example, the optimal pH for L-GA/XG and H-GB/CHI mixtures locate at pH 6.0 and 5.0 respectively (**Figures 6.2a** and **6.2d**). H-GB/CHI mixtures display an increase in gel turbidity or phase separation at pH above 5.0 (the pI of H-GB), due to the strong electrostatic complexation between the two oppositely charged biopolymers. The elastic properties of L-GA/CHI and H-GA/CHI mixtures increase with pH, but are limited by the pKa (~ 6.5) of CHI, and an optimal pH is not observed (**Figures 6.2b** and **6.2c**). Finally, L-GA/XG mixtures show phase separation at pHs below 5.5, far below the pI of L-GA (data not shown).

Looking at the effect of composition, L-GA/XG mixtures exhibit self-supporting properties at L-GA concentrations between 0.6 – 0.8 % w/v at pH 6.0, but lose them at higher L-GA contents (**Figure 6.2a**). Similar results are observed for L-GB/XG [9]. In comparison, the gel strength increases monotonously with gelatin concentration for all chitosan mixtures (**Figures 6.2b**, **6.2c** and **6.2d**).

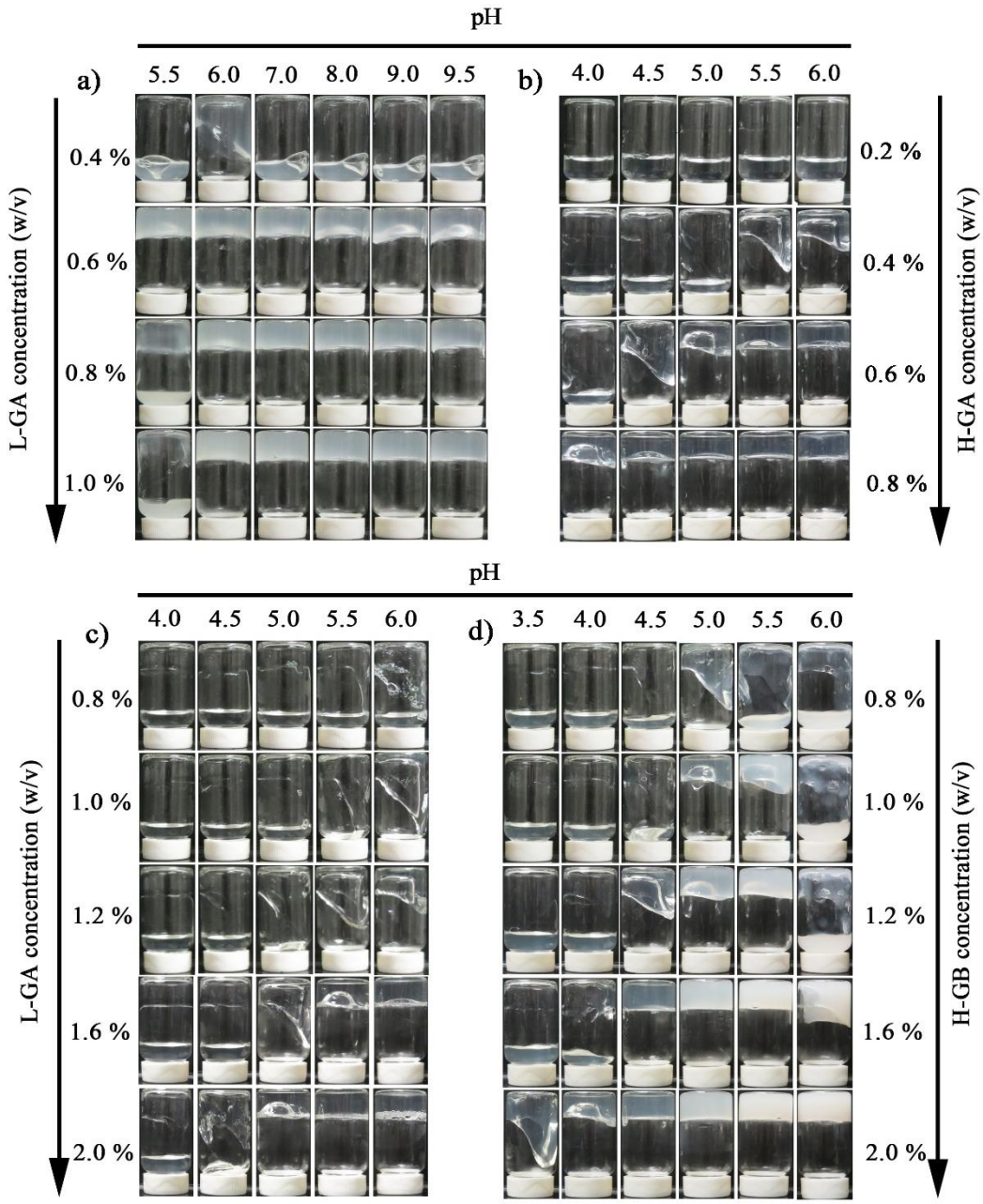

Figure 6.2 Effects of pH and gelatin concentration on the visual aspect of different mixtures: a) L-GA/XG, b) H-GA/CHI, c) L-GA/CHI and d) H-GB/CHI. The photos were taken after overnight storage.

Note that the critical gelling concentrations are always much lower for the mixtures ($c_{H\text{-}GB/CHI}$ = 0.8 % w/v, $c_{L\text{-}GA/XG}$ = 0.4 % w/v, $c_{L\text{-}GA/CHI}$ = 0.8 % w/v and $c_{H\text{-}GA/CHI}$ = 0.4 % w/v) compared to gelatin

alone ($c_{H\text{-}GB} \approx 2.0$ % w/v, $c_{L\text{-}GA} \approx 2.5$ % w/v and $c_{H\text{-}GA} \approx 1.0$ % w/v), confirming that a synergy occurs when mixing different types of gelatin and the two polysaccharides.

6.4.3 Time-resolved small amplitude oscillatory shear

The time-dependent rheological properties of different mixtures were measured and the results are shown in **Figure 6.3**. The elastic moduli (*G'*) of the individual XG and CHI solutions are time-independent, and always less than the values of the mixtures which are time dependent.

Consistent with our previous work [9], the *G'* of most mixtures initially increases rapidly followed by a slow increase, regardless of pH and composition. For some mixtures, an induction time is needed prior to the increase in *G'*. For example, see the results of L-GA/CHI mixtures at pH 4.5 and 5.0 (induction time: ~100 min and ~10 min) (**Figure 6.3e**). This is due to electrostatic repulsion between L-GA and CHI that hinders or prevents complexation in this low pH range.

The time-dependent storage modulus of the mixtures starts to differ in the initial period, with the relative magnitudes remaining in the same order during the whole period of measurement. The L-GA/XG and H-GB/CHI mixtures exhibit the highest moduli at pH of 6.0 and 5.0 respectively at the compositions studied (**Figures 6.3a** and **6.3c**). With respect to the gelatin to polysaccharide ratio, *G'* reaches a highest value for L-GA/XG mixture at ratio 3 (**Figure 6.3b**), but steadily increases as the ratio increases for H-GB/CHI and L-GA/CHI mixtures at a given pH (**Figures 6.3d** and **6.3f**). The magnitude of G_{8h}' agrees well with "table-top" rheology results. In order to identify the optimal pH for a particular protein/polysaccharide mixture we must consider both the rheological behavior as well as zeta potential values. The best gelation properties are always obtained near a pH where phase separation occurs, which may not be exactly at the isoelectric point of the protein.

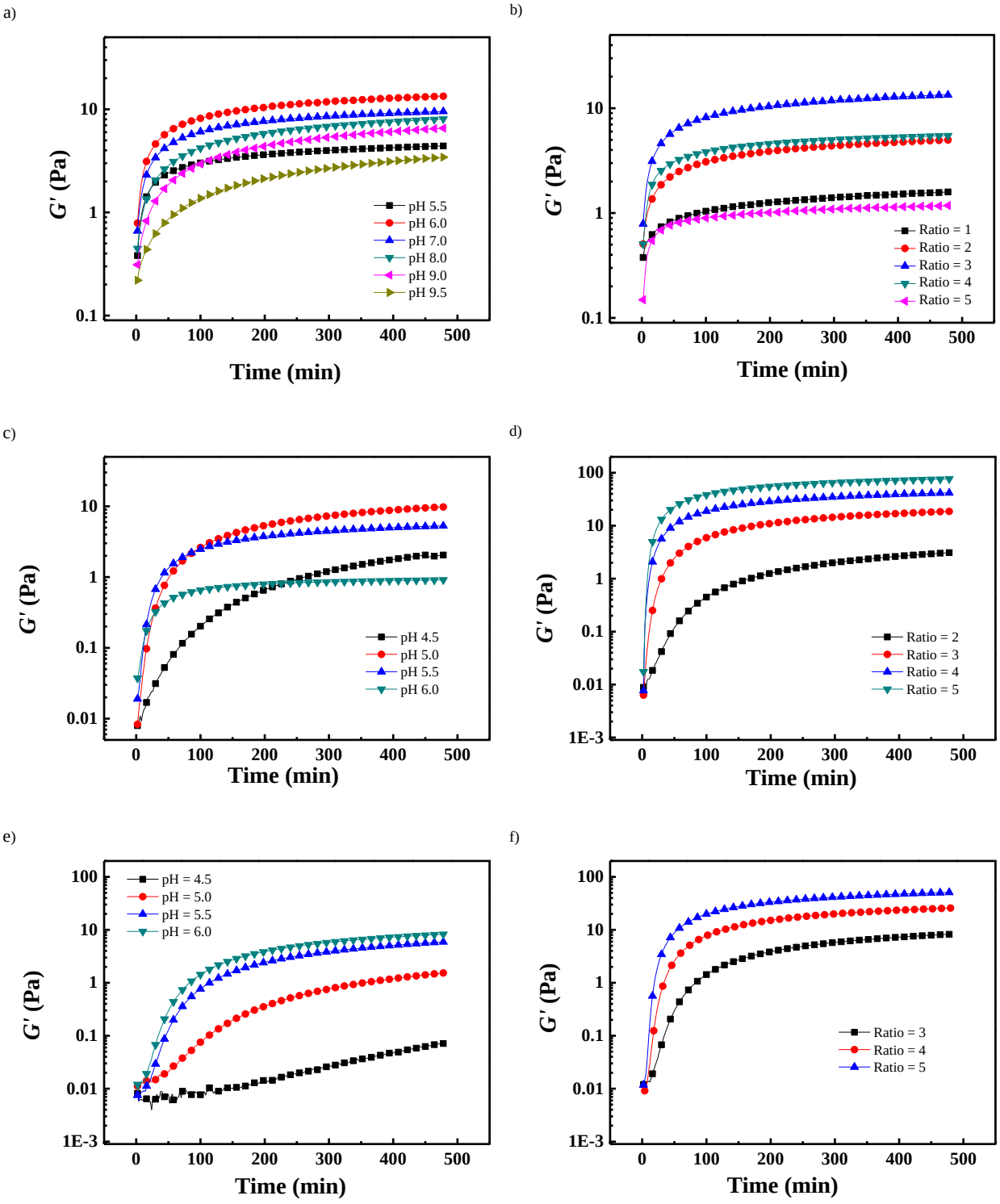

Figure 6.3 Evolution of *G'* as a function of time for a) the L-GA/ XG mixtures at ratio = 3 and different pHs, b) the L-GA/ XG mixtures at different ratios and pH 6.0, c_{XG} = 0.2 %, c) the H-GB/CHI mixtures at ratio = 2.5 and different pHs, d) the H-GB/CHI mixtures at

different ratios and pH 5.0, c_{CHI}= 0.4 %, e) the L-GA/CHI mixtures at ratio= 3 and different pHs, and f) the L-GA/XG mixtures at different ratios and pH 6.0, c_{CHI} = 0.4 %

L-GA and H-GB start to show a detectable *G'* at concentrations ≥ 1.2 % and ≥ 1.0 %, respectively. In order to quantitatively evaluate how the mixtures show enhanced rheological properties as compared to the solutions of pure components, the *G'* ratios of L-GA/CHI or H-GB/CHI mixtures, over the sum of *G'* of the neat L-GA or H-GB and CHI solutions in the corresponding mixtures, after 8 hrs, were calculated (**Figure 6.4**) – a ratio of 1 representing the case of linear additivity. For both mixtures with CHI, the ratio is significantly superior to 1 at low polysaccharide composition (> 10 for H-GB/CHI, ≈ 550 for L-GA/CHI), indicating a synergistic interaction between the components in solution. The ratio then decreases exponentially as the L-GA or H-GB concentration increases. In comparison, L-GA/XG mixtures display a maximum at L-GA = 0.6 % (**Fig. 6S1**).

a)

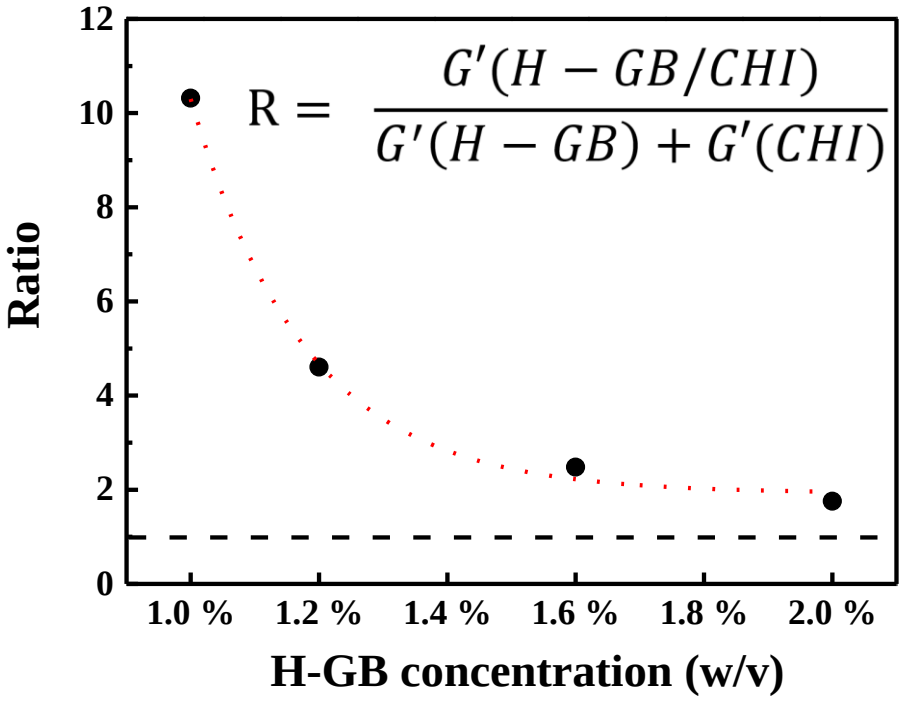

b)

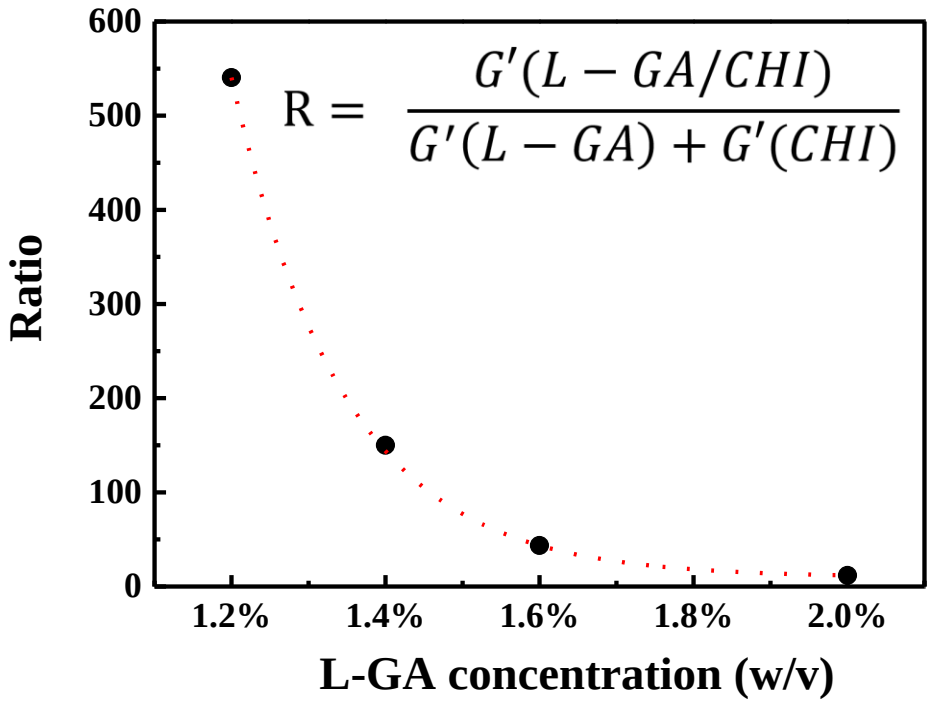

Figure 6.4 The ratio of *G'* of a) H-GB/CHI and b) L-GA/CHI mixtures over the sum of the *G'* of neat compositions at concentrations in the corresponding mixtures, as a function of gelatin concentration, 8 h after solution preparation (c_{CHI} = 0.4 % w/v).

6.4.4 CLSM

Figure 6.5 exhibits the microstructures of L-GA/XG, H-GB/CHI and L-GA/CHI at different pHs (L-GA/XG and L-GB/XG at pH 8.0, see **Figure 6S2**). L-GA/XG mixtures show a pH-dependent structural transition: the biopolymers display a colocalized microstructure at pH 5.5; then become less colocalized at pH 6.0 and finally change to a complementary microstructure above pH 6.0, indicating a segregative phase separation (Panel A). Note that the two biopolymers carry opposite net charges at all pH values studied except for pH 9.5 (**Figure 6.1**). In comparison, a segregative phase separation was also observed for L-GB/XG mixtures but only when the two biopolymers carry the same charges (**Figure 6S2**). This counter-intuitive result is probably related to the amphiprotic properties of proteins and to the particular charge distribution of L-GA.

H-GB/CHI mixtures display no visible microstructures at pHs below the pI of H-GB (i.e. pH 4.0-4.5), but a colocalized microstructure of biopolymer-rich and biopolymer-poor domains at pHs

equal and above the pI of H-GB (i.e. pH 5.0-5.5) (Panel B). No clear structures are observed for L-GA/CHI mixtures (Panel C).

The microstructures are much finer for gelatin/CHI mixtures compared to those of gelatin/XG mixtures. This is most probably due to the much lower molecular weight of CHI and/or the stiffer conformation of XG.

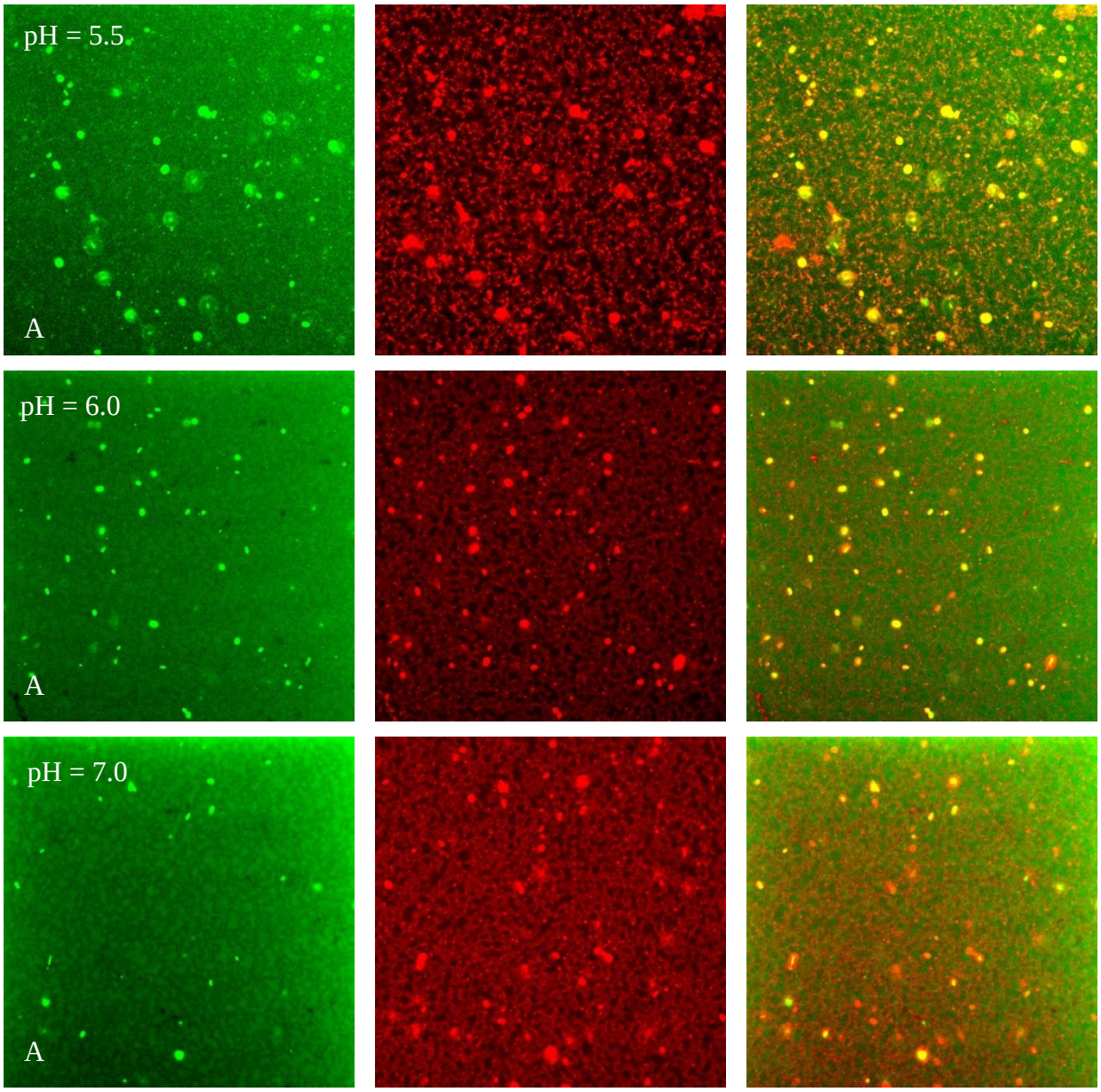

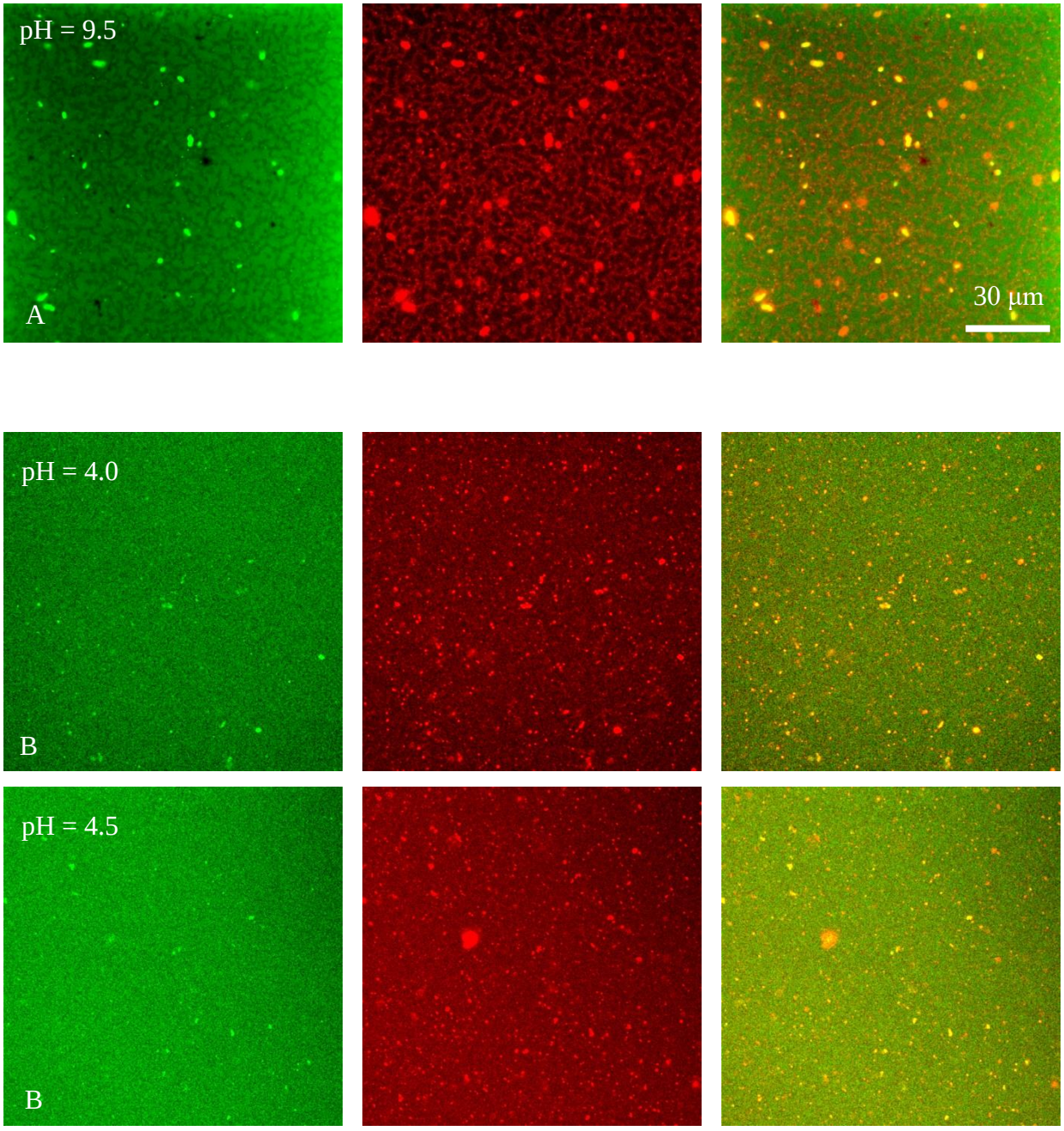
pH = 9.5
A
30 µm
pH = 4.0
B
pH = 4.5
B

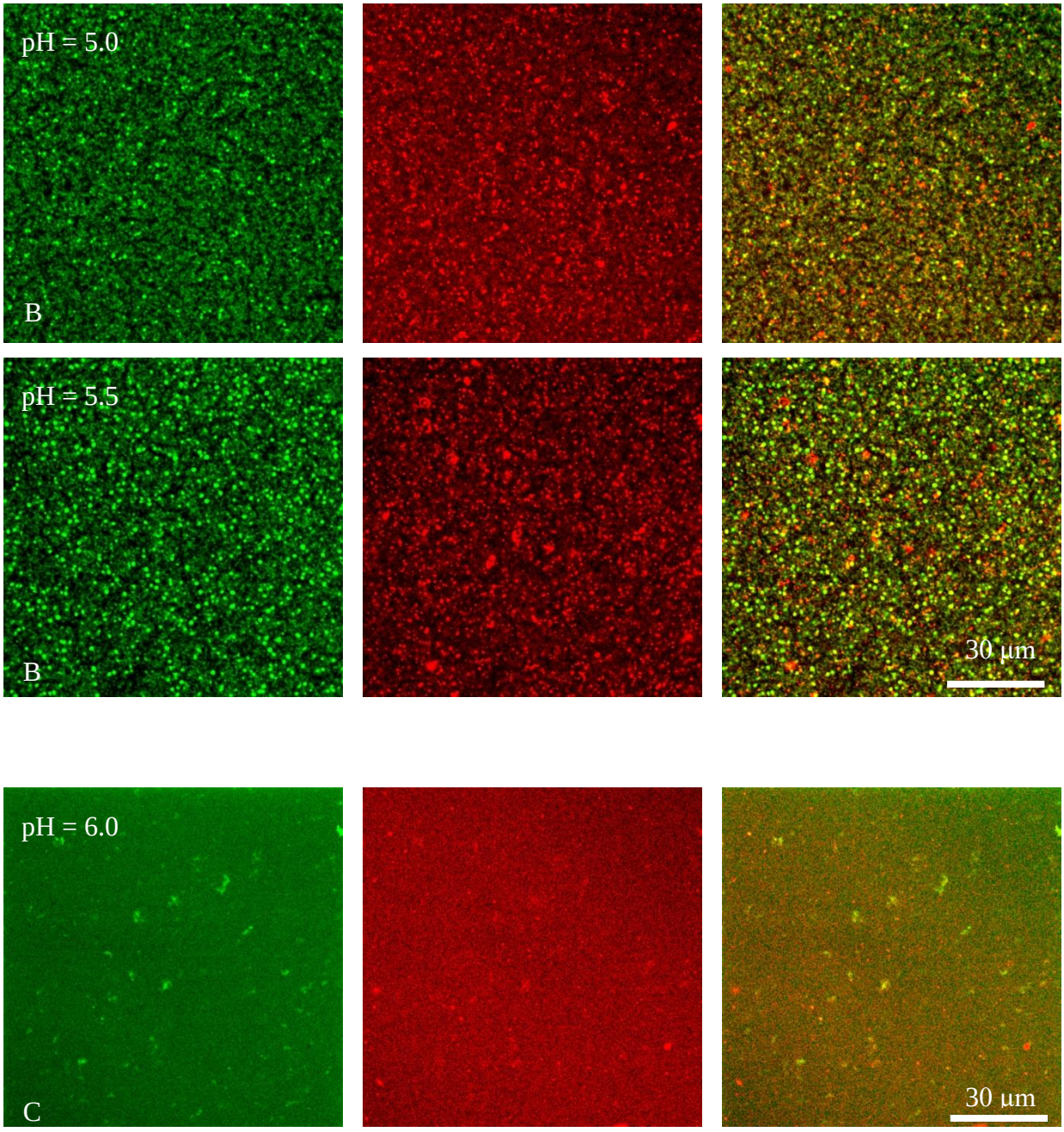

Figure 6.5 Microstructures of L-GA/XG (Panel A, ratio 3, 120 µm x 120 µm), H-GB/CHI (Panel B, ratio 4, 105 µm x 105 µm) and L-GA/CHI (Panel C, ratio 4, 105 µm x 105 µm) mixtures. Gelatin appears in red and XG or CHI in green. The images were taken after storage for 24 hrs.

6.4.5 Micro-DSC

Micro-DSC was used to study biopolymer conformation transitions and the results are shown in **Figure 6.6**. A XG solution at 1.0 % w/v exhibits two peaks at 35.6 (T_2) and 52.3 ^{o}C (T_3) in the heating cycle, with the second peak attributed to the XG order-to-disorder (helix-to-coil) transition upon heating. L-GA and H-GB solutions show peaks at 24-25 ^{o}C due to the gelatin helix-to-coil transition [23-25]. No visible peak is observed for CHI alone.

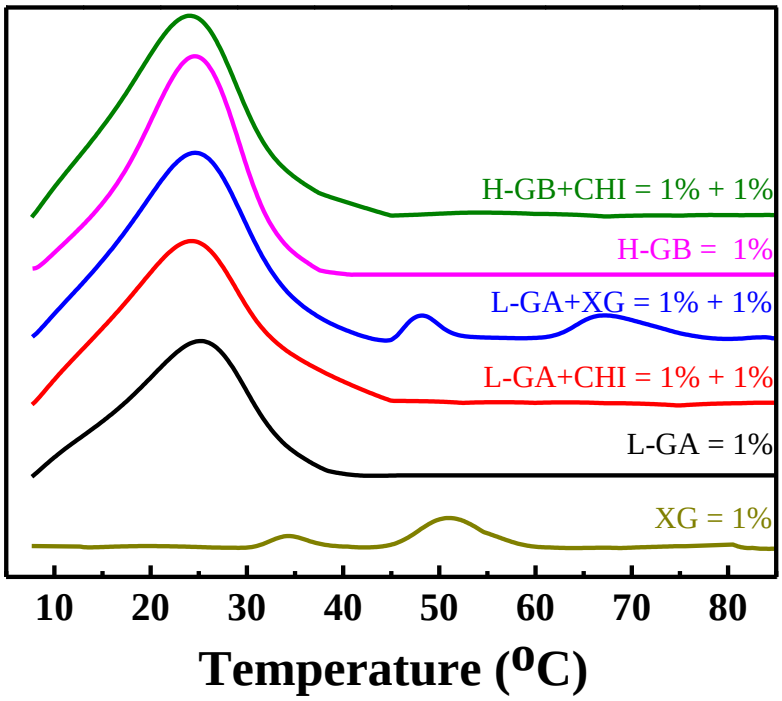

Figure 6.6 Micro-DSC heating curves shifted vertically for clarity. Scanning rate = 1 ^{o}C/min.

The enthalpy of the helix-to-coil transition of gelatin always increases in the presence of CHI or XG (**Table 6.1**). The enthalpies of 1.0 % L-GA in L-GA/XG and L-GA/CHI mixtures are even higher than that of 2.0 % w/v L-GA alone. In addition, L-GA exhibits a higher transition enthalpy when mixed with XG than with CHI. This indicates that both XG and CHI enhance gelatin triple helix formation, and gelation with XG is more effective than CHI. Furthermore, the two peaks of XG shift to higher temperatures and the enthalpies of helix to coil transition of XG increase by

adding L-GA compared to those of neat XG. This suggests that GA also helps XG to form more stable structures.

Table 6.1 Specific enthalpies and transition temperatures (peak maximum) of neat components and their mixtures during the second micro-DSC heating segment.

		Peak 1		Peak 2		Peak 3	
L-GA (%)	XG (%)	$T_1(^oC)$	$\Delta H_1{}^a$ (J/g)	$T_2(^oC)$	$\Delta H_2{}^b$ (J/g)	$T_3(^oC)$	$\Delta H_3{}^b$ (J/g)
-	1	-	-	35.6	0.49	52.3	1.54
1	-	25.2	14.33	-	-	-	-
2	-	24.8	18.29	-	-	-	-
1	1	24.6	20.42	48.1	0.78	67.2	2.04
L-GA (%)	CHI (%)			-	-	-	-
1	1	24.2	19.33	-	-	-	-
H-GB (%)	CHI (%)			-	-	-	-
1	-	24.6	19.83	-	-	-	-
2	-	24.9	24.42	-	-	-	-
1	1	24.0	22.13	-	-	-	-

a: normalized by the mass of gelatin;

b: normalized by the mass of XG;

6.4.6 Discussion

Based on our previous work [22] and the results above, the gelation mechanism of gelatin/polysaccharides aqueous mixtures can be divided into three steps (**Figure 6.7**):

1) The formation of soluble gelatin/polysaccharide complexes via electrostatic attraction occurs.

2) The decrease in the charge density of polysaccharides due to complexation reduces the distance between molecules and results in conformational transitions of polysaccharides when lowering the temperature. The transitions vary depending on the nature of the polysaccharide. For example, XG molecules undergo a coil-to-helix (disorder-to-order) transition whereas CHI molecules become less flexible upon cooling [26]. Moreover, side-by-side associations between the ordered XG domains leads to the formation of XG aggregates [27, 28].

3) Once cooling below the coil-to-helix transition temperature of gelatin, the gelatin triple helical structures form driven by hydrogen bonding, which concentrate and then bridge the complexes and/or aggregates. Finally, a colocalized network of biopolymer-rich domains is formed. This explains the observed increase in *G'* of gelatin/polysaccharide mixtures with time.

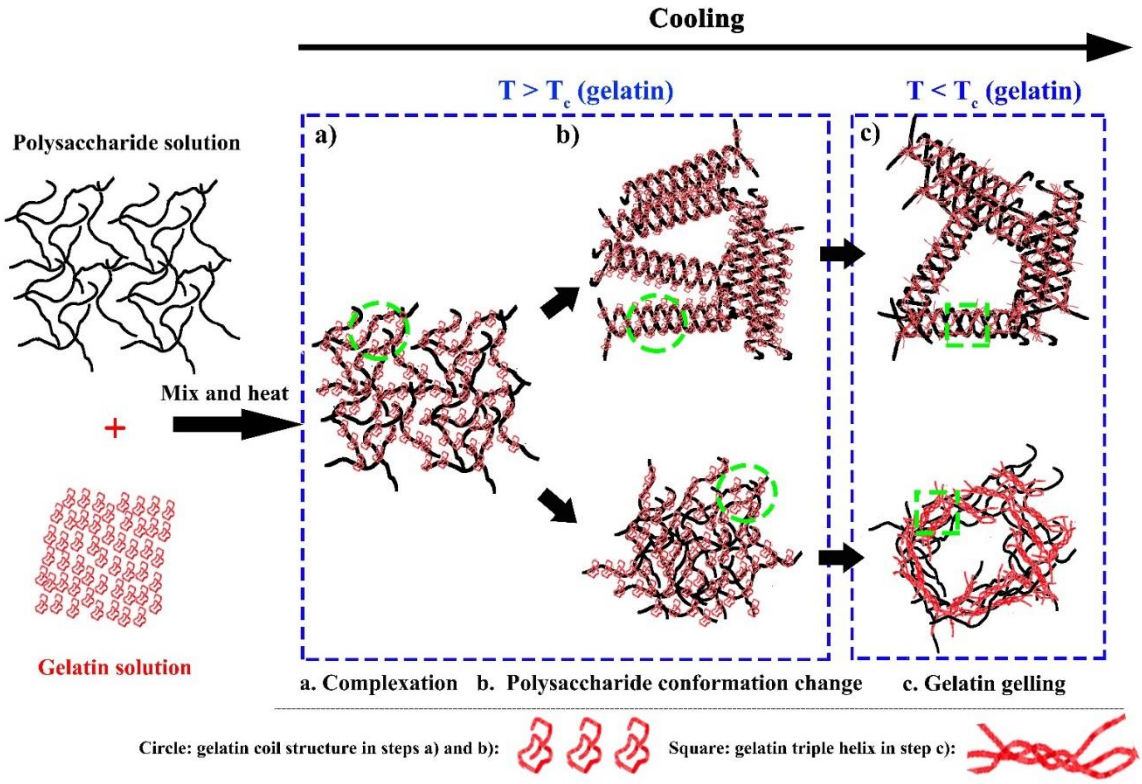

Figure 6.7 Gelation mechanism in gelatin/polysaccharide mixtures, based on their interactions and molecular conformations. XG molecules undergo a disorder-to-order transition and CHI molecules become less flexible upon cooling in step b.

The proposed mechanism is further supported by rheological temperature sweeps and turbidity measurements performed after heating to a homogeneous state, then cooling back to 20 °C (**Fig. 6.8**). L-GB/XG mixtures exhibit a gradual increase in *G'* and turbidity with time at 30 °C, whereas H-GB/CHI mixtures display no significant change. This confirms the formation of aggregates during the cooling process for gelatin/XG systems. The *G'* and turbidity of both mixtures increases with time when cooling down to 20 °C. indicating the development of the network structure.

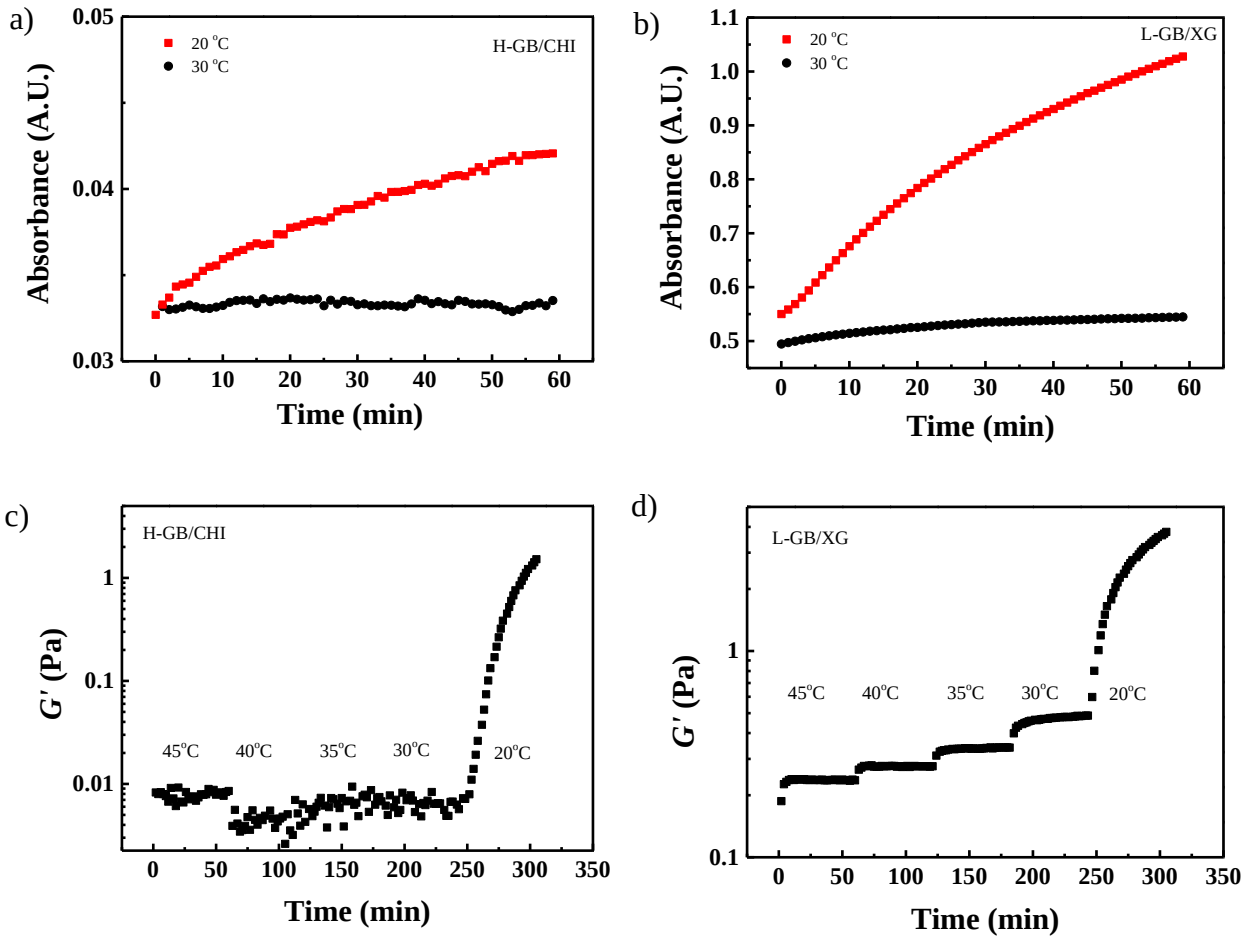

Figure 6.8 Time-resolved rheological and turbidity measurements at different temperatures, a) and c) H-GB/CHI, ratio = 4, pH 5.0; b) and d) L-GB/XG, ratio = 6, pH 5.5. Turbidity data were obtained at 600 nm.

6.5 Conclusions

The gelation of gelatin and charged polysaccharides aqueous mixtures occurs in three main steps depending on the coil-to-helix transition temperature of gelatin. When mixing gelatin and polysaccharides above the coil-to-helix transition temperature, complexation occurs by electrostatic attraction. The reduction in the charge density of polysaccharides shortens the distance between molecules, and induces a polysaccharide conformation change with decreasing temperature. Gelatin/XG mixtures can form aggregates in this temperature range due to the association between the ordered XG domains, whereas gelatin/CHI mixtures cannot, as evidenced by time-resolved rheological tests at different temperatures and turbidity measurements. Once

cooling down below the coil-to-helix transition temperature of gelation, the complexes and/or aggregates are concentrated and bridged by gelatin triple helix formation. This finally leads to a network of biopolymer-rich domains. A low extent of complexation may cause a segregative phase separation due to the repulsion between gelatin and polysaccharide, resulting in a complementary microstructure.

6.6 Acknowledgements

The authors acknowledge Dr. Nicolas Tran-Khanh from École polytechnique de Montréal for performing the CLSM observations, Dr. Françoise M. Winnik from University of Montreal for allowing us to use micro-DSC and Dr. Evgeniya Korchagina from University of Montreal for her help using micro-DSC and useful discussions. The authors also thank the Natural Sciences and Engineering Research Council of Canada (NSERC) and CREPEC for financial support, and the China Scholarship Council (CSC) for providing a scholarship to Mr. Wang.

6.7 Supporting information

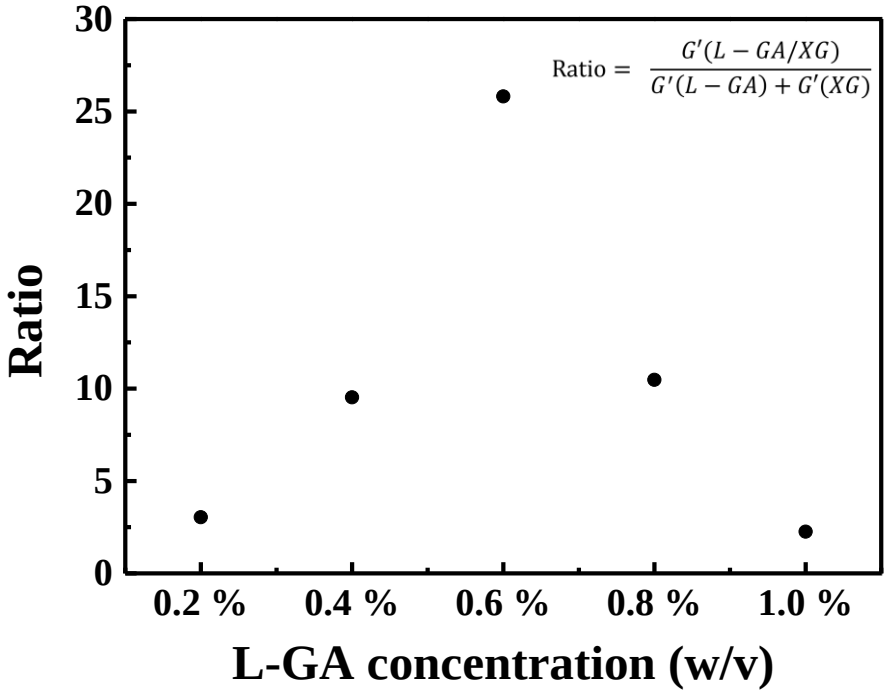

Fig. 6-S1 The ratio of *G'* of L-GA/XG mixtures over the sum of the *G'* of neat compositions at concentrations in the corresponding mixtures, as a function of gelatin concentration, 8 h after solution preparation (c_{XG} = 0.2 % w/v).

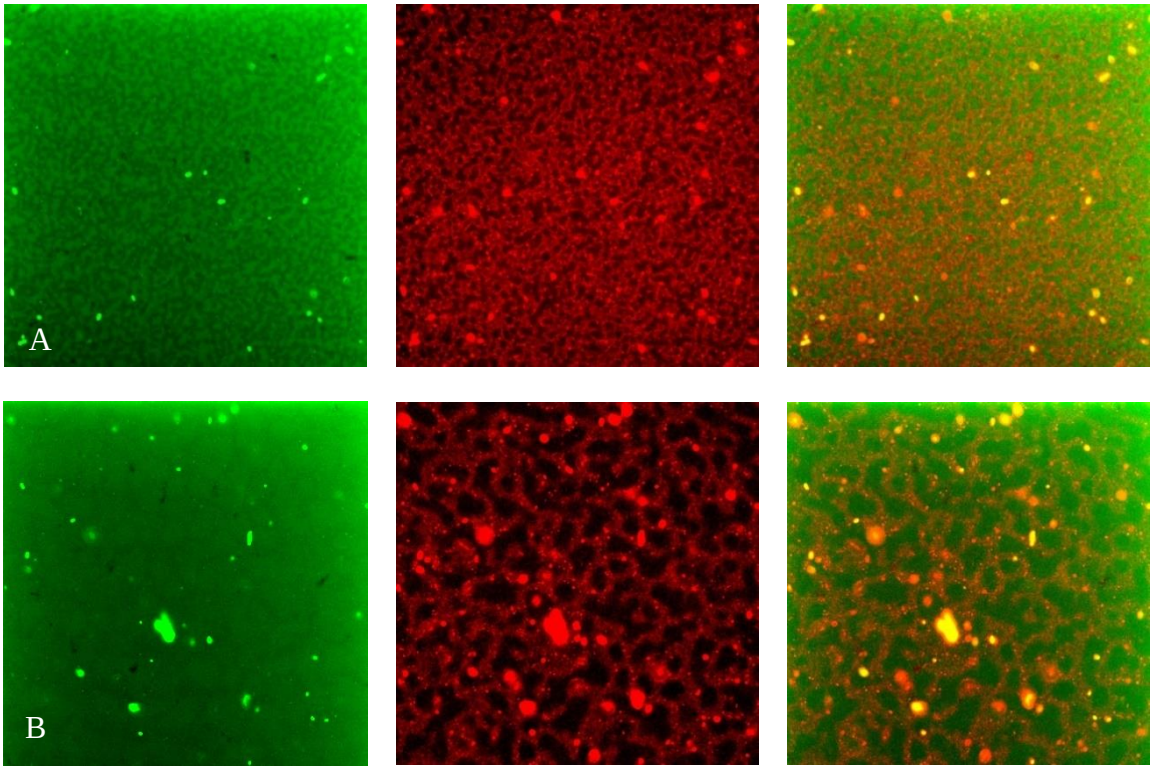

Figure 6-S2 Microstructures of L-GA/XG (Panel A, ratio 3, 120 µm x 120 µm) and L-GB/XG at pH 8.0 (Panel B, ratio 4, 105 µm x 105 µm). Gelatin appears in red and XG in green.

6.8 References

1. Schmitt, C. and Turgeon, S.L., *Protein/polysaccharide complexes and coacervates in food systems.* Advances in Colloid and Interface Science, 2011. **167**(1–2): p. 63-70.
2. Turgeon, S.L. and Laneuville, S.I., *CHAPTER 11 - Protein + Polysaccharide Coacervates and Complexes: From Scientific Background to their Application as Functional Ingredients in Food Products A2 - Kasapis, Stefan*, in *Modern Biopolymer Science*, I.T. Norton and J.B. Ubbink, Editors. 2009, Academic Press: San Diego. p. 327-363.
3. Schmitt, C., et al., *Structure and Technofunctional Properties of Protein-Polysaccharide Complexes: A Review.* Critical Reviews in Food Science and Nutrition, 1998. **38**(8): p. 689-753.

4. Le, X.T., Rioux, L.-E., and Turgeon S.L., *Formation and functional properties of protein-polysaccharide electrostatic hydrogels in comparison to protein or polysaccharide hydrogels.* Advances in Colloid and Interface Science, 2017. **239**: p. 127-135.
5. Wang, Y.F., Gao, J.Y., Dubin, P.L., *Protein separation via polyelectrolyte coacervation: selectivity and efficiency.* Biotechnology Progress, 1996. **12**: p. 356-362.
6. Zhu, A.-p., et al., *Interactions between N-succinyl-chitosan and bovine serum albumin.* Carbohydrate Polymers, 2007. **69**(2): p. 363-370.
7. van der Wielen, M.W.J., van de Heijning, W., and Brouwer, Y., *Cellulose Gum as Protective Colloid in the Stabilization of Acidified Protien Drinks*, in *Gums and Stabilisers for the Food Industry 14*, P.A. Williams and G.O. Phillips, Editors. 2008, The Royal Society of Chemistry: London, UK. p. 495-502.
8. Stokes, J.R., *Food Biopolymer Gels, Microgel and Nanogel Structures, Formation and Rheology*, in *Food Materials Science and Engineering*. 2012, Wiley-Blackwell. p. 151-176.
9. Wang, C.-S., et al., *Synergistic gelation of gelatin B with xanthan gum.* Food Hydrocolloids, 2016. **60**: p. 374-383.
10. Le, X.T. and Turgeon, S.L., *Rheological and structural study of electrostatic cross-linked xanthan gum hydrogels induced by [small beta]-lactoglobulin.* Soft Matter, 2013. **9**(11): p. 3063-3073.
11. Bertrand, M.-E. and Turgeon, S.L., *Improved gelling properties of whey protein isolate by addition of xanthan gum.* Food Hydrocolloids, 2007. **21**(2): p. 159-166.
12. Sanchez, C., et al., *Rheology of whey protein isolate-xanthan mixed solutions and gels. Effect of pH and xanthan concentration.* Food / Nahrung, 1997. **41**(6): p. 336-343.
13. Rabea, E.I., et al., *Chitosan as antimicrobial agent: Applications and mode of action.* Biomacromolecules, 2003. **4**(6): p. 1457-1465.
14. Riva, R., et al., *Chitosan and Chitosan Derivatives in Drug Delivery and Tissue Engineering.* Chitosan for Biomaterials Ii, 2011. **244**: p. 19-44.
15. Chen, R.-H., et al., *Advances in chitin/chitosan science and their applications.* Carbohydrate Polymers, 2011. **84**(2): p. 695-695.
16. Ravi Kumar, M.N.V., *A review of chitin and chitosan applications.* Reactive and Functional Polymers, 2000. **46**(1): p. 1-27.
17. Rinaudo, M., *Chitin and chitosan: Properties and applications.* Progress in Polymer Science, 2006. **31**(7): p. 603-632.
18. Wang, X.-Y., Wang, C.-S., and Heuzey, M.-C., *Complexation of chitosan and gelatin: From soluble complexes to colloidal gel.* International Journal of Polymeric Materials and Polymeric Biomaterials, 2016. **65**(2): p. 96-104.
19. Qaqish, R. and Amiji, M., *Synthesis of a fluorescent chitosan derivative and its application for the study of chitosan–mucin interactions.* Carbohydrate Polymers, 1999. **38**(2): p. 99-107.

20. Liu, C., et al., *Complex coacervation of chitosan and soy globulins in aqueous solution: a electrophoretic mobility and light scattering study.* International Journal of Food Science & Technology, 2011. **46**(7): p. 1363-1369.

21. de Kruif, C.G., Weinbreck, F., and de Vries, R., *Complex coacervation of proteins and anionic polysaccharides.* Current Opinion in Colloid & Interface Science, 2004. **9**(5): p. 340-349.

22. Wang, C., et al., *A mechanism for the synergistic gelation properties of gelatin B and xanthan gum aqueous mixtures.* Carbohydrate Polymers, Submitted.

23. Sarbon, N.M., Badii, F., and Howell, N.K., *The effect of chicken skin gelatin and whey protein interactions on rheological and thermal properties.* Food Hydrocolloids, 2015. **45**: p. 83-92.

24. Alqahtani, N.K., et al., *Effect of Oat Particle Concentration and Size Distribution on the Phase Behaviour of Mixtures with Gelatin.* Journal of Food and Nutrition Research, 2016. **4**(2): p. 69-75.

25. Cheow, C.S., et al., *Preparation and characterisation of gelatins from the skins of sin croaker (Johnius dussumieri) and shortfin scad (Decapterus macrosoma).* Food Chemistry, 2007. **101**(1): p. 386-391.

26. Chen, R.H. and Tsaih, M.L., *Effect of temperature on the intrinsic viscosity and conformation of chitosans in dilute HCl solution.* International Journal of Biological Macromolecules, 1998. **23**(2): p. 135-141.

27. Norton, I.T., et al., *Mechanism and dynamics of conformational ordering in xanthan polysaccharide.* Journal of Molecular Biology, 1984. **175**(3): p. 371-394.

28. Stephen, A.M. and Phillips, G.O., *Food polysaccharides and their applications*. Bacterial Polysaccharides. Vol. 160. 2010: CRC Press.

CHAPTER 7 ARTICLE 4: PROTEIN/POLYSACCHARIDE BASED HYDROGELS PREPARED BY VAPOR-INDUCED PHASE SEPARATION

Chang-Sheng Wang, [a] Nick Virgilio, [a*] Paula M. Wood-Adams, [b] Marie-Claude Heuzey [a*]

[a] Centre de Recherche sur les Systèmes Polymères et Composites à Haute Performance (CREPEC), Department of Chemical Engineering, Polytechnique Montréal, Montréal, Québec, H3C 3A7, Canada.

[b] CREPEC, Department of Mechanical and Industrial Engineering, Concordia University, Montréal, Québec, H3G 1M8, Canada.

This work has been submitted to *ACS Macro letters*

7.1 Abstract

The preparation of hydrogels via vapor induced phase separation (VIPS) has received limited attention. VIPS consists of exposing a solution containing a gelling agent to a vapor that induces gelation via mass transfer at the gas/liquid interface. We demonstrate, using mixtures of gelatin B and xanthan gum exposed to acetic acid vapors, that VIPS is efficient for the preparation of protein/polysaccharide mixed gels. This method prevents the typical precipitation of protein/polysaccharide complexes observed in the strong electrostatic attraction regime. It significantly extends the pH window associated with gel formation, and yields mechanically stronger gels as compared to other preparation techniques such as using glucono delta-lactone or the conventional dropwise pH adjustment technique. Finally, VIPS yields gels at very low gelling agent content, and for a variety of other mixed systems, including globular proteins such as bovine serum albumin.

7.2 Results and discussion

Protein/polysaccharide mixed gels have recently attracted much attention for the protection of bioactive molecules when used as encapsulation and delivery systems [1, 2], since gelation can occur without crosslinking agents or enzymes. Their mechanical properties can be tuned by controlling various parameters such as pH, ionic strength, protein to polysaccharide ratio and

temperature [2-4]. The two most common ways to prepare mixed gels are (1) mixing together aqueous solutions of protein and polysaccharide, followed by adjusting the pH by adding acidic (e.g. HCl) or alkaline (e.g. NaOH) solution; and (2) preparing two separate solutions of polysaccharide and protein both at the desired pH, and then mixing the solutions together. These methods are quick (pH changes within seconds), and usually result in precipitation instead of gelation at a pH well below (or above) the pI of protein, or at very low biopolymer concentrations.

One way to broaden the range of pH and composition for gel formation is to slow down the acidification (or alkalization) process to several minutes or hours. A typical example is to use glucono delta-lactone (GDL), which is an internal ester. It gradually hydrolyzes in solution, causing a slow decrease of pH over time (**Figure 7.1**, open symbols). The acidification rate increases with increasing GDL content, and the pH reaches a final value after 4-5 hrs. However, since GDL is a crystalline powder, stirring (15~20 min) is needed to dissolve and disperse it. This process has two problems: a) large aggregates or precipitates are formed due to the initial fast decrease in pH and b) the initial crosslinks or junctions between protein/polysaccharide complexes are continuously disrupted due to shear.

Another technique to slow down the acidification (or alkalization) process is vapor-induced gelation (also called vapor-induced phase separation or VIPS) [5]. This technique has until now received relatively little attention in the preparation of hydrogels. It has been tested exclusively for the preparation of chitosan/chitin hydrogel membranes [6], and as far as we know there are no reports for other gelling polysaccharides or proteins, or for mixed systems. The approach consists of using a closed vessel saturated with a volatile compound. By diffusing this compound via the gas/liquid interface into a solution of the gelling agent, a phase separation is induced leading to gelation. For example, chitosan hydrogels have been prepared following this approach by exposing the chitosan solution to ammonia vapors [6]. This method allows gels to form without mechanical perturbation during the entire gelation process, as opposed to gelling using GDL.

Herein, we compare all three gelation techniques and correlate the microstructural analysis to mechanical properties of mixed gels of gelatin B (GB, protein pI = 5.3) and xanthan gum (XG, a negatively charged polysaccharide). We demonstrate that VIPS significantly extends the range of pH and composition that can undergo gelation, including very low biopolymer concentrations.

VIPS of GB/XG mixtures was realized by exposing the solutions to vapors of acetic acid in a sealed chamber. Due to its volatility, acetic acid is gradually transferred into the protein/polysaccharide aqueous mixture across the gas/liquid interface, resulting in a gradual decrease of pH over time. The acidification rate is controlled by the acetic acid concentration (**Figure 7.1**, solid symbols), and the pH keeps decreasing after 24 h.

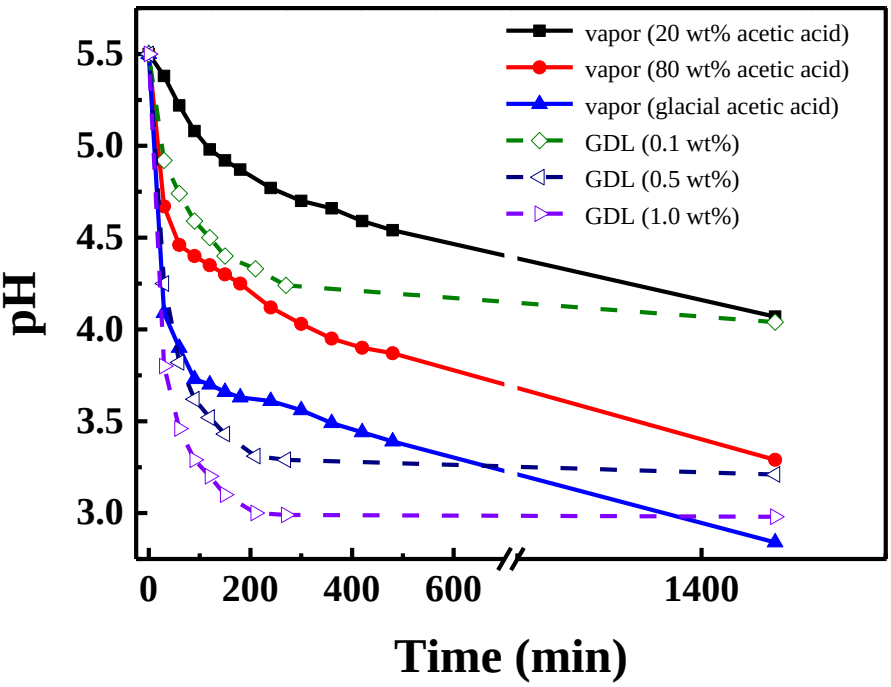

Figure 7.1. pH of a gelatin B solution (1.0 % w/v) as a function of time under different acidification conditions: acetic acid vapor (solid symbols, wt% in water) and GDL addition (open symbols).

Gelation by VIPS occurs locally from the top to the bottom of the vial, starting at the gas/liquid interface, and the gelation rate increases with the GB content (**Figure 7S1a**, see red dashed lines). Gels prepared by the VIPS technique display much less syneresis at a given composition compared to those prepared by GDL addition (**Figure 7.2a**). All mixed gels break down and form precipitates when heated at T ≈ 45 ^{o}C (**Figure 7.2a**). This process is irreversible due to the low pH (~3.0-4.0) of the mixtures. Adjusting pH to a similar value by adding an acidic solution following the conventional method results in the formation of precipitates (**Figure 7S1b**). The obtained mixed gels are stable in water and ethanol for a long time (more than one week).

The gelation behavior of the mixtures under VIPS also varies depending on the initial pH. For example, when starting at pH 5.5, where complexation between GB and XG has already occurred [7], very minor syneresis is observed; whereas at a higher initial pH, where the two biopolymers repel each other and are phase separated [8], heterogeneous gels (pH = 8.0, **Figure 7S1c**) with significant syneresis or viscoelastic liquids are obtained (pH = 10.0, **Figure 7.2b**).

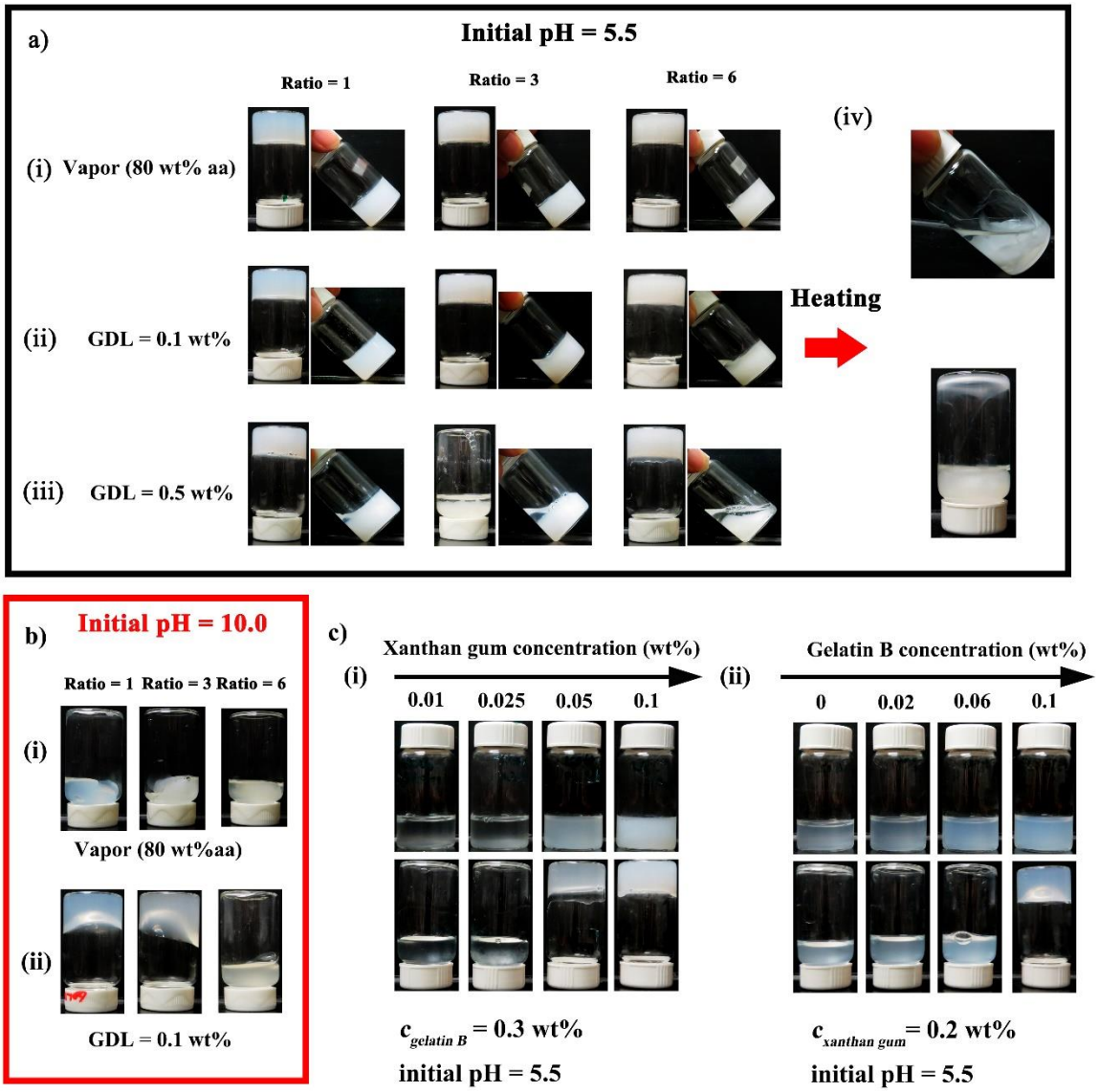

Figure 7.2. State of the mixtures in terms of gelation (upside down vials) and syneresis (tilted vials) after 24 h: a) initial pH = 5.5 and prepared (i) by exposing to vapor of 80 wt% acetic acid; (ii) with 0.1 wt% GDL; (iii) with 0.5 wt% GDL; (iv) gel destabilization after

heating; b) initial pH = 10.0 prepared (i) by exposing to vapor of 80 wt% acetic acid and (ii) with GDL addition; c) effects of (i) XG and (ii) GB concentration.

VIPS also significantly decreases the critical total biopolymer concentration required for gel formation, from 1.2 wt% for the conventional mixing method by dropwise pH control with HCl [7] to 0.3 wt% (**Figure 7.2c**). Note that the critical gelling concentration for a neat GB solution is 4.0 wt%, whereas XG is a non-gelling polysaccharide – this is more than an order of magnitude lower in concentration. This method can also be used to prepare mixed gels of globular proteins (*e.g.* bovine serum albumin) and polysaccharides (**Figure 7S1d**).

The gels produced by the GDL addition method differ in several aspects from those produced by VIPS due to the required mechanical stirring. With GDL, gelation occurs simultaneously over the whole volume (this is not an interfacial process), and is greatly affected by the GDL concentration and stirring time. For example, the mixture at a GB/XG ratio of 6 produces a gel when c_{GDL} = 0.1 wt%, but precipitates when c_{GDL} is 0.5 wt%, when stirred initially for 15 min (**Figure 7.2a**). No gels are formed when the GDL concentration increases to 1.0 wt%, regardless of GB/XG ratio. An increase in syneresis is observed when the GDL content increases for a given composition (**Figure 7.2a**), and the syneresis also increases significantly with increasing GB content at a constant GDL concentration. Note that extending the initial stirring time to 30 min leads to an increase in syneresis, and 90 min prevents gel formation (**Figure 7S1e**). A similar phenomenon also occurs in the VIPS technique if stirring is applied (**Figure 7S1e**). Note finally that for the GDL method, for a given GDL concentration, starting at a higher initial pH results in a higher final pH, which then results in a weaker mixed gel (**Figure 7.2b**).

Both slow acidification methods induce mixed gel formation significantly below the pI of GB, where the electrostatic attraction between the two biopolymers is very strong. The microstructures of the resulting mixed gels are characterized by the formation of biopolymer-rich and biopolymer-poor domains [7, 8]. Gels obtained by VIPS (using an 80 wt% acetic acid) comprises clear, sharp, colocalized networks of GB and XG, with colocalization increasing with GB concentration (**Figure 7.3**, Panel A, note the changing amount of green in the primarily yellow images). Increasing GB concentration and therefore complexation with XG also causes gradual neutralization of the system, and as a result, a more compact network structure is observed. Another striking feature is that the

two networks are very well defined, with very thin biopolymer-rich domains – contrasting sharply with gels prepared by the conventional method of dropwise pH control [7].

In comparison, mixed gels prepared by GDL addition (0.1 wt%) display less regular and more tenuous microstructures, with smaller biopolymer-poor domain size and more aggregated biopolymer-rich domains (**Figure 7.3**, **Panel B**). This becomes more obvious with increasing GB content, especially for the mixture at ratio 6. A direct consequence of this is the lower gel strength of gels prepared with GDL.

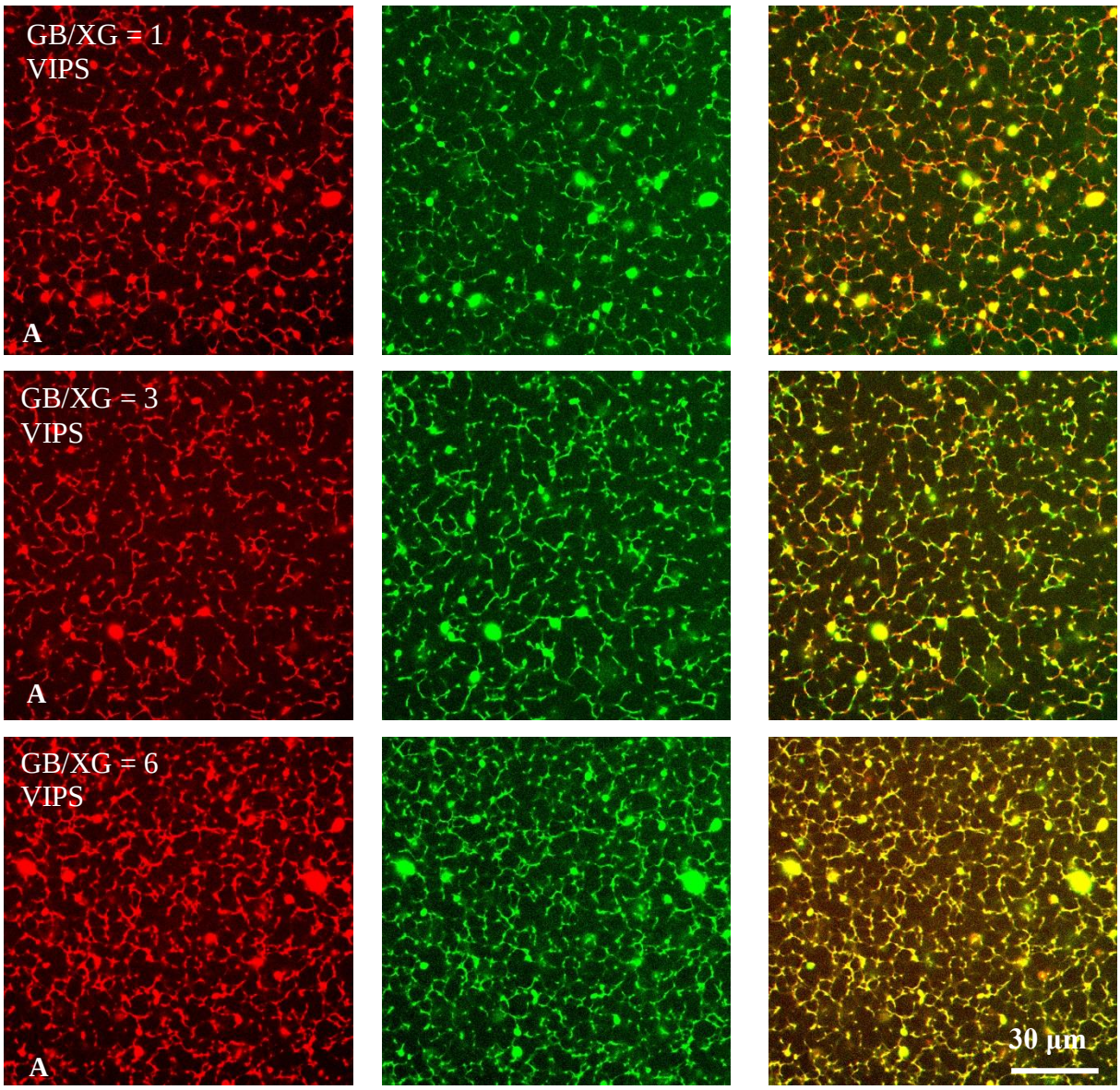

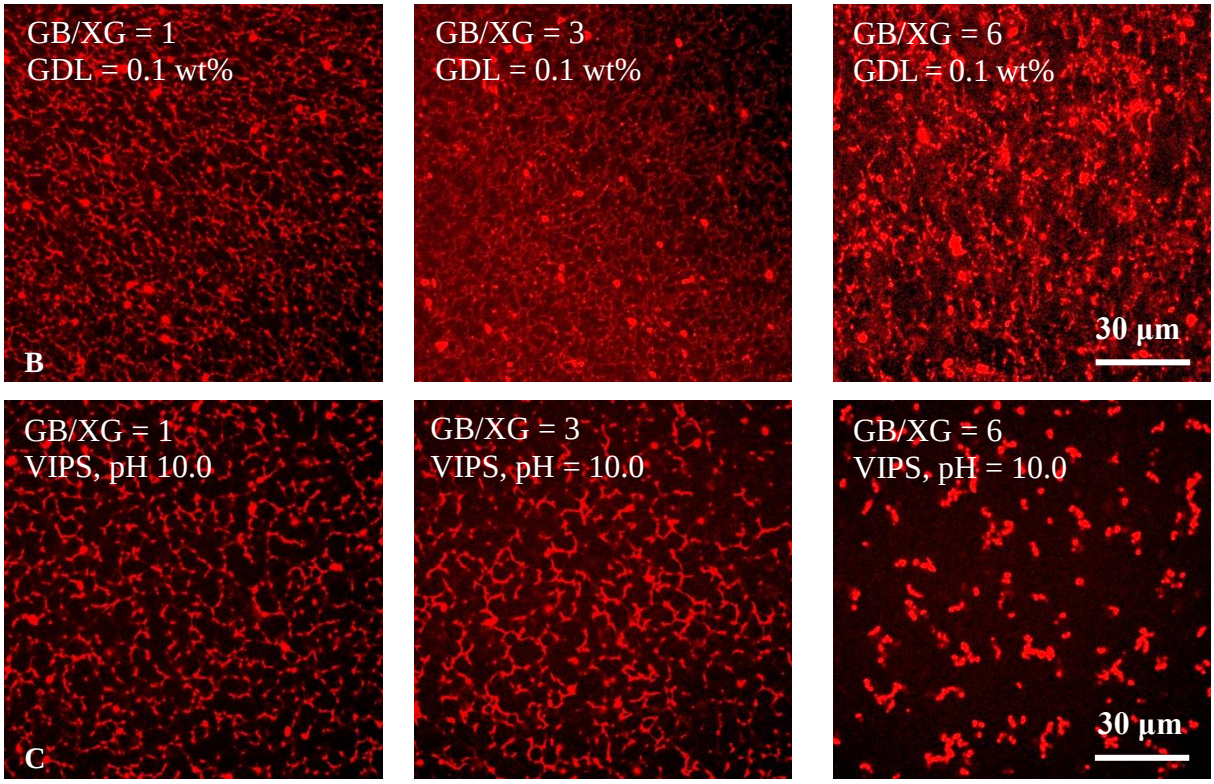

Figure 7.3. Microstructures of GB/XG (c_{XG} = 0.2 wt%) mixed gels prepared from an initial pH of 5.5 by VIPS using 80 wt% acetic acid (Panel A), and by GDL addition (Panel B); Panel C: mixed gels prepared from an initial pH of 10.0 by VIPS using 80 wt% acetic acid vapor. GB appears in red and XG in green with colocalized networks appearing yellow. The images were taken after 24 h storage.

Interestingly, increasing the initial starting pH reduces significantly the connectivity between the biopolymer-rich domains of gels prepared by VIPS (**Figure 7.3**, **Panel C** and **Figure 7S2a**). When starting at a higher pH, GB and XG are initially phase separated in solution [7, 8], as compared to the complexes that exist at pH 5.5. This indicates that the diffusion of hydrocolloids and how their electrostatic charges evolve with pH play important roles in establishing the final microstructure. More thorough investigations are required on these aspects.

We then characterized the gel strength of the mixed gels prepared with the VIPS, GDL, and conventional solution titration methods. Briefly, force/gap curves were obtained by monitoring the normal force as a function of decreasing gap distance using a commercial rotational rheometer (**Figures 7S3 to 7S5** show experimental setup and examples of force-displacement curves). The

force at break reported in **Figure 7.4** represents the maximum force before gel failure by compression puncture and is taken as a measure of gel strength.

Significant enhancement of the gel strength is observed for gels prepared by VIPS and GDL addition, as compared to the conventional method (dropwise pH adjustment) – at least by a factor of 20, and up to ~200. The VIPS samples exhibit significantly higher strengths than the GDL samples for GB/XG ratios of 3 and 6. For the slow acidification techniques, a maximum in strength is observed at a GB/XG ratio of 3. Increasing the acetic acid solution concentration yields stronger gels at a given GB/XG ratio due to the stronger attraction between GB and XG caused by the lower final pH.

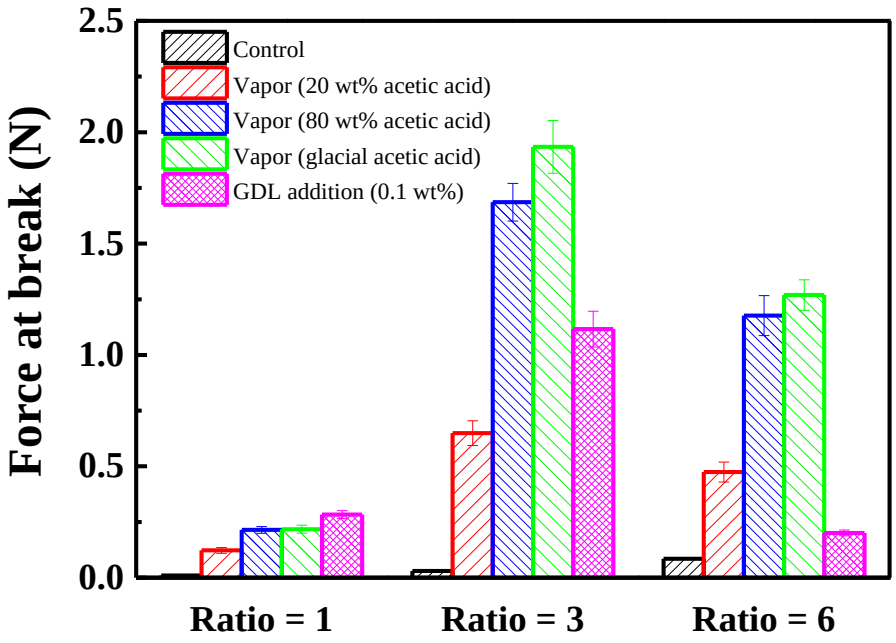

Figure 7.4. Force at break in compression of mixed gels at different GB/XG ratios, prepared by different methods after 24 h storage (c_{XG} = 0.2 wt%).

In summary, the gelation of GB/XG aqueous mixtures by slow acidification methods is affected by stirring, mixture composition, acidification rate, and the initial and final pH. Stirring has a significant impact on the resulting mechanical properties since it disrupts the initial network formed between GB/XG complexes. Less charged systems (*e.g.* high GB content) or faster decrease of pH (*e.g.* higher GDL content) leads to aggregation and/or precipitation and thus lower gel strength.

This can also cause syneresis and even prevent network formation. Finally, the initial pH has an effect on gelation by controlling the initial level of complexation between GB and XG, while the final pH controls how strongly GB and XG are bound to each other – which is ultimately reflected by the gel strength.

Therefore, two key steps are required for gelation to occur by acidifying the mixtures: complexation between GB and XG must first occur, and complexes must subsequently establish junctions to ultimately form a network. When starting at a relatively low initial pH (*e.g.* pH 5.5, close to the pI of GB), only the second step needs to occur since the complexes are already formed after solution mixing [7]. When starting at a higher pH, complexation must take place as pH decreases, since GB and XG are initially phase separated, followed by network formation. Since the integrity of the network determines the strength, VIPS, which does not involve mechanical stirring, generally yields stronger gels than those prepared with GDL.

At high initial pH with VIPS, complexation is limited by diffusion of the components, which results in inhomogeneous gels (*e.g.* initial pH = 8.0) or no gel formation (*e.g.* initial pH = 10.0). When using GDL with high initial pH, stirring accelerates the complexation step, but disrupts the initial network formation. The final pH affects the strength of the electrostatic attraction between GB and XG, potentially explaining why a lower final pH is associated with stronger mechanical properties.

In conclusion, we have demonstrated that vapor-induced phase separation (VIPS) can be used to prepare protein/polysaccharide mixed gels with increased gel strength, as compared to other conventional gelation techniques. This method allows mixed gel formation without mechanical perturbation, resulting in the formation of highly colocalized networks of GB and XG. Gelation induced by slow acidification is affected by several factors, including mechanical stirring, acidification rate, and the initial and final pH.

7.3 Experimental section

7.3.1 Materials

Gelatin (type B, G6650, bloom index ~75, molecular weight: 20-25 kDa, pI = 5.3) (GB) and xanthan gum (from *xanthomonas campestris*, G1253, molecular weight ≈ 2000 kDa) (XG) were

purchased from Sigma-Aldrich Canada. All other reagents and chemicals were of analytical grade and were used without further purification.

7.3.2 Preparation of GB, XG and GB/XG solutions

GB solutions (0.4-2.4 wt%) were prepared by allowing the protein to swell in Milli-Q water (18.2 Ω) for 15-20 min, followed by gentle stirring at 60 ^{o}C for 15 min. The solutions were used on the same day. XG solutions (0.4 wt%) were prepared by dissolving the powder into Milli-Q water at a stirring speed of 600-700 rpm for at least 12 h at room temperature, to ensure complete dissolution. Mixed GB/XG solutions with a fixed XG concentration (0.2 wt%) and different GB concentrations (0.2-2.0 wt%) were prepared by mixing equal volumes of GB and XG primary solutions under magnetic stirring at 60 ^{o}C for approximately 30 min.

7.3.3 Preparation of GB/XG mixed gels

For the glucono delta-lactone (GDL) addition method: the mixtures were stirred for 15 min to dissolve and disperse the GDL crystalline powder after its addition. Then, for "table-top" rheology, 6 mL of solution were transferred into 20 mL vials (Fisherbrand, O.D. × H (with cap): 28 x 61 mm), and for mechanical tests, 20 mL were transferred into petri dishes (O.D.× H: 50 x 11 mm) (see **Figure 7S3**). The mixtures were kept at room temperature for 24 h to allow gelation before analysis. For the vapor-induced method (VIPS), the GB/XG mixtures were first transferred into vials or Petri dishes, and then sealed in a chamber with acetic acid solutions in water (20-100 wt %) for 24 h to allow gelation before analysis.

7.3.4 Confocal laser scanning microscope (CLSM)

The mixed gels were observed with an Olympus IX 81 inverted Confocal Microscope (Olympus Canada Inc., Richmond Hill, ON, Canada). GB was stained with Nile Blue A (N0766, Sigma) in solution under magnetic stirring for 30 min before mixing with XG solutions. XG was covalently labeled with 5-(4,6-dichlorotriazinyl) aminofluorescein (DTAF) (D0531, Sigma) using a method described previously [23]. After mixing, solution samples were poured into Petri dishes. Observation of XG was made by excitation of DTAF at 488 nm, the emission being recorded between 510 and 550 nm. Observation of GB was made by excitation of Nile Blue A at 633 nm, the emission being recorded between 650 and 680 nm. Micrographs were taken using a 60x

objective lens at a 2048 x 2048 pixels resolution. All micrographs were subsequently analyzed using Image J software.

7.3.5 Mechanical properties

Gel mechanical properties in compression were probed with a stress-controlled Physica MCR 501 rheometer (Anton Paar, Graz, Austria). The gels were penetrated with a 12-mm diameter cylinder probe (modified using the disposable geometry shaft, **Figure 7S3**). A normal force-displacement (or gap) curve was obtained at a crosshead speed of 0.5 mm/s (**Figure 7S5**). To protect the instrument, the software was set to terminate the test when the normal force reaches 50 N, or the gap is less than 0.5 mm.

7.4 Acknowledgements

The authors thank the Natural Sciences and Engineering Research Council of Canada (NSERC) and CREPEC for financial support, and the China Scholarship Council (CSC) for providing a scholarship to Mr. Wang. The authors also acknowledge Mr. Matthieu Gauthier from Polytechnique Montreal for his assistance when using the rheometer for the compression tests.

7.5 Supporting information

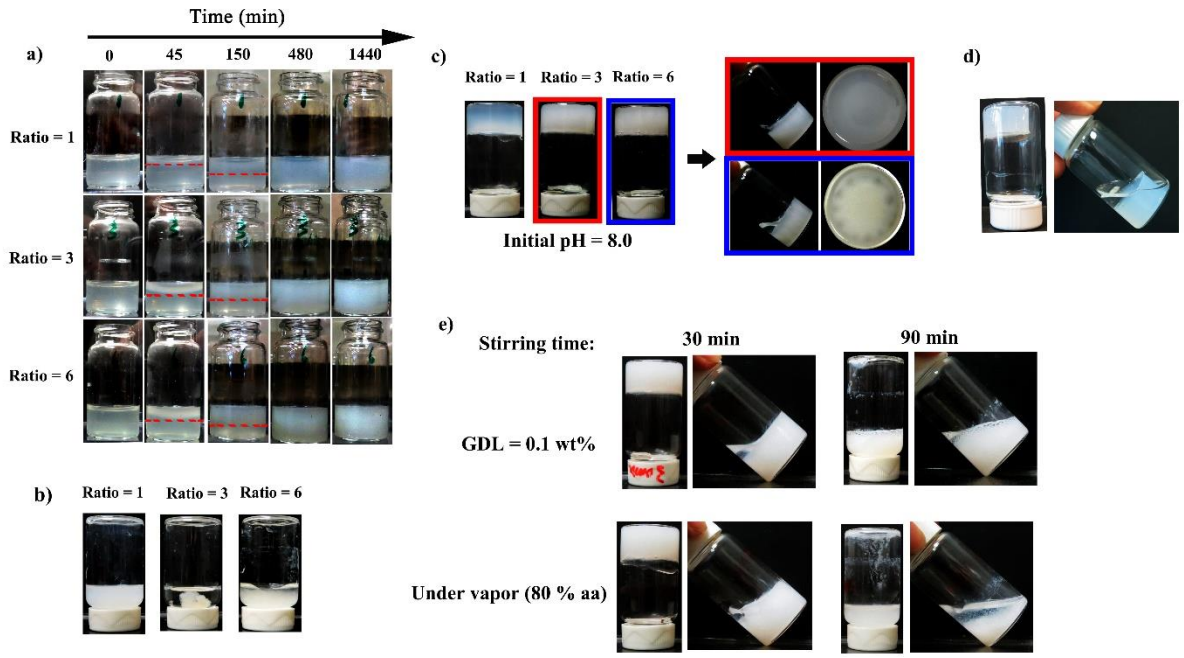

Figure 7-S1. a) Gelling kinetics of GB/XG mixtures exposed to acetic acid (80 wt%) vapor (GB/XG ratios: 1, 3 and 6; c_{XG} = 0.2%, initial pH: 5.5). The dashed line indicates the gel/liquid interface (gel phase on the top); b) Close-up view of mixtures when adjusting pH to ~4.0 using HCl in solution; c) gels prepared by VIPS, at an initial pH = 8.0; d) bovine serum albumin and XG mixed gels prepared by VIPS using acetic acid, c_{BSA} = 1.0 wt% and c_{XG}= 0.2 wt%; e) the effect of stirring time on the mixed gel formation, c_{GB} = 0.6 wt% and c_{XG} = 0.2 wt%.

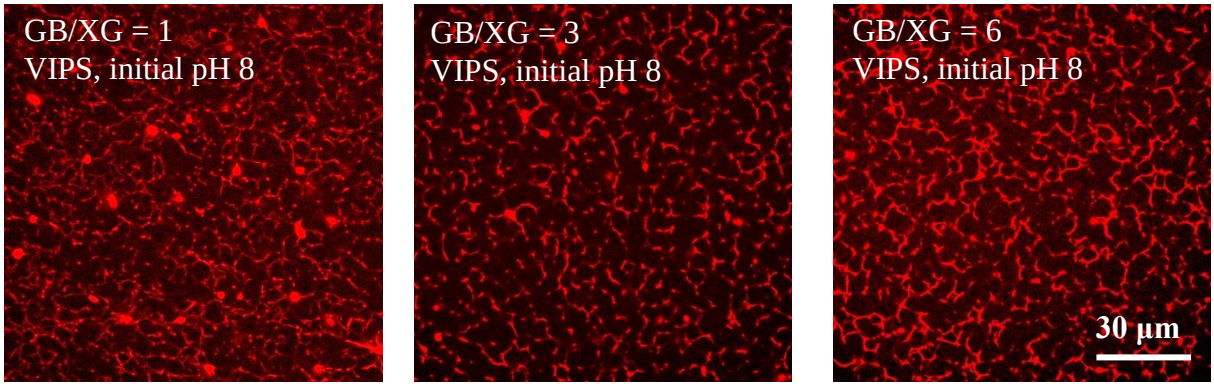

Figure 7-S2. Microstructures of GB/XG mixed gels prepared by acetic acid vapor (80 wt%) after 24 h with a starting pH of 8.0.

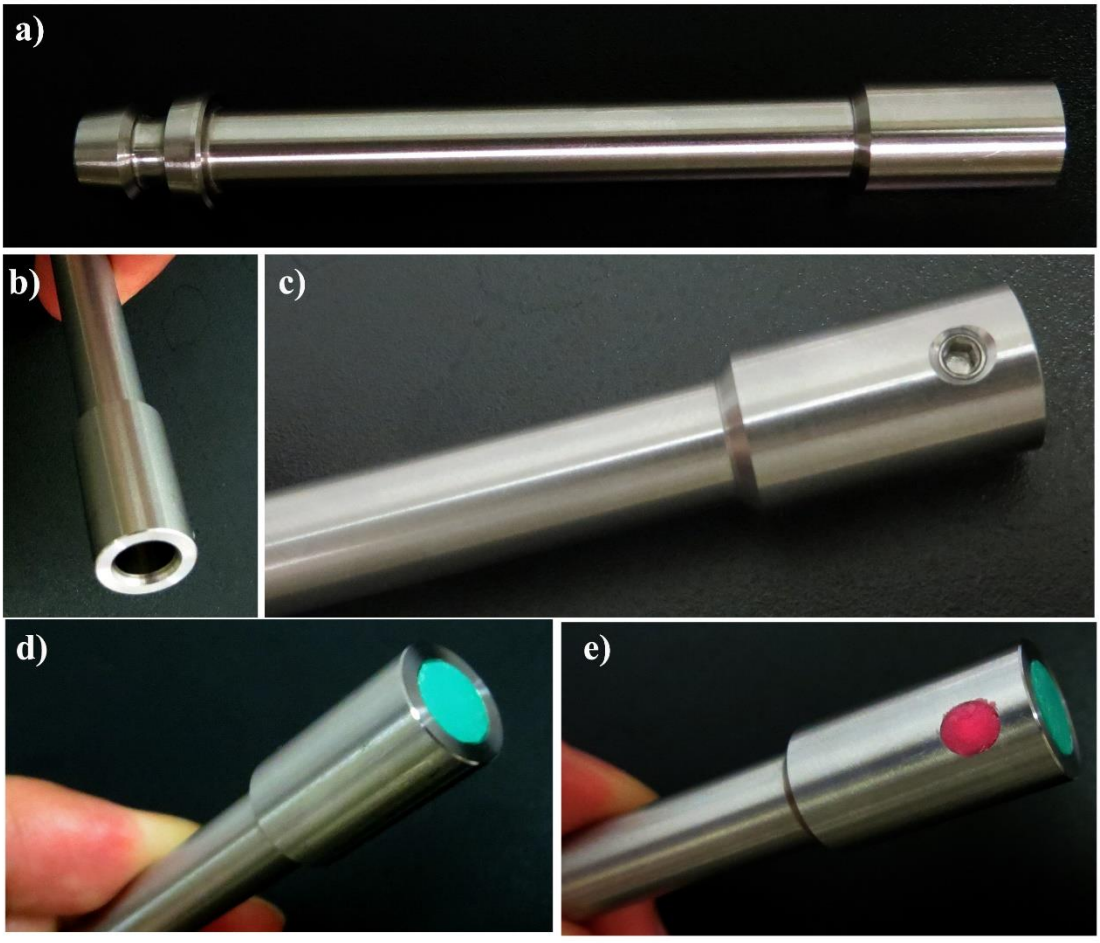

Figure 7-S3. Geometry setup for gel strength measurement.

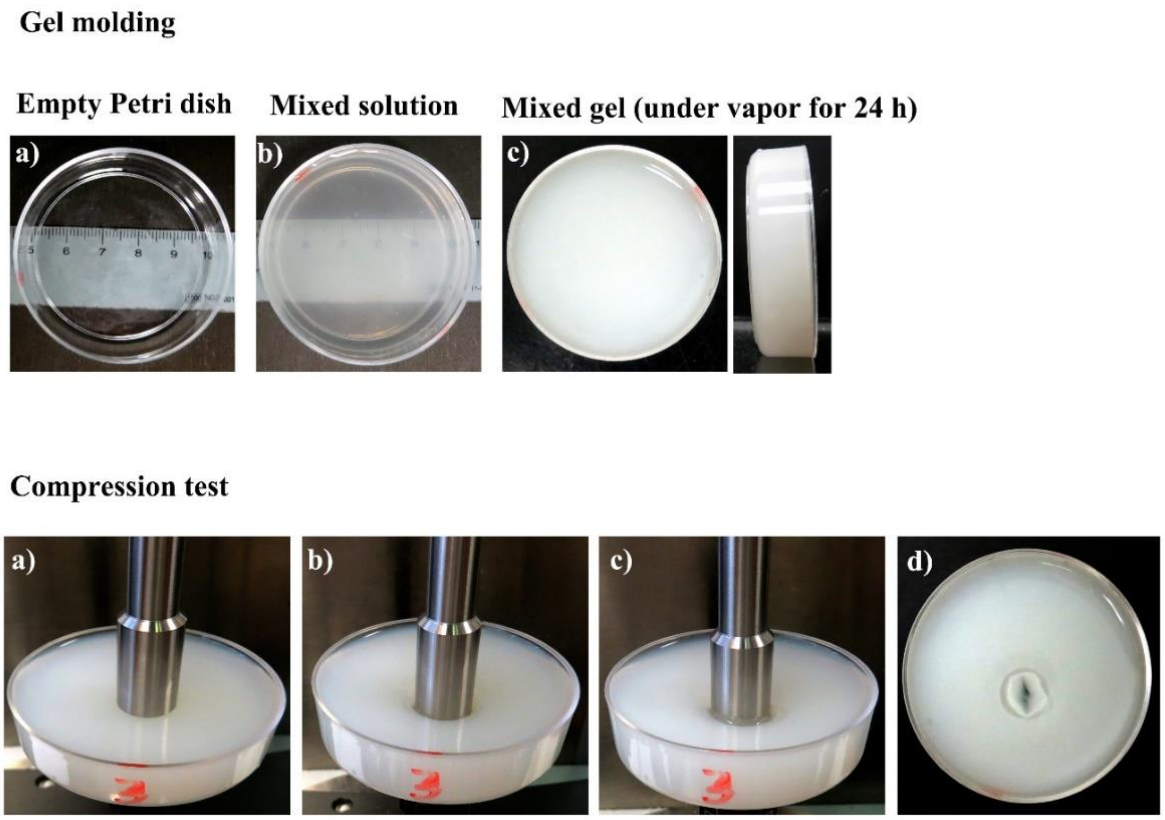

Figure 7-S4. Gel molding and compression test.

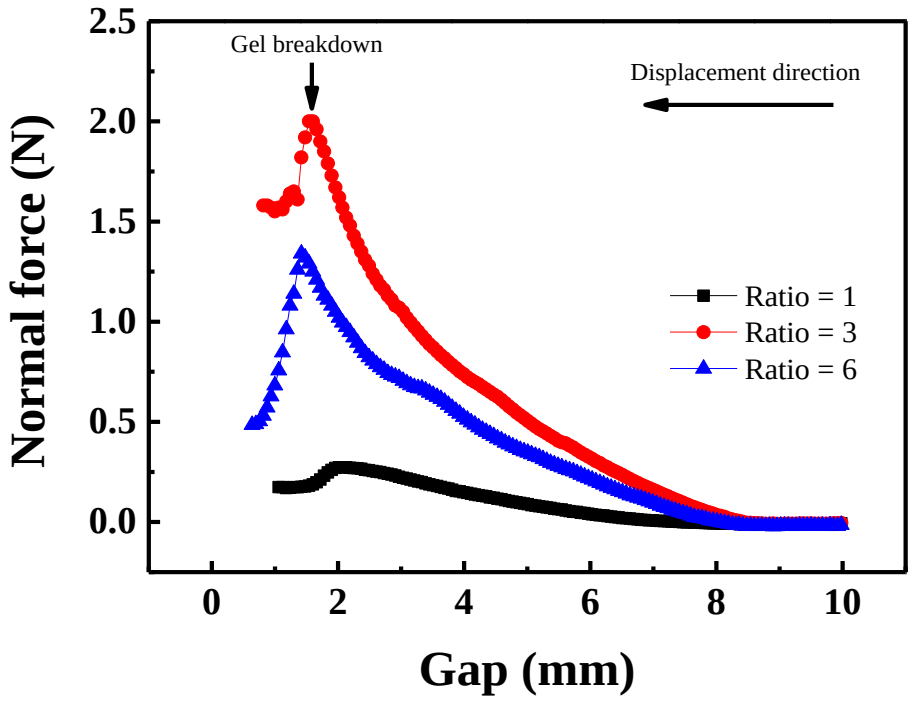

Figure 7-S5. Normal force vs. gap curve for GB/XG gels prepared by VIPS using glacial acetic acid.

7.6 References

1. Turgeon, S.L. and Laneuville, S.I., *CHAPTER 11 - Protein + Polysaccharide Coacervates and Complexes: From Scientific Background to their Application as Functional Ingredients in Food Products A2 - Kasapis, Stefan*, in *Modern Biopolymer Science*, I.T. Norton and J.B. Ubbink, Editors. 2009, Academic Press: San Diego. p. 327-363.
2. van der Wielen, M.W.J., van de Heijning, W., and Brouwer, Y., *Cellulose Gum as Protective Colloid in the Stabilization of Acidified Protien Drinks*, in *Gums and Stabilisers for the Food Industry 14*, P.A. Williams and G.O. Phillips, Editors. 2008, The Royal Society of Chemistry: London, UK. p. 495-502.
3. Turgeon, S.L. and Beaulieu, M., *Improvement and modification of whey protein gel texture using polysaccharides.* Food Hydrocolloids, 2001. **15**(4): p. 583-591.
4. Bertrand, M.-E. and Turgeon, S.L., *Improved gelling properties of whey protein isolate by addition of xanthan gum.* Food Hydrocolloids, 2007. **21**(2): p. 159-166.
5. Venault, A., et al., *A review on polymeric membranes and hydrogels prepared by vapor-induced phase separation process.* Polymer Reviews, 2013. **53**(4): p. 568-626.

6. Montembault, A., Viton, C., and Domard, A., *Rheometric Study of the Gelation of Chitosan in Aqueous Solution without Cross-Linking Agent.* Biomacromolecules, 2005. **6**(2): p. 653-662.

7. Wang, C.-S., et al., *Synergistic gelation of gelatin B with xanthan gum.* Food Hydrocolloids, 2016. **60**: p. 374-383.

8. Wang, C.-S, et al., *A Gelation Mechanism for Gelatin/Polysaccharide Aqueous Mixtures.* Food Hydrocolloids, Submitted.

CHAPTER 8 GENERAL DISCUSSION

Proteins and polysaccharides can form different types of networks when they are mixed in aqueous solutions: interpenetrated, phase separated and coupled networks. Mixed gels of proteins and polysaccharides have attracted more and more attention since gelation occurs without a crosslinking agent or an enzyme, and their mechanical properties can be tuned by many factors including pH, ionic strength, protein to polysaccharide ratio and temperature, according to the needs. The gelation properties have been examined for many protein/polysaccharide systems, however, the underlying mechanism is not yet fully understood.

In this work, we have systematically investigated the effects of environmental factors (*e.g.* pH, ionic strength, protein to polysaccharide ratio, temperature) and biopolymer intrinsic factors (*e.g.* gelatin Bloom index, xanthan gum molecular weight and polysaccharide type) on the gelation properties of gelatin and polysaccharide aqueous mixtures. By analyzing and comparing the results of zeta potential measurements, rheometry, confocal microscopy and micro-calorimetry analyses, for mixtures comprising of 4 types of gelatin (A and B) and 2 types of oppositely charged polysaccharides (xanthan gum and chitosan), we have established a general mechanism, on a molecular conformation level, for the gelation of gelatin/polysaccharide mixed systems. Specifically, the process is completed in three steps following a decrease in solution temperature T:

1) protein/polysaccharide complexes formation by electrostatic attraction at an initially elevated temperature T_1 (above the coil-to-helix transition temperature of gelatin (T_2));

2) as T decreases, the distance between polysaccharide molecules also decreases, along with polysaccharide conformational changes due to the neutralization effect of gelatin when temperature is in-between T_1 and T_2. This step depends on the nature of the polysaccharide. For example, side-by-side associations between xanthan gum ordered structures lead to the formation of aggregates, whereas chitosan molecules get closer to each other due to the neutralization effect of gelatin and become less flexible with decreasing temperature.

3) when $T < T_2$, there is an increase in local biopolymer concentration due to bridging of complexes and interpolymer complexes, caused by the formation of gelatin triple helices, leading to a network.

The proposed mechanism is supported by a number of quantitative and qualitative observations:

- The helix-to-coil transition temperature and conformational transition enthalpy of xanthan gum in the mixtures increase in the presence of gelatin, suggesting a conformational change due to complexation;
- The sol-to-gel enthalpy of gelatin in the mixtures is higher than that of pure gelatin, indicating the high local concentration caused by aggregation;
- The increase in turbidity and *G'* with time at 30 ^{o}C of gelatin/XG mixtures indicates the formation of XG aggregates in the second step.
- The microstructures are characterized by a network of biopolymer-rich domains, an indication of aggregates linked by gelatin;
- The viscoelastic properties decrease greatly when salt is added, and can be tuned by pH and protein to polysaccharide ratio, indicating the key role of electrostatic attractions;
- Mixed gels exhibit full heat-reversibility. The gelation behavior is controlled by gelatin, indicated by the fact that *G'* of the mixed gels, independently of pH, increases (*e.g.* L-GB/XG, pH 5.0-7.0) with the same power-law exponent after an initial period;

The key parameter for gel formation of gelatin/polysaccharide mixtures is the extent of complexation, which affects polysaccharide charge density and conformation. Low extent of complexation occurs at low gelatin contents or at a pH far from the pI of gelatin. The relatively high charge density of polysaccharides in this case weakens the interactions between the gelatin/polysaccharide complexes, making the final network formation unlikely. In contrast, too low charge density on the polysaccharides should be avoided in order to maintain the network structure. Therefore, we usually observe an optimal pH and/or an optimal ratio to obtain the highest *G'*.

It should be noted that our proposed mechanism still has some unknowns. For example, the specific temperature at which the complexation between gelatin and polysaccharides occurs remains undetermined, although we tend to believe that complex formation occurs rapidly initially when solutions are mixed at high temperature (~ 60 ^{o}C) by inferring from some indirect proofs (e.g. micro calorimeter). We tried using temperature-controlled confocal microscopy to provide direct information, but without success due to instrumental limitations (insufficient spatial resolution and poor temperature control).

Gelatins A and B also display some subtle differences. Gelatin A/xanthan gum mixtures show the highest *G'* at a pH (6.0) far below the pI of gelatin A (9.3), which differs from gelatin B/xanthan gum mixtures, which always display the highest *G'* near the pI of gelatin B. For both mixtures, phase separation occurs below the optimal pH by precipitation, whereas a complementary microstructure is formed above the optimal pH. The phenomena may be related to different charge distributions of the two types of gelatin. However, this hypothesis remains to be verified.

The proposed mechanism can be used to explain the gelation behavior of other linear proteins like gelatin (e.g. collagen) and polysaccharide mixtures since collagen is the parent protein of gelatin, and they have a lot of similarities, including helix-to-coil transition, etc. Care should be taken when explaining the gelation behavior of globular proteins/polysaccharides mixtures using our proposed mechanism, since globular proteins denature irreversibly when heated above their denaturation temperature. In this case, the complexes and interpolymer complexes might be bridged by the exposed hydrophobic regions of globular proteins caused by denaturation.

Throughout this project, in order to get reproducible results, particular care was required for the following aspects:

- First, the pH of gelatin/xanthan gum mixtures should be adjusted drop by drop at a very low speed using a micropipette (~1-2 μL per drop to 20-30 mL). In this work, 0.5-1 M HCl and NaOH solutions were used for pH adjustment;
- Second, “table-top” rheology results vary depending on sample size and vial size. Therefore, it is crucial to use the same sample mass and vial type (geometry, size) to assess gel formation and strength;
- Third, a rough surface Couette flow geometry was used to avoid possible slipping effect during rheological measurements;
- Fourth, a diluted and filtered Nile Blue A solution (0.1 wt%) must be used to avoid the presence of large aggregates in confocal images. A freshly prepared Nile Blue A solution is preferred since the fluorescence intensity decreases with time. Also, the grafting of DTAF on xanthan gum and of FITC on chitosan should be conducted in the dark to avoid fluorescence quenching.
- Fifth, the sample cell of the micro DSC instrument should be well cleaned in order to obtain reliable data. It was first cleaned manually by extensive rinsing with hot deionized water, and then with a continuous hot deionized water flow using a pump. A water-water baseline test

should always be done prior to each measurement to ensure no contamination of the sample cell.

CHAPTER 9 CONCLUSIONS AND RECOMMENDATIONS

9.1 Conclusions

Gelatin and polysaccharides form gels with enhanced viscoelastic properties in aqueous solutions compared to their pure component solutions at similar compositions. The gelation occurs in three main steps depending on the coil-to-helix transition temperature of gelatin. When mixing gelatin and polysaccharides above the coil-to-helix transition temperature near the pI of gelatin, complexation occurs by electrostatic attraction. The reduction in the charge density of polysaccharides shortens the distance between polysaccharide molecules, and induces a change in polysaccharide conformation when decreasing temperature. Once cooling down below the coil-to-helix transition temperature of gelatin, the complexes and/or aggregates are concentrated and bridged by gelatin triple helix formation.

The gel properties are determined by the extent of complexation, and thus they are affected by environmental factors like pH, ionic strength, protein to polysaccharide ratio, and biopolymer intrinsic characteristics like gelatin type and Bloom index, polysaccharide type and molecular weight. A low extent of complexation may cause a segregative phase separation, resulting in a complementary microstructure, whereas too strong complexation leads to associative phase separation by precipitation, characterized by an aggregated microstructure. Therefore, there typically exists an optimal ratio and/or an optimal pH for gelatin/polysaccharide mixtures.

Stronger interactions between gelatin/polysaccharide complexes lead to higher *G'*, as well as a denser network, as indicated by the effects of gelatin Bloom index. Increasing the XG molecular weight decreases the mobility of soluble and/or interpolymer complexes, which then weakens the concentrating effect and resulting gel properties. XG is more effective than CHI in enhancing the triple helix formation of gelatin due to its more rigid conformation and the ability to form aggregates.

This work provides a fundamental understanding of gelatin and polysaccharide interactions in solutions, and is an important guideline to design novel thickeners and/or gelling agents, encapsulation and delivery systems. It will also help to understand the interactions in other systems, such as globular proteins and polysaccharides.

9.2 Recommendations

The following aspects are recommended for more exploration in future work:

1) The charge distribution of gelatin A and gelatin B needs to be characterized in order to better explain the location of the optimal pH for the best gelation properties;

2) Edible films prepared from biopolymers have been attracting much attention in recent years due to their potentials to substitute for conventional plastics in food packaging. Since we now have a fundamental understanding of how gelatins and polysaccharides interact with each other in solution, it will be also very interesting to examine the film manufacturing properties of gelatin/polysaccharide mixtures;

3) It would be necessary to verify if the proposed mechanism can be applied to globular proteins or other linear proteins (e.g. collagen) and polysaccharides mixtures. This is of great interest since globular proteins exist widely in food products, and unlike linear proteins, globular proteins denature irreversibly upon heating above their denaturation temperature. Therefore, some corresponding modifications are expected. For example, the formed complexes and interpolymer complexes will probably be bridged by the exposed hydrophobic groups of globular proteins in step three above;

4) Emulsions formed by protein/polysaccharide mixtures will also be of great interest. Taking oil/water emulsions as an example, the local concentrations of proteins and polysaccharides will be increased due to the presence of oil. This may induce an increase in viscosity or gel formation of the dispersed phase, which then favors the stability of the formed emulsions.

5) Slow acidification method can also be used to prepare polysaccharide/polysaccharide mixed gels.

BIBLIOGRAPHY

1. Tolstoguzov, V. B. *Food Hydrocolloids* **1995,** 9, (4), 317-332.

2. Benichou, A.; Aserin, A.; Garti, N. *Journal of Dispersion Science and Technology* **2002,** 23, (1-3), 93-123.

3. Tolstoguzov, V. *Food Hydrocolloids* **2003,** 17, (1), 1-23.

4. van der Wielen, M. W. J.; van de Heijning, W.; Brouwer, Y., Cellulose Gum as Protective Colloid in the Stabilization of Acidified Protien Drinks. In *Gums and Stabilisers for the Food Industry 14*, Williams, P. A.; Phillips, G. O., Eds. The Royal Society of Chemistry: London, UK, 2008; pp 495-502.

5. Turgeon, S. L.; Laneuville, S. I., CHAPTER 11 - Protein + Polysaccharide Coacervates and Complexes: From Scientific Background to their Application as Functional Ingredients in Food Products A2 - Kasapis, Stefan. In *Modern Biopolymer Science*, Norton, I. T.; Ubbink, J. B., Eds. Academic Press: San Diego, 2009; pp 327-363.

6. Turgeon, S. L.; Schmitt, C.; Sanchez, C. *Current Opinion in Colloid & Interface Science* **2007,** 12, (4–5), 166-178.

7. Evans, J.; Zulewska, J.; Newbold, M.; Drake, M. A.; Barbano, D. M. *Journal of Dairy Science* **2010,** 93, (5), 1824-1843.

8. Beecher, J. W.; Drake, M. A.; Luck, P. J.; Foegeding, E. A. *Journal of Dairy Science* **2008,** 91, (7), 2553-2560.

9. Ako, K.; Nicolai, T.; Durand, D.; Brotons, G. *Soft Matter* **2009,** 5, (20), 4033-4041.

10. Langton, M.; Hermansson, A.-M. *Food Hydrocolloids* **1992,** 5, (6), 523-539.

11. Wagoner, T. B.; Foegeding, E. A. *Food Hydrocolloids* **2017,** 63, 130-138.

12. McClements, D. J. *Langmuir* **2005,** 21, (21), 9777-9785.

13. Laplante, S.; Turgeon, S. L.; Paquin, P. *Carbohydrate Polymers* **2006,** 65, (4), 479-487.

14. Lutz, R.; Aserin, A.; Wicker, L.; Garti, N. *Colloids and Surfaces B-Biointerfaces* **2009,** 72, (1), 121-127.

15. Li, Y.; Hu, M.; Xiao, H.; Du, Y.; Decker, E. A.; McClements, D. J. *European Journal of Pharmaceutics and Biopharmaceutics* **2010,** 76, (1), 38-47.

16. Guezey, D.; McClements, D. J. *Food Biophysics* **2006,** 1, (1), 30-40.

17. Ghosh, A. K.; Bandyopadhyay, P., *Polysaccharide-protein interactions and their relevance in food colloids*. INTECH Open Access Publisher: 2012.

18. Le, X. T.; Rioux, L.-E.; Turgeon, S. L. *Advances in Colloid and Interface Science* **2017,** 239, 127-135.

19. Ballester, S. I. L.; Turgeon, S. L.; Sanchez, C.; Paquin, P., Gelation of Undenatured Proteins with Polysaccharides. Google Patents: 2005.

20. Cooper, C.; Dubin, P.; Kayitmazer, A.; Turksen, S. *Current opinion in colloid & interface science* **2005,** 10, (1), 52-78.

21. Weinbreck, F.; de Vries, R.; Schrooyen, P.; de Kruif, C. G. *Biomacromolecules* **2003,** 4, (2), 293-303.

22. Seyrek, E.; Dubin, P. L.; Tribet, C.; Gamble, E. A. *Biomacromolecules* **2003,** 4, (2), 273-282.

23. Wang, C.-S.; Natale, G.; Virgilio, N.; Heuzey, M.-C. *Food Hydrocolloids* **2016,** 60, 374-383.

24. Le, X. T.; Turgeon, S. L. *Soft Matter* **2013,** 9, (11), 3063-3073.

25. Phillips, G. O.; Williams, P. A., *Handbook of Food Proteins*. Woodhead Publishing: 2011.

26. Dudley, J. T.; Karczewski, K. J., *Exploring Personal Genomics*. OUP Oxford: 2013.

27. Matalanis, A.; Jones, O. G.; McClements, D. J. *Food Hydrocolloids* **2011,** 25, (8), 1865-1880.

28. Jones, O. G.; McClements, D. J. *Comprehensive Reviews in Food Science and Food Safety* **2010,** 9, (4), 374-397.

29. Nishinari, K.; Zhang, H.; Ikeda, S. *Current opinion in colloid & interface science* **2000,** 5, (3), 195-201.

30. Hosseini-nia, T.; Ismail, A. A.; Kubow, S. *Journal of agricultural and food chemistry* **1999,** 47, (11), 4537-4542.

31. Funtenberger, S.; Dumay, E.; Cheftel, J. *Journal of Agricultural and Food Chemistry* **1997,** 45, (3), 912-921.

32. Otte, J.; Schumacher, E.; Ipsen, R.; Ju, Z.; Qvist, K. B. *International Dairy Journal* **1999,** 9, (11), 801-812.

33. Dickinson, E. *Trends in Food Science & Technology* **1997,** 8, (10), 334-339.

34. Katsuta, K.; Hatakeyama, M.; Hiraki, J. *Food Hydrocolloids* **1997,** 11, (4), 367-372.

35. Ikeda, S.; Foegeding, E. A.; Hardin, C. C. *Journal of Agricultural and Food Chemistry* **2000,** 48, (3), 605-610.

36. Boye, J. I.; Ma, C. Y.; Ismail, A.; Harwalkar, V. R.; Kalab, M. *Journal of Agricultural and Food Chemistry* **1997,** 45, (5), 1608-1618.

37. Verheul, M.; Roefs, S. P. *Journal of Agricultural and food Chemistry* **1998,** 46, (12), 4909-4916.

38. Aymard, P.; Nicolai, T.; Durand, D.; Clark, A. *Macromolecules* **1999,** 32, (8), 2542-2552.

39. Peng, X.; Ren, C.; Guo, S. *Trends in Food Science & Technology* **2016,** 54, 138-147.

40. Wierenga, P. A.; Meinders, M. B. J.; Egmond, M. R.; Voragen, F. A. G. J.; de Jongh, H. H. J. *Langmuir* **2003,** 19, (21), 8964-8970.

41. Wierenga, P. A.; Meinders, M. B. J.; Egmond, M. R.; Voragen, A. G. J.; de Jongh, H. H. J. *The Journal of Physical Chemistry B* **2005,** 109, (35), 16946-16952.

42. Bouyer, E.; Mekhloufi, G.; Le Potier, I.; de Kerdaniel, T. d. F.; Grossiord, J.-L.; Rosilio, V.; Agnely, F. *Journal of Colloid and Interface Science* **2011,** 354, (2), 467-477.

43. Pongsawatmanit, R.; Harnsilawat, T.; McClements, D. J. *Colloids and Surfaces a-Physicochemical and Engineering Aspects* **2006,** 287, (1-3), 59-67.

44. Benichou, A.; Aserin, A.; Garti, N. *Colloids and Surfaces a-Physicochemical and Engineering Aspects* **2007,** 294, (1-3), 20-32.

45. Grand View Research. http://www.grandviewresearch.com/press-release/global-gelatin-market

46. Babel, W.; Schulz, D.; Giesen-Wiese, M.; Seybold, U.; Gareis, H.; Dick, E.; Schrieber, R.; Schott, A.; Stein, W., Gelatin. In *Ullmann's Encyclopedia of Industrial Chemistry*, Wiley-VCH Verlag GmbH & Co. KGaA: 2000.

47. Djabourov, M.; Leblond, J.; Papon, P. *Journal de physique* **1988,** 49, (2), 319-332.

48. Williams, P.; Phillips, G.; McKenna, B. *Texture in food. Volume 1: Semi-solid foods* **2003**, 251-274.

49. Djabourov, M. *Contemporary Physics* **1988,** 29, (3), 273-297.

50. Joly-Duhamel, C.; Hellio, D.; Ajdari, A.; Djabourov, M. *Langmuir* **2002,** 18, (19), 7158-7166.

51. Joly-Duhamel, C.; Hellio, D.; Djabourov, M. *Langmuir* **2002,** 18, (19), 7208-7217.

52. Izydorczyk, M.; Cui, S. W.; Wang, Q. *Food carbohydrates: Chemistry, physical properties, and applications* **2005**, 293-299.

53. Stokes, J. R., Food Biopolymer Gels, Microgel and Nanogel Structures, Formation and Rheology. In *Food Materials Science and Engineering*, Wiley-Blackwell: 2012; pp 151-176.

54. Huber, K.; McDonald, A.; BeMiller, J., Carbohydrate Chemistry. In *Handbook of Food Science, Technology, and Engineering - 4 Volume Set*, CRC Press: 2005.

55. Morris, E. R. *Canadian Institute of Food Science and Technology Journal* **1979,** 12, (1), A14.

56. Rees, D. A.; Welsh, E. J. *Angewandte Chemie International Edition in English* **1977,** 16, (4), 214-224.

57. Stephen, A. M.; Phillips, G. O., *Food polysaccharides and their applications*. CRC Press: 2010; Vol. 160.

58. McCleary, B. V.; Amado, R.; Waibel, R.; Neukom, H. *Carbohydrate Research* **1981,** 92, (2), 269-285.

59. Katzbauer, B. *Polymer Degradation and Stability* **1998,** 59, (1), 81-84.

60. marketsandmarkets.com. http://www.marketsandmarkets.com/Market-Reports/xanthan-gum-market-171291392.html

61. Sworn, G., Xanthan Gum – Functionality and Application. In *Practical Food Rheology*, Wiley-Blackwell: 2011; pp 85-112.

62. Sworn, G., 8 - Xanthan gum. In *Handbook of Hydrocolloids (Second edition)*, Woodhead Publishing: 2009; pp 186-203.

63. Pelletier, E.; Viebke, C.; Meadows, J.; Williams, P. *Biopolymers* **2001,** 59, (5), 339-346.

64. Rochefort, W. E.; Middleman, S. *Journal of Rheology (1978-present)* **1987,** 31, (4), 337-369.

65. McClements, D. J., *Understanding and controlling the microstructure of complex foods*. Elsevier: 2007.

66. Morris, V. J., 1 - Polysaccharides: their role in food microstructure A2 - McClements, D. Julian. In *Understanding and Controlling the Microstructure of Complex Foods*, Woodhead Publishing: 2007; pp 3-39.

67. Morris, E. R.; Rees, D. A.; Young, G.; Walkinshaw, M. D.; Darke, A. *Journal of Molecular Biology* **1977,** 110, (1), 1-16.

68. Norton, I. T.; Goodall, D. M.; Frangou, S. A.; Morris, E. R.; Rees, D. A. *Journal of Molecular Biology* **1984,** 175, (3), 371-394.

69. Bertrand, M.-E.; Turgeon, S. L. *Food Hydrocolloids* **2007,** 21, (2), 159-166.

70. Stokke, B. T.; Christensen, B. E.; Smidsrod, O., *Macromolecular properties of xanthan*. 1998; p 433-472.

71. Copetti, G.; Grassi, M.; Lapasin, R.; Pricl, S. *Glycoconj J* **1997,** 14, (8), 951-961.

72. Morris, V. J.; Franklin, D.; I'Anson, K. *Carbohydrate research* **1983,** 121, 13-30.

73. Mourya, V.; Inamdar, N. N. *Reactive and Functional polymers* **2008,** 68, (6), 1013-1051.

74. Suginta, W.; Khunkaewla, P.; Schulte, A. *Chemical Reviews* **2013,** 113, (7), 5458-5479.

75. Rabea, E. I.; Badawy, M. E. T.; Stevens, C. V.; Smagghe, G.; Steurbaut, W. *Biomacromolecules* **2003,** 4, (6), 1457-1465.

76. Riva, R.; Ragelle, H.; des Rieux, A.; Duhem, N.; Jerome, C.; Preat, V. *Chitosan for Biomaterials Ii* **2011,** 244, 19-44.

77. Chen, R.-H.; Domard, A.; Muzzarelli, R. A. A.; Tokura, S.; Wang, D.-M. *Carbohydrate Polymers* **2011,** 84, (2), 695-695.

78. Grand View Research. http://www.grandviewresearch.com/industry-analysis/global-chitosan-market

79. Peter, M. G. *Journal of Macromolecular Science, Part A: Pure and Applied Chemistry* **1995,** 32, (4), 629-640.

80. Tan, S. C.; Khor, E.; Tan, T. K.; Wong, S. M. *Talanta* **1998,** 45, (4), 713-719.

81. Nilsen-Nygaard, J.; Strand, S. P.; Vårum, K. M.; Draget, K. I.; Nordgård, C. T. *Polymers* **2015,** 7, (3), 552-579.

82. Klinkesorn, U. *Food Reviews International* **2013,** 29, (4), 371-393.

83. Vachoud, L.; Zydowicz, N.; Domard, A. *Carbohydrate Research* **2000,** 326, (4), 295-304.

84. Chenite, A.; Buschmann, M.; Wang, D.; Chaput, C.; Kandani, N. *Carbohydrate polymers* **2001,** 46, (1), 39-47.

85. Cho, J.; Heuzey, M.-C. *Colloid and Polymer Science* **2008,** 286, (4), 427-434.

86. Cho, J.; Heuzey, M.-C.; Bégin, A.; Carreau, P. J. *Carbohydrate Polymers* **2006,** 63, (4), 507-518.

87. Cho, J.; Heuzey, M.-C.; Hamdine, M. *Macromolecular Materials and Engineering* **2007,** 292, (5), 571-581.

88. Lavertu, M.; Filion, D.; Buschmann, M. D. *Biomacromolecules* **2008,** 9, (2), 640-650.

89. Shu, X. Z.; Zhu, K. J. *International Journal of Pharmaceutics* **2002,** 233, (1–2), 217-225.

90. Draget, K. I.; Värum, K. M.; Moen, E.; Gynnild, H.; Smidsrød, O. *Biomaterials* **1992,** 13, (9), 635-638.

91. Montembault, A.; Viton, C.; Domard, A. *Biomacromolecules* **2005,** 6, (2), 653-662.

92. Ladet, S.; David, L.; Domard, A. *Nature* **2008,** 452, (7183), 76-79.

93. Rami, L.; Malaise, S.; Delmond, S.; Fricain, J.-C.; Siadous, R.; Schlaubitz, S.; Laurichesse, E.; Amédée, J.; Montembault, A.; David, L.; Bordenave, L. *Journal of Biomedical Materials Research Part A* **2014,** 102, (10), 3666-3676.

94. Gupta, A. N.; Bohidar, H. B.; Aswal, V. K. *Journal of Physical Chemistry B* **2007,** 111, (34), 10137-10145.

95. Turgeon, S. L.; Beaulieu, M.; Schmitt, C.; Sanchez, C. *Current Opinion in Colloid & Interface Science* **2003,** 8, (4-5), 401-414.

96. Selinheimo, E.; Kruus, K.; Buchert, J.; Hopia, A.; Autio, K. *Journal of Cereal Science* **2006,** 43, (2), 152-159.

97. Donato, L.; Garnier, C.; Novales, B.; Durand, S.; Doublier, J.-L. *Biomacromolecules* **2005,** 6, (1), 374-385.

98. Doumèche, B.; Picard, J.; Larreta-Garde, V. *Biomacromolecules* **2007,** 8, (11), 3613-3618.

99. Turgeon, S. L.; Beaulieu, M. *Food Hydrocolloids* **2001,** 15, (4), 583-591.

100. de Jong, S.; van de Velde, F. *Food Hydrocolloids* **2007,** 21, (7), 1172-1187.

101. Sanchez, C.; Schmitt, C.; Babak, V. G.; Hardy, J. *Food / Nahrung* **1997,** 41, (6), 336-343.

102. Turgeon, S. L.; Beaulieu, M. *Food Hydrocolloids* **2001,** 15, (4–6), 583-591.

103. Beaulieu, M.; Turgeon, S. L.; Doublier, J.-L. *International Dairy Journal* **2001,** 11, (11–12), 961-967.

104. Laneuville S I; Turgeon, S. L.; Sanchez, C.; Paquin, P. *Langmuir* **2006,** 22, (17), 7351-7357.

105. Eleya, M. O.; Turgeon, S. *Food hydrocolloids* **2000,** 14, (1), 29-40.

106. Eleya, M. O.; Turgeon, S. *Food hydrocolloids* **2000,** 14, (3), 245-251.

107. Ould Eleya, M. M.; Leng, X. J.; Turgeon, S. L. *Food Hydrocolloids* **2006,** 20, (6), 946-951.

108. Le, X. T.; Turgeon, S. L. *Food Hydrocolloids* **2015,** 49, (30), 216-223.

109. Laneuville, S. I.; Turgeon, S. L.; Sanchez, C.; Paquin, P. *Langmuir* **2006,** 22, (17), 7351-7357.

110. Zasypkin, D. V.; Dumay, E.; Cheftel, J. C. *Food Hydrocolloids* **1996,** 10, (2), 203-211.

111. Dumay, E.; Laligant, A.; Zasypkin, D.; Cheftel, J. *Food hydrocolloids* **1999,** 13, (4), 339-351.

112. Derkach, S. R.; Ilyin, S. O.; Maklakova, A. A.; Kulichikhin, V. G.; Malkin, A. Y. *LWT-Food Science and Technology* **2015,** 63, (1), 612-619.

113. Derkach, S. R.; Voron'ko, N. G.; Maklakova, A. A.; Kondratyuk, Y. V. *Colloid Journal* **2014,** 76, (2), 146-152.

114. Jin, W.; Xu, W.; Ge, H.; Li, J.; Li, B. *Food Hydrocolloids* **2015,** 51, 188-192.

115. Zhang, S.; Hsieh, F.-H.; Vardhanabhuti, B. *Food Hydrocolloids* **2014,** 36, 76-84.

116. Bryant, C. M.; McClements, D. J. *Food Hydrocolloids* **2000,** 14, (4), 383-390.

117. Wijaya, W.; Van der Meeren, P.; Patel, A. R. *Food Hydrocolloids* **2017,** 65, 35-45.

118. Çakır, E.; Foegeding, E. A. *Food Hydrocolloids* **2011,** 25, (6), 1538-1546.

119. Çakır, E.; Khan, S. A.; Foegeding, E. A. *International Dairy Journal* **2012,** 27, (1–2), 99-102.

120. Michon, C.; Cuvelier, G.; Launay, B.; Parker, A. *Carbohydrate Polymers* **1996,** 31, (3), 161-169.

121. Panouillé, M.; Larreta-Garde, V. *Food Hydrocolloids* **2009,** 23, (4), 1074-1080.

122. Holzwarth, G.; Prestridge, E. B. *Science* **1977,** 197, (4305), 757.

123. Rao, M. A., Measurement of Flow and Viscoelastic Properties. In *Rheology of Fluid and Semisolid Foods: Principles and Applications*, Springer US: Boston, MA, 2007; pp 59-151.

124. Kasapis, S.; Bannikova, A., Chapter 2 - Rheology and Food Microstructure A2 - Ahmed, J. In *Advances in Food Rheology and its Applications*, Ptaszek, P.; Basu, S., Eds. Woodhead Publishing: 2017; pp 7-46.

125. Wetzel, D. L. B.; Charalambous, G., *Instrumental Methods in Food and Beverage Analysis*. Elsevier Science: 1998.

126. Winter, H. H.; Mours, M., Rheology of Polymers Near Liquid-Solid Transitions. In *Neutron Spin Echo Spectroscopy Viscoelasticity Rheology*, Springer Berlin Heidelberg: Berlin, Heidelberg, 1997; pp 165-234.

127. Lopes da Silva, J. A.; Rao, M. A., Rheological Behavior of Food Gels. In *Rheology of Fluid and Semisolid Foods: Principles and Applications*, Springer US: Boston, MA, 2007; pp 339-401.

128. Grillet, A. M.; Gloe, L. M.; Wyatt, N. B., *Polymer gel rheology and adhesion*. INTECH Open Access Publisher: 2012.

129. Henning Winter, H., Gel Point. In *Encyclopedia of Polymer Science and Technology*, John Wiley & Sons, Inc.: 2002.

130. Winter, H. H.; Morganelli, P.; Chambon, F. *Macromolecules* **1988,** 21, (2), 532-535.

131. Djabourov, M.; Leblond, J.; Papon, P. *Journal de Physique* **1988,** 49, (2), 333-343.

132. Stading, M.; Hermansson, A.-M. *Food Hydrocolloids* **1990,** 4, (2), 121-135.

133. Stading, M.; Hermansson, A.-M. *Carbohydrate Polymers* **1993,** 22, (1), 49-56.

134. Muller, R.; Gerard, E.; Dugand, P.; Rempp, P.; Gnanou, Y. *Macromolecules* **1991,** 24, (6), 1321-1326.

135. Chambon, F.; Winter, H. H. *Journal of Rheology* **1987,** 31, (8), 683-697.

136. Albano, K. M.; Franco, C. M. L.; Telis, V. R. N. *Food Hydrocolloids* **2014,** 40, 30-43.

137. Giacomazza, D.; Bulone, D.; San Biagio, P. L.; Lapasin, R. *Carbohydrate Polymers* **2016,** 146, 181-186.